AD-A260 253

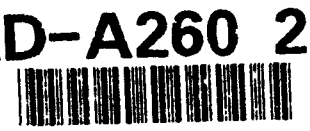

2

WL-TR-92-2110

COMBUSTION AND HEAT TRANSFER STUDIES UTILIZING ADVANCED DIAGNOSTICS: COMBUSTION STUDIES

D. R. Ballal, S. P. Heneghan, W. J. Schmoll, F. Takahashi, and M. D. Vangsness
University of Dayton
Dayton, OH 45469-0001

November 1992

FINAL REPORT FOR THE PERIOD September 11, 1987 to September 30, 1992

Approved for Public Release; Distribution is Unlimited

DTIC
ELECTE
FEB 17 1993
S E D

AERO PROPULSION AND POWER DIRECTORATE
WRIGHT LABORATORY
AIR FORCE MATERIEL COMMAND
WRIGHT-PATTERSON AIR FORCE BASE, OH 45433-6563

93-04577

93 2 16 134

NOTICE

When Government drawings, specifications, or other data are used for any purpose other than in connection with a definitely Government-related procurement operation, the United States Government incurs no responsibility nor any obligation whatsoever. The fact that the Government may have formulated, furnished, or in any other way supplied the said drawings, specifications, or other data, is not to be regarded by implication or otherwise in any manner construed, as licensing the holder or any other person or corporation, or as conveying any rights or permission to manufacture, use, or sell any patented invention that may in any way be related thereto.

This report is releasable to the National Technical Information Service (NTIS). At NTIS, it will be available to the general public, including foreign nations.

This technical report has been reviewed and is approved for publication.

W. M. Roquemore

Government Monitor
W. MELVYN ROQUEMORE
Fuels Branch
Fuels & Lubrication Division

Royce P. Bradley

Supervisor
ROYCE P. BRADLEY
Section Chief, Fuels Branch
Fuels & Lubrication Division
Aero Propulsion & Power Directorate

Division Chief
LEO S. HAROOTYAN, JR.
Chief, Fuels & Lubrication Division
Aero Propulsion & Power Directorate

If your address has changed, if you wish to be removed from our mailing list, or if the addressee is no longer employed by your organization, please notify WL/POSF, Wright-Patterson AFB, OH 45433-7103 to help us maintain a current mailing list.

Copies of this report should not be returned unless return is required by security considerations, contractual obligations, or notice of a specific document.

DISCLAIMER NOTICE

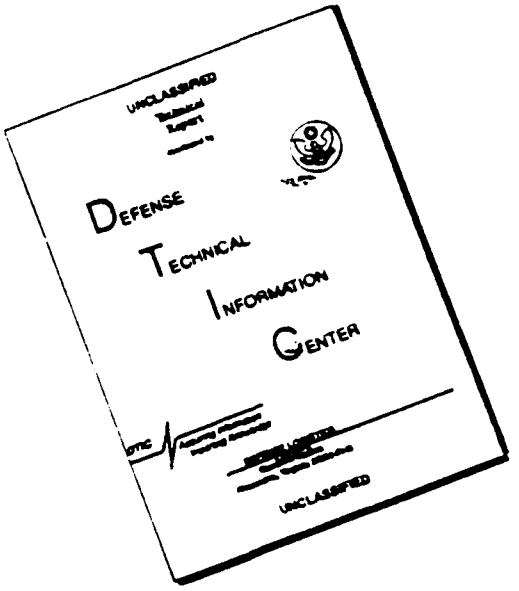

THIS DOCUMENT IS BEST QUALITY AVAILABLE. THE COPY FURNISHED TO DTIC CONTAINED A SIGNIFICANT NUMBER OF PAGES WHICH DO NOT REPRODUCE LEGIBLY.

REPORT DOCUMENTATION PAGE

Form Approved
OMB No. 0704-0188

Public reporting burden for this collection of information is estimated to average 1 hour per response, including the time for reviewing instructions, searching existing data sources, gathering and maintaining the data needed, and completing and reviewing the collection of information. Send comments regarding this burden estimate or any other aspect of this collection of information, including suggestions for reducing this burden, to Washington Headquarters Services, Directorate for Information Operations and Reports, 1215 Jefferson Davis Highway, Suite 1204, Arlington, VA 22202-4302, and to the Office of Management and Budget, Paperwork Reduction Project (0704-0188), Washington DC 20503

1. AGENCY USE ONLY (Leave blank)	2. REPORT DATE	3. REPORT TYPE AND DATES COVERED
	November 1992	Final 9/11/87 - 9/30/92

4. TITLE AND SUBTITLE
Combustion & Heat Transfer Studies Utilizing Advanced Diagnostics : Combustion Studies

5. FUNDING NUMBERS
C-F33615-87-C-2767
PE-62203
PR-3048
TA-05
WU-60

6. AUTHOR(S)
D. R. Ballal, S. P. Heneghan, W. J. Schmoll, F. Takahashi, and M. D. Vangsness

7. PERFORMING ORGANIZATION NAME(S) AND ADDRESS(ES)
University of Dayton
300 College Park
Dayton, OH 45469-0001

8. PERFORMING ORGANIZATION REPORT NUMBER

9. SPONSORING/MONITORING AGENCY NAME(S) AND ADDRESS(ES)
Aero Propulsion & Power Directorate
Wright Laboratory (WL/POSF)
Air Force Material Command
Wright-Patterson Air Force Base, OH 45433-6563
W. Melvin Roquemore, 513-255-6813

10. SPONSORING/MONITORING AGENCY REPORT NUMBER
WL-TR-92-2110

11. SUPPLEMENTARY NOTES

12a. DISTRIBUTION/AVAILABILITY STATEMENT
Approved for public release; distribution is unlimited.

12b. DISTRIBUTION CODE

13. ABSTRACT (Maximum 200 words)

A long-term goal of the Air Force is to develop near-stoichiometric gas turbine combustors that will burn broad-specification fuels, and have low maintenance and high durability. Towards meeting this goal, this program had two principal objectives: (1) to design and conduct experiments that will establish a fundamental understanding of lean blowout (LBO), swirling flames, kinetically controlled combustion, and turbine blade cooling, and (2) to provide data sets for evaluating and refining computer models of gas turbine combustor.

We successfully designed and operated several laboratory combustors. Two novel methods for CARS slit function were developed; these made possible precise and unambiguous measurements of flame temperature. We identified the complex sequence of events leading to LBO and obtained and analyzed LBO data for different combustor loadings. We investigated the effects of geometric, chemical, and turbulent flow parameters on the structure of the recirculation zone and the flame inside the combustor. Our heat transfer experiments showed that freestream turbulence augments flat plate heat transfer 2 to 2.5 times. Finally, benchmark-quality data for evaluating and refining computer models of gas turbine combustor were made available to industry. In this manner, the program objectives were met.

14. SUBJECT TERMS	15. NUMBER OF PAGES
Lean Blowout, Flame Stabilization, Combustor Design, Swirling Flames, Turbulent Combustion, Turbine Blade Cooling	213
	16. PRICE CODE

17. SECURITY CLASSIFICATION OF REPORT	18. SECURITY CLASSIFICATION OF THIS PAGE	19. SECURITY CLASSIFICATION OF ABSTRACT	20. LIMITATION OF ABSTRACT
Unclassified	Unclassified	Unclassified	UL

TABLE OF CONTENTS

DTIC QUALITY INSPECTED 3

Accesion For
NTIS CRA&I [X]
DTIC TAB [ ]
Unannounced [ ]
Justification .....
By .....
Distribution /
Availability Codes
Dist | Avail and / or Special
A-1

TABLES

FIGURES

PREFACE

This final report was submitted by the University of Dayton Research Institute (UDRI) under Contract No. F33615-87-C-2767, sponsored by the U.S. Air Force Wright Laboratory, Aero Propulsion and Power Directorate, Wright-Patterson Air Force Base OH. Dr. W. M. Roquemore of WL/POSF was the Air Force Technical Monitor; Dr. D. R. Ballal of the Applied Physics Division, UDRI, was the Principal Investigator; and Dr. E. H. Gerber, Head of the Applied Physics Division, UDRI, was the Project Supervisor of this research program. This report covers work performed during the period September 11, 1987 through September 30, 1992.

The Principal Investigator wishes to express his gratitude and appreciation to Dr. W. M. Roquemore, for his encouragement and support; to Ms. Ruth Rodak, UDRI, for technical editing; and to Ms. W. Barnes, UDRI, for report preparation.

SUMMARY

A long-term goal of the Air Force is to develop high-performance gas turbine engines with combustors that operate at near-stoichiometric conditions, burn broad-specification fuels, and have low maintenance and high durability. Towards meeting these broad goals, the Air Force Wright Laboratory, Aero Propulsion and Power Directorate (WL/PO) initiated a 5-year program of research with the University of Dayton Research Institute (UDRI), beginning in September 1987, with three principal objectives: (1) to design and conduct combustion experiments that will establish a fundamental understanding and data base on combustion stability, lean blowout (LBO), swirling flows, and *kinetically controlled* combustion; (2) to conduct experimental research and evaluate heat transfer models that can be used to design hot section components such as turbine blades; and (3) to develop research tools and perform the research that will eventually lead to the development of a high-temperature, thermally stable, JP-8 fuel.

To perform this research, we successfully designed and operated several laboratory combustors such as a step combustor, a bluff body combustor, and a swirl combustor, each of which simulated some important features of a practical gas turbine combustor. Thus, we ensured that our research results closely represent features of the combustion processes in practical combustors. Next, we documented a systematic and detailed sequence of events leading to Lean Blowout (LBO). We found that in a step combustor, these events comprised the attached-flame region, lifted shear flame, intermittent shear flame, the large-scale instability of the flame front, and finally LBO. For a bluff-body combustor, excess entrainment of cold reactants in the thick-flame region caused flamelet extinction, and in a swirl combustor, intermittent mixing and radial jet fluid ejection produced by large-scale vortices caused local flame extinction. These individual events clearly highlighted the complexity of LBO mechanism in a modern annular gas turbine combustor.

In a modern annular gas turbine combustor, flame is stabilized by a recirculation zone. Therefore, we investigated the effects of various parameters on the recirculation zone structure. We found that for flames anchored by the bluff body, wall confinement elongated the recirculation zone by accelerating the flow and narrowed it by preventing mean streamline curvature. In the limit of fast chemistry, the recirculation zone size decreases to its value for fully developed, cold turbulent flow wake. Finally, we discovered that swirl enhances flame stability significantly by creating a toroidal recirculation zone.

The structure of a turbulent flame in the primary zone of a gas turbine combustor is highly complex. Therefore, we conducted a systematic study of this structure. We observed that at low fuel flows a distinct flame attaches itself around the fuel nozzle. This so-called "attached flame" structure has the appearance of an inverted "classic coke bottle" and is remarkably stable. As the overall equivalence ratio falls below 0.65, large-scale, oscillatory axial movement of the flame begins; this eventually leads to LBO. The structure of the turbulent flame anchored by the bluff

body and enveloping the recirculation zone comprises: (1) an ignition-thin flame region in the vicinity of the flameholder base, (2) a reacting shear layer region of large-scale coherent structures, and (3) a thick-flame region in which entrainment is the dominant mechanism. Finally, the high-velocity gradients generated in the swirl combustor produce a thin diffusion layer, low Damkohler number, highly stretched flame structure.

In ramjet engines, jet afterburners, and gas turbine combustors, chemistry-turbulence interaction is important and controlling. We made successful correlations of the LBO in a step combustor against loading parameter (LP) for LP values extending over 3 orders of magnitude. Further, *a priori* calculation of LBO was done using a dissipation gradient approach of defining local perfectly stirred reactor regions in the step combustor. Such a network of stirred reactor nodes yielded good agreement with experimental data. We observed that in a bluff body combustor, for $\phi \leq 0.75$, combustion was *kinetically controlled* and requires a recirculation zone larger than that for cold flow in order to stabilize a flame. Such results indicate how compact the size of the primary zone of a gas turbine combustor can be, provided it operates at or near-stoichiometric equivalence ratios.

The free-stream turbulence level experienced by a turbine blade downstream of the combustor approaches 20 percent. We performed an investigation of the effects of free-stream turbulence up to 22%, on the flat plate heat transfer. We discovered that free-stream turbulence augments heat transfer 2 to 2.5 times. In practice, this means free-stream turbulence would cause a faster decay in the turbine blade film-cooling effectiveness, a reduction in the effective cooling length, or an increase in the film-cooling requirement.

To summarize, our experimental studies have made a valuable contribution by providing a physical understanding of turbulent combustion and heat transfer, and also by making available benchmark-quality data for evaluating and refining computer models used by industry to design gas turbine combustors. Now, the challenge is to produce new modeling codes that can be used with a sufficient degree of realism, confidence, and certainty to design practical combustion systems. The research work described above has led to 24 archival journal publications, 22 presentations at national and international meetings, and 10 internal reports. It has won three major national awards including the American Society of Mechanical Engineers (ASME) International Gas Turbine Institute's Outstanding Research Paper Award for 1992, and the American Institute of Aeronautics and Astronautics (AIAA)--1992 National Aerospace Highlights.

This final report describes the experimental work, theoretical results, and conclusions for all the combustion work performed on this contract. The combustion data sets are presented in a companion Report No. WL-TR-92-2111.

1. INTRODUCTION

1.1 Program Objectives

A long-term goal of the Air Force is to develop high-performance gas turbine engines with combustors that operate at near-stoichiometric conditions, burn broad-specification fuels, and have low maintenance and high durability. With these broad goals in mind, the Air Force Wright Laboratory, Aero Propulsion and Power Directorate (WL/PO) initiated a 5-year program of research with the University of Dayton Research Institute (UDRI), beginning in September 1987. This program had three principal objectives: (1) to design and conduct combustion experiments that will establish a fundamental understanding and data base on combustion stability, lean blowout (LBO), swirling flows, and *kinetically controlled* combustion; (2) to conduct experimental research and evaluate heat transfer models that can be used to design hot section components such as turbine blades; and (3) to develop research tools and perform the research that will eventually lead to the development of a high-temperature, thermally stable, JP-8 fuel.

1.2 Combustion Tasks

Traditional gas turbine combustor design methodology has been based on empirical correlations, experience, scaling of working designs, and extensive development testing. This approach has been amazingly successful. However, as the requirements of high- performance, compactness, and durability have increased, the error margin for achieving these goals has decreased and the cost of rig testing has dramatically increased. The mixing and combustion process in practical combustors involves complex recirculation zones, unknown chemical kinetics, two-phase flows, and turbulence. Simultaneous consideration of all these effects complicates their study. The objective of this program was to develop a fundamental understanding; therefore, we formulated five technical tasks to study combustion and heat transfer:

(1) Step Combustor Task,
(2) Bluff Body Combustor Task,
(3) Swirl Combustor Task,
(4) Perfectly Stirred Reactor (PSR) Task, and
(5) Heat Transfer Task.

This report describes the objectives, laser diagnostic instrumentation, test results, and conclusions for each of the five technical tasks. Finally, we analyze our entire combustion and heat transfer research from the viewpoint of program objectives, how we met those objectives, what new fundamental knowledge emerged, and what gaps, if any, were discovered that should form the basis of future research.

2. TEST FACILITY AND LASER DIAGNOSTICS

All the combustion tasks were performed in the Fundamental Combustion Laboratory located in Building 490, Test Cell 153, of the Fuels and Lubrication Division (WL/POSF) and the film-cooling studies were conducted in the Heat Transfer Laboratory located in Building 18C, Room 21 (WL/POTC).

2.1 Combustion Test Facility

This test facility is fully described by Ballal et al. [1]. At the heart of this facility is a turbulent flame burner located under an exhaust hood. On one side of the burner is an optics table on which a three-component LDA system is assembled; on the other side is another optical table which bears the CARS system. A breadboard optics table and a U-channel support structure are used to bind the two large optics tables. This smaller table has a square cutout through which the burner working section protrudes. The optical integration of LDA with the CARS system can be performed on this breadboard table.

The turbulent flame burner is mounted on a three-axis traversing platform and is connected to a high-pressure (110 psia) airflow delivery system. An intricate piping network is designed to supply large quantities of gaseous fuels such as propane, methane, hydrogen, and/or inert gases such as nitrogen, carbon dioxide, argon, and helium to the burner. Both the airflow and the fuel flow are accurately monitored. An exhaust hood routes the products of combustion out of the test cell. Finally, this test facility is well equipped with fire and laser safety features, utilities, and climate control systems. A powerful and dedicated MODCOMP/MODAC computer and many data acquisition computers are used to operate the facility, and to record and analyze data.

2.2 Heat Transfer Test Facility

The heat transfer facility essentially consists of a either a 20.3-cm-dia ASME or a 6.67 × 49.53 cm ASME planar free-jet nozzle (lip thickness = 0.64 cm) which supplies highly turbulent freestream airflow to a flat test plate (3.05 m long and 0.61 m wide) with an unheated starting length of 1.52 m, located many diameters downstream of the free-jet nozzle. The flat plate is electrically heated and embedded with hot film and 42 fine thermocouple probes for measuring surface temperature. The back face of the plate is insulated to minimize heat loss.

In a film-cooling arrangement, spanwise rows of slots (5 slots, 2.54 cm dia., l/d = 6) are used to inject a layer of coolant air over the flat plate and insulate it from the turbulent hot mainstream gases. These slots, which have a pitch-to-diameter ratio of 2, are inclined at a 30-degree angle and are located at the end of the unheated starting length. The effectiveness and heat transfer coefficient of the film can be measured at several locations (z/d = 5.5 to 40) along the length of the heat transfer table and downstream of the row of holes or slots for a range of values of freestream turbulence. This test facility is equipped with a hot-wire anemometer, an

LDA system, pressure transducers, pitot probes, thermocouples, and IBM-compatible PCs for data acquisition and analysis.

2.3 LDA System

Our three-component LDA system is essentially a refined version of the two-component system used by Ballal et al. [1]. The LDA system employs a three-beam two-channel optics to measure velocity components ± 45 degrees off-axis. It uses a 514.5-nm (green) laser beam and a 488-nm (blue) laser beam from an 15-W Spectra Physics Model 171 argon-ion laser. The 514.5-nm source beam is split into two channels using polarization separation and the 488-nm beam is used for the third channel (tangential velocity component). These laser beams are focused to the crossing volume by lenses with a focal length of 250 mm. The third channel beams are focused in a direction normal to the other two beams to minimize the size of the ellipsoidal probe volume of 175 μm × 1500 μm (for a two-component LDA system) to a probe volume equal to 100 μm in diameter (for a three-component LDA system). The scattered light is collected in the forward direction, 10 degrees off-axis. The LDA system incorporates Bragg cell frequency shifting of 10 MHz for the first two channels and 20 MHz for the third channel to eliminate directional ambiguity presented by measurements in swirl and/or recirculatory flows, and a three-channel time-coincidence data check circuit which guarantees a rapid acquisition of valid data (due to beam crossing) in highly turbulent flows. The calculated fringe spacing is approximately 3.6 μm. The LDA software comprises subroutines to filter spurious signals, for example, due to seed agglomeration, corrections to account for LDA signal biasing effects in combusting flows, and LDA data sampling rates.

A fluidized bed seeder was used to inject submicron size ZrO_2 seed particles (97% < 1 μm, seed rates > 10^8 particles/sec) into the flowing combustible mixture. Scattered signals were detected by TSI 1990C counter processors and processed by our custom-designed software which calculates turbulence intensity, shear stresses, higher moments (skewness and kurtosis), pdfs, and complex velocity correlations such as u'^2v'. A total of 4096 LDA realizations were collected at each measurement location and data sampling rates as high as 8 kHz in cold flows and 1 kHz in flames were obtained using this system. In our experiments, we employed the seeding of both single and multiple streams.

2.4 LDA Measurement Errors and Accuracy

In processing the LDA Doppler burst signal, typically 2^5 cycles/burst are requested and the spurious data are filtered by using the 3σ test of Rose and Johnson [2]. Applying the analysis of Yanta and Smith [3], the error in rms velocity was less than 3 percent and uncertainty in mean velocity was less than 1 percent at a 95 percent confidence limit. However, in recirculatory and reactive flows, the velocity statistical biasing was worst. Using the analysis of Glass and Bilger [4] and Edwards [5], the mean values can be overestimated up to 7 percent and the rms values underestimated up to 5 percent for turbulence intensity levels above 20 percent. The flow rates calculated from integrating the velocity profiles were 3 percent or less than the measured flow

rates. This difference is partly attributed to the plus-or-minus 1 percent measurement accuracy of the mass flow controller. To eliminate velocity biasing due to nonuniform seeding, the conditional data sampling technique of Libby et al. [6] was used by seeding particles into only the fuel jet or the annular coflowing air. This type of technique allowed us to track the convection and diffusion of one (seeded) fluid into another (unseeded) fluid in a manner similar to that used by Dibble et al. [7].

2.5 CARS System

The CARS system light source is provided by a Nd:YAG pulse laser with 10-ns time resolution. The frequency-doubled source green beam (532-nm) is equally divided into four parts. Two of these serve as the pump beams, while the other two pump a dye laser oscillator and amplifier. The dye laser is tuned to provide a red broad-band Stokes beam (110 FWHM) centered at 607 nm. The red Stokes beam and the two green pump beams are then focused together by a 25-cm focal length lens in a BOXCARS configuration. A 25-μm-x-250-μm measuring spot size is achieved. The CARS signal is collected by a Spex 1702 spectrometer, 1024 element DARSS camera, and Tracor-Northern multichannel analyzer. The raw data are processed by a MODCOMP minicomputer.

From the raw data, the temperatures are determined by comparing the actual nitrogen spectra to the calculated spectra, using a least square fit. The calculation of a nitrogen CARS spectrum requires knowledge of the instrument slit function. Early in our research, we recognized (see Appendices A and B) that accounting for the variation of slit function can increase the precision of the CARS data and the assumption that the slit function is constant and independent of temperature, laser beam intensity, and turbulence is also relaxed.

In Appendix A, we discuss the source of instrument slit function, its variability from shot to shot, and the various weighting schemes used to increase the CARS precision. We have fitted the collected CARS spectra using two parameters: slit width and temperature. This two-parameter least squares (TPLS) method allowed the calculation of temperature with almost no previous knowledge of the slit function except its general shape.

Appendix B describes a simple method of determining the slit function from the collected data at the actual temperature and turbulence level by applying the principle of local thermodynamic equilibrium. In general, the mean temperature is measured for two different curve-fit weighting schemes and two different values of half-width at half-maximum (HWHM) slit widths. The actual mean temperature and slit width are calculated by finding the intersection of the two lines (T vs. slit width at constant weighting). This four-point-intercept (4PI) method determines the correct average HWHM of the slit function to use, and thereby guarantees unambiguous temperature measurement. Since this method was easily adaptable to current software, it was used to analyze all the CARS data collected in all the combustion experiments.

2.6 CARS Precision and Accuracy

Usually, 500 samples were taken for each CARS measurement to ensure that the error in the rms temperature was less than 10 K, while 1500 samples were taken in the flame region where the rms values were expected to be large. As shown by Vangsness and Heneghan [8], the rms temperature is susceptible to CARS instrument noise. Overall, we estimated the CARS mean temperature measurement accuracy to be within 50 K, while the precision was well within 20 K. Unlike the LDA, CARS temperature measurements are time-averaged, without density biasing effects. We also discovered that once system parameters are optimized and the dye laser is tuned, the CARS system can run for long periods of time. For example, we obtained repeatability to within ± 20 K for a mean flame temperature of 1500 K after 4 days of operation.

3. COMBUSTION TASKS

3.1 Step Combustor Task

3.1.1 Objective. The provision of adequate LBO stability in aircraft gas turbine combustors is a long-term problem that is exacerbated by several current design trends. Therefore, the principal objective of this task was to investigate, understand, and model LBO in a step combustor that simulates the essential flow and heat release features of a modern annular aircraft engine combustor.

3.1.2 Step Combustor. In a modern annular gas turbine combustor (Figure 1), the flame is stabilized by producing a recirculation zone in the flow field. This zone is generated by a combination of *three* mechanisms, namely: (1) an axial swirling air jet associated with each fuel introduction, (2) sudden expansion of the axial swirling jets as they enter the primary zone, and (3) back pressure provided by an array of radial air jets at the end of the primary zone. Therefore, the step combustor was required to reproduce this type of recirculation pattern. Figure 2 shows a schematic diagram of this combustor whose design and development is fully described by Sturgess et al. [9].

Briefly, the research combustor consists of a 29-mm i.d. central fuel jet of gaseous propane surrounded by a 40-mm i.d. coaxial air jet located in a 150-mm diameter (nominal) circular cross section. This arrangement creates a reactive shear layer, *similar to that of a practical combustor*, in which combustion is initiated. A perforated conical baffle inserted five diameters upstream of the fuel tube serves to acoustically isolate the fuel supply from the combustion process. The duct is closed at its forward end to yield a 55-mm wide, backward-facing step. This step provides two inside-out recirculation zones that stabilize the flame. Also, the duct, which has an overall length of 735 mm, is restricted at its discharge end by an orifice plate of 45 percent exit blockage ratio. This simulates the back pressure provided by an array of radial air jets at the end of the primary zone. As shown in Figure 2, the step combustor is mounted vertically on a small wind tunnel. The combination of combustor and its extension chimney yields (L/D) ratios of 3.17, 4.9, and 6.5, respectively. Sturgess et al. [9] listed the unique design features of this step combustor.

3.1.3 Test Conditions. A three-component LDA system for velocity measurements and a CARS system for flame temperature measurements were arranged on two separate 1.22-m-x-2.44-m optics tables on either side of the combustor. Air was supplied to the combustor in the 510-Kg/hr-to-4,900-Kg/hr range at atmospheric pressure. The combustion laboratory provides gaseous propane and methane fuels up to 20 Kg/hr. Ignition of the combustor was satisfactorily accomplished in the recirculation zone with a small propane torch igniter attached to the side-plate fitting. Upon successful ignition, the torch igniter was removed and the fitting was capped. As the LOB condition was approached, the attached diffusion flame lifts from the fuel tube and is stabilized slightly downstream. This was the region of most interest and relevance to the present study.

3.1.4 Results. Before performing combustion tests, acoustic characteristics of this research combustor were investigated because it was feared that eddy-shedding off the step might result in satisfying the Rayleigh criterion, which, in turn, could set up resonance in the combustor and fuel supply tube. Appendix C describes our results.

(a) Acoustic Characteristics. Inlet conditions, combustor geometry and size, and outlet blockage were found to affect the acoustic characteristics. An acoustic isolator in the fuel tube and a step design that eliminated vortex generation at the inlet significantly decreased acoustic coupling. For a long combustor (L/D = 7.3), loud acoustic resonances resembling classic "rumble" were produced. In this combustor, dominant frequencies around 55 Hz and 170 Hz were observed corresponding to eddy-shedding from the step and the quarter-wave longitudinal mode, respectively. The short combustor (L/D =3) simply did not exert enough back pressure to confine a steady burning flame. In general, top-hat outlet restrictors produced noisier combustion than orifice plates. Finally, a research step combustor with a 4.9 L/D and fitted with an orifice plate with a 0.45 blockage ratio provided the best combination of LBO and freedom from acoustic coupling. This combustor operated in a stable and predicted manner under all the conditions of interest; therefore, its LBO performance was studied.

We documented the sequence of events leading to LBO. As the overall equivalence ratio was reduced below unity, the shear-layer *attached* flame moved further downstream into the combustor in a characteristic *lifted flame* position and form. Continuing reduction in the equivalence ratio produces an onset of flow instability in the lifted flame, increase in the amplitude of the instability, onset of intermittency, severe intermittency, and, finally, onset of strong axial flame instability. This sequence clearly highlights the complexity of the LBO mechanism in a modern annular gas turbine combustor.

(b) Isothermal Flow Field. To understand the effects of jet flow and step-on combustor flow-field development, measurements of velocity fields were performed using LDA in an isothermal constant density flow field. The fuel jet Reynolds numbers were in the 1,730-to-17,300 range and the air jet Reynolds numbers spanned the 7,200-to-72,000 range. These results are discussed in detail by Sturgess et al. [10].

The isothermal flow-field development in the combustor is shown in Figures 12 and 13 of Sturgess et al. [10]. It revealed the existence of three regions: near field, far-field, and step-recirculation regions. In the near-field region, the distinct high velocity coannular air jet and the low velocity central fuel jet quickly merge. However, the initial momentum difference between the jets is so large that entrainment of the central jet by the annular jet produces a central recirculation bubble. In the far-field region, the individual jets lose their identity and exhibit self-similarity. Finally, the step-recirculation region bounds the near-field and, partly, the far-field regions. The initial turbulence generation in the jet shear layers is in accordance with Prandtl

mixing length theory; however, downstream, the flow history effects start to dominate and turbulence profiles are totally unassociated with the local velocity profiles.

(c) Lean Blowout. Figure 3 shows the LBO performance of our research combustor. The trend of LBO vs. air loading for our research combustor appears to be similar to that for PSR; the latter approaches the characteristics of the future high-performance annular combustors. Thus, our research combustor correctly reproduced the LBO processes of a real gas turbine combustor. However, to obtain a complete lean stability map, the operation of the step combustor was necessary at subatmospheric pressure (to simulate high altitude) and with finite back pressure (to simulate the presence of dilution air jets). To study subatmospheric pressure effects, we developed a novel nitrogen dilution technique (Appendix D) that lowers reactant concentration and temperature by virtue of its heat capacity. It was found that: (1) the nitrogen dilution simulated the effects on chemical reaction rates of low pressures down to 0.1 atm, (2) the LBO was correlated by an air-loading parameter when the effective pressure was used for the actual pressure and the reaction order was made a function of excess nitrogen flow rate, (3) the range of ϕ covered by the variation in loading parameter in Figure 3 was from near-flammability limit (ϕ = 0.5) to near-maximum heat release rate (ϕ = 0.9), (4) nitrogen dilution enabled the air-loading parameter to be extended over 3 orders of magnitude, and (5) at LBO, the step combustor behaved like a PSR.

The effects of back pressure on the LBO were investigated; these results are presented in Appendix E. As shown in Figure 4, LBO was improved by an increase in the exit blockage. For lightly loaded combustor, an exit blockage of 45 percent provides the best combustion stability and optimal configuration. Further, we discovered that exit blockage exerts its influence through its effect on the jet and the recirculation zone shear layers. Other important conclusions that emerged are as follows.

(a) The back pressure (or exit blockage) did not directly affect the step recirculation zone; rather the fuel and air jet shear layers were affected. These shear layers influence both the central recirculation bubble and the step recirculation zone.

(b) The research combustor exhibited consistent and well-characterized flame behavior that depends on the equivalence ratio and exit blockage. The ability to reproduce this behavior will provide a stringent test of the realism of any numerical modeling of this combustor.

3.1.5 Analysis. We participated with Pratt and Whitney (East Hartford CT) in developing and evaluating various theories for the analysis and modeling of LBO. Details of this investigation are summarized in our joint paper attached as Appendix F. Principally, we evaluated the following analytical approaches.

(a) PSR Approach. In this approach, we successfully correlated LBO against the loading parameter (LP) derived from the chemical reaction rate theory (see Figure 3) but modified to include the effects of inert excess oxygen:

$$LP = m_{tot}/(VP^n), \tag{1}$$

$$m_{tot} = m_f + m_a + m_{nit}, \text{ and} \tag{2}$$

$$n = 2\,\phi_{LBO}/(1 + m_{nit}/m_a), \tag{3}$$

where V is the combustor volume, P is the operating pressure, n is the apparent global reaction order, and m denotes mass flow. Although the LP adequately handles the range of inlet variables covered in the experiment, it cannot be general. Indeed, Figure 10 of Appendix F clearly shows that this type of correlation does not have general validity even for a family of combustors with similar flow patterns but different scale and flow parameters.

(b) Characteristic Time Approach. This approach is based on the reaction-quench model which has a premise that at LBO, flame propagation will seize when the rate of mixing between small turbulent eddies of cold reactants and hot products is greater than the local chemical reaction rate. This quenching criterion gives:

$$(D + C_\mu K^2/\sigma_t \varepsilon) > \nu\,(1 + S_L/(\varepsilon \nu)^{0.25}), \tag{4}$$

where D is the laminar diffusion coefficient, K is the kinetic energy of turbulence, ε is the dissipation rate, C_μ is constant, σ_t is the turbulent Schmidt number, and S_L is the laminar flame speed.

Since the quenching criterion requires turbulence parameters for evaluation, isothermal flow CFD calculations were performed to provide this information at each grid node and quenching was examined on a point-by-point basis. Equation (4) did show limited promise in the step combustor in delineating between operating conditions where combustion was possible and where it was not.

(c) Local Stirred Reactor Modeling. In this approach, combustor volume is represented by an equivalent global stirred reactor network. This enables the calculation of stability from thermochemistry considerations. We applied Swithenbank's [11] dissipation gradient approach for defining PSR regions in the combustor. The resulting reactor was 44 percent of the combustor volume and corresponded reasonably well to the lifted flame observed in the real combustor. As shown in Figure 3, good agreement was found between predictions and experiments.

The eddy dissipation concept (EDC) of Magnessen and Byggstoyl [12] was used to construct a subgrid scale reactor model. In contrast to the characteristic time analysis and local stirred reactor modeling, this approach tests the individual reactor stability with the CFD calculations, and not after it. However, a characteristic time approach to LBO within the EDC model was implemented with fast chemistry for propane-air combustion and tested for an attached flame condition at rich condition. It was found that this model calculated the lifted flame condition but was unsuccessful in predicting the all-important attached flame-condition.

3.1.6 Highlights and Conclusions. We completed a systematic investigation of LBO and achieved the following results.

(a) A research step combustor was successfully developed and produced three important features of the flow field that affect LBO in a practical combustor: (1) a reactive shear layer at the exit to the fuel nozzle, (2) inside-out recirculation zones, and (3) back pressure provided by dilution air jets.

(b) The step combustor acoustic characteristics were optimized; this permitted its operation in a stable and predictable manner. A detailed sequence of events leading to LBO and comprising the attached-flame region, lifted shear flame, intermittent shear flame, and the large-scale instability of the flame front was observed.

(c) The combustor flow-field measurements revealed three regions: near-field, step-recirculation, and far-field regions. In these regions, the turbulent fuel-air mixing and entrainment were governed by a potential core, a central recirculation bubble, and a self-similar jet development, respectively.

(d) The LBO process (ϕ = 0.4 to 1.2) in the step combustor behaved like a PSR for LP values in the range 0.1 to 100 lb/s-ft^3-atm^2. Also, the LBO was successfully correlated with a standard LP derived from the PSR theory and using Swithenbank's [11] dissipation gradient approach.

3.2 Bluff Body Combustor Task

3.2.1 Objective. Bluff-body flameholders are widely used in ramjet engines, afterburners, and many other combustion systems to maintain a steady flame in a high-speed, turbulent, combustible mixture. Therefore, the main objective of this task was to investigate the effects of hardware geometry (BR and θ), approaching turbulence level (U and I), and chemistry (ϕ) on the stabilization of flame in a bluff-body combustor.

3.2.2 Bluff-Body Combustor. Figure 5 shows the test rig employed for these experiments. Several stainless-steel conical flame stabilizers were manufactured including two base diameters, measuring 4.44 cm and 3.18 cm and corresponding to 25 and 13 percent blockage

ratios, respectively; and four apex angles, θ = 30, 45, 60, and 90 degrees. Each stabilizer was mounted coaxially inside a 8-cm-x-8-cm-x-28.4-cm test section with rounded corners and four 5.64-cm-x-25.4-cm cut-outs for quartz windows. This test section was mounted on a vertical combustion tunnel. Different turbulence grids could be inserted 5.8 cm upstream of the base of the conical bluff body. Measurements of turbulence quantities, temperature, and mean wall-static pressure were performed downstream of the confined conical flame stabilizer, using a two-component LDA, CARS system, and precision micromanometer, respectively.

3.2.3 Test Conditions. Premixed methane-air flames were studied in our experiments. The mean annular velocities were 10, 15, and 20 m/s which covered a range of Reynolds number from $Re_d = 3x10^4$ to $6x10^4$. Zukoski and Marble [13] have pointed out that the bluff-body wake region becomes fully turbulent when $Re_d = U_a d/v \geq 10^4$. Four different equivalence ratios, 0.56, 0.65, 0.8, 0.9, were tested, corresponding to adiabatic flame temperatures of 1590 K, 1755 K, 1990 K, and 2130 K, respectively. The inlet turbulence intensity level was varied from 2 percent to 22 percent by using different grids.

3.2.4 Result. We investigated the turbulence and scalar fluctuation properties of confined turbulent recirculatory flame for different hardware geometries. These data were then interpreted to elucidate the recirculation zone structure, effects of flow confinement, the role of combustion-generated turbulence, and turbulence-kinetics interaction.

(a) Confined Recirculation Zone Structure. Appendix G describes the results of our investigations of the turbulent combustion properties and the structure of recirculation zone in a confined bluff-body combustor. The size, shape, and mean flow structure of the recirculation zone were determined by calculating the spatial distribution of the mean stream function ψ from the equation:

$$\psi = \int_0^r \rho U r \, dr. \qquad (5)$$

Also, knowing the value of $C_{p,min}$, we derived the maximum width W of the recirculation zone as:

$$W = R\,[1-\{(1-BR)/(1-C_{p,min})^{1/2}\}]^{1/2}. \qquad (6)$$

From Equation (1), the ratio of reverse to total mass flow rate m_r/m_t was calculated. This ratio represents the recirculation strength. Figure 6 shows a sketch of the confined recirculation zone and Table 1 lists the various recirculation zone parameters for confined cold flow, confined flame, and open flame, respectively. As seen in Table 1, the combustor wall confinement elongates the recirculation zone by 13 percent over cold flow and narrows it by 12 percent over an open flame. Also, mean reverse flow velocity and, hence, the recirculated mass flow, increase by 30 percent over their corresponding values in open flame. Finally, in Appendix G, we note

that the flow enveloping the recirculation zone resembles a normal mixing layer (i. e., a = +0.3 to -0.3).

(b) Influence of Geometry and Flow Parameters. In a paper attached as Appendix H, we describe the effects on recirculation zone structure and properties of blockage ratios (13 percent and 25 percent), cone angles (30, 45, 60, and 90 degrees), equivalence ratios (0.56, 0.65, 0.8, and 0.9), mean annular velocities (10, 15, and 20 m/s), and approach turbulence levels (2 percent, 17 percent, and 22 percent). Increasing the blockage ratio or the cone angle only slightly changed the recirculation zone length and volume. However, increasing the equivalence ratio from its lean extinction limit to near-stoichiometry decreased the recirculation zone length to half its original value and very close to its value in the cold flow. Also, the turbulent kinetic energy (TKE) drastically decreased, presumably due to suppression of turbulence by dilatation. Similarly, increasing the approach turbulence intensity drastically shortens the recirculation zone length close to its value in the cold flow.

(c) Scalar Fluctuations in Bluff-Body Stabilized Flames. We employed the CARS system to perform measurements of mean and rms temperature fluctuations in confined turbulent premixed methane-air flames stabilized on a conical flameholder. These results, which are given in Appendix I, revealed that the recirculation zone loses about 5 percent heat to outside and about 5 to 8 percent heat to the flameholder base. Also, low rms temperatures (~ 5 percent) suggest that a perfectly well-stirred reactor description of the recirculation zone is very close to valid. Blockage ratio, equivalence ratio or approach turbulence intensity did not alter the scalar field in any dramatic way. Finally, near the flameholder base, temperature pdfs reveal an extremely thin flame front. Downstream of this, temperature pdf is bimodal and suggests the presence of large-scale coherent structures within the reacting shear layer. Further downstream, a thick flame consisting of partially burned-unburned gas states develops.

(d) Chemistry and Turbulence Effects. We studied the effects of chemistry and approach turbulence intensity for confined, turbulent, and premixed bluff-body stabilized methane-air flames. These results are documented in Appendix J.

In this paper it is demonstrated that an increase in ϕ from 0.56 to 0.90 decreases the recirculation zone length dramatically from x/d = 2.35 to 1.32 (i.e., slightly shorter than that found in the cold flow (x/d = 1.52)). It also accelerated axial mean velocities downstream of the rear stagnation point. Both these effects are a result of increasing heat release rates and fast chemistry brought about by increasing the equivalence ratio towards stoichiometry. Also, as the approach turbulence intensity increases from 2 percent to 22 percent the recirculation zone length decreases rapidly from x/d = 2 to x/d = 1.2. Also, the location of maximum recirculation width shifts upstream from x/d ≈ 0.8 to 0.4.

3.2.5 Analysis. We analyzed the effects of wall confinement and combustion-generated turbulence on the bluff-body stabilized combustion.

(a) Influence of Wall Confinement. A bluff body confined in a pipe produces an aerodynamic blockage corresponding to the deflection of the mean separation streamline from its trailing edge. Wall confinement prevents any significant deflection of mean flow streamlines and also produces flow acceleration to elongate the recirculation zone as seen in Table 1. Consequently, in confined flames, TKE is produced by the interaction of Reynolds stress and shear strain (i.e., via the term uv $\partial U/\partial r$) and, therefore, restricted to the shear layer surrounding the maximum width of the recirculation zone. If the wall confinement is removed, as is the case in open flames, large mean streamline curvature and turbulent dilatation would combine to produce the widest recirculation zone, and generate larger axial and radial turbulence intensities and turbulent kinetic energy as compared to their values in a confined flow.

(b) Combustion-Generated Turbulence. Combustion affects the confined turbulent flow field in a variety of ways. Ballal [14] found that turbulent dilatation and viscous dissipation processes suppress flame turbulence, whereas turbulent advection and shear-generated turbulence augment flame turbulence. Depending on which processes dominate, combustion will either produce additional so-called combustion-generated turbulence or damp existing isothermal turbulence.

In our studies presented in Appendix G, radial variation of ratio (q_c/q) at two different axial locations clearly showed that the TKE is lower by as much as 70 percent in the combusting flow than in the cold flow. This result suggests that a minimum shear-generated turbulence is produced because wall confinement prevents deflection of mean flow streamlines and produces extremely low streamline curvature. In the absence of this strong turbulent production mechanism, the processes of turbulent dilatation and viscous dissipation take over to significantly damp cold flow turbulence. For the confined flame studied in Appendix G, we have calculated that at x/d = 0.8 and 2, the ratio of production/suppression of turbulence varies between 12 percent and 33 percent, respectively, in our fuel-lean (ϕ = 0.65), high-speed, confined flame.

(c) Recirculation Zone Structure. In these experiments, we observed that increasing the blockage ratio or approach flow turbulence, and in the limit of fast chemistry, the recirculation zone size decreases to its value for fully developed, cold turbulent flow wake. Thus, in the limit of a high Reynolds number, *mixing-controlled* combustion, the recirculation zone size can be predicted from the nonreactive turbulence modeling codes. In contrast, for *reaction-controlled* combustion, the recirculation zone is highly elongated. Intermediate between these two extremes, recirculation zone size and shape may vary with geometric (BR, θ), chemical (ϕ), and flow (U_a, I) parameters.

(d) Turbulent Flame Structure. From the experimental measurements of scalar fluctuations, we developed a model of the turbulent flame structure enveloping the recirculation zone. This model is sketched in Figure 7 and described below.

Turbulent combustion in the reacting shear layer is a *three-stage* preheat-ignition-propagation process. Near the base of the bluff body and along its edge, the flowing reactants are preheated and ignited by the heat flux transported radially outward from the recirculation zone. Within the region $x/L_r = 0\text{-}0.12$, ignition of the incoming reactants takes place and a thin flame that conforms to the "fast-chemistry" assumptions sits slightly oblique to the oncoming reactants. This type of flame can be successfully modeled by the Bray-Moss-Libby theory [15].

Downstream of this ignition-thin flame region ($x/L_r > 0.12$), the temperature remains either fairly constant or decreases slightly (i.e., $\partial C/\partial r \leq 0$). This suggests that no radial heat flux is transported and only entrainment of reactants and products is occurring downstream. In this region, large-scale coherent structures begin to grow within the reacting shear layer. These structures form as folds around the flame edge, then grow in size downstream to produce a convoluted reaction zone with many isolated pockets of hot-product and cold-reactant gas. These coherent bodies of gas are squeezed and stretched during their travel through the flame and the entrainment process causes their growth downstream, thereby thickening the flame.

Further downstream and in the vicinity of the rear stagnation point, the flame front is thick ($\approx$ 4.5 mm) and mass entrainment of fresh reactants is the dominant mechanism at work. In this region, large temperature fluctuations ($C_t \approx$ 25 percent-35 percent) are measured. Such fluctuations may acoustically couple with a sufficiently long duct and produce combustion instability or *rumble* in practical combustors. Clearly, the relatively simple statistical description of the wrinkled thin flame front is inadequate here. Rather, the "eddy-entrainment, combustion-in-depth" process of Ballal and Lefebvre [16] is at work. Thus, the instantaneous region of combustion is distributed throughout the time average of the combustion zone rather than being confined to a thin wrinkled laminar flame.

Scalar measurements of Shephard et al. [17] in confined premixed flames and the analysis of Libby and Bray [18] have found counter-gradient diffusion effects in these type of flames. However, they used thermocouples with relatively large wire sizes and it is possible that their flame temperature measurements could have suffered from relatively large experimental uncertainties or errors discussed earlier. On the other hand, direct, laser-diagnostics-based, nonintrusive measurements of axial and radial turbulent heat fluxes are required in the future to examine, in an unambiguous manner, if counter-gradient diffusion exists within these type of flows.

(e) Turbulence-Chemistry Interaction. From our observations on the chemistry and turbulence effects, we constructed, in Figure 8, a sequence of events leading to LBO (a consequence of

finite chemistry). Excess entrainment of cold reactants in the thick- flame region causes flamelet extinction; this increases the magnitude of the adverse pressure gradient downstream of the rear stagnation point. This, in turn, increases the entrainment of the cold reactant mixture, reduces the recirculation zone size towards the cold-flow value, and quenches the flame in the preheat-ignition region.

3.2.6 Highlights and Conclusions. Bluff-body flameholders are widely used in ramjet engines, afterburners, and many other combustion systems to maintain a steady flame in a high-speed, turbulent, combustible mixture. We performed a study of the structure of the recirculation zone and the turbulent flame surrounding it and found the following.

(a) Wall confinement elongates the recirculation zone by accelerating the flow and narrows it by preventing mean streamline curvature. For confined flames, turbulence production is mainly due to a shear-stress/mean-strain interaction. In the region of maximum recirculation zone width and around the stagnation point, the outer stretched flame resembles a normal mixing layer.

(b) In a confined flame, turbulent dilatation and viscous dissipation processes suppress flame turbulence, whereas turbulent advection and shear-generated turbulence augment flame turbulence. In our experiments, we found that because of the suppression of mean streamline curvature by confinement, the production of turbulence was only up to 33 percent of its damping due to dilatation and dissipation.

(c) The turbulent flame structure enveloping the recirculation zone comprises: (1) an ignition thin-flame region in the vicinity of the flameholder base, (2) a reacting shear-layer region of large-scale coherent structures, and (3) a thick-flame region in which entrainment is the dominant mechanism.

(d) LBO of the bluff-body, stabilized, turbulent flame occurs because excess entrainment of cold reactants in the thick-flame region causes flamelet extinction and increases the adverse pressure gradient. This, in turn, increases the entrainment of the cold reactant mixture and quenches the flame in the preheat-ignition region.

3.3 Perfectly Stirred Reactor Task

3.3.1 Objective. The function of an advanced combustor system in tomorrow's engine is to provide maximum heat release, high combustion efficiency, wide stability limits, minimum pressure loss, and multifuel capability. A PSR represents a laboratory simulation of the primary zone of an advanced combustor. Therefore, the objectives of this task were: (1) to design and fabricate a PSR, and (2) to perform preliminary experiments to investigate the limits of *kinetically controlled* combustion.

3.3.2 PSR Test Facility. We performed a literature review of previous PSR designs and overcame most of their deficiencies in our new design.

Figure 9 shows a schematic diagram of our PSR design. Essentially, it is a slightly modified version of the original toroidal design of Nenninger et al. [19]. We cast the two halves of the toroid in high-temperature alumina. The PSR specifications were: toroid volume = 250 ml, estimated mixture residence time = 1 to 6 ms, estimated mixing time = 50 to 150 μsec, feed pressure = 20 to 60 psig, feed temperature = up to 500 K, feed rate = 5 to 20 gms/s, Reynolds number for the circulating flow = 10^5, and reactor temperature = 1500 to 1950 K. This PSR receives a fuel/air mixture from a total of 33, 1.04-mm i.d. jets located on the outside circumference.

In our PSR design, intense mixing within the reactor volume, caused by multiple jet injection, ensures kinetically controlled combustion even at relatively high temperatures (1700 K). Also, residence time and reactor temperature are very representative of the operating conditions in the gas turbine primary zone. Finally, large reactor volume and relatively short residence times (below 10 ms) eliminate any possibilities of surface reactions. We completed the fabrication and installation of the test facility in Building 490, Room 151, W-PAFB. Figure 10 is a schematic diagram of the PSR test facility. The main components of the test facility are: (1) a toroidal WSR cast in alumina, (2) a stainless steel fuel jet ring, (3) alumina sleeves, (4) an exhaust section, and (5) a fuel and air flow system.

As seen in Figure 10, fuel and air are fed to the reactor through a complex network of check valves, solenoids, mass flow controllers, and pressure regulators. The Sierra mass flow controller ranges are: (1) main air, 0 to 500 SLPM; (2) fuel, 0 to 70 SLPM; and (3) exhaust air, 0 to 100 SLPM. Fuel and air are premixed and heated to different inlet temperatures a short distance upstream of the fuel jet ring. This premixed fuel-air mixture is injected into the PSR and ignited using a torch igniter. Check valves are placed in the fuel, air, and nitrogen lines to prevent flame flashback. The nitrogen line dilutes and lowers the reactor temperature in the vicinity of the stoichiometric operation, and also floods the reactor in case of a fuel-rich blowout. Finally, the products of combustion are exhausted through the PFR.

3.3.3 Tests Planned and Results Obtained. The PSR tests are designed to measure the global reaction rate, n, and the reaction order, k ($m = n/k$), for different JP fuels (i.e., changing activation energy), at LBO and rich blowout (RBO) conditions, and for a variety of inlet temperature conditions. Preliminary PSR tests (Figure 11) show LBO results for methane-air mixtures and a comparison between experiments and CHEMKIN [20] calculations. In addition, we have outlined below four experiments that should be performed in the future.

(a) Combustion Performance. Measurements of combustion efficiency and stability (LBO and RBO) should be performed for current military fuels such as Jet A, JP-8, JP-8+100, model compounds comprising JP-900 and endothermics, JP-900, and endothermic fuels. These experiments will cover values of LP ranging between ground and subatmospheric pressures, and inlet temperatures sufficiently high to prevaporize endothermic liquid fuels.

(b) Ignition/Stability. A nitrogen-dilution technique developed by Sturgess et al. (see Appendix D) should be used to simulate high altitude and measure ignition/stability loops.

(c) NO_x and Other Emissions. Advanced combustor designs of the future will produce a large quantity of thermal NO_x. The PSR apparatus offers a unique opportunity to investigate NO_x emissions.

(d) Soot and Radiation. Soot produces an infrared/visible target signature from aircraft and enhances radiative heat transfer to the combustor wall; this reduces combustor durability. We propose that the PSR be used to determine the critical equivalence ratio at sooting (see Takahashi and Glassman [21]) for various hydrocarbon fuels and mixtures including advanced jet fuels, and to measure the soot yield and exhaust radiation intensity as a function of the equivalence ratio and residence time.

3.3.4 Analysis. PSR theory is used to relate the LP to combustion efficiency, flame temperature, blowout limits, and pollutant emissions. The rate of reaction between fuel and air may be expressed by the material balance equation:

$$\eta_c \phi m_a = A V T^{0.5} \exp(-E/RT) \rho^n C_f^m C_o^{n-m}, \qquad (7)$$

where m_a is the air mass flow rate, A is the molecular collision factor, V is the combustion-zone volume, T is the reaction-zone temperature, E is the activation energy, R is the gas constant, C_f and C_o are fuel and oxygen concentrations, respectively, m is the exponent of fuel concentration, n is the reaction order, ρ is the density, ϕ is the equivalence ratio, and η_c is the combustion efficiency.

For JP fuels and weak mixtures, Lefebvre [22] has shown that:

$$(m_a/VP^2) \propto (1/(T^{1.5}\exp(E/RT))(1-\eta_c)(1-\eta_c\phi)/\eta_c \quad . \qquad (8)$$

Past experimental work of Longwell and Weiss [23] revealed that m = 0.75 and the reaction order, n, is 1.75 for fuel lean mixtures. Later work of Ballal and Lefebvre [24] showed that near the lean extinction limit and for gaseous fuels, m = 0.625 and n = 1.25.

For JP fuels and rich mixtures, n = 1.75, m = 0.75, and Equation (7) becomes:

$$(m_a/VP^{1.75}) \propto (\phi^{0.75}/(T^{1.25}\exp(E/RT))(1-\eta_c)^{1.75}/\eta_c \, . \qquad (9)$$

In Equations (7) through (9), it is evident that the combustor LP = (m_a/VP^n) is related to global reaction rate n, combustion efficiency η_c, fuel activation energy E, and flame temperature T. Also, we can analyze soot emissions from the PSR by writing the species conservation equation for soot:

$$m_a/\rho V (C_s - C_{so}) = R_f - A_t R_{ox}, \qquad (10)$$

where C_s and C_{so} are inlet and outlet soot concentrations, respectively, and R_f and R_{ox} are reaction rates for soot formation and oxidation steps, respectively. The reaction rate R_f will be determined by measuring the concentration of unburnt hydrocarbon and oxygen, while oxidation rate R_{ox} will be obtained from the model of Nagle and Strickland-Constable [25].

3.3.5 Highlights and Conclusions. A PSR is a laboratory combustor whose design simulates combustion processes in the primary zone of an advanced gas turbine combustor.

(a) We designed a toroidal PSR and cast its two halves in high-temperature alumina. This design eliminates most of the deficiencies and limitations of previous PSRs. Also, we designed and made operational a PSR test facility.

(b) Preliminary PSR tests yielded LBO equivalence ratios (ϕ = 0.42 to 0.50) versus the air loading (200 to 450 slpm) results for methane-air mixtures and a comparison between experiments and CHEMKIN [20] calculations over the reactor temperature of 1500K to 1800K.

(c) We have developed a PSR theory that relates the LP to combustion efficiency, flame temperature, blowout limits, and pollutant emissions. This analysis serves to illustrate how the global chemistry parameters for computer modeling can be derived from PSR experiments.

3.4 Swirl Combustor Task

3.4.1 Objective. Swirl is commonly used in gas turbine combustors to enhance fuel-air mixing, combustion intensity, and flame stabilization. Therefore, the objectives of this task were: (1) to study the stability of jet diffusion flames with and without swirl, and (2) to provide benchmark quality experimental data for the evaluation and development of PDF methods [26,27] of turbulent combustion modeling.

3.4.2 Swirl Combustor. Figure 12 shows the schematic of a swirl combustor. This combustor uses an arrangement of coannular swirling air and central fuel jets confined by a coflowing, nonswirling airflow with a uniform velocity distribution. In this combustor, a turbulent swirling jet diffusion flame is stabilized at the mouth of the central fuel tube. The central fuel tube (9.45-mm i.d., 0.2 mm lip thickness, and 806-mm length) is made of stainless steel. It is placed concentrically at the center of the outer annular air tube (26.92-mm i.d., 769-mm length). Three fuel tubes with lip thicknesses of 0.2, 1.2, and 2.4 mm were used. Both the tubes

are centered inside a vertical combustion chimney (150 mm × 150 mm × 483 mm) with 85-mm-radius rounded corners. The chimney has quartz windows (76 × 457 mm) on all sides to permit visual observation and laser diagnostics. A helical swirler unit is placed in the annular air tube, 96 mm upstream of the tube exit to ensure that disturbances caused by its vanes vanish. Four swirlers (26.9 mm long) with various vane helix angles (15, 30, 45, and 60 degrees) and one straight vane section with a zero helix angle were designed.

3.4.3 Test Conditions. All tests were performed at room temperature and atmospheric pressure. The fuel jet, air jet, and the external coflowing stream velocities were up to 30 m/s, 10 m/s, and 0.5 m/s, respectively. The flame stability limits were measured as follows. For a fixed annular- and coflowing-air flow rates, the fuel flow rate was increased gradually until the flame *attached* to the burner-rim *lifted* above the burner or simply extinguished (*blowoff*). Now, at the *lift* condition, fuel flow was: (1) decreased until the flame re-attached to the burner-rim (*dropback*), or (2) increased until the lifted flame extinguished (*blowout*).

A three-component LDA, CARS, and Mie scattering systems were used for a variety of conditioned and unconditioned measurements of mean and turbulent quantities. For a set of values of jet, annulus, and external velocity, measurements extending up to 34 jet diameters were made at a large number of radial locations up to ± 3.2 jet diameters.

3.4.4 Results. The flame stability limits essentially define the operational boundaries of a combustor. Here, we present results on three aspects of flame stability: flame lift, flame stability limits, and local extinction of flame due to large-scale vortex structure.

(a) Flame Lift. Figure 13a shows the stability limits of nonswirling methane jet diffusion flames for various fuel-tube lip thicknesses: sharp-edged (0.2 mm), medium thickness (1.2 mm), and flat-ended (2.4 mm). Appendix K provides detailed results on the lifting criteria.

The critical mean jet velocity at lifting (U_{jc}) for zero annular air flow was 21~22 m/s for sharp-edged and 19~20 m/s for medium-thickness and flat-ended fuel tubes. For a 2.4-mm tube, U_{jc} was least sensitive to an increase in annular mean air velocity and the attached flame region expanded significantly. Further, the results of Figure 13a demonstrate that the stability limits for 0.2- and 1.2-mm tubes are controlled by the flame-base mechanism proposed by Takahashi et al. [28], whereas for the 2.4- mm tube, the recirculation zone produced in the wake of the thick lip leads to flame stabilization.

(b) Flame Stability Limits. Figure 13b shows the effects of swirl on the stability limits for various fuel-tube lip thicknesses. These measurements were for swirl angles ranging from 15 to 60 degrees. Appendix L provides the detailed results. These results illustrate that the effect of swirl was insignificant for annular air velocity below 0.5 m/s, but swirl enhances flame stability in a striking manner above this value, particularly for the 60-degree vane swirler. As a result of

the strong swirl, the jet spread angle increases, entrainment goes up, and, in turn, flame stability is enhanced. Finally, for 1.2- and 2.4-mm fuel tubes, the impact of swirl on stability was relatively weak because recirculation in the wake of the fuel tube and local extinction were predominant in determining flame stability.

*(c) **Local Flame Extinction.*** To ascertain the effects of large-scale vortex structure on local flame extinction, we measured the velocity, crossing frequency, and size of these vortices. These data, presented in Table 2, were derived by relating the instantaneous Mie scattering images to jet intermittency having a value I (z,r,t) = 1 in jet fluid and I (z,r,t) = 0 in external fluid. The intermittency is the fraction of time the jet fluid is present at a particular location and the crossing frequency f_c represents the number of crossings from the jet to external fluid per unit time. Appendix M contains the Mie scattering flow visualization photographs and detailed results on local flame extinction.

In Appendix M are presented the results of LDA measurements of radial profiles of conditioned mean and rms values of axial and radial velocity. In the mixing layer, the jet fluid parcels had a higher mean axial velocity of outward movement than the external fluid parcels. These results demonstrate the intermittent mixing process due to large-scale vortices, the occasional radial jet fluid ejection, and the engulfment of the external fluid into the large-scale structure.

Further, we found that the radial velocity gradient of the mean radial velocity of the approach flow into the flame zone reaches approximately 500 s^{-1}; the critical strain rate beyond which a methane flame cannot be stabilized. This high velocity gradient suggests that conditions exist conducive to the local flame extinction due to the radial ejection of large-scale vortex (i.e., a thin diffusion layer, low Damkohler number, and highly strained flame zone).

3.4.5 Analysis. Our observations have led us to identify flame- lifting criteria, swirl effects on flame stability, and a mechanism of local flame extinction.

*(a) **Flame-Lifting Criteria.*** We have observed four major jet diffusion flame-lifting criteria and several subcategories, depending on the burner port geometry, flow conditions, and fuel types. The physical mechanisms responsible for these lifting phenomena are: Type I--(a) imbalance between the entrained stream velocity at the flame base and the local maximum burning velocity, (b) flow field disturbance around the flame base caused by pipe-flow turbulence; Type II--(a) local flame extinction at the breakpoint due to stretch generated by the large-scale, fuel jet vortices, (b) local extinction of the rim flame followed by blowout, and (c) local extinction of the lifted part of the flame followed by blowoff; Type III--extinction of combustion reactions in the immediate wake of a thick-lip fuel tube due to the lean flammability limit; and Type IV--extinction of the aerated wake flame due to the penetration of the fuel jet.

To elucidate the critical conditions at the stability limits, particularly Types II(a) and III described above, LDA measurements were made using a thick fuel tube (9.45-mm i.d. and 2.4-mm lip thickness) under near-limit conditions along the upper branch Type (II[a]) and the lower branch (Type III) of the stability limit curve. These measurements show that when the large-scale vortex of the jet fluid is ejected radially, the flame zone is quenched locally due to the outward shift of the high fuel concentration and engulfment motion of the vortices. Thus, the Type IIa stability is observed if the flame-base stability is secured at either very low coflowing air velocities (<0.17 m/s) for the sharp-edge nozzles or high velocities (<1.9 m/s) for thick-lipped nozzles. The lean-limit extinction lifting (Type III) occurs for thick-walled tubes for both methane and hydrogen.

(c) Flame Stability and Extinction. Our analysis of the experimental data has shown that for lip thicknesses less than the minimum quenching distance of the methane-air mixture (0.2 mm), an increase in the annular air velocity markedly decrease the critical mean jet velocity at lifting. However, strong swirl enhances the flame stability significantly by creating a toroidal recirculation zone. For larger lip thicknesses, the effect of swirl on the stability limit was weak because the recirculation zone in the wake of the fuel-tube lip and local flame extinction were predominant in determining flame stability. Specifically, LDA measurements in the breakpoint region of a near-limit swirling flame revealed the turbulence-flame interaction which leads to local extinction followed by lifting.

3.4.6 Highlights and Conclusions. Swirl is commonly employed in modern combustors to enhance fuel-air mixing, combustion intensity, and flame stabilization. Therefore, we completed a fundamental investigation of the effects of swirl on flame stability and found the following.

(a) We discovered four major flame lifting criteria: Type I--imbalance between entrained stream velocity and burning velocity; Type II--disturbance caused by pipe-flow turbulence vortices; Type III--LBO in the vicinity of flame base; and Type IV--extinction of flame due to fuel jet penetration.

(b) Swirl improved flame stability by a factor of 2 (jet velocity doubled from 4 m/s to 8 m/s for the attached flame) by creating a toroidal recirculation zone. However, for a fuel tube with 2.4 mm lip thickness, swirl did not noticeably influence the stability.

(c) In a jet diffusion flame, intermittent mixing and radial jet fluid ejection produced by large-scale vortices cause local flame-quenching or extinction of a thin, highly stretched diffusion flame interface.

3.5 Heat Transfer Task

3.5.1 Objective. The freestream turbulence level experienced by a turbine blade downstream of the combustor approaches 20 percent. Until very recently, heat-transfer and film-cooling data for turbine blade design were obtained for very low values of freestream turbulence. This led to an underestimation of the turbine blade surface temperatures which, in practice, can significantly reduce its lifetime. Therefore, the objective of this task was to study the effects of freestream turbulence on flat plate heat transfer and provide a data base for realistic predictions of turbine blade heat transfer using computer codes.

3.5.2 Heat Transfer Rig. Essentially, the heat transfer facility described in Section 2.2 employs either the 20.3-cm-dia ASME or a 6.67-x-49.53 cm ASME planar free-jet nozzle (lip thickness = 0.64 cm). The 3.05-m-long and 0.61-m-wide flat test plate was located many diameters downstream of the free-jet nozzle. The flat plate, which is embedded with hot film and 42 fine thermocouple probes for measuring surface temperature was electrically heated. The back face of the plate was insulated to minimize heat loss.

3.5.3 Test Conditions. In our tests, the mean velocities ranged between 7 and 40 m/s and the rms values were between 1 and 6 m/s. The turbulence scales, which ranged from $L/y_{max} = 0.5$ to 5, were measured using a hot wire coupled with an HP 3562 dynamic signal analyzer. The signal analyzer provided a frequency spectrum and either this spectrum or its inverse, the autocorrelation coefficient, were used to calculate turbulence scales. A three-component LDA system, which produced a measurement ellipsoid of 25 μm × 3 mm, was used to obtain velocity and shear stress profiles. Finally, thermocouples provided the heat transfer coefficients at seven different locations covering z/d = 7 to 53.

3.5.4 Results. Appendix N gives the plots of wall-jet heat-transfer data obtained from our experiments and a variety of literature sources. These data cover Reynolds numbers from 10^5 to 10^7 and the corresponding Stanton numbers from 10^{-3} to 10^{-2}. It is clear that, in the presence of a free-stream turbulence level up to 20 percent, the resulting heat-transfer coefficients are 2 to 2.5 times higher than the turbulent flat plate heat transfer in the absence of free-stream turbulence. Also, as stated in Appendix N, our wall-jet data superimposed on the engine data indicated similar levels of heat transfer.

To gain insight into the effects of free-stream turbulence on heat transfer, measurements of turbulence velocities, Reynolds stresses, and scales were measured. These results revealed that the center-line velocity and velocity profiles were locally similar and the rms fluctuations are nearly constant across the wall layer. The normalized Reynolds stresses (such as u'v') are initially negative, then change sign at $y_{max} = 0.6$ and remain positive thereafter. This trend was similar to those observed in other planar wall-jet studies [29].

3.5.5 Analysis. Our experimental results on heat transfer and turbulence flow-field were analyzed to study the effects of free-stream turbulence on turbine blade heat transfer.

Our analysis of experimental results indicates a linear relationship between the heat transfer coefficient and the freestream turbulence intensity. However, additional parameters (such as the ratio (L/δ) and Re_θ) make for a complex functional relationship of the form proposed by Blair and Werle [30]:

$$St\text{-}St_0/St_0 = F(Tu, \alpha, \beta), \qquad (11)$$

where $\alpha = (L/\delta) + 2$ and $\beta = 3 \exp(-Re_\theta/400 + 1)$.

We also performed some development and evaluation of mathematical models for boundary layer heat transfer in the presence of high free-stream turbulence. A two-dimensional boundary layer code TEXSTAN was modified to solve the set of modeled equations and to compare their predictions with measurements of temperature fluctuations and fluctuation gradients. As shown in Figure 14, these predictions were compared to the Blair and Werle [30] data. The predicted heat transfer rates are higher than those estimated by the turbulent Prandtl number models. They also agree quite well with the experimental measurements at high levels of free-stream turbulence. However, for low values of free-stream turbulence, the model overpredicts both Stanton number and skin friction, $C_f/2$. Two possible reasons for this are (1) improper free-stream thermal boundary conditions or (2) improper choice of model constants.

3.5.6 Highlights and Conclusions. We performed an investigation of the effects of free-stream turbulence on flat plate heat transfer. This study yielded the following conclusions:

(a) Under high free-stream turbulence conditions, our data yielded values of heat-transfer coefficients ($St = 0.005$) similar to those obtained on a turbine blade in actual engine tests. Thus, free-stream turbulence augments heat transfer 2 to 2.5 times. This confirmed the validity and importance of these data sets to practical turbine blade cooling.

(b) Our analysis indicates a linear relationship between heat transfer and turbulence level. However, additional parameters (such as the ratio (L/δ) and Re_θ) make for a complex correlation.

(c) Predictions based on a modified two-dimensional TEXSTAN code show a good qualitative agreement but slightly higher than measured values of St and $C_f/2$. This provides confidence in the ability of modeling codes to predict the effects of high free-stream turbulence on heat transfer in practical systems.

4. HIGHLIGHTS AND CONCLUSIONS

In this section we analyze our entire effort from the viewpoint of program objectives; how we met those objectives; what new knowledge of interest to modelers and combustor designers emerged; how this knowledge can be used to evaluate, refine, and develop workable models based upon a sound fundamental understanding; and finally, what gaps, if any, were discovered that should form the basis of future research.

A logical starting point for our investigation was to examine the fundamental requirements of the combustor design and modeling needs of the reactive flow. Of all the combustor design requirements, combustion stability is the most important since it causes a loss in the engine operating envelope and impedes aircraft safety. Stability is also intimately tied to combustion efficiency, pollutant production, and combustion instability phenomenon such as rumble and screech. Therefore, we studied LBO in a research step combustor. This study produced results that had direct applicability to the Pratt and Whitney-type annular combustor design. The design and stability of flameholders in an engine reheat (afterburner) pipe have important implications to military engines. Our investigation of bluff-body stabilized flames produced a detailed knowledge of turbulent flame structure, propagation, and LBO of a flame held on a conical bluff body confined in a combustor. To minimize size and weight, in an ideal near-stoichiometric combustor of the future, chemical reaction and not turbulent mixing should be rate controlling. A PSR represents such a combustor and we conducted research to understand the performance of this type of combustor. Swirl is commonly used in practical combustors to enhance the combustion stability of a turbulent diffusion flame. Thus, we designed a swirl combustor and performed research on flame liftoff and blowout phenomenon in a turbulent swirling diffusion flame. Finally, our analysis and experiments on film-cooling provide the fundamental knowledge required to assess turbine blade-cooling effectiveness.

4.1 Highlights

4.1.1 Laboratory Combustor Development. We successfully designed and operated several laboratory combustors. Each combustor simulated some important features of a practical gas turbine combustor. For example, the step combustor produced the three important features of the practical combustor flow field; that is, the reactive shear layer, inside-out recirculation zones, and back pressure to confine the combustion process. Engine companies such as Pratt & Whitney employ these three features of the flow field to stabilize flames in modern annular combustors. Moreover, data obtained from these combustors closely represent features of the combustion processes in practical combustors.

4.1.2 CARS Measurements in Combustors. We recognized that in highly turbulent confined flames in practical combustors the CARS slit function would vary from shot to shot and depend on temperature, laser beam intensity, and turbulence. Therefore, we developed two novel methods of CARS temperature calculation. In the first method, we fitted the collected

CARS spectra using two parameters, slit width and temperature. This TPLS method increased precision and allowed the calculation of temperature without *a priori* knowledge of the slit function. In the second method, we used the principle of local thermodynamic equilibrium so that the actual mean temperature and slit width were calculated by finding the intersection of the two lines (T vs. slit width at constant weighting). This 4PI method guaranteed unambiguous temperature measurement.

Overall, we found the CARS mean temperature measurement accuracy to be within 50 K, while the precision was well within 20 K. We also discovered that once system parameters are optimized and the dye laser is tuned, repeatability is within ± 20 K for a mean flame temperature of 1500 K, after 4 days of operation.

4.1.3 LBO Mechanism. We successfully observed and documented a systematic and detailed sequence of events leading to LBO in practical combustors. We found that in a step combustor, these events comprised the attached-flame region, lifted shear flame, intermittent shear flame, the large-scale instability of the flame front, and finally LBO. For a bluff-body combustor, excess entrainment of cold reactants in the thick-flame region caused flamelet extinction, increased the adverse pressure gradient and the entrainment of the cold reactant mixture, and quenched the flame in the preheat-ignition region. Finally, in a swirl combustor intermittent mixing and radial jet fluid ejection produced by large-scale vortices caused local flame extinction of a thin, highly stretched, diffusion-flame interface. These individual events clearly highlight the complex LBO mechanism in a modern annular gas turbine combustor.

4.1.4 Recirculation Zone Structure. The flow field in a modern annular gas turbine combustor may be categorized into three regions: near-field, recirculation, and far-field regions. Flame is stabilized by a recirculation zone which bounds the near-field and far-field regions. Therefore, we investigated the effects of various parameters on the recirculation zone structure. We found that back pressure (or exit blockage) did not directly affect the step recirculation zone; rather the fuel and air jet shear layers were affected. These shear layers influence both the combustor central recirculation bubble and the inside-out step recirculation zones.

In contrast, for flames anchored by the bluff body, wall confinement elongated the recirculation zone by accelerating the flow and narrowed it by preventing mean streamline curvature. In the limit of fast chemistry, the recirculation zone size decreases to its value for fully developed, cold turbulent flow wake. In contrast, for *reaction-controlled* combustion, the recirculation zone is highly elongated. Finally, we discovered that swirl enhances flame stability significantly by creating a toroidal recirculation zone. However, for a fuel tube with an appreciable lip thickness, swirl did not noticeably influence stability because the central recirculation bubble generated in the wake region of the fuel tube successfully anchored the flame.

4.1.5 Turbulent Flame Structure. The structure of a turbulent flame in the primary zone of a gas turbine combustor is highly complex, involving contorted flame fronts and rapid chemical reactions. When the mixing process is dominated by large-scale turbulence, a high degree of unmixedness exists inside the combustor. Such a combustor design has good flame stability and high-altitude relight capability, but poor combustion efficiency and soot emission characteristics. When small-scale turbulence is the controlling factor, this leads to a compact, efficient, and clean-burning combustor design, but with a low combustion stability and poor relight performance.

The turbulent flame structure that appears in the combustor prior to LBO determines the extinction process. Therefore, we conducted a systematic study of this structure. We observed that at low fuel flows a distinct flame attaches itself around the fuel nozzle. This so-called "attached flame" structure has the appearance of an inverted "classic coke bottle" and is remarkably stable. As the overall equivalence ratio falls below 0.65, large-scale, oscillatory axial movement of the flame begins; this eventually leads to LBO. The structure of the turbulent flame anchored by the bluff body and enveloping the recirculation zone comprises: (1) an ignition-thin flame region in the vicinity of the flameholder base, (2) a reacting shear layer region of large-scale coherent structures, and (3) a thick-flame region in which entrainment is the dominant mechanism. Finally, the high-velocity gradients generated in the swirl combustor produce a thin diffusion layer, low Damkohler number, highly stretched flame.

4.1.6 Chemistry-Turbulence Interaction. In ramjet engines, jet afterburners, and gas turbine combustors, intense turbulent mixing and the nonlinearity of the chemical kinetics terms make the chemistry-turbulence interaction important and controlling.

We made successful correlations of the LBO in a step combustor against LP for LP values extending over 3 orders of magnitude. Further, *a priori* calculation of LBO was done using Swithenbank's [11] dissipation gradient approach of defining local PSR regions in the step combustor. Such a network of stirred reactor nodes yielded good agreement with experimental data.

We observed that chemistry-turbulence interaction also affected the structure of the recirculation zone and LBO in the bluff-body combustor. Faster chemistry decreased the recirculation zone length to half its original value. Also, TKE decreased dramatically due to suppression of turbulence by dilatation. Increasing the reactant turbulence intensity drastically shortens the recirculation zone length close to its value in the cold flow. The distribution of both shear stresses and TKE shifts from the outer periphery of the recirculation zone to radially inward locations. Finally, higher reactant turbulence also increased rms temperature fluctuations.

Such results indicate how compact the size of the primary zone of a gas turbine combustor can be, provided it operates at or near-stoichiometric equivalence ratios. Detailed examination of our data indicates that for $\phi \leq 0.75$, combustion is *kinetically controlled* and requires a recirculation zone larger than that for cold flow in order to stabilize a flame.

4.1.7 Free-stream Turbulence and Heat Transfer. The free-stream turbulence level experienced by a turbine blade downstream of the combustor approaches 20 percent. We performed an investigation of the effects of free-stream turbulence on flat plate heat transfer. We discovered that free-stream turbulence augments heat transfer 2 to 2.5 times. In practice, this means free-stream turbulence would cause a faster decay in the turbine blade film-cooling effectiveness, a reduction in the effective cooling length, or an increase in the film-cooling requirement. Also, our data yielded heat-transfer coefficients around St = 0.005 under high free-stream turbulence conditions which are close to those obtained on a turbine blade in actual engine tests. Thus, our research confirmed the validity and importance of these data sets to practical turbine blade-cooling.

4.1.8 Implications to Modeling. The combustor modeling strategy is essentially based upon the simultaneous solution of the conservation equations of fluid dynamics and chemical kinetics within a framework of appropriate physical and mathematical assumptions. Knowledge of the interaction between chemistry and turbulence is obtained by inspecting the various terms constituting the conservation equations of continuity, momentum, scalar transport, scalar dissipation, and turbulent kinetic energy. This exercise revealed marked differences between the magnitude of the terms that dominate the nonreactive and the reactive flows. For example, in practical combustors, mostly shear generation and scalar fluxes--not the normal stresses-- cause turbulence production. Finally, it was found that pressure gradients and velocity-pressure correlations were nonnegligible and important in turbulent combusting flows.

The fact that the research combustors behave as PSRs is important in modeling the LBO. Our experimental data were used by Dr. Sturgess of Pratt and Whitney, East Hartford CT, in developing novel combustor modeling schemes (see Appendices D, E, and F). The two main modeling approaches that enabled the calculation of stability from thermochemistry considerations are those of Swithenbank [11] and Magnessen and Byggstoyl [12].

Based on Swithenbank's [11] dissipation gradient approach, local volumes enclosing the highly turbulent portion of the combustor and the ones with the fuel-air mixture within the flammability limits defined the PSRs. The resulting reactor was 44 percent of the combustor volume and corresponded reasonably well to the lifted flame observed in the real combustor. The eddy dissipation concept (EDC) of Magnessen and Byggstoyl [12] was used to construct a subgrid scale reactor model. In contrast to the Swithenbank [11] model, this approach tests the individual reactor stability with the CFD calculations. It was found that this model calculated the lifted flame condition but was unsuccessful in predicting the all-important attached flame condition. Thus, our experimental studies show that improvements and refinements to modeling codes are required.

Finally, we discuss what gaps, if any, were found in our knowledge that should logically form the next step in future turbulent combustion studies.

Although we designed a toroidal PSR and installed the test facility capable of providing fuel-air mixtures to the PSR, we could not complete all the tests. Preliminary PSR tests yielded a comparison between experiments and CHEMKIN [20] calculations, and served to illustrate how the global chemistry parameters for computer modeling could be derived from PSR experiments. Given that we obtained successful correlations of LBO in a step combustor using the PSR theory and that the recirculation zone produced by the bluff body also behaves as a PSR, it would have been very appropriate to obtain further confirmation of this behavior from the PSR tests.

Another problem of theoretical and practical interest in turbulent reacting flow fields is the effect of turbulence on chemical kinetics. The treatment of chemical kinetic equations in combustion modeling entails a very expensive and complex computational effort because solutions to several hundred kinetic equations must be obtained. This reduction in effort may be possible if PSR experiments could be designed to isolate a few important elementary chemical kinetic reactions that dominate the combustion process. This type of investigation should be performed in the future.

4.2 Conclusions

Summarized below are the important results and conclusions of this 5-year multifaceted research program in turbulent combustion and heat transfer using advanced laser diagnostics.

(a) We successfully designed and operated several laboratory combustors (e.g., the step combustor, bluff-body combustor, PSR, and swirl combustor) each capable of simulating some important features of a practical gas turbine combustor. Thus, the test data from these combustors represent a very cost effective and valid means of understanding the combustion processes in a practical combustor.

(b) We developed two novel methods of accounting for the variation in the CARS slit function due to turbulence, beam intensity, and temperature. These methods have made possible the precise, repetitive, and unambiguous measurements of temperature in highly turbulent, confined flames. Now, mean flame temperature measurements can be performed within 50 K, while the CARS precision is well within ± 20 K.

(c) Our studies of LBO revealed a detailed sequence of events such as attached flames, lifted shear flames, and intermittent shear flames. Large-scale instability of the flame front, excess entrainment of cold reactants in the thickened flame front, reaction-controlled combustion, and intermittent mixing followed by radial jet fuel ejection were the primary causes of flame extinction in the step combustor, bluff-body combustor, PSR, and swirl combustor, respectively.

(d) Our investigations of the effects of various parameters on the structure and size of the recirculation zone revealed that (1) back pressure does not affect the recirculation zone, (2) wall

confinement and reaction-controlled combustion strongly affect its size, and (3) swirl creates a toroidal recirculation zone which, in turn, enhances flame stability.

(e) Chemistry-turbulence interaction affects the structure of the recirculation zone and LBO in combustors. Faster chemistry decreased the recirculation zone length to half its original value, whereas slower chemistry (near LBO) produced a rapid growth in flame temperature fluctuations. Increasing the reactant turbulence intensity drastically shortened the recirculation zone length close to its value in the cold flow. These results indicate how compact the size of the primary zone of a gas turbine combustor can be, provided it operates at or near stoichiometric equivalence ratios.

(f) We discovered that free-stream turbulence augments flat plate heat transfer by 2 to 2.5 times. In practice, this means that free-stream turbulence would cause a faster decay in the turbine blade film-cooling effectiveness, a reduction in the effective cooling length, or an increase in the film-cooling requirement.

(g) Our experimental data were used by Dr. Sturgess of Pratt and Whitney, East Hartford, CT in developing two novel combustor modeling schemes based on the work of Swithenbank [11] and Magnessen and Byggstoyl [12]. It was found that the models calculate the lifted flame condition but are unsuccessful in predicting the attached flame condition.

To summarize, our experimental studies have made a valuable contribution by providing a physical understanding of turbulent combustion and heat transfer, and also by making available benchmark-quality data for evaluating and refining computer models used by industry to design gas turbine combustors. Now, the challenge is to produce new modeling codes that can be used with a sufficient degree of realism, confidence, and certainty to design practical combustion systems.

REFERENCES

1. Ballal, D. R., Lightman, A. J., and Yaney, P. P., "Development of Test Facility and Optical Instrumentation for Turbulent Combustion Research," AIAA Journal of Propulsion and Power, Vol. 3, 1987, pp. 97-104.

2. Rose, W. C., and Johnson, D. A., "Turbulence in a Shock-Wave Boundary-Layer Interaction," AIAA Journal, Vol. 13, 1975, pp. 884-889.

3. Yanta, W. J., and Smith, R. A., "Measurement of Turbulence Transport Properties Using an LDA," AIAA-73-169, Washington, D.C., 1973.

4. Glass, M., and Bilger, R. W., "The Turbulent Jet Diffusion Flame in Coflowing Stream-Some Velocity Measurements," *Combustion Science and Technology*, Vol. 18, 1978, pp. 165-177.

5. Edwards, R. V. (Ed.), "Report of the Special Panel on Statistical Particle Bias Problems in Laser Anemometry," Trans. ASME, J. Fluids Engineering, Vol. 109, 1987, pp. 89-93.

6. Libby, P. A., Chigier, N., and LaRue, J. C., "Conditional Sampling in Turbulent Combustion," Progress in Energy and Combustion Science, Vol. 8, 1982, pp. 203-231.

7. Dibble, R. W., Hartmann, V., Schaefer, R. W., and Killman, W., "Conditional Sampling of Velocity and Scalars in Turbulent Flames Using Simultaneous LDA-Raman Scattering," Experiments in Fluids, Vol. 5, 1987, pp. 103-113.

8. Vangsness, M. D., and Heneghan, S. P., "Coherent Anti-Stokes Raman Spectroscopy: System Characterization and Reproducibility," CI-92-36, Central States Section, The Combustion Institute, Columbus OH, April 26-28, 1992.

9. Sturgess, G. J., Sloan,D. G., Lesmerises, A. L., Ballal, D. R., and Heneghan, S. P., "Design and Development of a Research Combustor for Lean Blow Out Studies," *ASME, Journal of Engineering for Gas Turbines and Power*, Vol. 114, 1992, pp. 13-20.

10. Sturgess, G. J., Lesmerises, A. L., Heneghan, S. P., Vangsness, M. D., and Ballal, D. R., "Isothermal Flowfields in a Research Combustor For Lean Blowout Studies," Paper No. 91-GT-37, *ASME, Journal of Engineering for Gas Turbines and Power*, 1991.

11. Swithenbank, J., "Flame Stabilization in High Velocity Flow," in H. B. Palmer and J. M. Beer (eds.), Combustion Technology-Some Modern Developments, Academic Press, 1974, pp. 125.

12. Magnessen, B. F., and Byggstoyl, S., "A Model of Flame Extinction In a Turbulent Flow," in L. Bradbury (ed.), Turbulent Shear Flows, Berlin: Springer Verlag, 1985, pp. 67-78.

13. Zukoski, E. E., and Marble, F. E., "The Role of Wake Transition in the Process of Flame Stabilization on Bluff Bodies," in A. H. Lefebvre et al. (eds.), AGARD *Combustion Researches and Reviews*, London: Butterworths Publishing Co., 1955, pp 167-180.

14. Ballal, D. R., "Combustion-Generated Turbulence in Practical Combustors," AIAA *Journal of Propulsion and Power*, Vol. 4, 1988, pp. 123-134.

15. Bray, K. N. C., "Turbulent Flows With Premixed Reactants," in *Turbulent Reacting Flows*, P. A. Libby and F. A. Williams (eds.), New York: Springer Verlag, 1980, pp. 115-183.

16. Ballal, D. R., and Lefebvre, A. H., "The Structure and Propagation of Turbulent Flames," *Proceedings of the Royal Society*, Vol. A344, London, 1974, pp. 217-234.

17. Shephard, I. G., Moss, J. B., and Bray, K. N. C., "Turbulent Transport in a Confined Premixed Flame," *Nineteenth Symposium (International) on Combustion*, Pittsburgh, PA: The Combustion Institute, 1982, pp. 423-431.

18. Libby, P. A., and Bray, K. N. C., "Countergradient Diffusion in Premixed Flames," *AIAA Journal*, Vol. 19, 1981, 205-213.

19. Nenninger, J. E., Kridiotis, A., Chomiak, J., Longwell, J. P., and Sarofim, A. F., "Characterization of a Toroidal Well-Stirred Reactor," Twentieth Symposium (Int.) on Combustion, Pittsburgh PA: The Combustion Institute, 1984, pp. 473-479.

20. Kee, R. J., Rupey, F. M., and Millar, J. A. ,"CHEMKIN II: A Fortran Chemical Kinetics Package for the Analysis of Gas Phase Chemical Kinetics," Sandia Report 89-8009, Livermore CA: Sandia National Laboratory, 1989.

21. Takahashi, F. and Glassman, I., "Sooting Correlations for Premixed Flames," Combust. Sci. Technol., Vol. 37, 1984, pp. 32-36.

22. Lefebvre, A. H., *Gas Turbine Combustion*, New York: Hemisphere Publishing Corp., 1983.

23. Longwell, J. P., and Weiss, M. A., "High Temperature Reaction Rates in Hydrocarbon Combustion," Industrial and Engineering Chemistry, Vol. 47, 1955, pp. 1634-1643.

24. Ballal, D. R., and Lefebvre, A. H., "Weak Extinction Limits of Turbulent Flowing Mixtures," ASME Journal of Engineering for Power, Vol. 101, 1979, pp. 343-348.

25. Nagle, J., and Strickland-Constable, R. F., "Oxidation of Carbon Between 1000-2000C," Proc. Fifth Carbon Conf., Vol. 1, 1962, pp. 154-163.

26. Pope, S. B., "PDF Methods for Turbulent Reactive Flows," Progress in Energy and Combustion Science, Vol. 11, 1985, pp. 119-192.

27. Anand, M. S., Pope, S. B., and Mongia, H. C., "A PDF Method for Turbulent Recirculatory Flows," U. S.-France Joint Workshop on Turbulent Reactive Flows, Rouen, France, July 1987.

28. Takahashi, F., Mizomoto, M., Ikai, S., and Tsuruyama, K., "Stability Limits of Hydrogen-Air Coflowing Jet Diffusion Flames," AIAA 90-0034, 1990.

29. Launder, B. E., and Rodi, W., "The Turbulent Wall Jet-Measurements and Modeling," Annual Reviews of Fluid Mechanics, 1983, pp. 429-458.

30. Blair, M. F., and Werle, M. J., "Combined Influence of Freestream Turbulence and Favorable Pressure Gradients on Boundary Layer Transition and Heat Transfer," Report No. R81-914388-17, United Technologies Research Center, 1981.

Table 1. **Recirculation Zone Parameters in a Bluff Body Stabilized Turbulent Premixed Flame.**

Conical Stabilizer
$\theta = 45°$, BR = 25%, $\phi = 0.65$, $Re_d = 5.7 \times 10^4$

	Confined Cold Flow	Confined Flame	Open Flame
(L/D)	1.5	1.70	1.85
(W/d)	0.55	0.58	0.65
(U_r/U_a)*	-0.24	-0.40	-0.30
$(\dot{m}_r/\dot{m}_t)$	0.20	0.13	0.10
(u'/U_a)	0.3	0.24	0.32
(v'/U_a)	0.26	0.17	0.28
(q_c/q)	1.0	0.64	1.12

*at x/d = 0.8, r/d = 0.3

Table 2. **Characteristics of the Large-Scale Vortex Structures in a Turbulent Jet Diffusion Flame.**

U_j (m/s)	z (mm)	$r_{1/2}$ (mm)	$U_{1/2}$ (m/s)	$f_{c1/2}$ (Hz)	l (mm)
6	15	5.0	5.1	704	3.6
10	15	5.3	7.0	1100	3.2
15	5	5.5	3.6	1130	1.6
15	15	5.5	9.1	1330	3.4
15	25	5.3	12.1	1230	4.9
15	50	5.4	---	1190	---

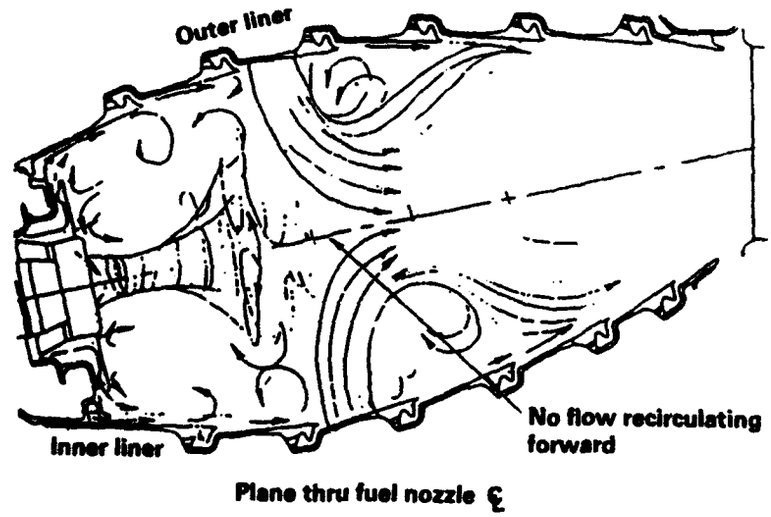

Figure 1. Cross section through a modern annular gas turbine combustor

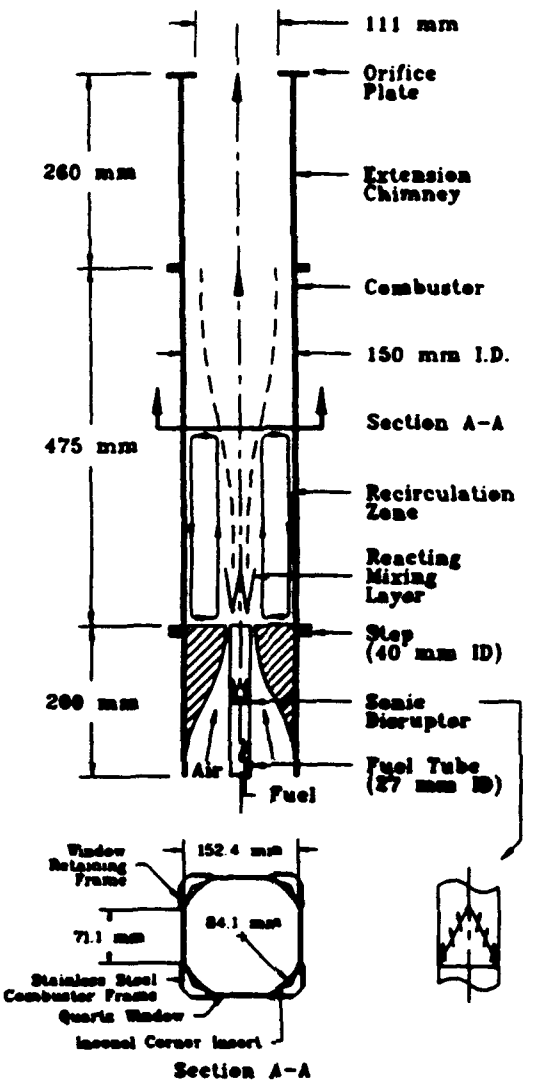

Figure 2. Schematic diagram of a step combustor

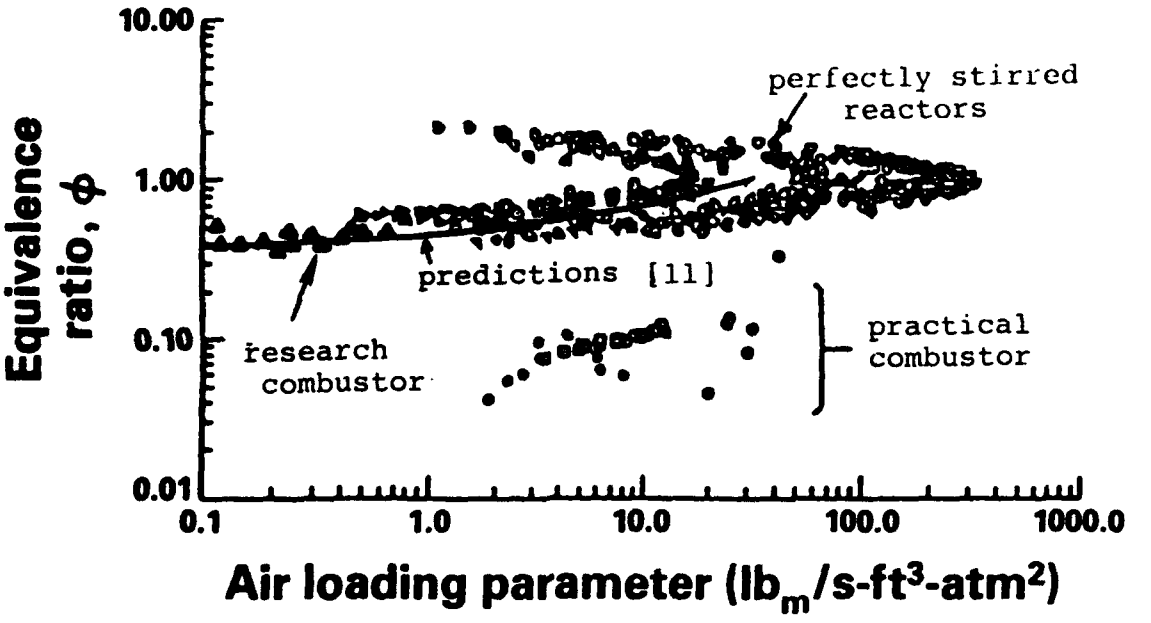

Figure 3. LBO performance of a step combustor and predictions [11]. Also shown for comparison are LBO data from PSR and practical gas turbine combustors.

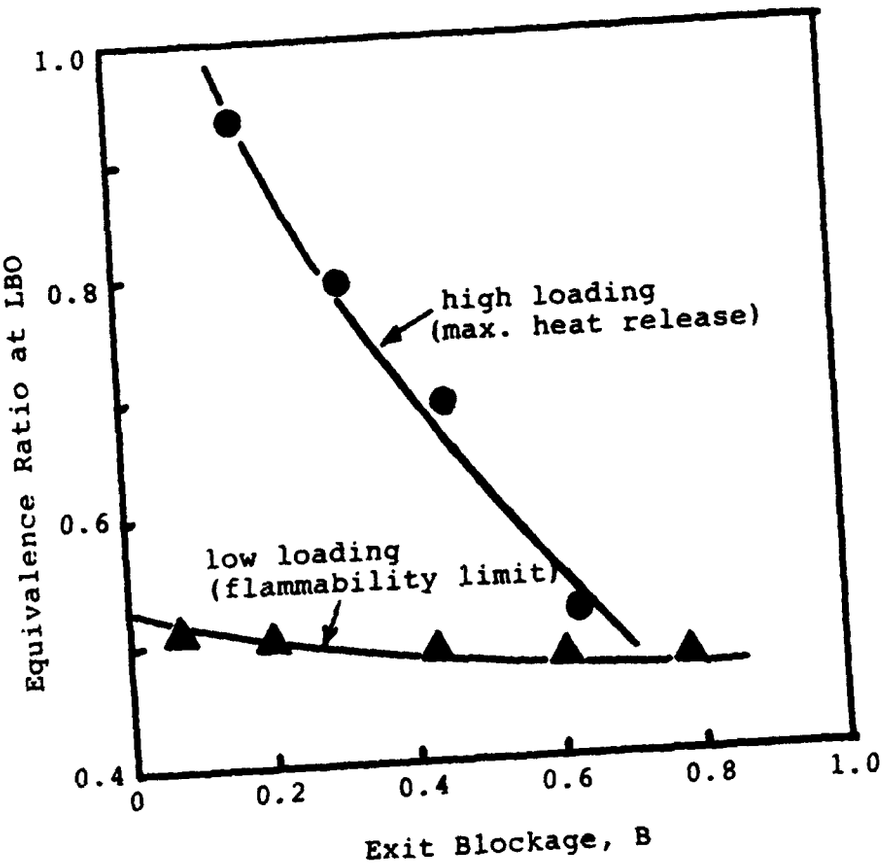

Figure 4. Influence of exit blockage on LBO equivalence ratio for low and high combustor loadings (combustor L/D = 4.9)

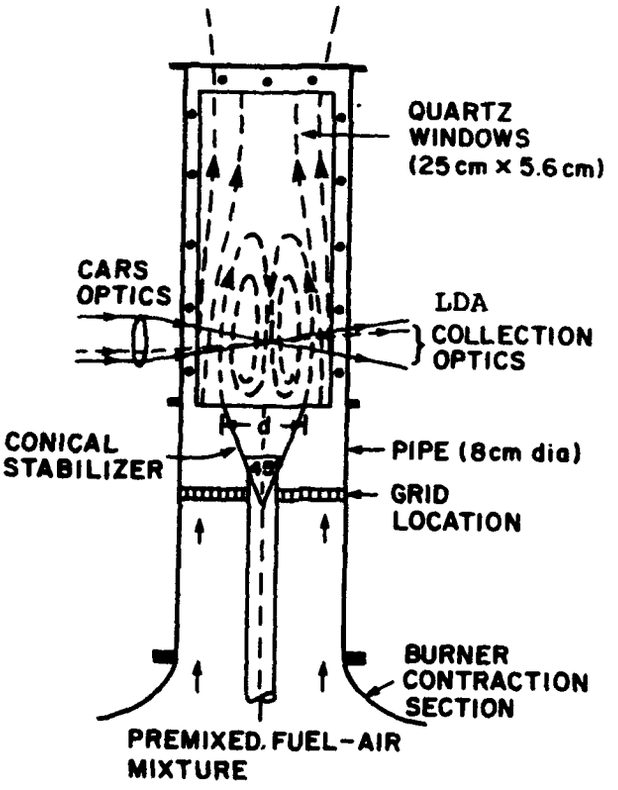

Figure 5. Schematic of a bluff body combustor

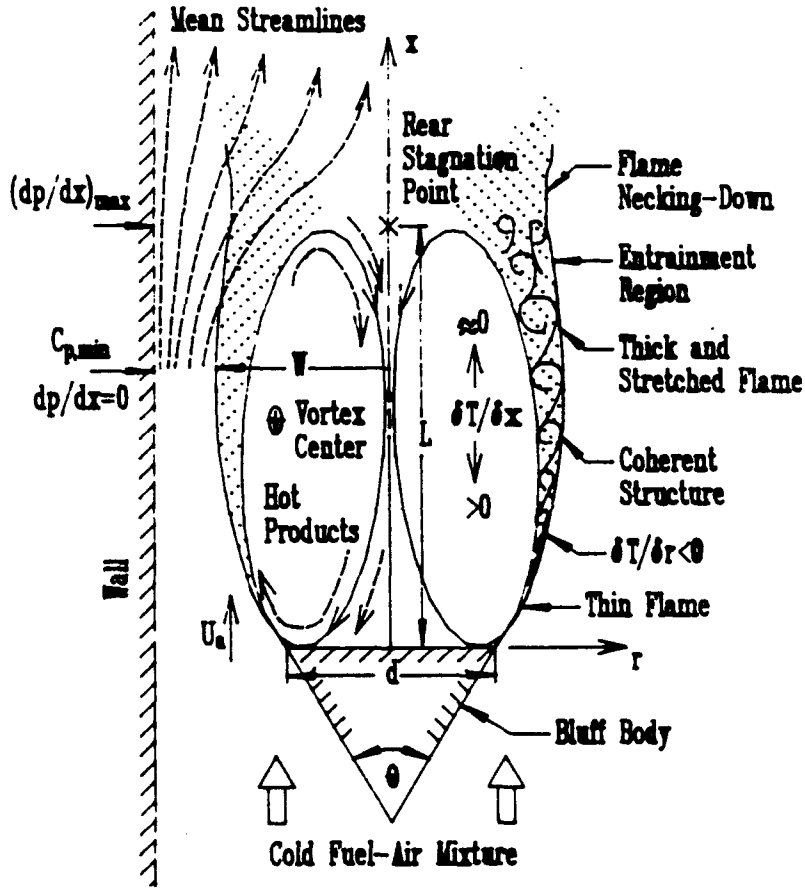

Figure 6. Sketch of a confined recirculation zone produced by a bluff body

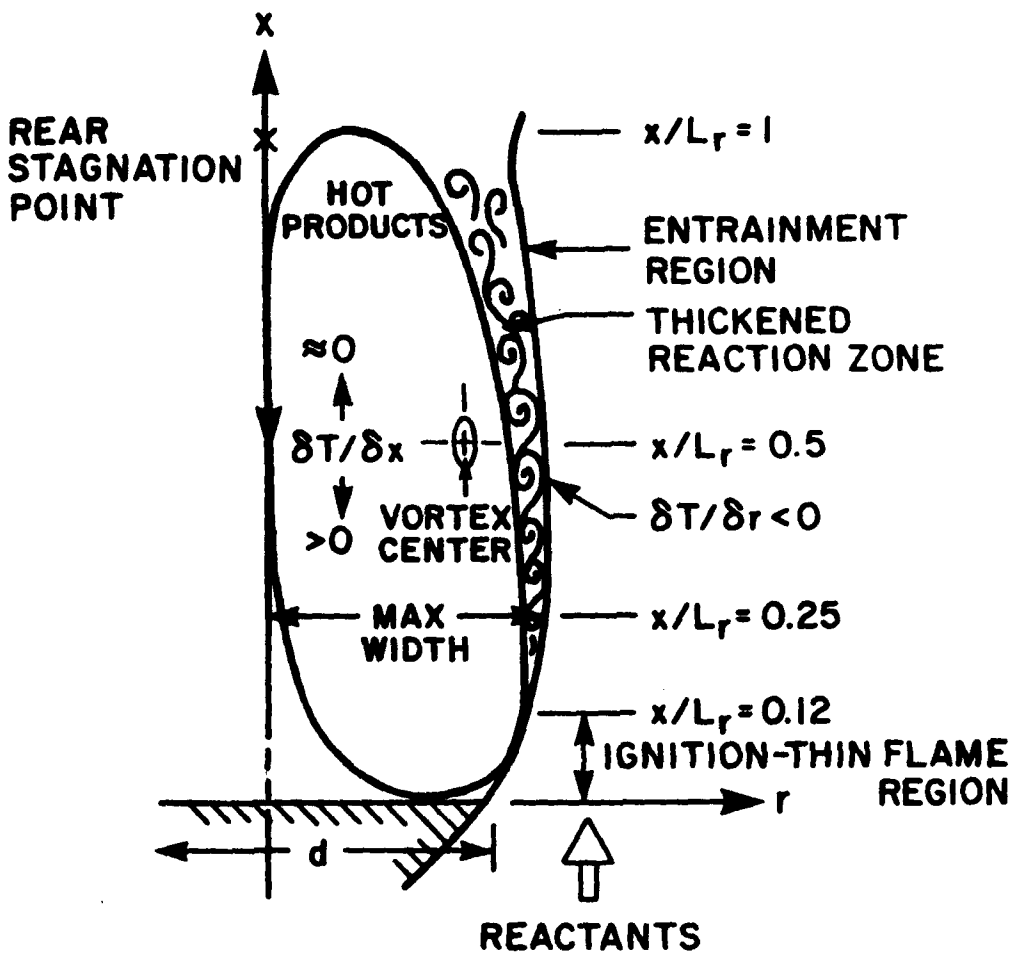

Figure 7. Schematic diagram of a turbulent flame structure enveloping the recirculation zone

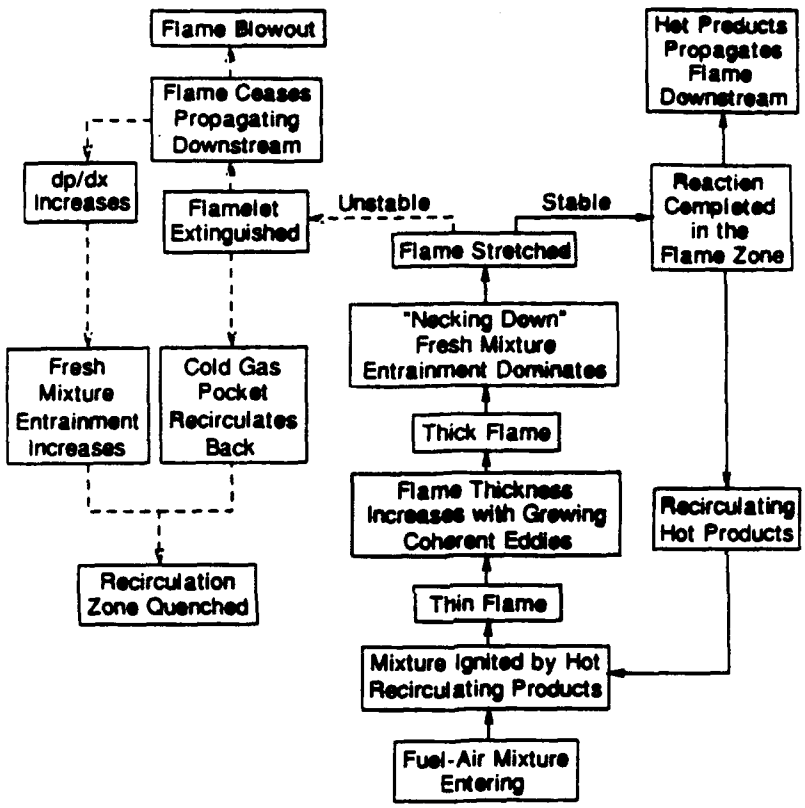

Figure 8. Flow chart illustrating the mechanism of bluff body flame stabilization and LBO

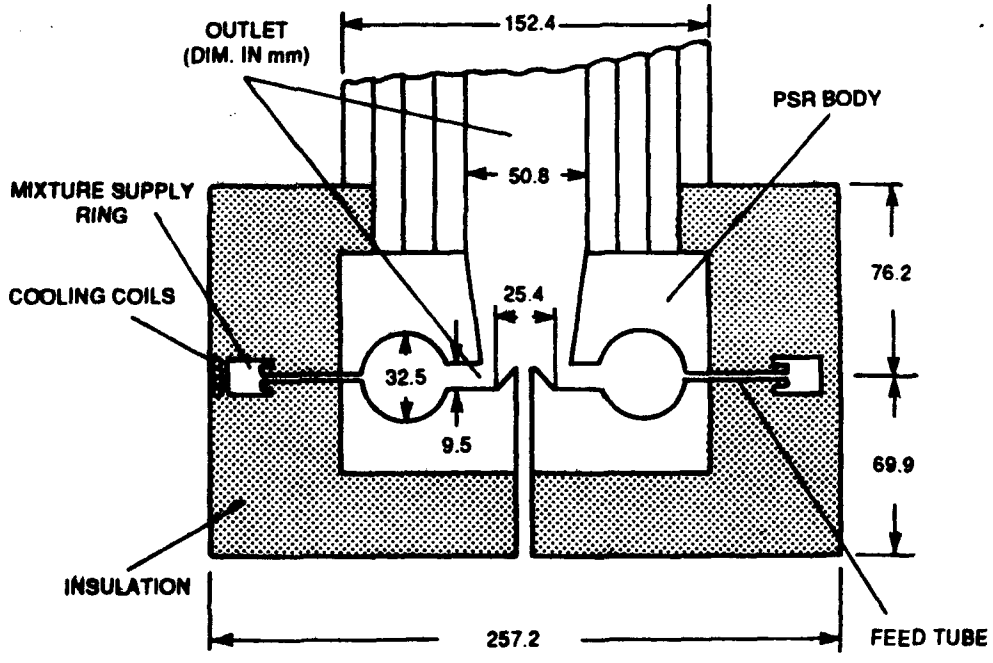

Figure 9. Schematic diagram of a toroidal PSR

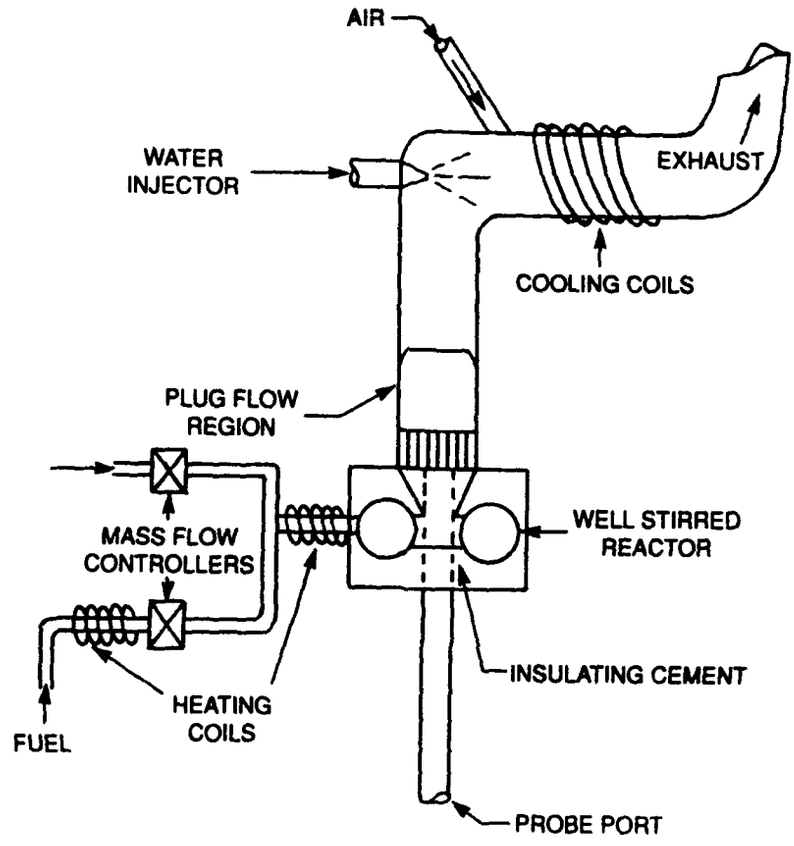

Figure 10. Schematic diagram of a PSR test facility setup

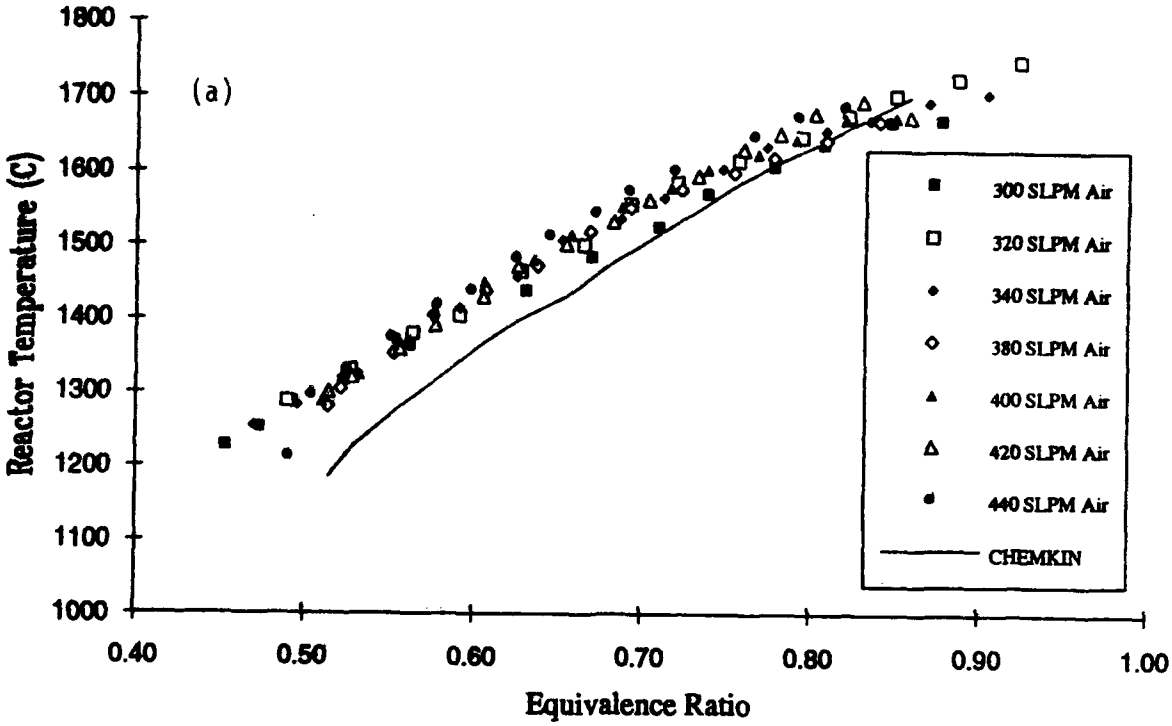

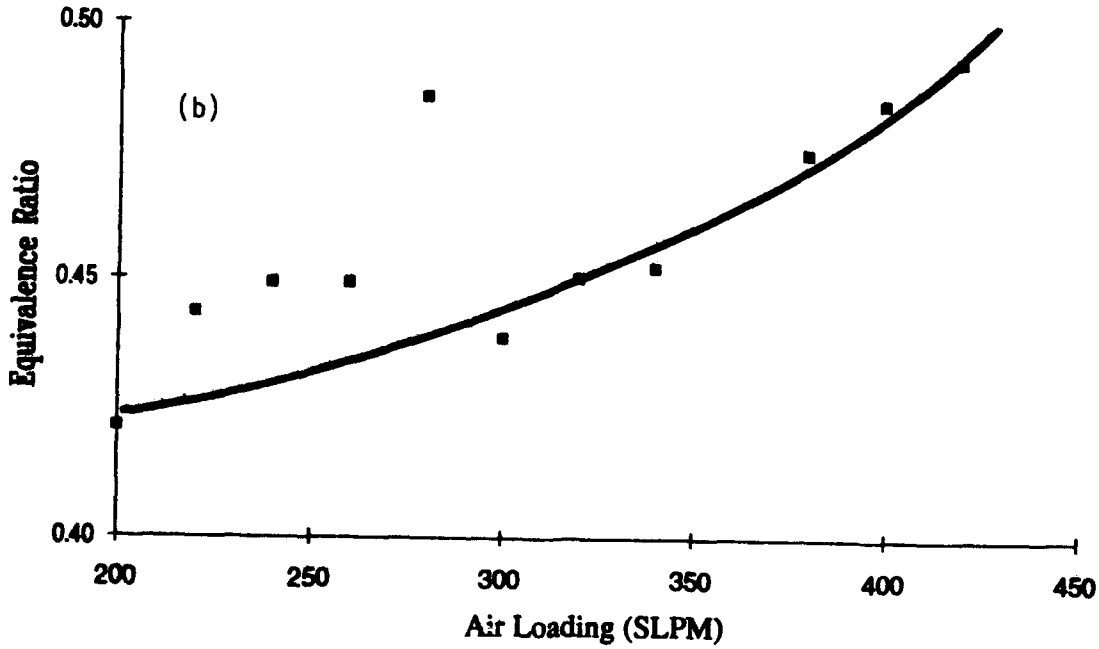

Figure 11. Preliminary PSR test results on methane-air mixtures illustrating; (a) comparison between measurements and CHEMKIN [20] predictions, and (b) LBO limits

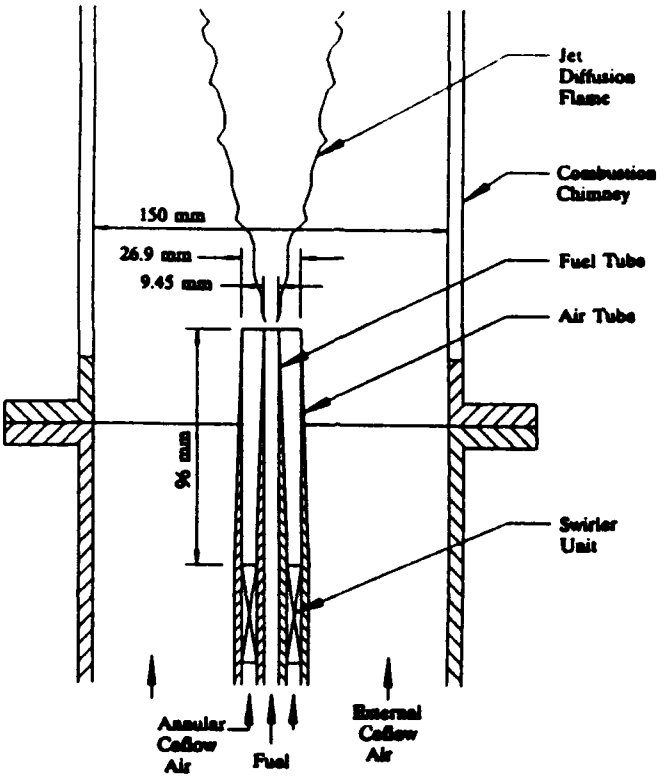

Figure 12. Schematic diagram of a swirl combustor

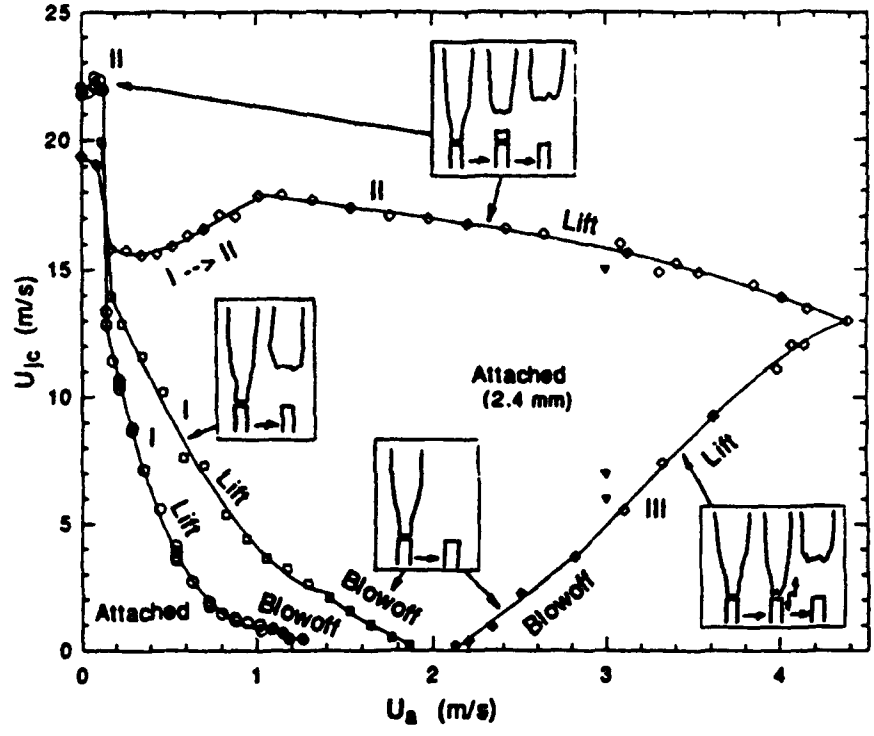

(a)

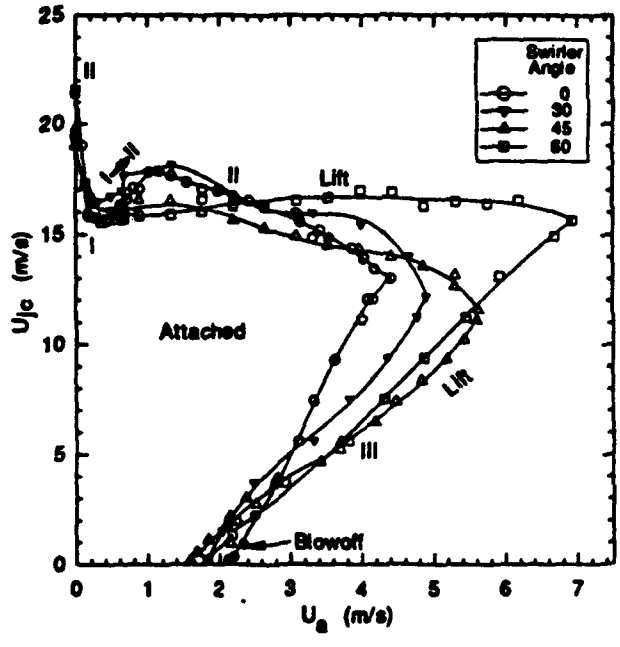

(b)

Figure 13. Stability limits of methane-air jet diffusion flames; (a) non-swirling flame, (b) swirling flames

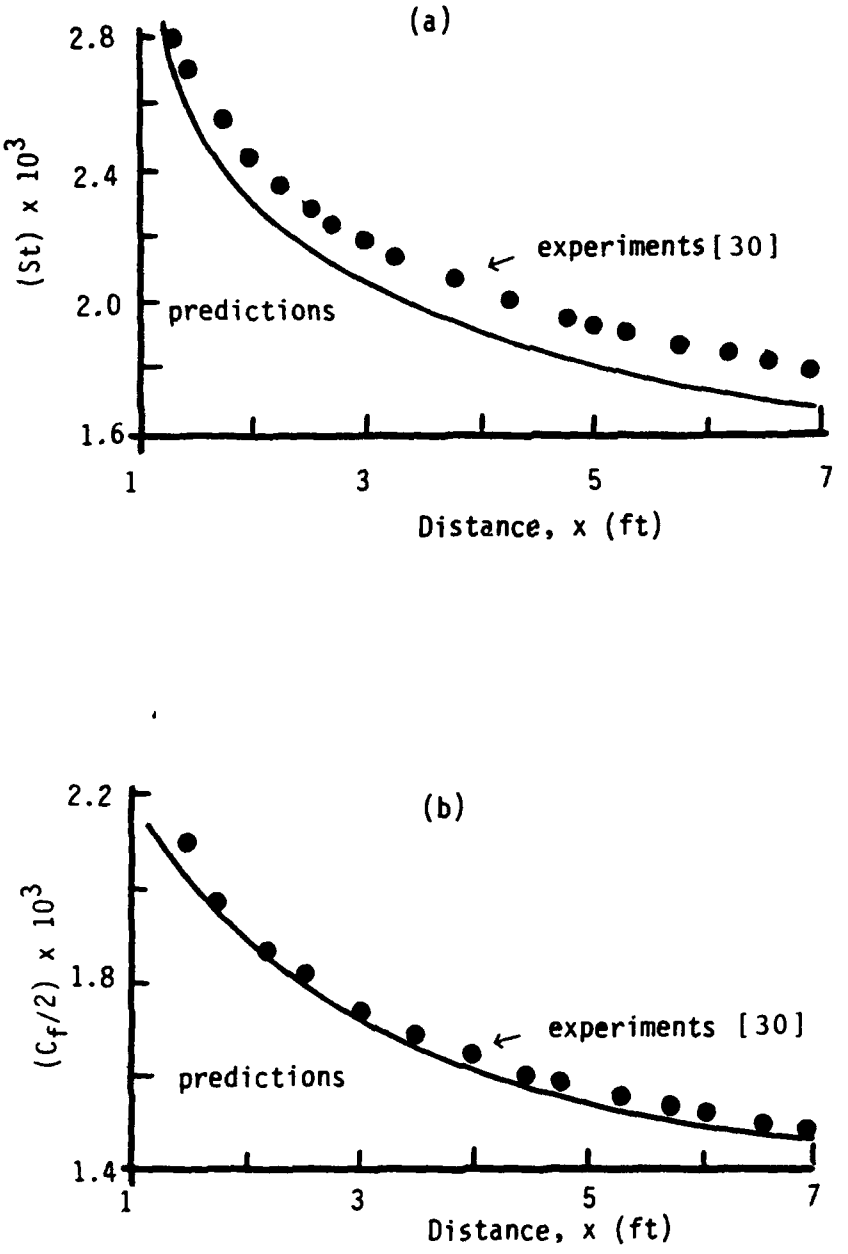

Figure 14. Comparison between TEXSTAN code predictions and experimental results for a flat plate heat transfer in the presence of high freestream turbulence level; (a) variation of Stanton number with downstream distance, and (b) variation of skin friction with downstream distance

APPENDIX A

ANALYSIS OF SLIT FUNCTION ERRORS IN SINGLE-SHOT COHERENT ANTI-STOKES RAMAN SPECTROSCOPY (CARS) IN PRACTICAL COMBUSTORS

By

Shawn P. Heneghan and Marlin D. Vangsness
University of Dayton, Dayton, Ohio

Published in Reviews of Scientific Instruments Vol. 62, No. 9, pp. 2093-2099, September 1991.

Analysis of slit function errors in single-shot coherent anti-Stokes Raman spectroscopy (CARS) in practical combustors

Shawn P. Heneghan and Marlin D. Vangsness
University of Dayton, 300 College Park, Dayton, Ohio 45469-0140

(Received 10 September 1990; accepted for publication 1 May 1991)

The temperature determined by a single-shot coherent anti-Stokes Raman spectroscopy (CARS) system is directly related to the half width at half maximum of the instrument slit function. Therefore, an accurate knowledge of the instrument slit function is necessary to determine temperature with CARS. However, in turbulent systems, the input slits of the spectrometer may be removed in order to guarantee signal throughput and establish the necessary dynamic range. In this case, the physical input slits of the spectrometer are replaced with apparent slits created by focussing the input beams near the entrance plane of the spectrometer. The slit function will then depend on the physical relationship among all of the optical components, the probe volume, and the dispersive performance of the spectrometer and detector, as well as the optical path through density and temperature gradients which may not be invariant in a turbulent system. The presence of high temperatures and turbulence levels can effect the size of the CARS signal origin and the optical path, and as a result, the slit function is not invariant. Ignoring these changes can result in large root mean square temperatures (decreased precision) as well as mean temperature errors. The variability of the slit width can be accounted for on a shot-to-shot basis by using a two parameter (HWHM of the slit function and temperature) fitting routine. For temperatures greater than 1200 K there is convergence on a best curve implying both a temperature and a slit width. This method can be used alone or in concert with various weighting schemes to improve the precision. There are two major advantages gained by allowing the slit function to vary in a CARS system: (a) it allows an increase in the precision; (b) it allows temperatures to be calculated without the assumption that the slit function does not change with temperature or turbulence or position within the flame. In fact, it allows the temperature to be determined with almost no previous knowledge of the slit function except the general shape. These two advantages combine to significantly simplify the study of turbulent combusting systems with CARS and to improve the precision, both point-to-point and shot-to-shot, of CARS.

I. INTRODUCTION

Single pulse coherent anti-Stokes Raman spectroscopy (CARS) has shown effectiveness in the determination of temperature and concentration of major species such as H_2, N_2, and O_2 as early as 1976.[1] The usefulness of CARS was expanded greatly with the introduction of the BOXCARS[2] set up to enhance spatial resolution. In 1983, Greenhalgh, Porter, and England[3] demonstrated the usefulness of CARS in turbulent combustion processes, while Goss *et al.*[4] described a system that was capable of measuring both temperature and concentration in nearly all turbulent systems because of its large dynamic range (300–2500 K). Since its advent, CARS has been used to measure temperature and species concentration in a variety of hostile environments. The theory and application of CARS have been reviewed several times.[5–7]

Despite the well-developed theory of CARS signal generation, including laser lineshapes,[8,9] and dye laser mode noise,[10] there has been almost no attempt to consider the instrument slit function, the remaining major broadening source of the CARS signal. The slit function needed to accurately calculate the actual collected spectra cannot be derived *a priori* but rather a calculated spectrum, neglecting the slit function, is convolved with a "guesstimate" of the slit function until the final convolved spectrum is a "good fit" with the collected spectrum at a particular temperature.

The function that gives the best fit is then assumed to be independent of temperature turbulence in the optical path. This slit function is then convolved with theoretically calculated nitrogen spectra to generate a temperature-dependent library of spectra. These generated spectra are then used in various least square fitting routines with temperature as the only variable to determine the best fit and estimate of the actual temperature.

In this article we show that the slit function in turbulent measurements is not invariant from shot to shot. This variation shows itself by a decrease in precision[11] of the CARS system, and can be corrected by using a two-parameter (half width half maximum of the slit function and temperature) fitting routine instead of the standard one-parameter (temperature) routine. While the two-parameter fit adds computational complexity to the analysis, it makes the determination of the slit function easier. In addition, using two parameters results in better precision and significantly better average fits. We present a theoretical description of a possible source of the slit function which

accounts for the variability.

Finally, a discussion concerning the effects of various weighting schemes is included because CARS temperatures have been determined using a variety of weighting schemes to increase the precision (that is improve the reproducibility) of the CARS instrument. While these weighting schemes tend to increase the precision of the CARS system, they affect the accuracy to varying degrees, as noted by Snelling *et al.*,[12] the selection of weighting coefficients appears to be a compromise between increasing the precision, and avoiding mean temperature shifts. A description of various weighting schemes is included in the Appendix, and an explanation of how they tend to minimize the variations introduced by a varying slit function is included in the discussion. We will also show how the mean temperature shifts associated with these weighting schemes can be eliminated.

II. EXPERIMENTAL DESCRIPTION

The CARS system hardware and software are described by Goss, Trump, and Roquemore.[13] A Nd:YAG (Quanta Ray DCR-2) laser, a Tracor Northern Spectrometer (TN-1710) with Diode Array Rapid Scanning Spectrometer (DARSS), a Spex $\frac{1}{4}$ meter grating spectrometer, and a ModComp Classic 32/85 Computer comprise the major components of the system. The major purpose of this system was the investigation of highly turbulent combusting system. Therefore, in order to guarantee signal throughput despite possible beam steering and establish the necessary dynamic range, we have used Goss *et al.*'s 1983 design[4] in which there are no physical input slits on the spectrometer. Instead, the input beams are focused near the entrance plane of the spectrometer, creating effective or apparent slits.

The Nd:YAG laser is operated near full power. The infrared radiation is doubled and the resulting green light is used in the optical system. The 150 mJ pulses of light have a linewidth (half width at half maximum, HWHM) less than 0.5 cm^{-1}. The spatial distribution of the green beams is nearly TEM_{01}^{*} ("donut mode") with a diameter of about 7 mm. The green beam is divided into four beams of equal intensity. Two of these become the pump beams, while the other two pump a dye laser oscillator and amplifier.

The dye laser is nearly coaxially pumped and concentration tuned. The oscillator cavity is 15 cm long with flat reflectors and an output coupler of about 30%. The dye (Rhodamine 640) concentration is adjusted until the dye laser is tuned to 607.3 Å (spectral HWHM about 60 cm^{-1}). The output of the dye laser is then transformed with a telescope to match the green beam characteristics.

The red dye beam (Stokes beam) and the two green beams (pump beams) are then focused together in a "BOXCARS" configuration. The input lens is 25 cm focal length with input half angles of about 0.05 radians. The signal is optimized after initial lineup by adjusting the actual Stokes beam input angle and collimation.

The CARS signal is collected and focused onto the "apparent" slits of a Spex ($\frac{1}{4}$ m) spectrometer with a cylindrical lens. The signal is then collected with a DARSS TN-6132 camera and sent to both the Tracor Northern Spectrometer and the Modcomp computer where it is stored on tape for future analysis. The dispersion of the spectrometer and camera is 1.24 cm^{-1} per digital readout (pixel) on the camera. The detector is 2.5 cm wide and contains 1024 pixels (about 25 μ/pixel).

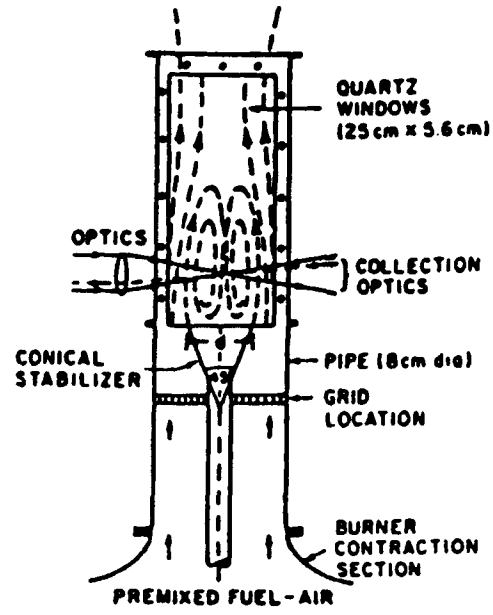

FIG. 1. Bluff body combustor used to generate a turbulent confined flame.

The methane-air flame was stabilized by a conical bluff body. Fuel and air were premixed at an equivalence ratio of 0.65 and passed by the fluff body at a velocity of about 15 m/s. The CARS data used in this study were collected at a position that was off-axis by $\frac{1}{10}$ of the bluff body diameter and downstream by $\frac{6}{10}$ diameters. This position was expected to give a flame temperature nearly equal to adiabatic flame temperature (1755 K) with a very low RMS.[14,15] Figure 1 shows the burner configuration. The combustion characteristics of the enclosed flame have been described previously.[16]

The spectral basis sets (each covering 250–2500 K in 10 K increments) were generated using a combination Gaussian and Lorentzian profile as follows:

$$\text{slit function} = a \times G \otimes L + (1 - a) \times G,$$

where G is a normalized Gaussian, HWHM = s cm^{-1}, and L is a normalized Lorentzian, HWHM = 1.8 s cm^{-1}, $a = 1/(1 + 0.75\ s)$, s varied from 2.0 to 4.0 by 0.2 increments, $\otimes$ is meant to convolve (HWHM is the half width at half maximum).

This combination creates an effective slit function that exhibits the width of a Gaussian, but the wings of a Lorentzian, while still being normalized. Nearly all the broadening is determined by the Gaussian portion of the slit function. The Lorentzian helps fit the legs of the spectra. The

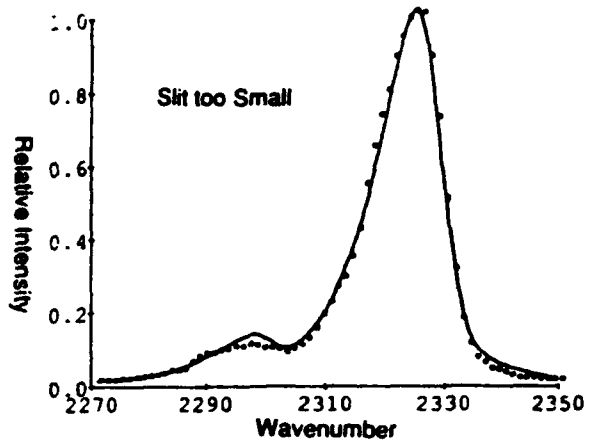

FIG. 2. Best fit to typical CARS data using too small a slit width. Notice the best fit underestimates the width of the data near 2320 cm^{-1} and overestimates the height of the data near 2300 cm^{-1} (data, ■, best fit,–).

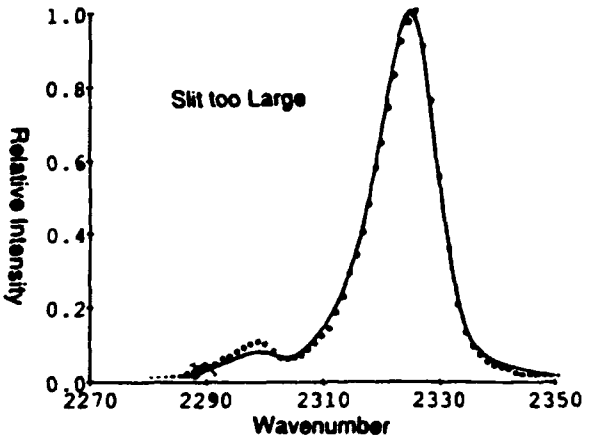

FIG. 3. Best fit to typical CARS data using too large a slit width. Notice the best fit overestimates the width of the data near 2320 cm^{-1} and underestimates the height of the data near 2300 cm^{-1} (data, ■, best fit,–).

width of the slit function is the critical parameter in determining the temperature, and hereafter the HWHM of the Gaussian (s) is used to describe the total function, and will be referred to as the slit width.

A weighted least-squares fitting routine described by Goss *et al.*[4] was used to obtain the best least-squares fit. This fitting routine allowed a weighting factor to be set on all points with frequencies below 2306 cm^{-1} (i.e., the excited vibrational band of N_2), emphasizing these points in the data analysis. We have used three different weights for these points: 1, 4, and 10.

III. RESULTS AND DISCUSSION

During the course of analysis of CARS data on this burner, it became obvious that the instrument slit width was not a constant. Most of the problem has been attributed to heating of the optical breadboard. The installation of heat shields helped to minimize the problem, but did not eliminate it. As a result, it was necessary to determine the slit width of the system at operating conditions. Attempts to understand the entire source of the slit function and to determine the exact nature of the slit function in our system after the burner was heated, led to the discovery that the slit width was not invariant. Not only did the width of the slit function change with changes in the temperature/turbulence level in the burner, but it varied from shot to shot and from one location to another within the burner. An analysis of the probable sources of the slit function reveals that there is no fundamental reason to assume that the slit width of the system should remain constant, independent of the optical path that varies with temperature, density, gradient changes, and turbulence levels, and consequently location in the burner. However, since variations of the average slit width with position have been described and accounted for previously,[17] we shall limit our discussion to shot to shot variations.

Figures 2 and 3 show the type of fit that can be expected (using no weighting factors) when slit widths that are either too small or too large are used. Looking at a series of temperature data showed that no one slit width was adequate to fit all of the data. Subsequently, we permitted the slit width to vary. That is, instead of allowing only the temperature to vary, we allowed the computer to scan a variety of spectra sets, each generated with a different s, and then to select the temperature and slit width of the spectra with the best fit.

Table I shows the type of mean and RMS temperatures acquired using the "best fit" method (the temperature acquired by allowing the slit width and temperature to vary), and fits associated with $s = 2.2$ cm^{-1} (the room temperature slit width), 2.4 cm^{-1}, and 2.7 cm^{-1} (a slit width with significant implications to be described in detail below). There are several observations to be made. There is a general decrease in the RMS value as the slit width decreases or weighting, w_i, increases. The mean temperature decreases with increasing weighting for the small slit

TABLE I. Comparison of mean and RMS temperatures and fit parameters vs slit width and weighting (all values in Kelvin).

	Slit ($w_i = 1$) in cm^{-1}			
	2.2	2.4	2.7	variable avg. = 2.42
Mean	1737	1712	1672	1704
RMS	102	104	109	89
Fit	18.4	18.2	19.2	15.8
	Slit ($w_i = 4$)			
	2.2	2.4	2.7	variable avg = 2.44
Mean	1717	1699	1671	1690
RMS	74	75	77	70
Fit	13.2	13.0	13.9	11.1
	Slit ($w_i = 10$)			
	2.2	2.4	2.7	variable avg. = 2.48
Mean	1708	1694	1671	1682
RMS	67	68	70	67
Fit	9.5	9.3	9.8	7.9

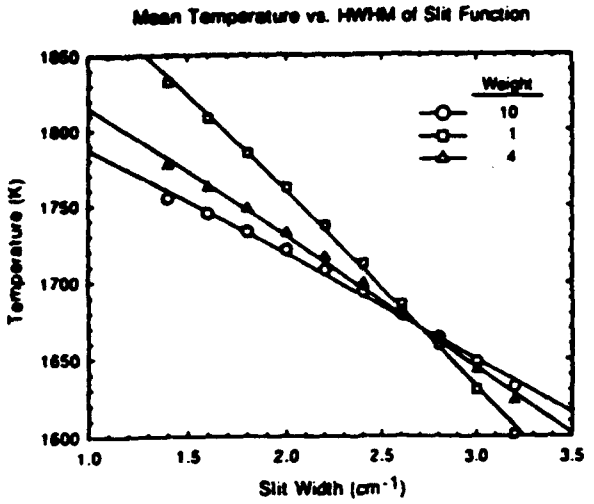

FIG. 4. Measured mean CARS temperature vs HWHM of slit function weighting factors of 1, 4, or 10 assigned to the "hot band" of nitrogen.

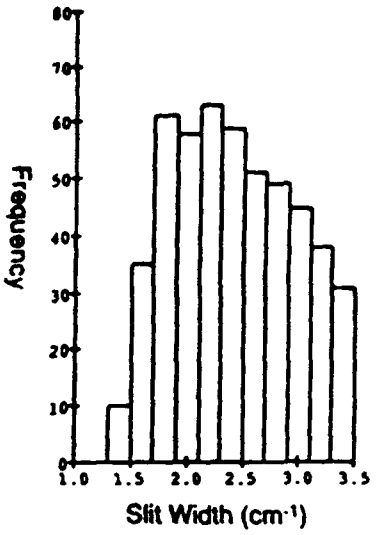

FIG. 5. Distribution of "best" slit widths in turbulent CARS measurement as determined by two-parameter (HWHM and temperature) least-squares fit.

widths, while it is essentially constant for 2.7 cm^{-1}. The fit variable has a minimum using fixed slit widths.

Figure 4 shows a plot of the mean temperature vs slit width s at constant weighting. The intersection of the graphs at one point is important, because it describes the average slit width for which the weighting does not affect the mean temperature. This slit width, as described previously,[17] is the only value of the average slit width that yields the same temperature independent of the vibrational quantum number (v). If we assume local thermodynamic equilibrium (LTE) is applicable, then the rotational temperature of the first excited state and the ground state must be equal, and further they must equal the vibrational temperature. In that case, changing the weighting on the $v = 1$ peak should have no effect on the mean temperature. The only HWHM consistent with the assumption of LTE is the one determined by the intersection of the three lines in Fig. 4. This can be reasoned by realizing that all of the information about temperature is contained in the shape of the $v = 0$ rotational band. The rotational temperature can be obtained by setting $w_v = 0$. By increasing the weight of the $v = 1$ band, the rotational temperature of the "hot band" is now considered in the fitting process as well as the vibrational temperature. If we assume that LTE applies, then the rotational and vibrational temperatures are the same, and the average temperature measured should not depend on the weighting factor used. This value of the slit width ($s = 2.7$ cm^{-1}) yields a mean temperature of 1672 K and RMS of 108 K (unity weighting) or 70 K (weighting by 10).

Conversely, allowing the slit width to vary for each spectra collected yields better fits on average than any average slit width. Since two parameters are used to fit the spectra, it is not surprising that the fit parameter is improved. However, in addition, the precision of the measurement is significantly increased (for unity weighting). The mean temperature is 32° higher than found using 2.7 cm^{-1}. For weighting equals 10, the increase in precision is only a few degrees and the change in the mean from 2.7 cm^{-1} has decreased to only 11 K. Weighting the $v = 1$ peak has a similar effect on the RMS temperature as allowing the slit width to vary. The measured mean temperature will vary with the slit width selected. The strength of the variation decreases with increasing weighting.

If we believe that the rotational and vibrational temperatures are in equilibrium, then we cannot accept 2.2 cm^{-1} as the appropriate slit width at the flame temperature and turbulence level. While there is a small difference between the $s = 2.7$ cm^{-1} slit width (temperature equals 1672 K) and the average temperature using a best fit slit width (1704), this difference essentially disappears when a weighting factor of 10 is used. This combination of variable slit width and weighting factor of 10 yields the best precision (67 K).

The slit width that provides the best fit to the data varies widely. The distribution of the slit widths is shown in Fig. 5. It is surprising to note the "best" slit width varies over a large range from 1.0 $cm^{-1} < s < 3.0$ cm^{-1}. Since the CARS is a nonlinear process, there is no reason to believe that the average best slit is the same as the best average slit width. However, the variable slit should yield a temperature that is invariant with weighting since the individual "best" slits should each exhibit equal rotational and vibrational temperatures.

The magnitude of the change in the mean temperature (for the variable slit) as the weighting is changed is an indication of systematic errors in the CARS system. As described above, if the vibrational temperature and the rotational temperature are in equilibrium, then putting increased emphasis on the $v = 1$ peak should not affect the mean temperature. Since it does, it is indicative of an apparent vibrational temperature that is different than the apparent rotational temperature. The less the mean temperature changes with weighting, the smaller the difference

between the rotational and vibrational temperature. There are three major sources of such a discrepancy: (a) inaccuracies in the spectral libraries; (b) nonlinearities in the detector; and (c) errors in the dye tuning curve.

The small variation of this mean temperature with weighting indicates that the sum of the errors from these three sources is not large. The actual temperature at this burner location can be described by the boundaries of these various "best methods" calculations. That is, the mean temperature is between 1671 and 1704 K. The RMS temperature is best represented by the variable slit with weighting 10, or 67 K.

The major benefit of allowing the slit width to vary is that the slit width need no longer be determined prior to the experiment. It is necessary that the shape of the slit function be determined, as in this case where a shape has been used that can be represented by one variable. Further, the assumptions that the slit function is invariant with temperature and turbulence need no longer be used. This assumption has been verified only in the case of simple flat flame burners, and even then its veracity is model dependent.[12] Also, the alternate methods for determining the mean temperature provide an internal check on the systematic errors of the system. Finally, as an additional benefit, it can be used to improve the precision of the CARS instrument.

IV. ORIGIN OF THE SLIT FUNCTION

The slit function is convolved from many sources, including the pump laser bandwidth and the resolving power of the spectrometer (the classic slit function of the spectrometer) and broadening caused by the detector. However, the limiting resolution is determined by either the spectrometer or the pump laser linewidth.[18] The combined bandwidth for these two sources does not exceed 0.6 cm^{-1} HWHM. The broadband pump laser has a width HWHM < 0.5 cm^{-1}. The spectrometer itself has a resolving power of 0.1 Å at 5000 Å or about 0.2 cm^{-1}. The combination, from the spectrometer and linewidth $(0.4^2 + 0.2^2)^{0.5}$, is about 0.5 cm^{-1} HWHM. This is in full agreement with similar estimates by Eckbreth,[7] and obviously small compared to any of the values measured in our system.

The contribution of the diode array arising from crosstalk has been discussed by Morris and McIlrath[19] and Eckbreth,[7] and for our TN-6132 DARSS, operating well below saturation, is about 1.8 cm^{-1}. To account for a slit width of about 2.5 cm^{-1} would require an additional broadening mechanism with a width of about 1.5 cm^{-1}.

The only other major source of broadening (due to the instrument) is the spatial extent of the CARS signal. As noted by Snelling, Sawchuck, and Smallwood,[20] the width of a room temperature signal will increase with any defocusing of the signal at the detector array. Therefore, the important consideration here is not the actual probe volume, but the size of the image of the probe volume at the detector. In classical spectroscopy, the light is gathered and input to the spectrometer with the appropriate F# through input and output slits. In our CARS experiment no slits are used, but rather the beam is focused at a position where the slits should be, creating effective slits.

The input beam is dispersed (in frequency) by the spectrometer while the spatial characteristics (neglecting diffraction) are refocused at the output (detector). The output spread in space is therefore a function of the beam spread in space, due to frequency, and the beam spread in space, due to the size of the input beam. The detector output is then interpreted as arising entirely from the frequency components in the CARS signal. Following this one step further, the input to the spectrometer is at best the diffraction limited image of the actual source spot of the CARS system. Therefore the instrument function includes a convolution of the probe volume size, modified by the system transfer function.

If we estimate the probe volume following Eckbreth[7] we calculate between 30 and 60 μm diameter (transverse to the propagation direction). In this case the collecting and focusing optics would need to introduce an aberration factor of less than 2 for the output beam to have a spatial extent of about 60 μm. If we use a significantly smaller estimate of the probe volume[21] then optical train would need to produce a proportionately greater aberration to account for a 60 μm diameter. In our detector, this spatial extent would be indicative of a half width of 1.5 cm^{-1} HWHM (based on our DARSS camera and resolution of 25 μm per pixel and 1.24 cm^{-1} per pixel.) It is obvious that this could be a major source of the instrument slit function, as the vector sum of the identified instrument broadening sources $(1.8^2 + 0.6^2 + 1.5^2)^{0.5}$ is 2.4 cm^{-1} and depends on the spatial extent of the CARS signal.

Further, the actual size of the probe volume is highly dependent on the optical path and focussing characteristics of the three beams as they approach the crossing point in the BOXCARS setup. The beam steering and defocusing characteristics of combusting/turbulent media have also been recognized previously. Goss recognized the problem of turbulence[4] and even discussed it in terms of log-amplitude theory.[22] However, Goss worked strictly with collinear CARS geometry to eliminate the difficult problems associated with beam wander and interaction-volume overlap. Bédué *et al.*[23] have noted that beam steering and defocusing can have several effects on the CARS signal, including changing the apparent resolving power of the spectrograph as a result of beam spreading at the plane of the entrance slit. In the BOXCARS geometry, even small changes in focusing or direction can affect the overlap volume and the resultant slit function. Our observation of a varying slit width is consistent with previous observations and theory concerning the probe volume.

V. EFFECT OF WEIGHTING

It has been noted that using a weighting scheme has the advantage of increasing the precision of the CARS system. In general, it has been observed that placing additional weighting on the $v = 1$ portion will reduce the measured root mean square (RMS) temperature. We have shown that the precision of the CARS system can be in-

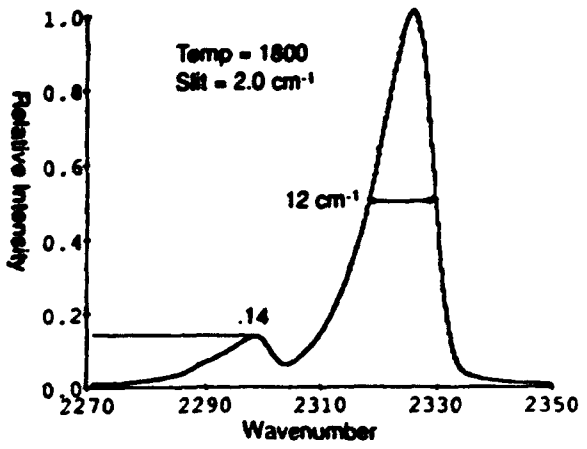

FIG. 6. Effect of slit on width of $v = 0$ peak vs the ratio of $v = 1/v = 0$ shown for HWHM = 2.0 cm^{-1}.

creased without any weighting scheme if the CARS slit width is allowed to vary.

To understand how increasing the weighting of the low-frequency portion of the N_2 vibration spectra increases the precision, consider that the CARS signal is composed of two peaks. The first peak ($v = 0$) contains only information concerning the rotational temperature of the lowest vibrational level. The second peak ($v = 1$) contains information concerning both the rotational temperature of the higher vibrational peak, and also all the information concerning the vibrational temperature. The vibrational temperature is contained in the height (normalized to the first peak), while the rotational temperature is in the width. The slit width (2 cm^{-1}) is narrow compared to the vibrational spacing (30 cm^{-1}) but wide compared to the rotational spacing. It will therefore affect the width of the rotational band more than the ratio of the vibrational band peak heights. Figures 6 and 7 show how two different slit widths produce spectra with significantly different widths in the $v = 0$ band, but with an essentially constant ratio of peak heights ($v = 1/v = 0$). Since the curves are normalized to the maximum signal (always the $v = 0$ peak), forcing the curve to fit the peak height of the $v = 1$, peak height places significant emphasis on the vibrational temperature. The slit width, since it is small compared to the peak spacing, does not change the ratio of the peak heights, but can obviously change the full width at half maximum (FWHM). Increasing the weighting of the $v = 1$ band increases the precision (reduces the RMS) by essentially removing the sensitivity of the CARS instrument to the width of the slit function. That is, by emphasizing the vibrational temperature (not strongly dependent on the slit width) versus the rotational temperature (strongly dependent on the slit width) would result in an increase in the precision in any system where the slit function was not constant.

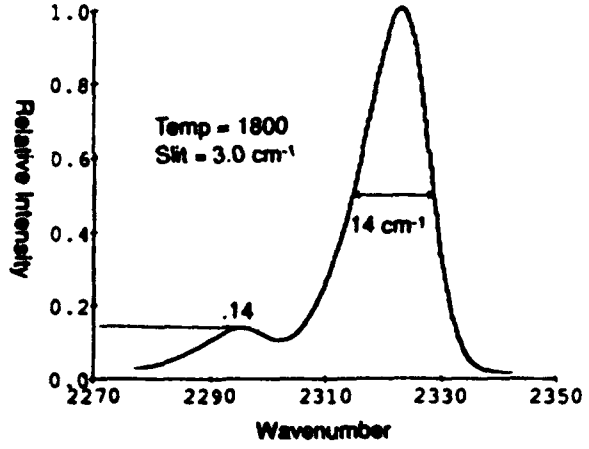

FIG. 7. Effect of slit on width of $v = 0$ peak vs the ratio of $v = 1/v = 0$ shown for HWHM = 3.0 cm^{-1}.

VI. RECOMMENDATIONS AND APPLICABILITY

There has been and continues to be significant effort in the development of CARS as a diagnostic for turbulent combustion systems. Much of this effort is directed towards determination of the slit function, establishing weighting factors for curve fitting routines, and increasing the precision of the CARS systems. The technique described here should be useful to help determine the appropriate slit width, and to increase the precision. In the study of highly turbulent systems, where no physical input slits are used, this technique may be necessary to acquire accurate mean and RMS temperatures.

If signal throughput can be maintained even through narrow slits, the importance of such a correction decreases. Obviously, in the limit that the input slit to the spectrometer goes to zero, the appropriate slit function depends only on the spectrometer, and not on any of the source and focusing optics (assuming that the spectrometer is matched) and would be invariant from shot to shot. As the slits to the spectrometer are opened to increase signal throughput, or if the input F# is too large, then variations of the apparent slit width can occur from shot to shot. The magnitude and importance of these variations will depend on the amount of beam steering and focusing caused by any turbulence of non-linear beam propagation effect. The less turbulent a system, the smaller the slit width variation.

ACKNOWLEDGMENT

This work was supported by the U. S. Air Force Wright Research and Development Center, Aero Propulsion and Power Laboratory, Ohio, under Contract No. F33615-87-C-2767 with W. M. Roquemore serving as Technical Monitor and D. R. Ballal serving as Principal Investigator.

APPENDIX

There have been four basic weighting schemes:

1. Linear least squares—no weighting[1]
   Fitting to a linearized function ln S_v vs $J(J+1)$;
2. Nonlinear least squares—weighting low frequencies[22] minimize $\Sigma(S_i - T_i)^2 w_i$;
3. Nonlinear least squares—minimizing[24]

$\Sigma(\ln S_i - \ln T_i)^2 T_i$;

4. Weighted nonlinear least squares Fit[12]
minimize $\Sigma(S_i - T_i)^2/\sigma_i^2$,

where S_i refers to the signal, T_i refers to the theoretical signal, J is the rotational quantum number, i refers to the particular pixel/frequency, σ refers to the noise associated with the actual signal, $w_i = 1$ if frequency $> 2306\ \text{cm}^{-1}$, $w_i = 1, 4$, or 10 if frequency $< 2306\ \text{cm}^{-1}$.

Weighting scheme 2 has the obvious effect of placing additional weight on the low frequency portion of the N_2 vibrational spectrum. These low frequencies are associated with transitions arising from N_2 in the first excited vibrational state ($v = 1$). Even at 1800 K this portion of the spectrum is only about 15% as strong as the portion resulting from the $v = 0$ population. That is, it places most of the emphasis of the fitting routine on those positions with the weakest signals.

Weighting scheme 3 exhibits a similar tendency as scheme 2 as follows:

5. $(\ln S_i - \ln T_i)^2 T_i = T_i[\ln(S_i/T_i)]^2$;

6. $= T_i \ln(1 + \Delta_i/T_i)^2$, where $\Delta_i = T_i - S_i$;

7. $\cong T_i[1 + \Delta_i/T_i + (\Delta_i/T_i)^2/2]$ and since $\Sigma\Delta_i/T_i = 0$ and ΣT_i is nearly constant;

8. minimizing $\Sigma(\Delta_i)^2/T_i$.

This shows that to first-order approximation, the nonlinear least-square analysis (based on Poisson statistics) is a least-square fit with a weighting factor $= 1/T_i$. This is essentially the same result suggested by Bevington,[25] that the method of maximum probable likelihood using Poisson statistics can be approximated by a least-squares fit (based on Gaussian statistics) with $\sigma_i^2 = S_i$.

It is not obvious that weighting scheme 4 also places increased weighting on the smaller values. However, according to Snelling *et al.*,[12] the CARS noise can be determined as a quadratic function of the CARS signal [Eq. (9)]:

9. $\sigma_i^2 = \text{constant} + kS_i + mS_i^2$. k accounts for shot noise, m accounts for CARS noise.

Since m is difficult to determine, the CARS noise is estimated by 4% of the signal. This method puts less emphasis on pixels with zero signal than does scheme 2, but still tends to emphasize small signals as compared to large signals.

[1] W. B. Roh, P. W. Schreiber, and J. P. E. Taran, Appl. Phys. Lett. **29**, 174 (1976).
[2] A. C. Eckbreth, Appl. Phys. Lett. **32**, 421 (1978).
[3] D. A. Greenhalgh, F. M. Porter, and W. A. England, Combust. Flame **49**, 171 (1983).
[4] L. P. Goss, D. D. Trump, B. G. MacDonald, and G. L. Switzer, Rev. Sci. Instrum. **54**, 563 (1983).
[5] S. A. J. Druet and J. P. E. Taran, Prog. Quantum Electron. **7**, 1 (1981).
[6] R. J. Hall and A. C. Eckbreth, in *Laser Applications*, edited by J. F. Ready and R. K. Erf (Academic, New York, 1984), pp. 213–309, Vol. 5.
[7] A. C. Eckbreth, *Laser Diagnostics for Combustion Temperature and Species* (Billing and Sons, Abacus, Worcester, Great Britain, 1988).
[8] M. A. Yuratich, Mol. Phys. **38**, 625 (1979).
[9] R. E. Teets, Opt. Lett. **9**, 226 (1984).
[10] D. A. Greenhalgh and S. T. Whittley, Appl. Opt. **24**, 907 (1985).
[11] The term precision is used to describe the reproducibility of the instrument, and should not be confused with accuracy. The measured root mean square (RMS) temperature of a known constant temperature source is used as a quantitative measure of the precision of the CARS system.
[12] D. R. Snelling, G. J. Smallwood, R. A. Sawchuck, and T. Parameswaran, Appl. Opt. **26**, 99 (1987).
[13] L. P. Goss, D. D. Trump, and W. M. Roquemore, Exp. Fluids **6**, 189 (1988).
[14] E. E. Zukowski and F. E. Marble, *AGARDograph No. 9, Combustion Researches and Reviews* (Butterworths, London, 1955), pp. 167–180.
[15] T. H. Chen, L. P. Goss, D. D. Trump, and W. J. Schmoll, AIAA/ASME/SAE/ASEE Joint Propulsion Conference, AIAA-88-3194, Boston, MA, July 11–13, 1988.
[16] J. C. Pan, W. J. Schmoll, and D. R. Ballal, Trans. ASME (1991).
[17] S. P. Heneghan, M. D. Vangsness, and J. C. Pan, J. Appl. Phys. **69**, 2692 (1990).
[18] A. C. Eckbreth, *Laser Diagnostics for Combustion Temperature and Species*, (Billing and Sons, Abacus, Worcester, Great Britain, 1988), p. 255.
[19] M. B. Morris and T. J. McIlrath, Appl. Opt. **18**, 4145 (1979).
[20] D. R. Snelling, R. A. Sawchuck, and G. J. Smallwood, Appl. Opt. **23**, 4083 (1984).
[21] S. P. Heneghan and M. D. Vangsness (unpublished).
[22] L. P. Goss and G. L. Switzer, "Laser Optics/Combustion Diagnostics," final report AFWAL-TR-86-2023, Wright-Patterson Air Force Base, OH (1985).
[23] R. Bédué, P. Gastebois, R. Bailly, M. Péalat, and J. P. Taran, Combust. Flame **57**, 141 (1984).
[24] M. Pealat, P. Bouchardy, M. Lefebvre, and J. P. Taran, Appl. Opt. **24**, 1012 (1985).
[25] P. R. Bevington, *Data Reduction and Error Analysis for the Physical Sciences* (McGraw-Hill, New York, 1969).

APPENDIX B

SIMPLE DETERMINATION OF THE WIDTH OF THE SLIT FUNCTION IN SINGLE-SHOT COHERENT ANTI-STOKES RAMAN SPECTROSCOPY

by

Shawn P. Heneghan, Marlin D. Vangsness, and John C. Pan
University of Dayton, Dayton, Ohio

Published in Journal of Applied Physics, Vol. 69, No. 4, pp. 2692-2693, February, 1991.

Simple determination of the width of the slit function in single-shot coherent anti-Stokes Raman spectroscopy

Shawn P. Heneghan, Marlin D. Vangsness, and John C. Pan
University of Dayton, Dayton, Ohio 45469-0110

(Received 27 July 1990; accepted for publication 5 November 1990)

The determination of temperatures using single-shot coherent anti-Stokes Raman spectroscopy normally requires an accurate measurement of the instrument slit function. This slit function is normally determined at a known temperature, and then assumed to be the applicable function at all temperatures and independent of the optical path which varies with density or temperature gradients. In this communication we show a simple method of determining the width of the slit function from the collected data at the actual temperature and turbulence level. This method depends on local thermodynamic equilibrium and is a generally applicable technique to determine the instrument slit function. It is limited to temperatures in excess of 1100 K, as it requires that there be a nonzero signal in the $v = 1$ vibrational level of N_2.

Single-shot coherent anti-Stokes Raman spectroscopy (CARS) has been used to evaluate temperatures in highly turbulent flames[1,2] by comparing actual nitrogen spectra to calculated spectra. The calculation of a nitrogen CARS spectrum requires knowledge of the instrument slit function. To determine the slit function, nitrogen spectra are calculated and compared with spectra collected at a known temperature (often room temperature). The difference between the two spectra is attributed to the instrument slit function, which is then determined and assumed to remain constant, independent of temperature and turbulence level. The correct evaluation of the slit function is critical to the operation of a CARS system.

In recent experiments with enclosed flames, we have gathered significant evidence that the slit function at high temperature and turbulence was not the same function that was applicable at room temperature and no turbulence. Further, the slit function was not independent of the location of the diagnostic volume inside the flame. The variation in slit function can be attributed to changes in the optical path as a result of density and temperature gradients. By applying the principle of local thermodynamic equilibrium (LTE), we have determined a quick and efficient method of calculating the mean and root-mean-square (rms) temperatures and the width of the slit function applicable to the temperature and turbulent conditions under study.

We have determined point-to-point variations in the slit functions of 5%–10%, which would have caused errors in the measured mean temperatures of 15–30 K. This technique is applicable to the study of temperatures greater than 1100 K, but loses sensitivity at lower temperatures, because it depends on a nonzero signal level in the region of 2300 cm^{-1}, the portion of the spectrum associated with $N_2(v = 1)$.

The CARS system is essentially the same as described by Goss *et al.*[1] A box configuration[3] is used to generate the CARS signal, which is collected by a Spex spectrometer, diode array rapid-scanning spectrometer camera, and Tracor Northern multichannel analyzer. The collected signals are stored on tape by a MODCOMP Classic 32/85 computer.

The spectral basis sets are generated using a combination Gaussian and Lorentzian profiles as follows: slit function $= 0.35 \times G \circledast L + 0.65 \times G$, where G is a normalized Gaussian, half width at half maximum (HWHM) $= \sigma$ cm^{-1}, and L is a normalized Lorentzian, HWHM $= 1.8\,\sigma$ cm^{-1}; σ varied from 2.0 to 4.0 by 0.2 increments, and $\circledast$ is meant to convolve. Nearly all the broadening is determined by the Gaussian portion of the slit function. The Lorentzian helps fit the legs of the spectra. Many different shapes have been proposed for the slit function, but is the HWHM which is most critical in determining the temperature, and hereafter the entire slit function will be represented by its Gaussian width (HWHM).

The enclosed flame has been described previously.[4] The bluff-body-stabilized methane flame has an adiabatic flame temperature of about 1755 K. The mean temperature is expected to be near adiabatic in the recirculation zone, while the rms temperature is expected to be under 50 K. The radial profile of the flame is expected to be nearly flat to the edge of the flame[5] (about 23 mm from the center).

We have noted (Fig. 1) that the mean temperature is very nearly a linear function of the Gaussian width (HWHM). A linear relation holds regardless of the weighting used in the least-squares fitting routine for frequencies below 2306 cm^{-1} (those frequencies associated with the nitrogen molecule in vibrational state $v = 1$). Further, the slope of the lines varies with the weighting (curves 2 and 3 of Fig. 1). This same trend, i.e., increasing the weighting on the $v = 1$ peak causing a shift in the mean temperature, was noted by Snelling *et al.*[6] The interesting point in Fig. 1 is the intersection of the three lines, since obviously if the HWHM were selected appropriately, the mean temperature would not change with changing the weighting on the $v = 1$ portion of the spectra.

If we assume that LTE is applicable, then the rotational temperature of the first excited state and ground state must be equal, and further, they must equal the vibrational temperature. In that case, changing the weighting

 0021-8979/91/042692-02$03.00 © 1991 American Institute of Physics

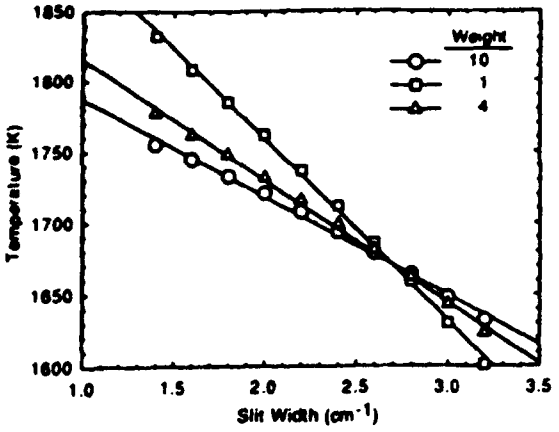

FIG 1 Mean temperatures (K) vs HWHM and weighting.

on the $v = 1$ peak should have no effect on the mean temperature. The only HWHM consistent with the assumption of LTE is the HWHM determined by the intersection of the lines for different weighting schemes.

Table I shows how this method has been used to determine the mean temperature in the bluff body flame, as well as the HWHM which establishes LTE. In general, the mean temperature is measured for two different weighting schemes and two different HWHMs (four measurements). The actual mean temperature and HWHM are calculated by finding the intersection of the two lines (T_{mean} vs HWHM at constant weighting). The mean temperature and rms temperature can be determined by interpolation (extrapolation).

TABLE I. Radial position (R), mean temperatures (K), and slit functions, variation of "best" slit function with position (27 mm downstream).

Weight	R (mm)	Temperature $\sigma = 3.0$	Temperature $\sigma = 2.0$	Intersection HWHM	Intersection Temperature
1	0	1631	1761	2.67	1674
10		1650	1722		
1	4.5	1653	1780	2.67	1695
10		1672	1742		
1	8.9	1649	1777	2.57	1704
10		1674	1744		
1	13.3	1658	1786	2.66	1702
10		1678	1748		
1	15.6	1656	1784	2.61	1706
10		1679	1748		
1	17.8	1666	1793	2.68	1706
10		1684	1754		
1	20.0	1672	1798	2.68	1712
10		1690	1759		
1	22.2	1676	1802	2.70	1714
10		1693	1762		

The measured room-temperature HWHM for this particular optical setup was determined to be about $\sigma = 2.2$ cm^{-1}. The error in using this function versus the intersection position would have been as large as 30 K. The point-to-point error would have been less, but still could have showed artificial temperature gradients caused by treating a changing slit function as constant.

The slit function is an important component in the CARS system analysis, as the mean temperature is directly proportional to the slit width. It has not always been easy to determine the appropriate width of the slit function. This problem may be exacerbated when highly turbulent flames are enclosed in chimneys, as it may be necessary to measure the slit function at the temperature and turbulence intensity of the flame. This HWHM can be easily determined by calculating the mean temperature using two HWHMs and two weighting schemes. The intersection of the two lines (T_{mean} vs HWHM at constant weighting) shows the only HWHM which is consistent with local thermodynamic equilibrium.

Assumptions concerning the constancy of the slit function with temperature and turbulence intensity are inconsistent with the assumption of LTE. The method presented here allows the experimenter to determine the HWHM at every location and thereby guarantees that LTE is maintained.

This work was supported by the U.S. Air Force Wright Research and Development Center, Aero Propulsion and Power Laboratory, Wright Patterson Air Force Base, OH, under Contract No. F33615-87-c-2767 with W. M. Roquemore serving as Technical Monitor and D. R. Ballal serving as Principal Investigator.

[1] L. P. Goss, D. D. Trump, B. G. MacDonald, and G. L. Switzer, Rev. Sci. Instrum. 54, 563 (1983).
[2] A. C. Eckbreth, *Laser Diagnostics for Combustion Temperature and Species* (Billing, Worcester, Great Britain, 1988).
[3] A. C. Eckbreth, Appl. Phys. Lett. 32, 421 (1978).
[4] J. C. Pan, W. J. Schmoll, and D. R. Ballal, Trans. ASME (to be published).
[5] E. E. Zukowski and F. E. Marble, *Combustion Researches and Reviews*, AGARDograph No. 9 (Butterworths, London, 1955), pp. 167–180.
[6] D. R. Snelling, G. J. Smallwood, R. A. Sawchuck, and T. Parameswaran, Appl. Opt. 24, 99 (1987).

APPENDIX C

ACOUSTIC CHARACTERISTICS OF A RESEARCH STEP COMBUSTOR

by

S. P. Heneghan, M. D. Vangsness, and D. R. Ballal
University of Dayton, Dayton, Ohio

A. L. Lesmerises
WRDC, Wright-Patterson Air Force Base, Ohio

G. J. Sturgess
Pratt and Whitney, East Hartford, Connecticut

Published as AIAA Paper No. 90-1851, July 1990. To Appear in AIAA Journal of Propulsion.

ACOUSTIC CHARACTERISTICS OF A RESEARCH STEP COMBUSTOR

S. P. Heneghan[1], M. D. Vangsness[1], D. R. Ballal[1], A. L. Lesmerises[2], and G. J. Sturgess[3]
[1]University of Dayton, Dayton, OH; [2]WRDC, Wright-Patterson Air Force Base, OH;
[3]Pratt and Whitney, East Hartford, CT.

Abstract

For a gas turbine combustor, combustion stability and freedom from acoustic coupling are the two essential design requirements. Here, acoustic characteristics of a research step combustor are investigated by measuring acoustic fluctuations, lean blowout, and visual observations of flame behavior. This combustor was designed to serve as a test bed for evaluating lean blowout and refining combustor design modeling codes.

It was found that inlet conditions, combustor geometry and size, and outlet blockage affected the acoustic characteristics. An acoustic isolator in the fuel tube and a step design that eliminated vortex generation at the inlet significantly decreased acoustic coupling. For a long combustor (L/D = 7.3), loud acoustic resonances resembling classic "rumble" were produced. In this combustor dominant frequencies around 55 Hz and 170 Hz were observed corresponding to eddy shedding from the step and the quarter-wave longitudinal mode respectively. The short combustor (L/D =3), simply did not exert enough back pressure to confine a steady burning flame. In general, top-hat outlet restrictors produced noisier combustion than orifice plates. Finally, a research step combustor with L/D = 4.9 and fitted with an orifice plate of blockage ratio = 0.45 provided the best combination of LBO and freedom from acoustic coupling. This combustor operated satisfactorily under all the conditions of interest and its LBO performance resembled that of a well-stirred reactor.

Nomenclature

A	=	cross sectional area (o-outlet, c-combustor)
ALP	=	air loading parameter (m/VP^n)
B	=	outlet area blockage ratio (A_o/A_c)
D, d	=	equivalent diameter, obstacle dimension
f	=	frequency (o-fundamental, h-harmonic)
I	=	intensity, amplitude
L	=	combustor length
LBO	=	lean blowout
LPM	=	litres per minute
m	=	mass flow through the combustor
n	=	reaction order, number
P	=	pressure
Re	=	Reynolds number
St	=	Strouhal number
U	=	mean velocity (a-air, f-fuel, j-jet)
V	=	combustor volume
v	=	volume flow rate (a-air, f-fuel)
x	=	axial distance
ϕ	=	equivalence ratio
λ	=	wavelength, velocity ratio (U_a/U_f)
ν	=	kinematic viscosity

Copyright © 1990 American Institute of Aeronautics and Astronautics, Inc. All rights reserved.

1. Introduction

An essential requirement in the design of new stoichiometric combustors and high thrust output afterburners is that steady combustion can be initiated and sustained over a wide range of flight conditions. Combustion-induced oscillations commonly known as *rumble* and *screech* severely limit the flame stability range of practical combustors. They can also compromise hot-section durability, induce mechanical vibrations in the engine-airframe components, and couple with the aerodynamics of other engine modules. Therefore, knowledge of acoustic characteristics of combustors is important from a design viewpoint.

The provision of adequate combustion stability, and freedom from acoustic coupling in aircraft gas turbine combustors is a long-term problem that is exacerbated by several current design trends. Further, the solution to this problem is made difficult by deficiencies in present calculation methods and by conflicting design criteria. Therefore, a joint U. S. Air Force, Industry, and University research program is being carried out to (i) study acoustic coupling and its effects upon the combustor performance, (ii) improve understanding of the physical processes involved in lean blowout (LBO), and (iii) evaluate and refine the combustor design modeling codes on the basis of experimental measurements.

In a modern annular gas turbine combustor, flame is stabilized by producing a recirculation zone in the flowfield. As shown in Fig. 1, this zone is formed by a combination of *three* mechanisms, namely an axial swirling air jet associated with each fuel introduction, sudden expansion of the axial swirling jets as they enter the primary zone, and back-pressure provided by an array of radial air jets at the end of the primary zone. To achieve low unburned hydrocarbon emissions, Pratt & Whitney currently tailors these combustor flow control mechanisms to produce an "inside-out" recirculation pattern, as illustrated in Fig. 1. Recently, Sturgess et al. [1] designed and developed a research step combustor that reproduces the recirculation pattern of the practical combustor, and closely simulates those essential features of its flowfield that control flame stability and lean blowout. This combustor is geometrically simple for ease of experimentation and computation, and provides adequate optical access for nonintrusive measurements. Its configuration and dimensions represent a series of compromises between different design criteria.

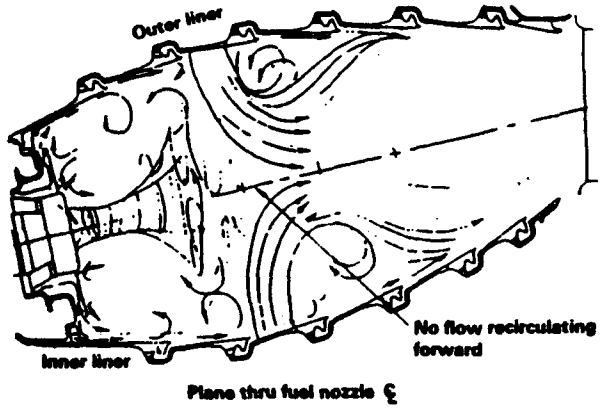

Fig. 1: Flow patterns in a modern annular combustor showing swirl and recirculation dominating the "inside-out" primary zone.

This paper describes *three* design stages in the development of the research step combustor. Acoustic analyses of the combustor prior to its manufacture were made using the lumped impedance-admittance techniques of Putnam [2] and also by the MSC/NASTRAN finite element code. These analyses suggested potentially strong acoustic coupling between the combustor, fuel tube, and the step. Acoustic characteristics of each design configuration were measured and improved upon (decoupled) in the subsequent design stage until a *final* design of the research combustor emerged that was relatively free of acoustic coupling effects. Experimental measurements of acoustic pressure fluctuations, lean blowout, and visual observations of the flame behavior are reported.

2. Research Step Combustor

Configurations: Figures 2a-c show *three* configurations of the research combustor, three step designs, and a schematic diagram of the vertical wind tunnel which supplies reactants to the combustor. Common to all the combustor configurations is an arrangement of coannular air (40 mm O. D.) and fuel (27 mm I. D.) jets that feed air and gaseous propane to a 55-mm-wide sudden expansion step. The step establishes a recirculation zone which increases residence time, recycles hot combustion products, and thus provides a source of continuous ignition for the incoming cold reactants. In this manner, a flame is stabilized in the research combustor. The combustor is 475 mm long, 150 mm square cross section with rounded corner fillets of 84 mm radius, and has glass windows on all four sides for optical access. On the top of this combustor sits an inconel chimney extension, of either 508 mm or 260 mm length. The chimney may be fitted, at its exit, either with a top hat (Fig. 2a) or with an orifice plate (Fig. 2c) of different blockage ratios. This outlet restriction exerts a specific amount of back pressure for stabilizing the confined flame.

As illustrated in Fig. 2a, the research combustor is bolted to a 150 mm I. D., 200 mm long tube with a bellmouth annular inlet that supports the step. This tube is mounted on top of a vertical wind tunnel that supplies reactants to the

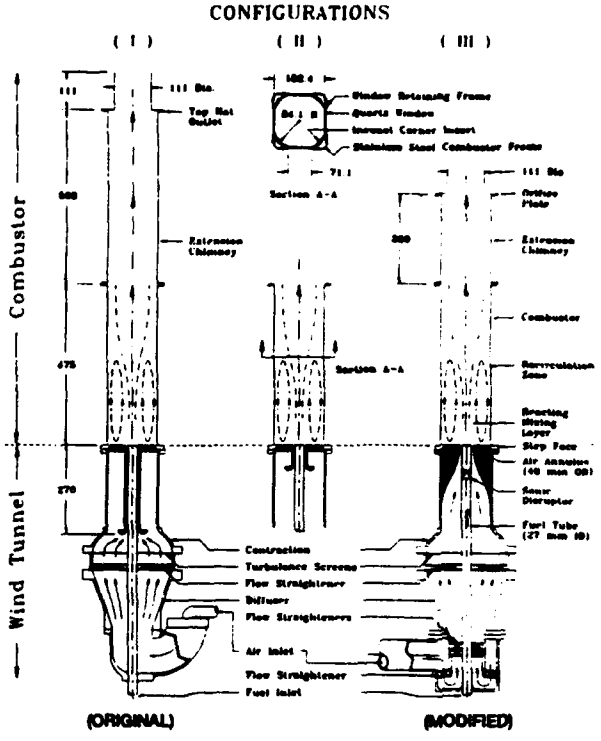

Fig. 2: Various configurations of the combustor, step, and vertical wind tunnel: (a) combustor configuration I-long combustor, (b) combustor configuration II-short combustor, (c) combustor configuration III-final (optimized) combustor.

research combustor. Figure 2b shows the research combustor with its plan view and a short inlet step. In Fig. 2c, the combustor is fitted with a short extension, an orifice plate, and a step having a smooth convergent inlet.

Figures 3a-b illustrate the influence of outlet configuration on the static pressure distribution along the combustor wall. Both these figures show plots of $\Delta P = (P_{atm} - P)$ vs. downstream distance. It is evident from Fig. 3b that outlet blockage causes atmospheric pressure to be attained well inside the combustor due to the *vena contracta* formed in the outlet restrictor. This terminates the combustion process and also defines the exit boundary condition for CFD calculations.

In general, combustion in any of the above combustor configurations can exhibit sensitivity to various physical processes such as:

(1) Transition from laminar to turbulent flow due to variation in throughput rate of reactants;

(2) Flame shifts due to pressure gradients created by step size, combustor length, outlet configuration, and stoichiometry;

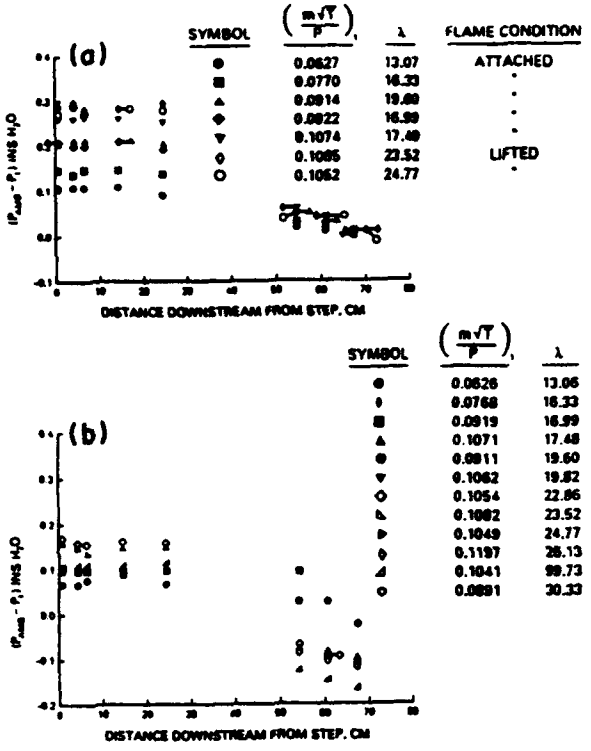

Fig. 3: Axial distribution of wall static pressure for reacting flow: (a) Pressure distribution with free outlet, (b) Pressure distribution with orifice plate (B = 0.45).

(3) Acoustic coupling that depends upon disturbances in the inlet streams, combustor length, inlet/outlet configuration, operating conditions, and flame type and location;

(4) Opposing effects of combustor back-pressure and acoustic resonance in the combustor;

(5) Opposing effects of chemical reaction-rate control and mixing-rate limit for a non-premixed flame.

Past Work: A good deal of research has been performed on the acoustic waves created by combustion in long pipes, multiple-port burners, residential heating units, and oil fired furnaces. This work is summarized by Putnam [2] and others [3-6]. Some of these instabilities can be predicted reasonably well by the Rayleigh criteria [2]. In contrast, practical combustors, some research combustors such as the one under investigation, and afterburners have complex flowfields with recirculation zones and swirl, elaborate fueling arrangements, and cross sections of varying shapes. The acoustics of these devices is unique and depends upon flow pattern, equivalence ratio, and hardware configuration. Research in this area is of relatively recent origin [7-10] and leads to a conclusion that significant differences in acoustic characteristics are realized with even *minor* changes in combustor configuration. Therefore, a combination of careful experimentation and phenomenological analyses was used to investigate the acoustic characteristics and then eliminate acoustic coupling in our research step combustor.

3. Acoustic Characteristics

Experimental Setup: Tests were made of the various research combustor configurations shown in Fig. 2. Gaseous propane and methane were used as fuels. Ignition was accomplished by means of a removable propane torch which protruded through a hole drilled in one wall of the combustor. A steady continuous blue flame filling the combustor indicated good combustion stability and relative freedom from acoustic coupling. The fuel burned in the reacting mixing layer (see Fig. 2c) to which the step recirculation zone fed hot products of combustion. For methane, flame could not be stabilized, even with complete tunnel length and a large outlet blockage. Acoustic frequency spectra were measured using a microphone and Kistler pressure transducers (Model 211 B5 series). These pressure signals were fed into a dual-channel FFT Spectrum Analyzer (Nicolet Model 660) the output of which was connected to a chart recorder (Hewlett-Packard Model HP 7035B). Acoustic spectra were recorded for several combinations of combustor inlet conditions, step and fuel tube designs, combustor lengths (475-983 mm), outlet restrictions (top-hats or orifice plates with B = 0-62%), and fuel and air flow rates given by Re_a = 2.5-10.5 x 10^4 and Re_j = 0.37-1.46 x 10^4 respectively.

Vertical Wind Tunnel

Acoustic Characteristics: As seen in Fig. 2, the research combustor-wind tunnel combination has a very complex geometry. Moreover, at an early stage, it was recognized that any air and fuel flow fluctuations produced within the wind tunnel itself would be amplified by the combustion process confined by the combustor. Initially, the wind tunnel shown in Fig. 2a was being supplied with a 25-mm-dia. line dumping air into a 100-mm-dia. U-shaped inlet. Two pressure transducers, one mounted in the wind tunnel air inlet, and the other at its exit, revealed the acoustic spectra shown in Fig. 4. The frequency peaks of 260, 390, 660, and 837 Hz were present in the wind tunnel (Fig. 4a). The amplitude of these peaks increased with an increase in airflow rate. When the research combustor configuration I was mounted on the top of this wind tunnel, additional frequency peak at 55 Hz appeared in the acoustic spectra (Fig. 4b). As will be explained later, this frequency is associated with the eddy-shedding frequency inside the combustor.

Acoustic Sources and Modifications: The acoustic fluctuations in the wind tunnel were traced to three sources, namely (i) sudden expansion of the airflow from the 25-mm-dia. flexible hose to the 100-mm-dia. U-shaped inlet produced extensive and periodic flow vortices, (ii) vortex shedding at the bell-mouthed entrance of the step, (iii) a short aggressive diffuser (area ratio = 2.172, included angle = 15°) which is not uniformly filled with the airflow at its entrance.

To significantly reduce, if not to totally eliminate, these acoustic fluctuations, the following design modifications to the

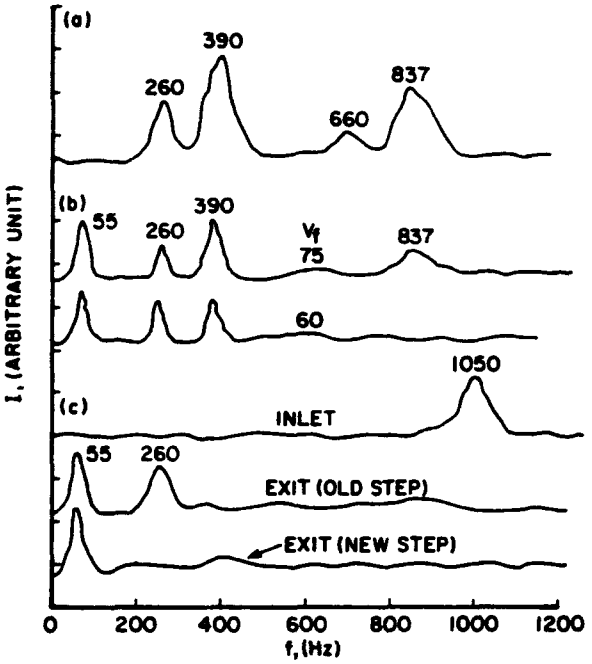

Fig. 4: Acoustic characteristics of the vertical wind tunnel: (a) Wind tunnel only (v_a = 1100 LPM), (b) Wind tunnel + Combustor configuration I + Outlet top-hat (B = 0.45) at v_a = 3200 LPM, (c) Modified wind tunnel (v_a = 3200 LPM)

wind tunnel were made. First, the 25-mm-dia. flexible air supply hose was replaced by a 7-m-long, 100-mm-dia. pipe. This pipe was connected to a newly designed 90 ° air inlet section sketched in Fig. 2c. This modification eliminated any sudden flow expansion and periodic vortex shedding. Second, the step intake length was shortened as shown in Fig. 2b to trap the toroidal shed vortex into a dead space just upstream of the combustor. Finally, an additional set of honeycombs and a flow straightening screen were added, just at the entrance to the short diffuser to improve the inlet airflow distribution. Figure 4c shows the acoustic characteristics of this modified wind tunnel. It can be seen that all frequencies, except the lowest one (260 Hz), have been eliminated.

As for the acoustic peak at 260 Hz, the following explanation is offered: vortex shedding off an obstacle (of the type presented by the bell-mouthed step entrance) usually has a Strouhal number, St = f d/U in the range 0.2 to 0.4. For an annulus air velocity of 35 m/s and the bell-mouth step width of 25.4 mm, vortex shedding frequencies fall in the range 177-354 Hz, or a mean value of 265 Hz represents the vortex shedding frequency of eddies shed off the entrance obstacle. It was recognized that this frequency was sufficiently low to interfere with the acoustic characteristics of our combustor. Therefore, and as shown in Fig. 2c, a new step was designed to eliminate the trapped vortex. Acoustic characteristics measured with the new step in place are plotted in Fig. 4c. These show an absence of any peak at 260 Hz. Finally, this new and modified wind tunnel was employed in the acoustic characterization of the following three combustor configurations.

Combustor

Acoustic Characteristics-Combustor Configuration I: Tests were performed on the research step combustor-configuration I shown in Fig. 2a. Acoustic frequency spectra were recorded for many combustor design and operating variables, such as different fuel and air velocities, fuel tube diameters, extension chimney lengths, and outlet blockage. When the flame was stabilized in the shear layer close to the fuel tube exit, combustion-generated noise increased dramatically. An oscillatory mode of burning was also observed in the vicinity of lean blowout (LBO). This oscillatory cycle comprised flame extinction in the shear layer, downstream re-ignition, flashback, shear layer burning, shear layer extinction, and so on. In the results plotted in Fig. 5, dominant frequencies around 55 Hz, 170 Hz, 390 Hz, and 850 Hz were observed.

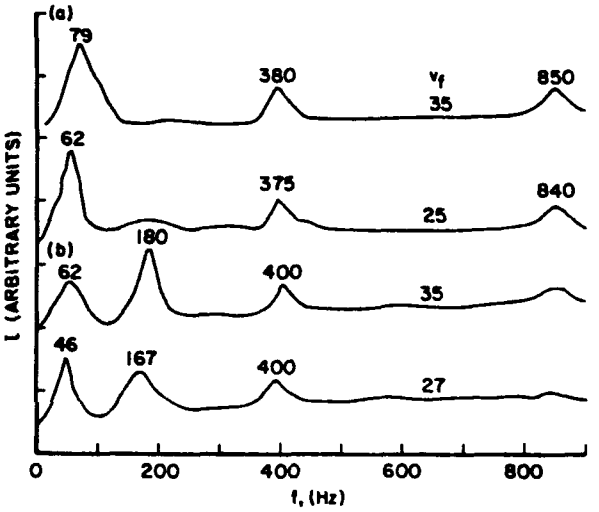

Fig. 5: Acoustic characteristics of the research step combustor configuration I at v_a = 1000 LPM: (a) Top-hat outlet (B = 0.45), (b) Orifice plate outlet (B = 0.45).

Acoustic Sources and Modifications: As described below, the frequency peaks noted in Fig. 5 correspond to eddy-shedding off the step, fundamental quarter-wave longitudinal acoustic mode for the combustor, and the two frequencies originating in the vertical wind tunnel. These latter frequencies coincide with the *calculated* organ-pipe harmonics of the 55 Hz frequency. Thus, the combustor-wind tunnel system was closely coupled and the Rayleigh criterion was being satisfied so that the oscillations were driven [2]. This meant that even the frequencies of 390 Hz and 837 Hz, well suppressed by the wind tunnel design modifications, were slightly augmented by the combustion process. To decrease the magnitude of all the observed acoustic fluctuations, various alternatives were considered, such as switching air and fuel flow lines and designing a tri-jet system. However, it was concluded that the acoustic isolation of the fuel tube from the combustor was the single best modification that would drastically attenuate noise and decrease acoustic coupling. Some experimental evidence that such a modification would work was available in the work of Whitelaw and coworkers [7-9]. These workers found

that by locating an orifice close to the pressure node, in the upstream duct, about one quarter of the wavelength from the dump plane, radiated sound intensity decreased by around 10 dB. Thus, it became clear that our modification should (i) eliminate line-of-sight access between fuel tube inlet and combustor inlet to prevent propagation of acoustic waves, (ii) decrease inlet length and thereby shift acoustic oscillations to higher frequencies, corresponding to the frequency of the quarter-wave mode for the new effective inlet length, (iii) add pressure drop to the fuel system to damp the acoustic over-pressure propagating from the combustor.

Various acoustic isolation schemes such as plugging the fuel tube with steel wool and/or ball (BB) shot were tried. Although these damped the acoustic fluctuations satisfactorily, they would not pass LDA seed particles through the tube. Finally, a perforated conical cap was designed as shown in Fig. 6, and fitted inside the fuel tube about 125 mm upstream of its exit. This device was very successful at acoustically decoupling the fuel tube from the vortex shedding frequency of 55 Hz in the main combustor. It significantly reduced the combustor noise and vibration. However, there was a trade-off in that the 125 mm (12% tube length) section of the fuel tube is still acoustically coupled. This length of the fuel tube is required for the fuel flow to develop a uniform velocity profile prior to issuing out into the combustor.

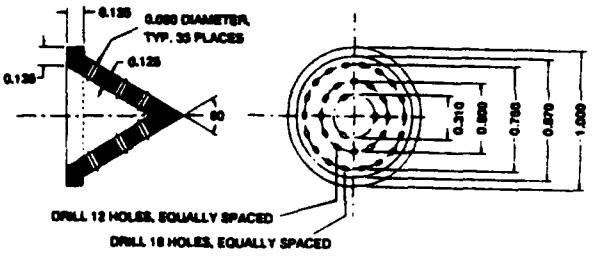

Fig. 6: Sketch of a perforated conical cap used for the acoustic isolation of the fuel tube from the main combustor.

Further tests, with the above modifications in place, still produced disappointingly loud acoustic resonance resembling the classic gas turbine combustor *rumble*. Also, the noise level increased with an increase in the reactant mass flow through the combustor, and as LBO was approached. Moreover, it visibly affected the flame lift and stability. Cylindrical combustors with long aspect ratios (L/D > 3) are generally known to be strongly susceptible to classic organ-pipe resonances [10] and lead to interesting side effects such a flame flashback [11].

In their work on axisymmetric dump combustors and gas turbine augmentors, Sivasegaram and Whitelaw [7] and Sivasegaram, et al. [8] have observed rough combustion and low-frequency oscillations around 55 Hz. For combustors with L/D > 6, these authors have suggested that the dominant frequency may be associated either with vortex shedding or with acoustic quarter-waves in their combustor.

The effects of large-scale eddy shedding and the acoustic-vortex interactions produced in Ramjet-type dump combustors are further elucidated by Kailasanath et al. [12, 13] and Schadow et al.[14]. In their earlier work, Kailasanath et al.[12] find a strong coupling between the first longitudinal acoustic mode frequency of 446 Hz and the unforced natural vortex shedding at 405 Hz. In their later work [13], the acoustics of both the inlet and the combustor are coupled. A low-frequency oscillation of 150 Hz, corresponding to the quarter-wave mode in the inlet, is observed and changing the inlet length changes this frequency. The merging patterns of the large-scale shed vortices are modified significantly [13, 14] when either the combustor acoustic mode or the inlet mode is changed.

For the combustor configuration I under study here, small air annulus passage and acoustic isolation of the fuel tube suggest that effectively the combustor dome region is acoustically closed. Depending upon the exit blockage, the combustor exit would be either acoustically open or closed. Assuming a uniform temperature in the combustor configuration I, a quarter-wave longitudinal acoustic frequency of 170 Hz was calculated. This suggests that the lowest frequency of 55 Hz detected by the pressure transducer is *not* the quarter-wave longitudinal frequency.

There is an additional non-stationary process present in the combustor, and that is the eddy-shedding off the step. For a Strouhal number in the range, St = 0.2-0.4, and assuming that the characteristic velocity is equal to the velocity of jet shear layer (or annulus air velocity) we obtain the calculated range of eddy shedding frequency as 40-90 Hz. In general, and as shown in Fig. 5, increasing the fuel flow (or combustor heat release) pushed the shedding frequency higher (up to 79 Hz) and also increased its amplitude. At high airflow rates (above 2000 LPM) and with large outlet blockage (> 45%) shedding frequency was as high as 90 Hz. Without or with top hats (B = 45%), the observed shedding frequency was in the range 45-63 Hz, i. e., the mean observed value was close to 55 Hz. In contrast to the observations of Kailasnath et al. [12], coupling between shedding frequency and the quarter-wave frequency did not occur in our combustor.

Acoustic Characteristics-Combustor Configuration II: To eliminate these resonances, we performed tests with a short (L/D < 3) configuration II combustor as sketched in Figure 2b. These tests were with ϕ = 0.76, Re_a = 24,827, Re_j = 6,027 and U_a/U_j = 26.2. It was observed that peaks in the frequency spectra for both combustor configurations I and II were the same despite the length reduction which should have produced higher frequencies. Finally, even with a large outlet blockage of 0.62, the combustor behaved as though it had an acoustically open outlet.

When the magnitude of the acoustic phenomena is considered, the amplitude of lowest frequency of 55 Hz was almost 5-10 times lower for a short combustor than for a long

combustor. For both the combustors I and II, amplitude of low frequency peaks sharply at the 45% outlet blockage condition. Now, since any resonance is destabilizing, it was expected that the shorter combustor (configuration II) would exhibit better stability than the longer combustor (configuration I) and LBO's would be clear and consistent. In practice, while the latter observation is found to be valid, the results of Fig. 7 show stability trends opposite to what was expected. A main reason is that the configuration II combustor was too short to contain the flame for equivalence ratios greater than lean blowout, and considerable back pressure was required to sustain burning in the combustor. Both Sivasegaram and Whitelaw [7] and Sivasegaram et al. [8] make similar observations with regard to flame holding in a short combustor ($L/D < 2$). For this reason, combustor configuration III of Fig. 2c was finally examined.

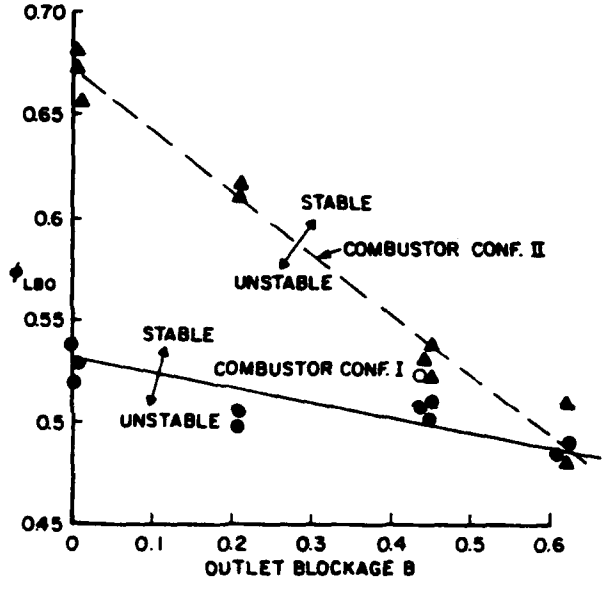

Fig. 7: Combustion stability (as measured by ϕ_{LBO} vs. B) of combustor configurations I and II in the near-turbulent flow regime (Re_a < 23,000). Note that m/VP' $(U_a - U_f/U) = 0.8$ configuration I and = 1.6 for configuration II.

Acoustic Characteristics-Combustor Configuration III: In all the tests, we observed that this combustor configuration operated at significantly reduced noise levels and exhibited much steadier combustion. As seen in Fig. 8a, acoustic spectra showed that the quarter-wave longitudinal mode frequency increases from 190 Hz to 222 Hz as the fuel flow is increased above its value for the LBO. These observations essentially remained valid even when the airflow was increased and when the shorter extension chimney was fitted with different outlet blockage (see Fig. 9). Figure 8b shows a comparison between the acoustic characteristics of combustor configurations I and III. It is observed that for combustor configuration III, peaks in the acoustic spectra exist at significantly higher frequencies, well above the eddy shedding frequency. This acoustic decoupling greatly attenuates the low-frequency *rumble* in this combustor configuration III. Moreover, for airflow rates all the way up to 7,000 LPM, combustor configuration III maintained a marked reduction in acoustic output at the step shedding frequency. Therefore, this configuration was adopted for further studies on the choice of a suitable combustor outlet configuration.

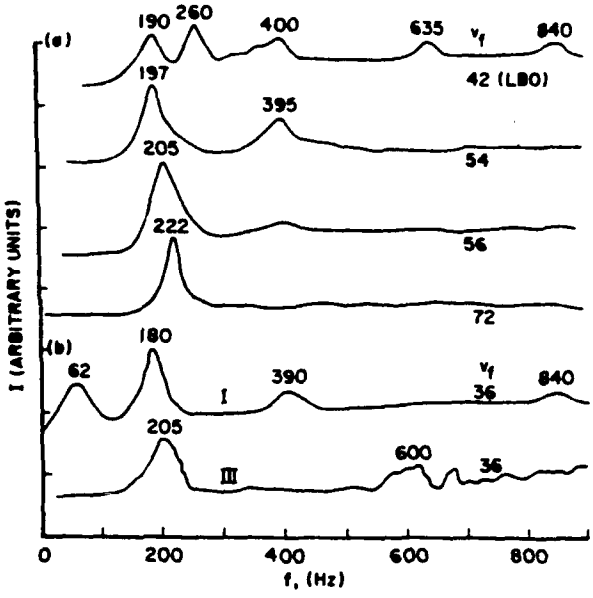

Fig. 8: Acoustic characteristics of the research step combustor configuration III with an orifice plate outlet (B = 0.45): (a) Effect of increasing the fuel flow rate at v_a = 2000 LPM, (b) Comparison of combustor configurations I and III at v_a = 1500 LPM.

Outlet Configuration: In deciding the optimum combustor outlet configuration, whether fully open, orifice plate, or short top-hat, the following *four* positive and *three* negative considerations come into play:

(1) back pressure stabilizing the flow in the step recirculation zone,

(2) outlet restriction accelerates the flow and terminates the chemical reactions for fuel-lean mixtures,

(3) top-hat configuration imposes the zero streamline gradient exit boundary condition for CFD calculation,

(4) the top-hat behaves as a high impedance to low-frequency pressure changes,

(5) outlet restriction necessitates additional combustor length to prevent the exit streamline curvature from influencing the step recirculation zone,

(6) outlet restriction produces acoustically closed exit boundary,

(7) outlet restriction provides a hot, potential source of reignition at LBO.

The combustor was run with three outlet configurations: free (B = 0), orifice plates (B = 0.45, 0.62), and top hats (B = 0.45 with L/D = 1 and 2.1). The following observations were made.

In general, the top hats resulted in noisier combustion than did the orifice plates. In Fig. 9, it is seen that for equal outlet blockage (i) orifice plate produced a broader acoustic frequency spectrum than the top-hat outlet, (ii) for an orifice plate, peaks in the acoustic spectra (205 Hz and 600 Hz) were found at a higher frequency than for a top-hat (140 Hz and 515 Hz). For an outlet blockage of 62%, both, top-hat and orifice plate were so loud that the combustor could not be operated comfortably over a long period.

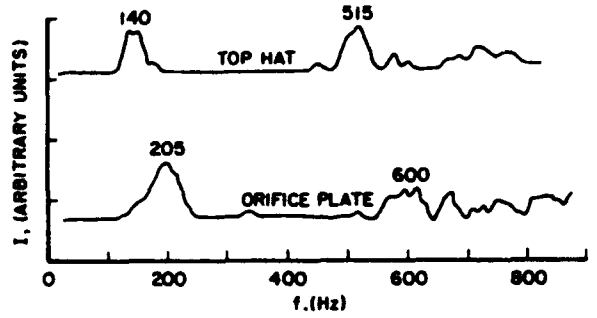

Fig. 9: Acoustic characteristics of top-hat and orifice plate outlet restrictions of same blockage ratio (B = 0.45) for combustor configuration III (v_a = 1500 LPM, v_f = 36 LPM).

Given the propensity of the top-hat restrictors to produce large acoustic fluctuations with strong peaks, and the requirement of the combustor to provide flame stability over a broad range of air and fuel flows, a choice of orifice plate with B = 0.45 was made. This choice was dictated by the conflicting requirements of low noise (B < 0.62), good flame stabilization (B > 0.21), and for achieving fully turbulent burning conditions without producing axial instability of the flame or LBO. In this way, the final configuration of the combustor for stable operation and relative freedom from acoustic coupling was arrived at.

4. Combustor Performance

Lean Blowout: The research combustor was designed to study LBO and other combustion processes such as attached flame, lifted flame, and large-scale axial instability eventually leading to LBO. Accordingly, visual observations of the flame, and a series of measurements of LBO, wall static pressure distribution, and wall temperature distribution were made. A wide range of fuel and air flows from semi-laminar to fully turbulent regime (Re_a = 2.5-10.5 x 10^4, and Re_j = 0.37-1.46 x 10^4) were investigated.

Figure 10 illustrates the LBO vs. air loading parameter (ALP) characteristics of this combustor. These values of LBO are in general agreement with experimental data from other well-stirred reactors [1]. Also, they are lower than the LBO values for combustor configurations I and II. This is because the acoustic fluctuations present in combustor configurations I and II augment flame instabilities in the combustor and cause premature LBO.

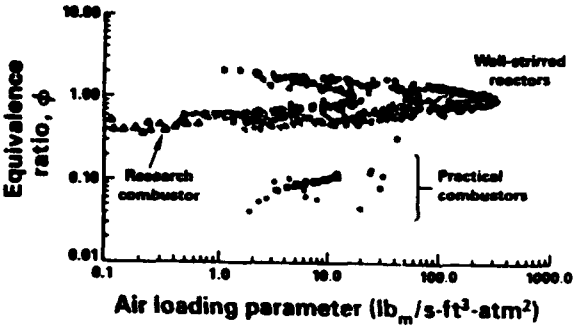

Fig. 10: Lean Blowout performance of the research step combustor as compared with the well-stirred reactor and practical gas turbine combustors.

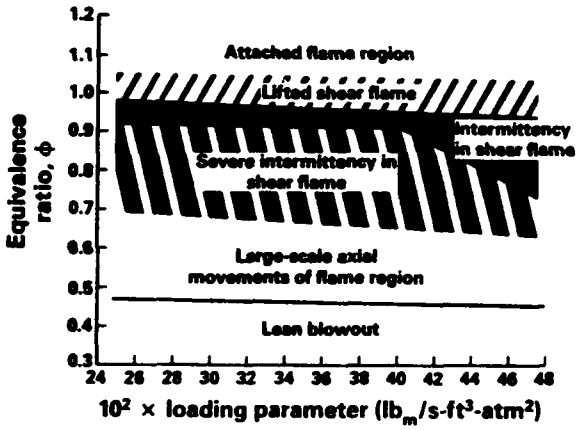

Fig. 11: Research step combustor performance illustrating the different flame regimes that eventually lead to LBO.

Flame Regimes: The flame features that appear in the combustor prior to LBO are sketched in Fig. 11. At a given airflow or ALP, a corresponding fuel flow can be found at which a distinct flame attaches itself around the inner edge of the step. This so called "attached flame" region is realized in our combustor for or above stoichiometric overall equivalence ratios. Also, the flame attachment is found to be very sensitive to acoustic fluctuations. An intense blue annular flame, in contact with the attached flame and anchored by it, appears in the jet shear layer region. The resultant flame structure has the appearance of an inverted "classic coke bottle" shape and is remarkably stable a little downstream of the confluence of the fuel and air jets. As the overall equivalence ratio falls below 0.9, the lifted shear flame develops severe intermittency, becomes ragged in appearance, and resembles a typical "turbulent flame brush." Below ϕ = 0.65, large-scale, oscillatory axial movement of the flame begins and this

eventually leads to LBO. Finally, as the ALP is increased, it is seen that the limits of each region are narrowed, each region intrudes sharply into the adjacent region, and eventually LBO occurs almost instantaneously.

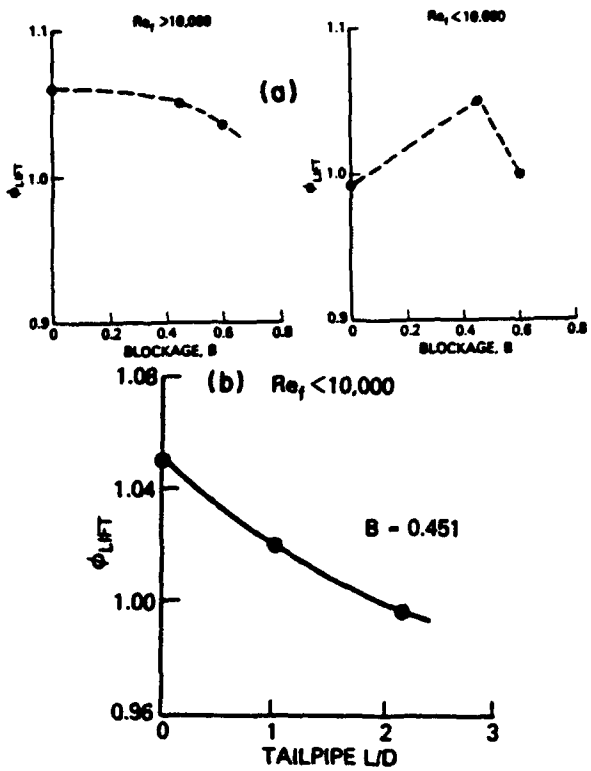

Fig. 12: Effect of outlet blockage, B on equivalence ratio for flame lift: (a) Orifice plate blockage, (b) Influence of top-hat aspect ratio.

The flame characteristics shown in Fig. 11 are influenced by the outlet blockage and the type of this blockage. For example, Fig. 12 compares equivalence ratios at flame lift for orifice blockage and for top-hat L/D at fixed blockage. These results show that the 45% blockage top-hat with a L/D = 2.11 and a 60% blockage orifice plate have the same ϕ_{lift}. Figure 13 shows the effect of orifice blockage on the equivalence ratio for the onset of large-scale axial movements of the flame that are an immediate precursor to blowout. A comparison between the data plotted in Figs. 12 and 13 shows the stabilizing effect of back pressure on combustion (low ϕ_{lift}) and the destabilizing effect of increased acoustic activity (high ϕ_{axial}).

5. Concluding Remarks

In this paper, we explored *three* combustor configurations and found influences of combustor upstream conditions, combustor geometry, combustor outlet blockage, and, to a minor extent, fuel/air flow conditions, on the acoustic characteristics of a research combustor. Broad similarities to the observations of other researchers [7, 10, 13, 14] were noted, and at the same time acoustic characteristics unique to our research step combustor were highlighted. Since this

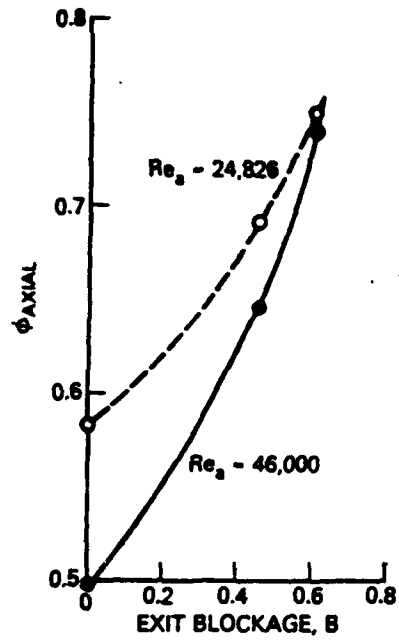

Fig. 13: Influence of orifice plate outlet blockage, B on the equivalence ratio for the onset of axial instability in the lifted flame.

research combustor simulates certain features of a practical gas turbine combustor, similar effects are likely to be present in practical combustors to a varying degree. This is especially disconcerting because the provision of steady combustion and freedom from acoustic coupling are the two main requirements of a good combustor design, be it a swirl combustor [7], a bluff body combustor [8], or a ramjet combustor [10].

We noted that both the fuel supply and the air supply had to be acoustically isolated from the main combustion process to significantly decrease acoustic coupling. In a modern annular gas turbine combustor, air swirl vanes and fuel metering inside the fuel injector provide the necessary acoustic isolation. However, and unless the air supply is sonically isolated from the combustion zone, combustor *rumble* or *screech* may be produced. Generally, the pressure drop across the combustor liner is low enough that the air boundaries for inflow are acoustically soft so that resonances can occur. Next, the aspect ratio (L/D) of the practical combustor should be well below 5 to prevent the generation of acoustic standing waves and quarter-wave longitudinal type resonances. While, the modern annular gas turbine combustor falls well within a safe range of aspect ratio, some types of the newer dual-stage combustors for low exhaust emissions may be approaching the upper limit of the safety criteria. Finally, most practical combustors provide sufficient back pressure to main a stable flame in the combustor. This is achieved by blocking the outlet via a smooth exit contraction or a turbine nozzle stator guide vane. All these design features contribute to producing favorable acoustic characteristics for the practical combustors.

The understanding of the acoustic characteristics of the research combustor and the subsequent development to eliminate spurious interactions have resulted in a vehicle that is well suited for its intended purpose of investigating flame stability with reference to aircraft gas turbine engines.

Acknowledgment

This work was supported by the U. S. Air Force, Wright Research and Development Center, Aero Propulsion and Power Laboratories, under Contract No. F33615-87-C-2767 to University of Dayton, Dayton, Ohio, (Monitor: Dr. W. M. Roquemore) and Contract No. F33615-87-C-2822 to Pratt and Whitney Aircraft, East Hartford, CT., (Monitor: 1Lt. A. L. Lesmerises).

References

1. Sturgess, G. J., Sloan, D. G., Lesmerises, A. L., Heneghan, S. P., and Ballal, D. R., "Design and Development of a Research Combustor for Lean Blowout Studies," ASME Paper No. 90-GT-143, To appear in *Transactions of ASME, Journal of Engineering for Gas Turbines and Power*, 1990.

2. Putnam, A. A., *Combustion Driven Oscillations in Industry*, Elsevier, New York, 1971.

3. Blackshear, P. L., Rayle, W. D., and Tower, L. K., " Study of Screeching combustion in a 6-Inch Simulated Afterburner," *NACA TN 3567*, 1955.

4. Kilham, J. K., Jackson, E. G., and Smith, T. J. B., "An Investigation of Tunnel Burner Noise," *Institution of Gas Engineers Journal*, Vol. 1, pp. 251-266, 1961.

5. Marble, F. E., and Candel, S. M., "An Analytical Study of the Nonsteady Behavior of Large Combustors," *Seventeenth Symposium (International) on Combustion*, The Combustion Institute, Pittsburgh, PA, 1978, pp. 761-770.

6. El Banhawy, Y., Melling, A., and Whitelaw, J. H., "Combustion Driven Oscillations in a Small Tube," *Combustion and Flame*, Vol. 33, pp. 281-290, 1978.

7. Sivasegaram, S., and Whitelaw, J. H., "Oscillations in Axisymmetric Dump Combustors," *Combustion Science and Technology*, Vol. 52, pp. 413-419, 1987.

8. Sivasegaram, S., Thompson, B. E., and Whitelaw, J. H., "Acoustic Characterization Relevant to Gas Turbine Augmentors," *AIAA Journal of Propulsion and Power*, Vol. 5, pp. 109-115, 1989.

9. Heitor, M. V., Taylor, A. M. K. P., and Whitelaw, J. H., "Influence of Confinement on Combustion Instabilities of Premixed Flames Stabilized on Axisymmetric Baffles," *Combustion and Flame*, Vol. 57, pp. 109-121, 1984.

10. Crump, J. E., Schadow, K. C., Yang, V., and Culick, F. E. C., "Longitudinal Combustion Instabilities in Ramjet Engines: Identification of Acoustic Modes, " *AIAA Journal of Propulsion and Power*, Vol. 2, pp. 105-109, 1986.

11. Vaneveld, L., Horn, K., and Oppenheim, A. K., "Secondary Effects in Combustion Instabilities Leading to Flashback," *AIAA Journal*, Vol. 22, pp. 81-88, 1984.

12. Kailasanath, K., Gardner, J. H., Boris, J. P., and Oran, E. S., "Numerical Simulation of Acoustic-Vortex Interactions in a Central-Dump Ramjet Combustor" *AIAA Journal of Propulsion and Power*, Vol. 3, pp. 525-533, 1987.

13. Kailasanath, K., Gardner, J. H., Boris, J. P., and Oran, E. S., "Acoustic-Vortex Interactions and Low-Frequency Oscillations in Axisymmetric Combustors," *AIAA Journal of Propulsion and Power*, Vol. 5, pp. 165-171, 1989.

14. Schadow, K. C., Crump, J. E., Mahan, V. A., Nabity, J. A., Wilson, K. J., and Gutmark, E., "Large Scale Coherent Structures as Drivers of Ramjet Combustion Instabilities," *1985 JANNAF Propulsion Meeting*, 1985.

APPENDIX D

LEAN BLOWOUT IN A RESEARCH COMBUSTOR AT SIMULATED LOW PRESSURES

by

G. J. Sturgess
Pratt & Whitney, EAst Hartford, Connecticut

S. P. Heneghan, M. D. Vangsness and D. R. Ballal
University of Dayton, Dayton, Ohio

A. L. Lesmerises,
WRDC, Wright-Patterson Air Force Base, Ohio

Published as ASME Paper No. 91-GT-359. To Appear in Transactions of ASME, Journal of Engineering for Gas Turbines & Power.

Lean Blowout in a Research Combustor at Simulated Low Pressures

G. J. STURGESS, Pratt & Whitney, East Hartford, Connecticut

S. P. HENEGHAN, M. D. VANGSNESS and D. R. BALLAL
University of Dayton, Dayton, Ohio

A. L. LESMERISES, WRDC, Wright-Patterson Air Force Base, Ohio

ABSTRACT

A propane-fueled research combustor has been designed to represent the essential features of primary zones of combustors for aircraft gas turbine engines in an investigation of lean blowouts. The atmospheric pressure test facility being used for the investigation made it difficult to directly approach the maximum heat release condition of the research combustor. High combustor loadings were achieved through simulating the effects on chemical reaction rates of sub-atmospheric pressures by means of a nitrogen diluent technique. A calibration procedure is described, and correlated experimental lean blowout results are compared with well-stirred reactor calculations for the research combustor to confirm the efficacy of the calibration.

NOMENCLATURE

A	Pre-exponential rate constant (may also include convenient unit conversion factors)
B	Combustion efficiency
C	E/$\mathscr{R}$
E	Activation energy
F	Temperature correction factor
K	Mass ratio of excess nitrogen to fuel
m	Volumetric fractional concentration
$\dot{m}$	Mass flow rate
$\dot{m}'''$	Volumetric rate of oxidant mass consumption
n	Effective order of global chemical reaction
P	Pressure
R	Global reaction rate expression
$\mathscr{R}$	Universal gas constant
T	Reaction temperature
V	Volume associated with combustion
α	Molar fraction of CO in products of reaction
β	Molar fraction of CO_2 in products of reaction
γ	Defined by Eq. (4)
ϕ	Fuel/air equivalence ratio

Subscripts

air	Air
f	Carbon monoxide in products of reaction, fuel
LBO	Lean blowout
N_2	Excess nitrogen as diluent
o	Oxygen in products of reaction
Tot	Inlet sum of air, propane and excess nitrogen

INTRODUCTION

A propane-fueled research combustor, Fig. 1, has been designed (Sturgess et al., 1990) and developed (Heneghan et al., 1990) to investigate lean blowouts in simulated primary zones of the combustors for aircraft gas turbine engines. The fundamental flow features of a gas turbine combustor primary zone, within which the flame is held, are generated by the geometrically-simple design of the research combustor.

The research combustor consists of co-axial jets with a 29.7 mm inside diameter central fuel jet surrounded by a 40 mm diameter annular air jet. The fuel is gaseous propane. The jets are located centrally in a 150 mm nominal diameter duct. A backward-facing step at the jet discharge plane completes the sudden expansion, giving a step height of 55 mm. The step provides a recirculation region that can stabilize the flame. The combustor test section incorporates flat quartz windows to provide optical access. Curved metal fillets, located in the corners of the test section, reduce and distribute the vorticity generation due to wall secondary flows, and so eliminate their impact on the bulk flowfield in the combustor. An orifice plate with a 45 percent blockage ratio forms the exit from the combustor.

When operated in a fuel-rich mode, the flame in the combustor is very stable and is anchored in the jet shear layers by a pilot flame attached to the step near the outer edge of the air supply tube. Fuel for this flame is recirculated from downstream by the step recirculation zone; ignition is by hot

Presented at the International Gas Turbine and Aeroengine Congress and Exposition
Orlando, FL June 3-6, 1991

gases also recirculated. As the bulk equivalence ratio is reduced the flame becomes less stable, and eventually reaches a point where the pilot flame becomes detached from the base region (lifts), and the entire flame structure becomes stabilized downstream, Fig. 2. Thus, there are two distinct operating modes for the combustor: a fully anchored flame, and a lifted flame.

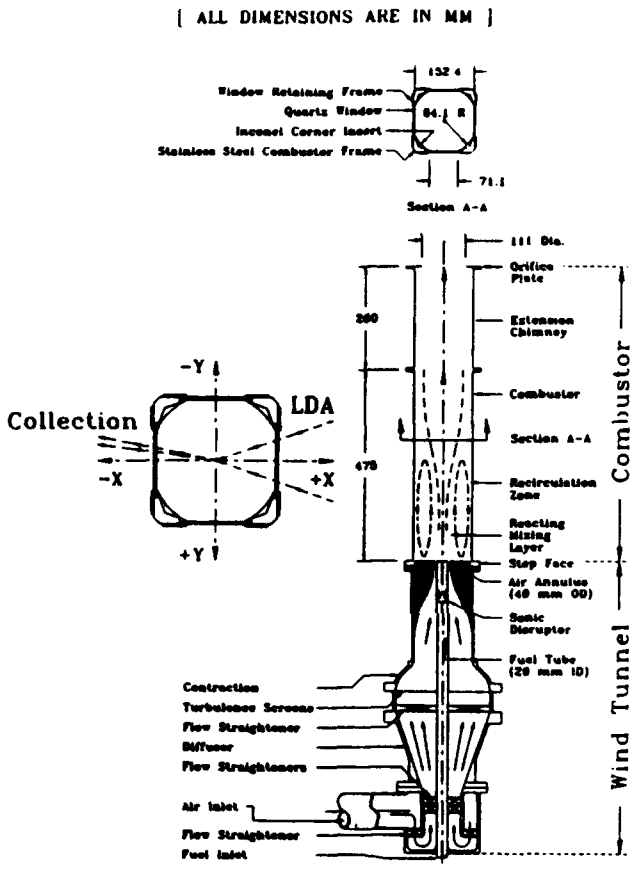

Fig. 1 Cross-Section of Research Combustor

As a consequence of the flame-lift, a significant degree of partial premixing of the reactants takes place upstream of the lifted flame position. When the equivalence ratio is further reduced, the flame becomes progressively less stable (Heneghan et al., 1990) in its lifted condition, and eventually flows out. This lean blowout limit at atmospheric pressure has been found to correspond to a fuel equivalence ratio (around 0.5) that is very close to the lean flammability limit of propane in air (Lewis and von Elbe, 1987). Due to the partial premixing, the combustor lean blowout performance characteristic has been observed to be consistent with that of well-stirred reactor data (Sturgess et al., 1990).

Lean blowout is strongly affected by chemical reaction rates. Application of chemical reaction rate theory to well-stirred reactors has resulted in the formulation of the gas loading parameter $\dot{m}/(VP^nF)$, where n is the effective order of the reaction, F is a temperature correction factor, V is the reactor volume, $\dot{m}$ is the oxidant mass flow rate, and P the operating pressure, against which the equivalence ratio at blowout is frequently plotted. The concept of the well-stirred reactor can provide a simplified description of practical combustors. Bragg (1953) originated the view that any reasonably efficient practical combustor should consist of an initially well-stirred reactor section for ignition and flame holding, followed by a plug-flow reactor section for burnout. Since the research combustor was designed specifically to reproduce the major features of an aircraft gas turbine combustor primary zone (Sturgess,et al., 1990), it might be expected to conform to well-stirred reactor behavior. The lean blowout behavior supports this expectation. Therefore, the loading parameter can be used to define lean blowout performance.

The research combustor is being tested in a facility that operates at atmospheric pressure and which was limited to maximum propane flow rates of about 20 kg/hr. Under these circumstances, sufficient loading to approach the maximum heat release condition of the research combustor cannot be achieved. However, to investigate the lean blowout phenomenon thoroughly, it is desirable to probe the flowfields for flames that are anchored and lifted at both lightly-strained and heavily-strained flame conditions. Heavily-strained flames occur at high loadings, and in practice, result from combustor operation at a given airflow with low air inlet temperatures and low (sub-atmospheric) pressures. Reducing air inlet temperatures alone to achieve high loadings without choking the combustor requires very low temperatures, and this demands drying of the air to avoid severe icing problems. Given these difficulties, alternative methods of achieving heavily-strained flames were needed.

The quantities involved in the loading parameter are those which influence the speed at which chemical activity converts reactants to products. When the combustor inlet conditions cannot be manipulated to achieve a desired loading, the chemical reaction can be influenced by some other means to yield a similar rate of reactants conversion. If pressure is made the variable of influence, then a suitably altered chemical reaction would reflect the "simulated pressure".

Low pressures can be simulated by the introduction of an inert diluent that slows down the chemical reaction in approximately the same way that low pressures do. The addition of the diluent has two effects - first, it lowers the concentration of reactants, and second, it lowers the reaction temperature by virtue of its heat capacity. Thus, tests may be made at atmospheric pressure and high loading still achieved.

Such a simulation technique for achieving high loadings while operating at room temperature and atmospheric pressure was developed for the research combustor.

SIMULATION TECHNIQUE

A number of techniques for simulating low combustion pressures are available, e.g. Lefebvre and Halls (1959), Lefebvre (1961) and Greenhough and Lefebvre (1956), using water as the diluent. However, water is inconvenient for the present purposes. It requires pre-heating of the inlet air to ensure complete vaporization of the droplets. Gaseous nitrogen has also been used with success (Norster, 1968), and does not require pre-heating. Although a direct calibration for nitrogen was not available, nitrogen as a diluent is extremely convenient for the present purposes, and was therefore selected.

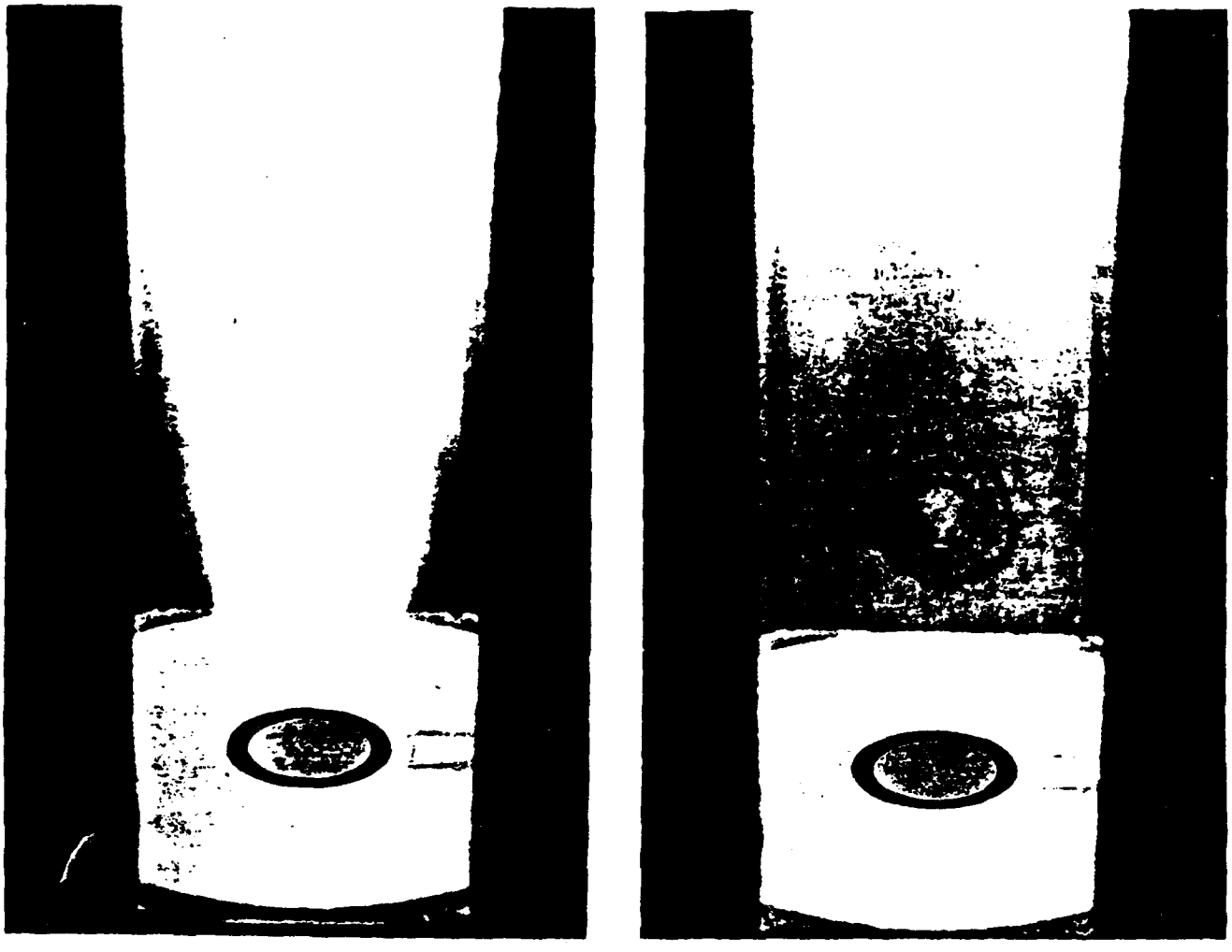

Fig. 2 Photographs of Anchored and Lifted Flame Operation

THEORETICAL BACKGROUND

Consider the combustion of the general hydrocarbon C_xH_y in air, and let the equivalence ratio ϕ be such that there is an excess of air, i.e., $\phi < 1.0$. Also, let the combustion efficiency be such that B is the fraction of fuel that is actually burned. The unburned fuel will not pass through the combustor unchanged, but will, in general, appear in the exhaust as carbon monoxide, hydrogen and lower hydrocarbons. In modern combustors the lower hydrocarbons are always small in quantity under normal circumstances; further, the fast reaction rate of hydrogen suggests that it too, will not be a significant product. Therefore, a simple bimolecular global reaction can be proposed,

$$\phi C_xH_y + (x + y/4)O_2 + 79/21(x + y/4)N_2 = \alpha CO + \beta CO_2 + y/2\phi H_2O + 79/21(x + y/4)N_2 + (1 - \phi B)(x + y/4)O_2 \quad (1)$$

where all of the hydrogen in the fuel is burned to water vapor, and the inefficiency is reflected solely in the CO/CO_2 balance. This is reasonable because of the relatively slow conversion of CO to CO_2. Nitrogen is assumed inert. The molar fractions α and β are found from C/O balances.

For propane this reaction becomes,

$$\phi C_3H_8 + 5O_2 + 18.8095N_2 = 10\phi(1-B)CO + \phi(10B - 7)CO_2 + 4\phi H_2O + 18.8095N_2 + 5(1 - \phi B)O_2 \quad (2)$$

Note that with this simple reaction mechanism CO_2 disappears from the products for a fractional conversion less than or equal to 0.7.

Let K be the mass ratio of diluent nitrogen to fuel. The reaction expression becomes,

$$\phi C_3H_8 + 5O_2 + 18.8095\gamma N_2 = 10\phi(1 - B)CO + \phi(10B - 7)CO_2 + 4\phi H_2O + 18.8095\gamma N_2 + 5(1 - \phi B)O_2 \quad (3)$$

so that the additional mass of N_2 is $18.8095 \times 28 (\gamma - 1)$.

Hence,

$$\gamma = (\phi K/11.9697 + 1) \quad (4)$$

Eqs. (3) and (4) together provide the volumetric fractional concentrations of oxidant and fuel present in the exhaust, i.e.,

$$m_f = \frac{10\phi(1-B)}{G} \quad (5)$$

where,

$$G = 10\phi(1 - B) + \phi(10B - 7) + 4\phi + 18.8095\gamma + 5(1 - \phi B)$$

and,

$$m_o = \frac{5(1-\phi B)}{G} \qquad (6)$$

From the kinetic theory of gases a reaction rate expression in Arrhenius form can be derived for bimolecular, single-step reactions. Longwell et al. (1953) have proposed that for lean mixtures this takes the form,

$$\phi B\dot{m}''' = Am_o m_f P^2 T^{-3/2} \exp(-E/\Re T) \qquad (7)$$

where $\dot{m}'''$ is the volumetric rate of oxidant mass consumption.

Although Longwell and others have proposed fractional indices in Eq. (7) to accord with the results of various experiments, for the present purposes a pure second order reaction in pressure and first order in concentrations is taken. In Eq. (7), E is a reaction rate constant (activation energy), and A can incorporate a pre-exponential rate constant as well as various unit conversion factors and other constant terms as may be convenient. T is the reaction temperature, and $\Re$ the universal gas constant.

Rearranging Eq. (7) into a form incorporating the loading parameter yields,

$$\frac{\dot{m}_{air}}{VP^2} = \frac{Am_o m_f}{\phi B} \frac{1}{T^{3/2}\exp(E/\Re T)} \qquad (8)$$

Combining Eqs. (5), (6) and (8) gives,

$$\frac{\dot{m}_{air}}{VP^2} = \frac{A(1-B)}{B} \frac{2(1-\phi B)}{(\phi(1.4-B)+79/21\gamma+1)^2} \frac{1}{T^{3/2}\exp(E/\Re T)} \qquad (9)$$

Eq. (9) represents the appropriate global kinetic expression for the reaction rate of propane in air with additional nitrogen. With K equal to zero, it also represents a similar expression for propane in pure air.

A reaction rate simulation can be obtained if,

$$\left(\frac{\dot{m}_{air}}{VP^2R}\right)_{simulation} = \left(\frac{\dot{m}_{air}}{VP^2R}\right)_{desired} \qquad (10)$$

where R is the appropriate reaction rate expression from the right-hand side of Eq. (9), i.e., with $K > 0$ and $P = 1$ atmos. for simulation and $K = 0$ and $P < 1.0$ atmos. for desired reaction rate. If it is taken that the presence of the diluent has no effect on the rate constants, the identity represented by Eq. (10) can be written,

$$\left(\frac{P^2R}{A}\right)_{simulation} = \left(\frac{P^2R}{A}\right)_{desired} \qquad (11)$$

Thus, A does not have to be described explicitly. A typical value for E is 26,613 gm.cal./gm.mole, for near-stoichiometric mixtures (Clarke et al., 1960).

Figs. 3 and 4 may be used to compare the left- and right-hand sides of the identity for an equivalence ratio of 0.9 and inlet temperature of 300K. Fig. 3 shows the effect of pressure on propane/air combustion, while Fig. 4 shows the effect of nitrogen addition on the combustion at one atmosphere pressure. The similarities of the two curves are obvious.

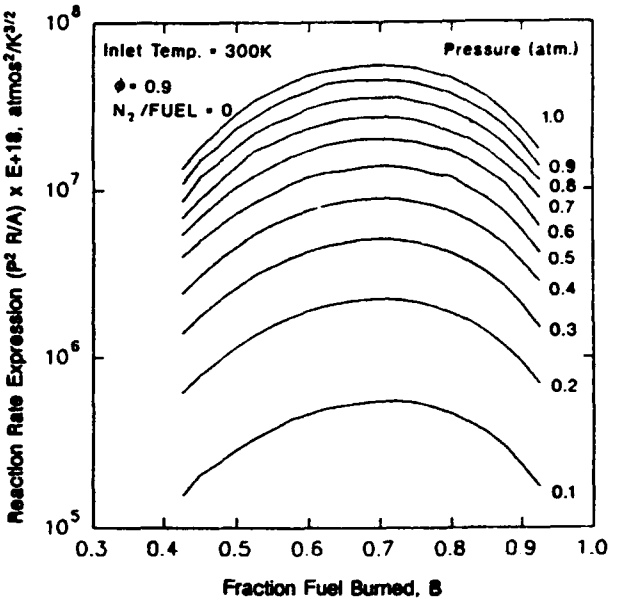

Fig. 3 Variation of Reaction Rate Expression (Eq. 11) with Pressure

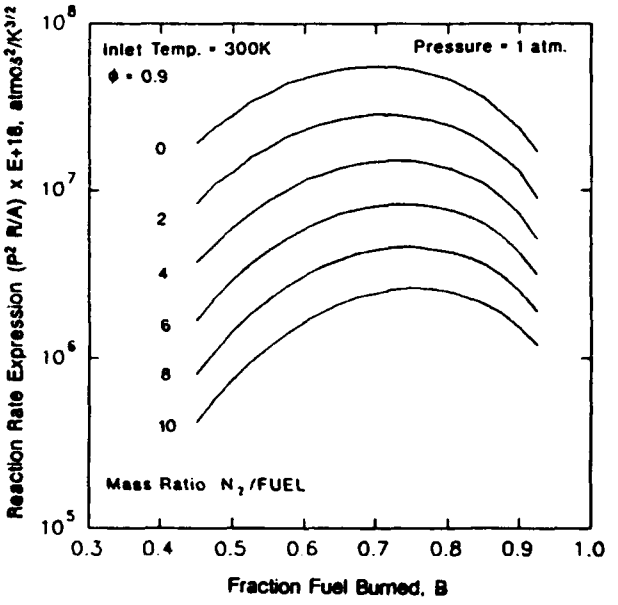

Fig. 4 Variation of Reaction Rate Expression (Eq. 11) with Diluent Addition

NEED FOR CALIBRATION

The simplified reaction mechanism and rate expression used to derive the simulation are only a convenient representation of reality. A given rate expression cannot be expected to adequately represent all the actual reactions taking place so that the expression is appropriate over wide ranges of operating conditions. Therefore, if the simulation technique is to be used for other than merely comparative purposes, some form of calibration is required.

Various global Arrhenius rate expressions have been published in the literature to represent propane/air combustion at different conditions, e.g., Greenhough and Lefebvre (1956), Clarke et al. (1960) and Herbert (1960). One that is more appropriate for low equivalence ratios (around 0.5) is given by,

$$\dot{m}''' = A m_o^{0.5} m_f^{0.5} P T^{-0.5} \exp(-56{,}600/\Re T) \qquad (12)$$

This has the form of Eq. (7), but different fractional indices and rate constants. When the simulation is based on Eq. (12) rather than Eq. (7), considerable differences result.

As is to be described, comparison of curves like Figs. 3 and 4 can be used to obtain the relationships between nitrogen to fuel mass ratio and the equivalent reaction pressure. This has been done in Figs. 5 and 6 for an equivalence ratio of 0.9 and a mixture initial temperature of 300K, using simulations based on Eqs. (7) and (12) respectively. For given combustion efficiency and nitrogen/fuel mass ratio, the differences in equivalent pressure from the two curves are marked. This illustrates vividly the need for calibration of the technique.

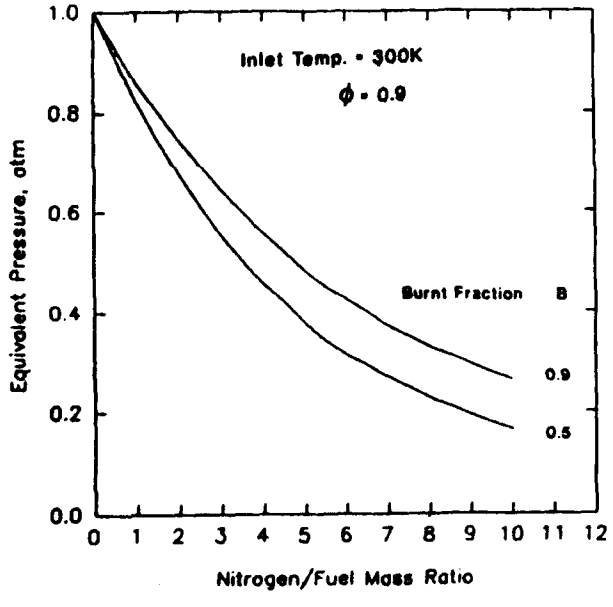

Fig. 5 Dependency of Simulated Pressure on Diluent Addition for a Global Reaction Rate Based on Indices for ϕ = 1.0 (Eq. 7)

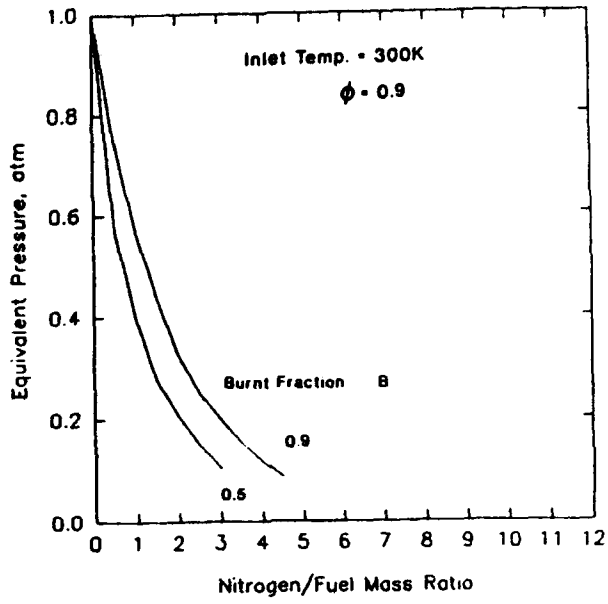

Fig. 6 Dependency of Simulated Pressure on Diluent Addition for a Global Reaction Rate Based on Indices for ϕ = 0.5 (Eq. 12)

CALIBRATION

An ideal calibration would be based on a comparison of the simulated pressure technique against true low pressure tests in the same reactor. Unfortunately, such a direct approach was not immediately available for the research combustor. Therefore, an indirect approach is used. This maintains the bimolecular reaction mechanism Eq. (3), unchanged, but calibrates the Arrhenius reaction rate expression that goes with it.

Fortunately, a calibration of the Arrhenius rate expression for propane/air/excess nitrogen systems has already been carried out by Kretschmer and Odgers (1972), and their work has been utilized here.

Kretschmer and Odgers used for their calibration experimental results from spherical stirred reactors and gas turbine combustors, burning fuels from propane to aviation kerosene over a wide range of operating conditions including pressures from 0.1 to 5.4 atmospheres and inlet temperatures from 200K to 900K; equivalence ratios equal to and less than unity were included. Analysis of these data resulted in a rate expression giving the calibrated form for Eq. (8) as,

$$\frac{\dot{m}_{air}}{V P^2 \phi} = \frac{A(m_o m_f)^{\phi}}{\phi B} \frac{1}{T^{2\phi-0.5} \exp(C/T)} \qquad (13)$$

where C is E/$\Re$. For an equivalence ratio of unity, Eq. (13) is identical to Eq. (8); while for an equivalence ratio of one-half, it is identical with the form of Eq. (12). Now, however, the exponential rate constant contained in C is a complex function of equivalence ratio and reactant inlet temperature. This variation arises because of the empirical character given to the rate equation.

Fig. 7 gives the dependency on ϕ of B at blowout for 300K inlet temperature as produced by Kretschmer and Odgers. This dependency is compared with earlier recommendations also given in Kretschmer and Odgers (1972).

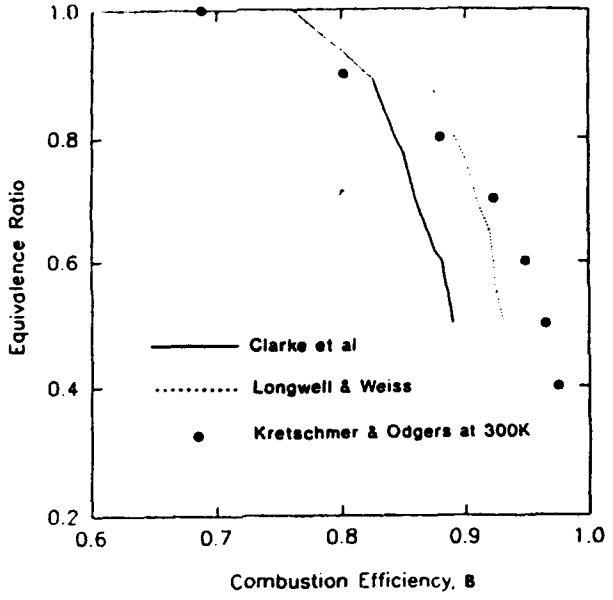

Fig. 7 Variation of Combustion Efficiency at Blowout with Equivalence Ratio, from Several Sources

Unfortunately, Kretschmer and Odgers assumed a reaction mechanism that was different from that given in Eq. (2). Hence, their expression for m_f was different from that given in Eq. (5). Therefore, it was necessary to derive a variation of C, containing the exponential rate constant, with ϕ that was appropriate to the present reaction mechanism.

The derivation of an appropriate C was done through Eq. (13) so that,

$$C = T\,[\ln (m_{f,new}/m_{f,Kretschmer})\, \exp(C/T)_{Kretschmer}] \quad (14)$$

A comparison between the variations of two C's with equivalence ratio for an inlet temperature of 300K is shown in Fig. 8. Although the differences are small, it should be remembered that C is eventually to be used in an exponential relationship. The variation of C for the present reaction mechanism is conveniently represented by the polynomial,

$$C = 14{,}926.5 + 73{,}774.7\phi - 109{,}826\phi^2 + 35{,}933.3\phi^3 \quad (15)$$

which has a correlation coefficient of 0.99998 and a maximum error of -54.3K in the range $0.4 < \phi <= 1.0$.

Eqs. (13) and (15) establish the form of the global reaction rate, and relate it to the selected reaction mechanism.

The calibration of simulated pressure may now be constructed for a range of equivalence ratios. The appropriate reaction rate expressions, one with variation in pressure and the other with variation in diluent mass flow rate, can be compared as functions of pressure and nitrogen/fuel mass ratio respectively. The intersection of these expressions represents a common value of reaction rate expression indicating equivalency of pressure and nitrogen/fuel mass ratio. This enables the relationship between diluent mass flow rate and simulated pressure to be established. Fig. 9 gives an example of this technique for a ϕ of 0.8; Fig. 10 shows the resulting calibration curves for an inlet temperature of 300K.

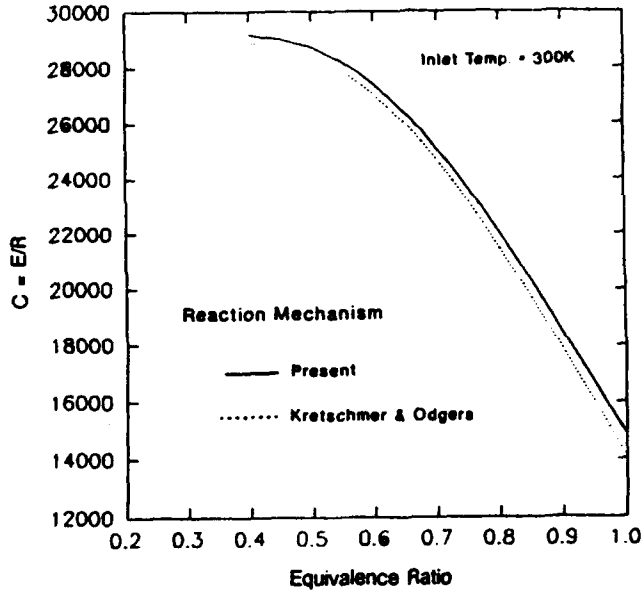

Fig. 8 Comparison of Dependencies of Activation Energy on Equivalence Ratio for Kretschmer and Odgers Reaction Mechanism and Present Reaction Mechanism

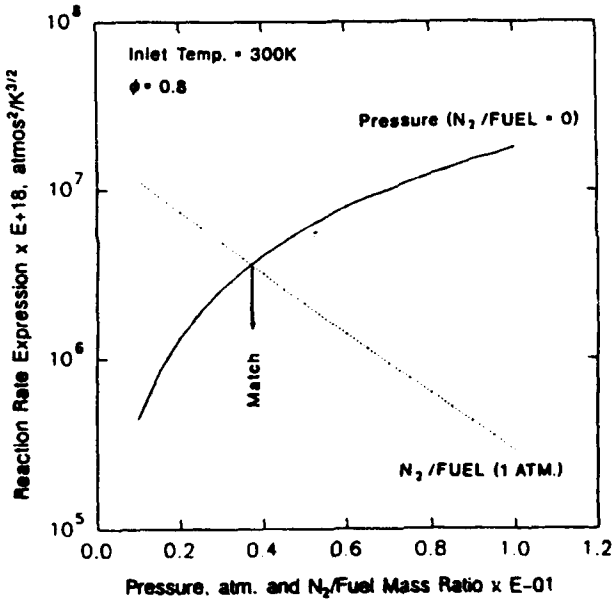

Fig. 9 Relationship Between Low Pressure and Simulated Reation Rates for ϕ = 0.8

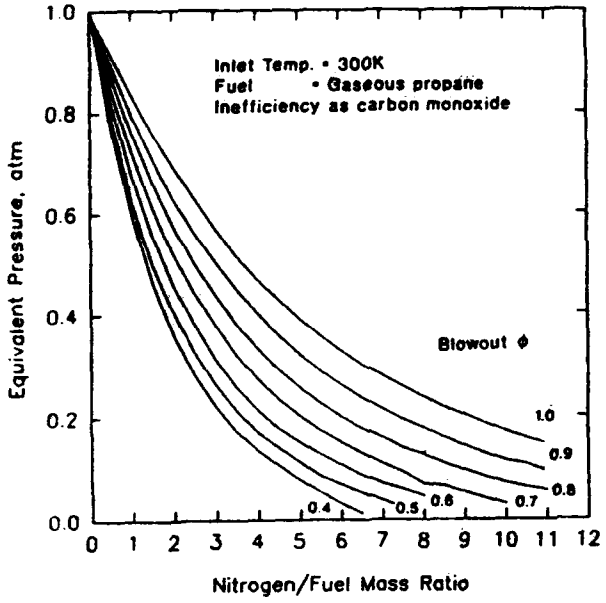

Fig. 10 Nitrogen-Simulation Calibration Curve at 300K

Fig. 10 can be considered valid for well-stirred and partially-stirred reactors. Although the empirical adjustment of the global Arrhenius reaction rate expression may be considered as being valid for a wide variety of hydrocarbons burning in air, the simulation calibration is for propane only. Further, it is limited to fuel-lean mixtures, as the figure indicates. The calibration shown is for 300K inlet temperatures; Swithenbank (1974) contains sufficient information to construct curves for inlet temperatures from 200K to 900K.

EXPERIMENTAL RESULTS

After the ignition sequence was completed and the desired airflow established with the anchored flame condition (Sturgess et al., 1990), gaseous nitrogen was introduced into the air supply line to the research combustor. This was done far upstream so that the excess nitrogen was uniformly mixed with the air entering via the annular air jet surrounding the fuel jet. The nitrogen flow rate was set at a desired level, and a blowout sequence obtained by reducing the fuel flow rate until the flame was extinguished. Ignition was reestablished, the airflow reset at the previous value in conjunction with the fuel flow, a new nitrogen flow rate was selected, and blowout was again obtained.

This procedure was repeated until a maximum nitrogen flow condition was reached. The combustor has been operated with nitrogen mass flow rates up to 55 percent of the air mass flow rate. No difficulties were encountered at this extreme condition. Repeatability and hysteresis were checked through obtaining blowouts by turning down the nitrogen flow rate range, and also by holding nitrogen and fuel flow rates constant while the airflow rate was increased. In addition, test points were repeated on different days with a different observer.

Examples of the basic results are displayed in Fig. 11, and show at a given airflow that increasing the nitrogen flow rate linearly increases the fuel flow rate at which a blowout takes place. In the figure, the multiple tests points shown at a given nitrogen flow rate for the 0.653 lbm/sec (0.075 kg/sec) airflow represent the day-to-day repeatability of the blowout.

Increasing the combustor airflow increases the fuel flow at which blowout occurs, but does not change its dependency on the nitrogen flow rate.

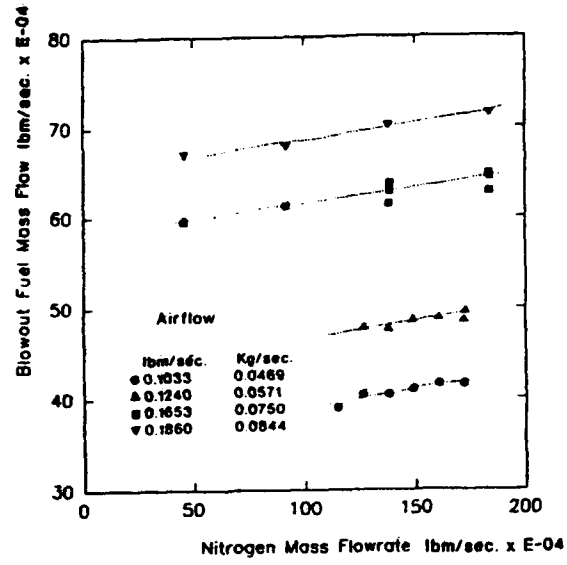

Fig. 11 Relationship Between Fuel Flow at Blowout and Nitrogen Flow at Several Airflows in the Research Combustor

Fig. 12 gives an indication of the range of equivalent pressures represented by the nitrogen simulation, for various airflows. It ranges from just less than one atmosphere down to one-tenth of an atmosphere for these tests. The equivalent pressures were obtained from Fig. 10 for the blowout conditions given in Fig. 11. When the equivalent pressures are displayed against the mass ratio of nitrogen to fuel at blowout in this form, the data for the different airflows collapse onto a single curve representing the blowout characteristic for the research combustor. Note that for nitrogen to fuel mass ratios greater than about 5, there is a loss of effectiveness of the technique.

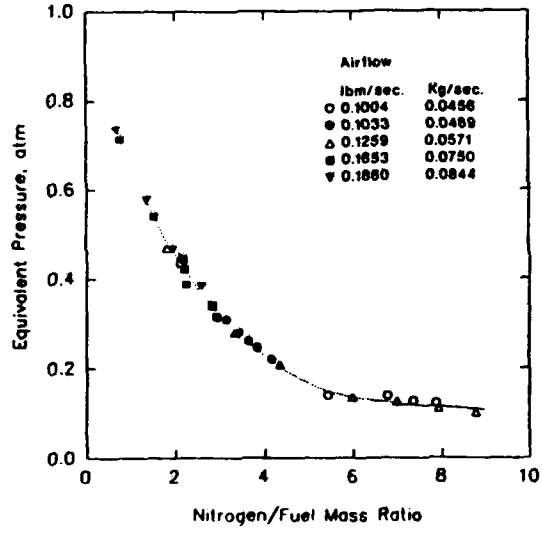

Fig. 12 Relationship Between Equivalent Pressure and Nitrogen to Fuel Mass Ratio at Blowout in the Research Combustor

When excess nitrogen is introduced into the air supply, the visual appearance of the flame and its behavior does not change from that observed for zero excess nitrogen, (Sturgess et al., 1990), (Heneghan et al., 1990). Fig. 13 gives a description of the flame behavior at constant airflow as the nitrogen flow rate is increased. Visually, there is no change in the equivalence ratio at which flame lift takes place. The equivalence ratio for lean blowout does increase, in accord with the behavior of Fig. 11. Blowout with excess nitrogen follows the same sequence of events as was observed for zero excess nitrogen (Sturgess et al., 1990), (Heneghan et al., 1990).

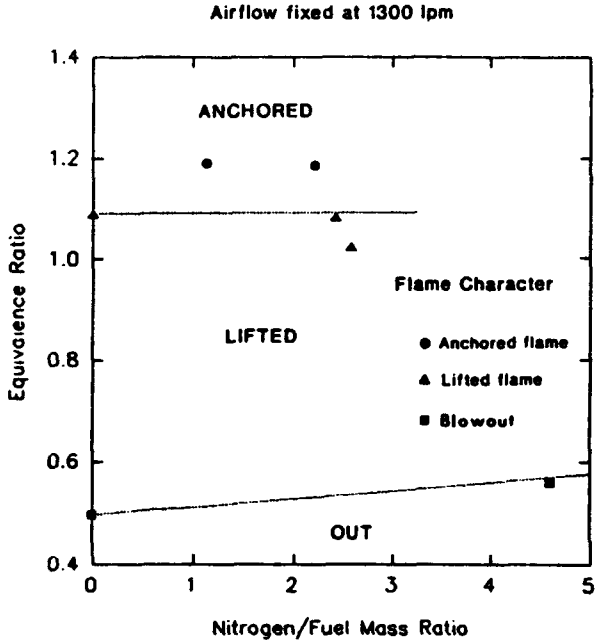

Fig. 13 Flame Behavior in the Research Combustor at Fixed Airflow as Nitrogen to Fuel Mass Ratio Is Varied

CORRELATION OF EXPERIMENTAL DATA

As described above, the equivalence ratio at blowout, ϕ_{LBO}, of a well-stirred reactor can be related to the gas loading parameter, $\dot{m}/VP^nF$, for the combustor. Here, the mass flow rate is interpreted as $\dot{m}_{Tot}$, which is the sum of the air, excess nitrogen and fuel mass flow rates. The fuel is included in this sum since its volume is not insignificant; the nitrogen flow rate is generally several times that of the fuel. Thus, the residence time in the reactor is materially affected by these flows.

For the present experiments the temperatures of the reactants were not varied, and the values for air, excess nitrogen and propane were sensibly equal. Therefore, the temperature correction factor F, is taken as unity as a matter of convenience.

The pressure is interpreted as the effective pressure, and depends on the quantity of excess nitrogen flowing, as given by Fig. 12.

The (constant) volume is taken as the total combustor volume minus the volume of the combustor associated with flame lift.

The apparent order of the reaction, n, is taken as equal to 2 ϕ for lean mixtures. However, this is for propane/air systems. When a diluent is present, the order is reduced. The expression,

$$n = \frac{2\phi_{LBO}}{(1+\dot{m}_{N2}/\dot{m}_{air})} \qquad (16)$$

is used to account for this. When no excess nitrogen is present, Eq. (16) reverts to the pure air form.

In Fig. 14 the data in terms of ϕ_{LBO} and $\dot{m}_{Tot}/VP^n$ are plotted in logarithmic form. The measured data define most of the lean portion of the stability loop for the research combustor. The data cover points at atmospheric pressure with zero excess nitrogen, as well as those at atmospheric pressure with excess nitrogen; a variety of airflows were used.

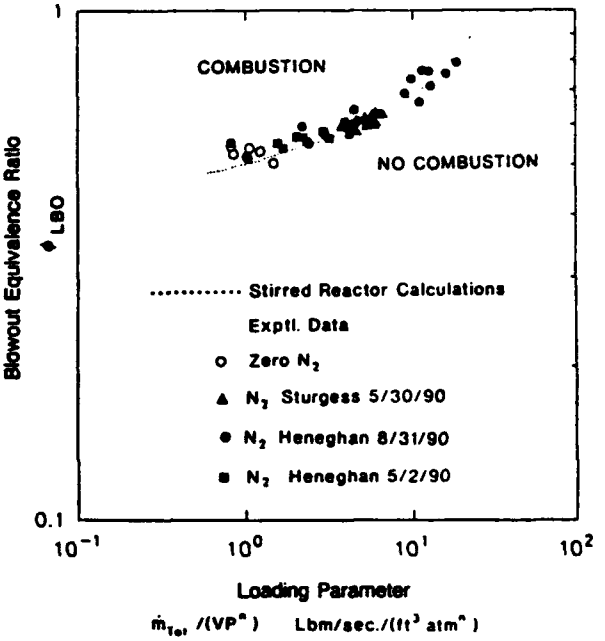

Fig. 14 Correlated Blowout Data for the Research Combustor, and Comparison with the Calculated Well-Stirred Reactor Blowout Characteristic for the Research Combustor

The figure shows that the loading parameter correlates the blowout equivalence ratios very well. This can be appreciated when considering the repeatability shown in Fig. 11. The blowout data extend over three orders of magnitude of loading parameter, and range from a blowout equivalence ratio of around 0.5 to around 0.8.

VERIFICATION OF CALIBRATION

Use of the simulation calibration curves for effective pressure (Fig. 12), resulted in a very satisfactory correlation of experimental lean blowout data obtained at constant true pressure for wide ranges of air and excess nitrogen flows. Fortunately, since the research combustor with zero excess nitrogen appeared to behave like a well-stirred reactor (Sturgess et al., 1990), (Heneghan et al., 1990), an independent check of the calibration can be made through the use of well-stirred reactor theory.

Swithenbank (1974) presented a dissipation gradient approach for defining perfectly-stirred regions of combustors. This approach was applied to the research combustor, using a

computational fluid dynamics (CFD) calculation to provide the turbulence characteristics.

Based on the dissipation gradient analysis, the rapid-stirring region of the research combustor was identified as the volume enclosing the highly turbulent portion of the flow. It was found that the surface contour enclosing 96 percent of the turbulence kinetic energy and 99 percent of its rate of dissipation corresponded to a surface over which the total dissipation gradient had a value of 10.0, which is 100 times the value recommended by Swithenbank. This well-stirred region extended over most of the length of the combustor, with exceptions of portions of the step recirculation zone and the stagnation region on the upstream face of the orifice plate placed at the combustor exit.

While the turbulence characteristics of a flow can be used to define a region of rapid mixing, this alone is not a sufficient condition for a well-stirred reactor. For stable reaction to take place within the rapid mixing region, the fuel and air mixture must locally fall inside the flammability limits, a source of continuous ignition (mixture at exit temperature) must be present, and local flow velocities must not exceed the local turbulent burning velocity.

CFD analysis was again used to provide necessary information to determine places within the defined rapid mixing region where stable combustion could take place for conditions close to blowout. On the basis of these calculations and the observations of the lifted flame position, which was found to remain roughly constant as equivalence ratio was reduced, a suitable well-stirred reactor volume was defined. This was 44 percent of the total combustor volume, and corresponded to a lifted flame mean position of about 40 cm (16 inches) from the central portion of the step, assuming that the flame completely filled the cross-section. Visual observations of the flame indicated that on the centerline of the combustor the closest position to the step-plane of the lifted flame was about 16 cm (6 inches) downstream. Of course, the real flame never completely filled the cross-section.

With a well-stirred reactor defined, the stirred reactor network code MARK2I by David Pratt and Brian Pratt was used to make calculations for the research combustor. The MARK2I code uses the CREK chemical kinetics code (Pratt and Wormeck, 1976) and a hydrocarbon reaction mechanism by Roberts et al. (1972). The research combustor near blowout was modeled in MARK2I as a single, perfectly-stirred reactor with separate air and fuel inlets, and a single discharge of products; there was no recirculation of products. It was operated with gaseous propane as fuel and air as oxidant, with equal inlet temperatures of 293K. The volume was that defined above, although two other volumes were used for spot-checks to see the sensitivity to volume. This was done because of the uncertainty associated with the flame position. (The results for the range of volumes were subsequently correlated successfully by the loading parameter, via the volume term incorporated in it.) The model was operated at a number of air mass flow rates, with several pressure levels of atmospheric and less, for each airflow. No cases with excess nitrogen were run.

Shown on the stability plot of Fig. 14 is a line representing the blowout characteristic calculated by the well-stirred reactor code. The line runs through the correlated experimental blowout data very nicely, thereby confirming that the research combustor is behaving as a well-stirred reactor. Furthermore, since the loading variation in the well-stirred reactor calculations was achieved through variations in mass flow rate and true operating pressure while the experimental data were correlated on the basis of mass flow rate and equivalent pressure, the agreement verifies the calibration (Fig. 12) of the nitrogen dilution technique.

DISCUSSION

A technique has been presented whereby the lean reaction of gaseous propane in air at sub-atmospheric pressures can be simulated by approximating the sub-atmospheric pressure reaction rate with a reaction rate at atmospheric pressure in the presence of excess gaseous nitrogen as a diluent.

The technique has been calibrated through the assumption of a one-step global reaction mechanism for propane/air/excess nitrogen systems in which nitrogen remains inert, and where combustion inefficiency is accounted for solely through the CO/CO_2 balance in the products. A global reaction rate expression in Arrhenius form for a bimolecular, single-step reaction was calibrated using experimental data from the literature. Finally, the relationship between excess nitrogen and the equivalent pressure was established by comparing appropriate reaction rate expressions with separate variation in pressure and diluent mass flow rate. This relationship forms a calibration for the simulation technique at blowout conditions. The calibration is valid for well-stirred and partially-stirred reactors using propane as a fuel in a lean mixture with air. The specific calibration curve presented is for 300K inlet temperature of reactants, although similar curves for other temperatures are readily constructed.

Lean blowout data in a research combustor, obtained using the simulation technique, were successfully correlated using the conventional loading parameter in which the pressure term was taken as the equivalent pressure obtained from the calibration. The range of equivalence ratios covered by the variation in loading parameter was from near the flammability limit to near the maximum heat release rate; the range of loading parameter obtained extended over three orders of magnitude. These were achieved at atmospheric pressure and with a limited range of mass flow rates. The lean stability of the research combustor was completely defined by these data.

The combustor was operated without difficulty with an excess nitrogen mass flow rate up to 60 percent of the air mass flow rate. At this condition the equivalent pressure corresponded to 0.1 atmosphere. However, it is not recommended that the maximum excess nitrogen flow rate be greater than about 45 percent of the air mass flow rate. This is because of inaccuracies in the calibration curve (lower right-hand corner of Fig. 10), at operating conditions with very high levels of excess nitrogen.

The effective order of the reaction when excess nitrogen is used becomes a function of the mass ratio of excess nitrogen to air, as well as equivalence ratio at blowout. There was no visual evidence that the excess nitrogen changed the flame characteristics in any way from that observed without excess nitrogen.

A final check on the accuracy of the calibration was made by comparing the correlated experimental results using the simulation against well-stirred reactor calculations based on propane/air systems for true sub-atmospheric pressures. This comparison was justified since it was known from the initial test

results (Sturgess et al., 1990), (Heneghan et al., 1990) that the research combustor had well-stirred reactor lean blowout performance when operated at atmospheric pressure without any excess nitrogen. The subsequent agreement in the stirred reactor calculation comparison confirmed the accuracy of the calibration.

The demonstration of the successful calibration for the nitrogen dilution simulation of low operating pressures opens an important possibility for small-scale facility combustion experiments. Their operating range may be extended for certain low pressure effects in an easy, inexpensive and safe fashion while the convenience of operating at atmospheric pressure is maintained.

Experimental lean blowout data have been obtained in the research combustor over a wide range of equivalence ratios. These data will provide a good data base for lean blowout modeling. The fact that the research combustor has been definitively shown to behave as a well-stirred reactor when operated in the lifted flame condition is an important help in understanding, and hence modeling, the lean blowout process.

CONCLUSIONS

1. The nitrogen dilution technique for simulating the effects on chemical reaction rates of low pressures has been successfully calibrated. The calibration removes the simulation from being a qualitative technique, to being a quantitative one. It permits certain low pressure combustion effects to be examined while maintaining the convenience of operating at atmospheric pressure.
2. The lean blowout data obtained in a research combustor via the low pressure simulation technique were correlated by the familiar loading parameter when the effective pressure was used for actual pressure and the reaction order was made a function of the excess nitrogen.
3. Nitrogen dilution enables the loading parameter for the research combustor to be extended over three orders of magnitude, and the blowout equivalence ratio to be increased from near the flammability limit to close to the maximum heat release condition. This enables the lean stability of the combustor to be adequately defined.
4. The research combustor at blowout conditions behaves like a classical well-stirred reactor.

ACKNOWLEDGEMENTS

This work was supported by the U.S. Air Force Wright Research and Development Center, Aero Propulsion and Power Laboratory, under Contract No. F33615-87-C-2822 to Pratt & Whitney, East Hartford, CT, (Contract Monitor: Lt. A. L. Lesmerises) and Contract No. F33615-87-C- 2767 to University of Dayton, Dayton, OH, (Contract Monitor: Dr. W. M. Roquemore).

REFERENCES

Bragg, S. L., Aeronautical Research Council, Paper No. 16170, CF 272, U.K., September 1953.

Clarke, A. E., Odgers, J., and Ryan, P., "Further Studies of Combustion Phenomena in a Spherical Reactor," *Proc. 8th. Symposium (International) on Combustion*, The Combustion Institute, 1960, pp. 983-994.

Greenhough, V. W., and Lefebvre, A. H., "Some Applications of Combustion Theory to Gas Turbine Development," *Proc. Sixth Symposium (International) on Combustion*, Reinhold Publishing Co., 1956, pp. 858-869.

Heneghan, S. P., Vangsness, M. D., Ballal, D. R., Lesmerises, A. L., and Sturgess, G. J., "Acoustic Characteristics of a Research Step Combustor," AIAA Paper No. AIAA-90-1851, presented at AIAA/SAE/ASME/ASEE 26th. Joint Propulsion Conference, Orlando, Florida, July 16-18, 1990.

Herbert, M. V., "A Theoretical Analysis of Reaction Rate Controlled Systems; Part II," *Proc. 8th. Symposium (International) on Combustion*, The Combustion Institute, 1960, pp. 970-982.

Kretschmer, D., and Odgers, J., "Modeling of Gas Turbine Combustors - A Convenient Reaction Rate Equation," Trans. ASME, *Journal of Energy Power*, July 1972, pp. 173-180.

Lefebvre, A. H., and Halls, G. A., "Simulation of Low Combustion Pressures by Water Injection," *Proc. Seventh Symposium (International) on Combustion*, Butterworths Scientific Publications, London, 1959, pp. 654-658.

Lefebvre, A. H., "Some Simple Techniques for the Performance Evaluation of Gas Turbine Combustion Systems," Experimental Methods in Combustion Research, Edit. J. Surugue, AGARD, Pergamon Press, 1961.

Lewis, B., and von Elbe, G., Combustion, Flames and Explosion of Gases, 3rd. Edition, Academic Press, 1987.

Longwell, J. P., Frost, E. E., and Weiss, M. A., "Flame Stability in Bluff-Body Recirculation Zones," *Ind. Eng. Chem.*, Vol. 45, No. 8, 1953, pp. 1629-1633.

Norster, E. R., "Subsonic Flow Flameholder Studies Using a Low Pressure Simulation Technique," *Proc. Intl. Prop. Symp. Combustion in Advanced Gas Turbine Systems*, Edit. I. E. Smith, Cranfield Intl. Symp. Series, Vol. 10, Pergamon Press, 1968, pp. 79-94.

Pratt, D. T., and Wormeck, J. J., "CREK - A Computer Program for Calculation of Combustion Reaction Equilibrium and Kinetics in Laminar or Turbulent Flow," Rpt. No. WSU-ME-TEL-76, Dept. Mech. Engrg., Washington State University, 1976.

Roberts, R., Aceto, L. D., Kollrack, R., Teixeira, D. P., and Bonnell, J. M., "An Analytical Model for Nitric Oxide Formation in a Gas Turbine Combustor," *AIAA J.*, Vol. 10, No. 6, June 1972, pp. 820-826.

Sturgess, G. J., Sloan, D. J., Lesmerises, A. L., Heneghan, S. P., and Ballal, D. R., "Design and Development of a Research Combustor for Lean Blowout Studies," ASME Paper No. 90-GT-143, presented at the Gas Turbine and Aeroengine Congress and Exposition, Brussels, Belgium, June 11-14, 1990.

Swithenbank, J., "Flame Stabilization in High Velocity Flow," Combustion Technology - Some Modern Developments, Edit. H. B. Palmer and J. M. Beer, Academic Press, 1974, pp. 91-125.

APPENDIX E

EFFECTS OF BACK PRESSURE IN A LEAN BLOWOUT RESEARCH COMBUSTOR

by

G. J. Sturgess
Pratt & Whitney, East Hartford, Connecticut

S. P. Heneghan, M. D. Vangsness and D. R. Ballal
University of Dayton, Dayton, Ohio

A. L. Lesmerises and D. Shouse
Wright Laboratories, Wright-Patterson Air Force Base, Ohio

Published as ASME Paper No. 92-GT-81. To Appear in Transactions of ASME, Journal of Engineering for Gas Turbines & Power.

Effects of Back-Pressure in a Lean Blowout Research Combustor

G. J. STURGESS
Pratt & Whitney
East Hartford, Connecticut

S. P. HENEGHAN, M. D. VANGSNESS and D. R. BALLAL
University of Dayton
Dayton, Ohio

A. L. LESMERISES and D. SHOUSE
Wright Laboratories, Wright-Patterson Air Force Base
Dayton, Ohio

ABSTRACT

Experimental information is presented on the effects of back-pressure on flame-holding in a gaseous fuel research combustor. Data for wall temperatures and static pressures are used to infer behavior of the major recirculation zones, as a supplement to some velocity and temperature profile measurements using LDV and CARS systems. Observations of flame behavior are also included. Lean blowout is improved by exit blockage, with strongest sensitivity at high combustor loadings. It is concluded that exit blockage exerts its influence through effects on the jet and recirculation zone shear layers.

INTRODUCTION

Combustion stability is extremely important in gas turbine engines for aircraft use. It is becoming more difficult to ensure that adequate stability margins can be maintained because of current design trends toward airblast atomization of liquid fuel, high temperature rise, and low emissions combustors.

As part of a comprehensive research program to investigate, understand and model lean blowouts in the combustors of aircraft gas turbine engines (Sturgess et al., 1991a), three combustors are utilized. These vehicles consist of a research combustor, a technology combustor, and a generic gas turbine combustor, that reflect the three-phase approach to the problem. The purpose of the research combustor is to yield fundamental information on the lean blowout process to assist in understanding the events taking place in blowout, and so guide in modeling them.

In gas turbine combustor design, it is generally recognized that the end of the flame-holding primary zone is determined by the transverse combustion air jets entering through the combustor liners (Lefebvre, 1983). For combustors using either pure airblast, or hybrid pressure-atomizing primary/airblast secondary fuel injectors, it has been observed that dynamic interactions can occur between the axially-directed jets of atomized fuel/air mixture from the injectors, and these transverse combustion air jets. Recirculation zones of the "external" (Gupta et al., 1984) or "inside-out" type (Sturgess et al., 1990) seem to be especially prone to this behavior. The interaction can be exacerbated if the airflow through the combustor dome (including the injectors) is a significant proportion of the combustor total flow, and if the transverse air jets are close to the dome.

It was therefore felt that the important back-pressure effect exerted on the flame through the presence of the combustion air jets should be included in any simulation of a gas turbine combustor primary zone.

In the research combustor, which was intended for the study of the breakdown of flame stabilization in the primary zone, the essential features of a typical primary zone of modern combustors were reproduced in simplified form (Sturgess et al., 1990). Combustion air jets were not included directly due to the complication involved; however, the back-pressure of these jets was represented by means of exit blockage from the combustor.

RESEARCH COMBUSTOR

The research combustor consists of a central fuel jet of gaseous propane surrounded by an unheated co-axial air jet, with the confluence of the jets centrally located in a nominally circular cross-section duct (Sturgess et al., 1991b). The duct is closed at its forward end to give a backward-facing step. The combustor exit is open to the atmosphere; low pressure effects on lean blowout are simulated by means of dilution through injection of excess nitrogen into the air supply (Sturgess et al., 1991c). The combustor is mounted vertically on an airflow-conditioning unit, that traverses through a cut-out in a fixed optical bench, Figure 1.

Presented at the International Gas Turbine and Aeroengine Congress and Exposition
Cologne, Germany June 1-4, 1992
This paper has been accepted for publication in the Transactions of the ASME
Discussion of it will be accepted at ASME Headquarters until September 30, 1992

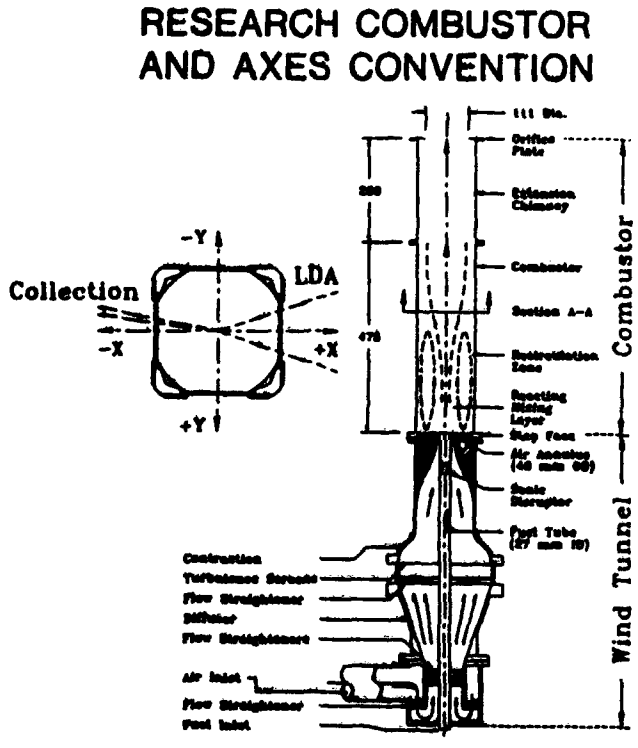

Fig. 1 Research Combustor, Showing Axes Convention

The combustion tunnel was designed and constructed in two sections – a fixed upstream window section providing optical access as needed, and a replaceable downstream chimney. The chimney is available in two lengths, and the combustor can be run with either of these, or with no chimney at all. The combustor has a hydraulic diameter of 150 mm, giving length to diameter (L/D) ratios of 3.167, 4.9 and 6.513 respectively, depending on the chimney arrangement. The inner diameter of the fuel tube is 29.97 mm with a 2-degree half-angle taper over 120mm of its length, and the outer diameter of the air passage at discharge is 40 mm.

Provision is made for exit blockage. The geometric values of exit blockage are 21.0, 45.1 and 62.0 percent of the combustion cross-section. These blockages are achieved by means of thin orifice plates. For the 45.1 percent geometric blockage, "top-hat" exits with tailpipe length to diameter (L/D) values of 1.0 and 2.1 respectively, are also available.

The optical windows can be replaced by metal plates containing arrays of thermocouples for wall temperature measurements, and tappings for static pressure measurements. The combustor may be run with any combination of windows and plates.

LDA ARRANGEMENT

Mean and fluctuating velocity component measurements are obtained by means of a laser-Döppler anemometer (LDA) system (Sturgess et al., 1991b), using 10-degrees off-axis forward scattering. The effective probe volume is 50 x 300 x 750 μm.

The combustor is mounted vertically in the facility (Sturgess et al., 1990), and its centerline constitutes the z-axis, with zero taken as the plane of the step. The x- and y-axes are diametral to the combustor cross-section, with the x-axis aligned with the LDA axis. Velocities parallel to and increasing in the direction of the z-axis, and velocities normal to and directed away from this axis, are also considered positive.

The effective optical window within which data may be taken is defined by: $-68.7 < x < +68.7$ mm, and $-22 < y < 33$ mm; in the downstream direction it is $+2 < z < 358$ mm. This window permits reasonable access to the major flow field features (Sturgess et al., 1991b)

For error assessments, see Sturgess et al. (1991b).

CARS ARRANGEMENT

The laser source for the coherent anti-Stokes Raman Spectroscopy (CARS) optics is a Nd:YAG pulse laser with 10 ns time resolution. The frequency-doubled source green beam (532 nm) is equally divided into four parts; two of these serving as pump beams, while the remaining two pump a dye laser oscillator and amplifier. The dye laser is tuned to provide a red broad-band Stokes beam (110 FWIIM) centered at 607 nm. The red Stokes beam and the two green pump beams are then focused together by a 25 cm focal length lens in a BOXCARS configuration. A 25 x 250 μm measuring spot size is achieved. The CARS signal is collected by a Spex 1702 spectrometer, 1024-element DARSS camera, and Tracor-Northern multichannel analyzer (Figure 2). The raw data are processed by a MODCOMP minicomputer.

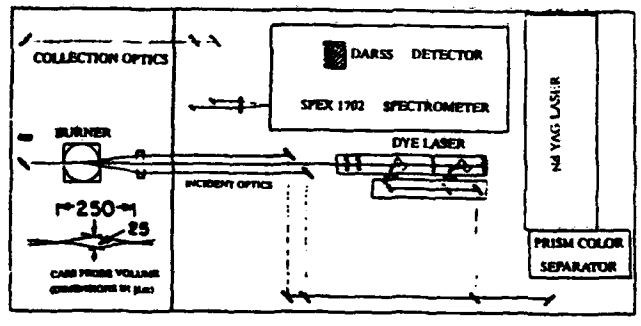

Fig. 2 Arrangement of the CARS System Optics

From the raw data the temperatures are determined by comparing the actual nitrogen spectra to the calculated spectra, using a least-squares fit. The calculation of a nitrogen CARS spectrum requires knowledge of the instrument slit function. Error problems associated with the assumption of a constant slit function when the optical path contains density and/or temperature gradients are avoided by use of a simple method of determining slit functions from the collected data at actual temperature and turbulence levels, by applying local thermodynamic equilibrium principles (Heneghan et al., 1991). This method has been shown to yield improvements in the precision of the CARS measurement (Heneghan and Vangsness., 1991).

Both fuel and air flows were monitored by separate electronic flow control units to within ±0.5 percent and ±1.5 percent respectively. The combined error produced an uncertainty of ±1.5 percent in equivalence ratio, or ±30K in

temperature. Usually, 500 samples were taken for each CARS measurement to ensure that the error in RMS temperature was less than 10K. The RMS temperature is susceptible to CARS instrument noise (Heneghan and Vangsness, 1990). However, in combusting flow the temperature fluctuations are much greater than the instrument noise, and thus the measurement precision (reproducibility) is good. It is estimated overall, that the CARS mean temperature measurement accuracy is within 50K, while the precision is well within 20K. Unlike the LDA, CARS temperature measurements are time-averaged without density-biasing effects.

ISOTHERMAL FLOW FIELD

Development of the isothermal flow field in the research combustor with a free outlet is fully discussed in Sturgess et al. (1991b). Briefly, at a simulated blowout condition, the annular air jet immediately entrains the central fuel jet, generating a small central recirculation bubble of length 17 mm with a beginning about 15 mm downstream of the jet confluence. The individual jets thus quickly merge as they expand into the combustor, and soon lose their identities. This merging is complete by 138 mm from the step. The step generates a large recirculation zone of axial length 7.7 step heights, and with vortex centers about 3.1 step heights downstream.

The addition of exit blockage by orifice plate exerts an obvious effect on the radial profiles of mean axial velocity as the flow accelerates along the combustor centerline to form a vena contracta in the exit plane, with a toroidal recirculation zone forming on the forward face of the orifice plate. For the 4.9 L/D combustor the near-field is unaffected, but the centerline flow acceleration is evident as close as 125 mm downstream from the step-plane. Figures 3 and 4 demonstrate this at 125 and 300 mm stations respectively, for 45.1 percent blockage. Note that the acceleration effect is ameliorated to some extent by the expansion of the combined jets into the combustor.

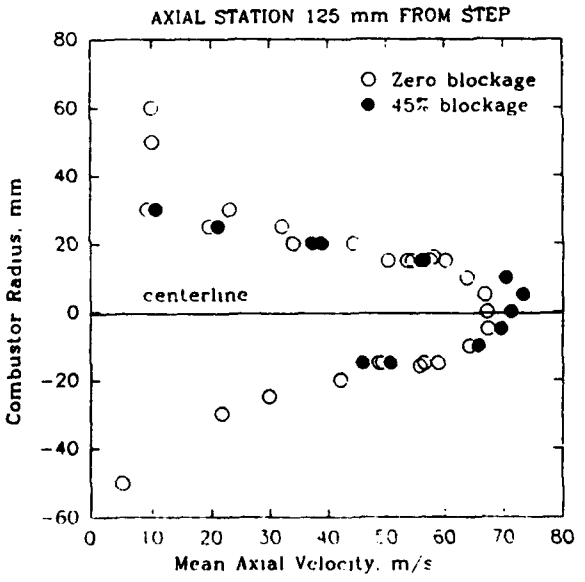

Fig. 3 Radial Profiles of Mean Axial Velocity in Isothermal Flow at 125 mm Downstream from the Step-Plane, Showing Central Flow Net Acceleration with Exit Blockage

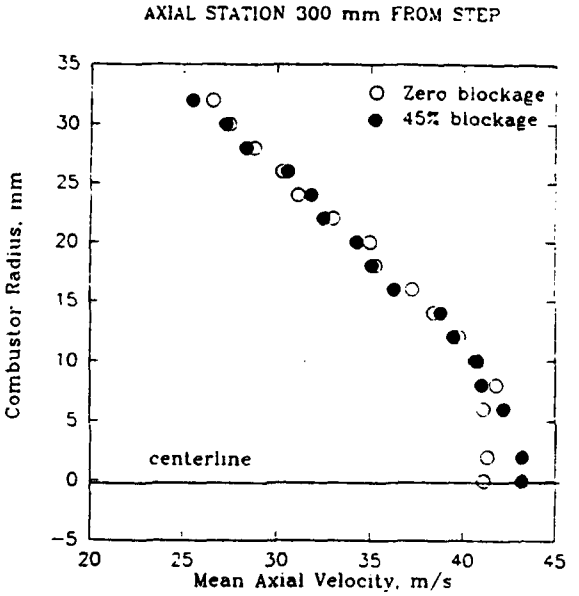

Fig. 4 Radial Profiles of Mean Axial Velocity in Isothermal Flow at 300 mm Downstream from the Step-Plane, Showing Central Flow Net Acceleration with Exit Blockage

There were no changes apparent in the fluctuating velocities with the addition of exit blockage.

The flow field with reaction present is the process of being measured. The features described under isothermal conditions are unchanged in character by the heat release.

EFFECTS OF BLOCKAGE ON FLAME BEHAVIOR

The research combustor operates with three basic flame conditions, depending on the equivalence ratio. For $\phi > 1.05$ approximately, a thin, sheath-like pilot flame is anchored close to the step near the outer diameter of the air passage (Sturgess et al., 1991c). The fuel source for this pilot flame is the step recirculation zone. The major heat release is then precipitated downstream in more or less distributed fashion, by the action of this pilot. Downstream flame-holding takes place in the shear layers associated with the central and step recirculation zones (Sturgess et al., 1991b). For $\phi < 1.05$ approximately, the pilot flame is highly intermittent (Roquemore et al., 1991), and the main flame is lifted (Sturgess et al, 1991c), allowing considerable premixing of reactants to take place prior to combustion. The lifted flame is positioned between 160 to 300 mm from the step-plane. When ϕ reaches 1.5 to 2.0 and before a rich blowout, a separated flame condition is again established where the pilot flame is no longer apparent to the eye, but the main flame does not lift in this case. It is located about 30 to 40 mm downstream from the step.

Lean blowout data were correlated on the basis of a combustor loading parameter (Sturgess et al., 1991c), derived from reaction rate theory as,

$$LP = \dot{m}_{Tot} / (VP^{n}F)$$

where for gaseous fuels and with simulation of low pressures by excess nitrogen injection,

$$\dot{m}_{Tot} = \dot{m}_{fuel} + \dot{m}_{air} + \dot{m}_{nitrogen}$$

V = reactor volume

P = effective pressure

n = apparent global reaction order
$= 2\phi / (1 + \dot{m}_{nitrogen} / \dot{m}_{air})$

ϕ = equivalence ratio

F = temperature correction factor (to 400K)
$= 10^{0.00143 T_{in}} / 3.72$

T = inlet temperature of reactants in K.

Use of LP for blowout correlations follows from the adoption of a stirred reactor modeling approach (Sturgess et al., 1991a). It also forms a useful way of characterizing the degree of "flame straining" present in the combustor.

Figure 5 provides a map of flame behavior as a lean blowout is approached, obtained by visual observation. The combustor L/D was 4.9, and the exit was a 45.1 percent blockage orifice plate. Inlet temperatures for the reactants were constant at 293K, and no excess nitrogen was injected. The Reynolds number of the annular air jet was in the range of 24,800 to 46,000. The attached and lifted flame conditions are illustrated in Figure 2 of Sturgess et al. (1991c).

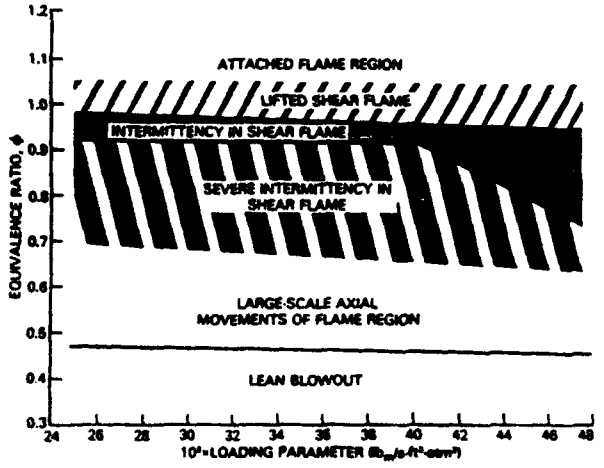

Fig. 5 Flame Behavior as Lean Blowout is Approached at Low Combustor Loadings with 45 Percent Exit Blockage

The range of loading parameter in Figure 5 is such that lean blowouts were obtained close to the flammability limits for propane/air mixtures at ambient conditions (Lewis and von Elbe, 1961). The flame behavior seen is both reversible and repeatable. Flame lift can be seen at about 1.05 equivalence ratio, and is insensitive to loading parameter over the limited range covered. Subsequent tests (Sturgess et al., 1991c) with injection of excess gaseous nitrogen into the air stream showed no effects on equivalence ratio for flame-lift. When the fuel flow was progressively reduced at constant airflow, or the airflow was progressively increased at constant fuel flow, the same sequence of flame events leading to a blowout took place. These events are shown on Figure 5. Eventually, an oscillatory flow situation develops, with large-scale axial movements of the entire lifted flame about a mean position. This motion leads, in due course, to lean blowout.

The existence of the sequence of flame behaviors did not qualitatively change with differences in exit blockage. However, the equivalence ratio for flame lift was observed to decrease slightly with increase in blockage due to orifice plates (Figure 6). Similar behavior was observed with increase in tailpipe L/D for the 45.1 percent blockage top-hat section (Figure 7).

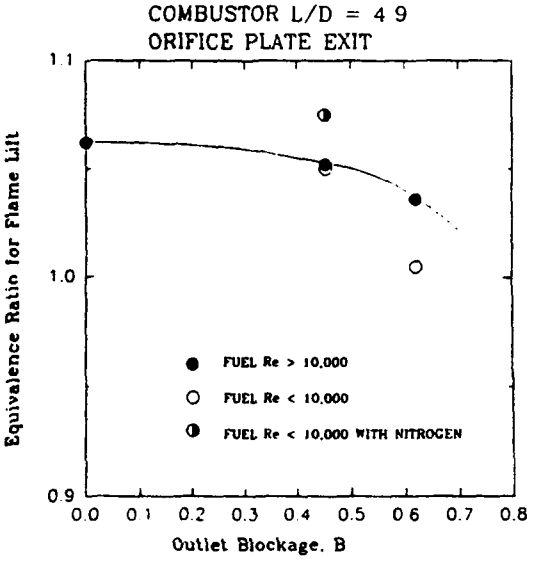

Fig. 6 Dependence of Equivalence Ratio for Flame Lift on Exit Blockage for Low and Intermediate Combustor Loadings

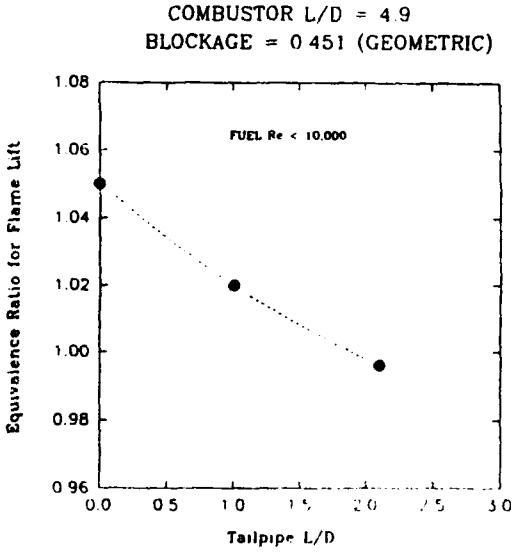

Fig. 7 Dependence of Equivalence Ratio for Flame Lift on Tailpipe Length for 45 Percent Geometric Exit Blockage

The significance of the 10,000 Reynolds number for the fuel jet in Figures 6 and 7 is that this value represents a critical threshold for transition to turbulent flow for propane (Lewis and von Elbe, 1961).

A fairly strong influence on the equivalence ratio for the onset of the large-scale axial oscillation of the lifted flame was observed, as shown in Figure 8. Increased blockage raises this equivalence ratio and is therefore destabilizing, opposite to the effect on flame lift. Note the significance of air jet Reynolds number.

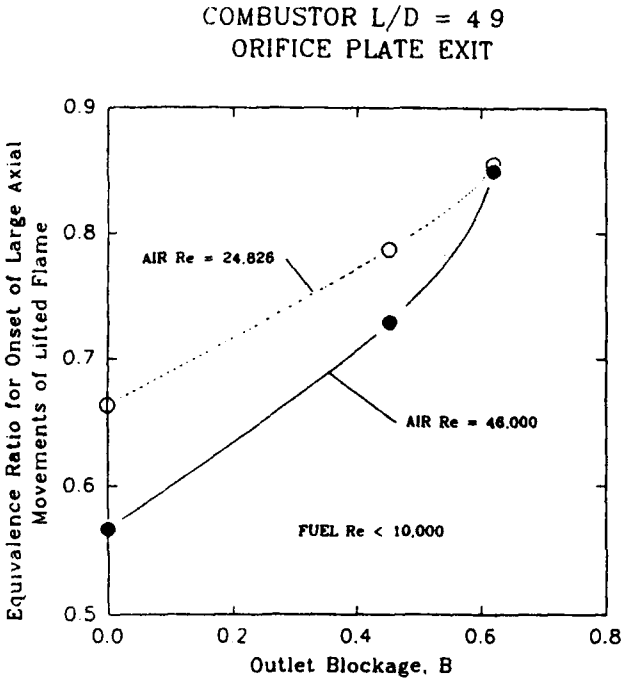

Fig. 8 Influence of Exit Blockage and Combustor Loading on Equivalence Ratio for Onset of Axial Movements of the Lifted Flame

It is apparent that the loss of the important pilot flame marks the beginning of a lean blowout sequence. A similar importance of the pilot flame is observed as a rich blowout is approached. Figure 9 shows the dependence of rich equivalence ratio for loss of the pilot flame (to result in a separated main flame), on exit blockage in the 4.9 L/D combustor. Note that on the rich-side, decreasing equivalence ratio denotes a maximum loss of stability at 45.1 percent blockage. At given blockage this rich equivalence ratio for pilot flame loss decreases as the combustor loading is increased; Figure 10 demonstrates this for the 4.9 L/D combustor at 45.1 percent exit blockage by orifice plate.

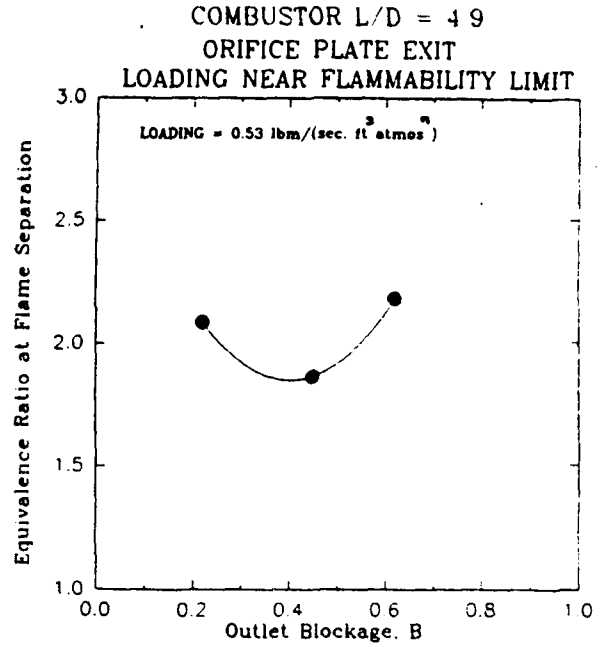

Fig. 9 Dependence of Equivalence Ratio for Flame Separation on Exit Blockage for Low Combustor Loading

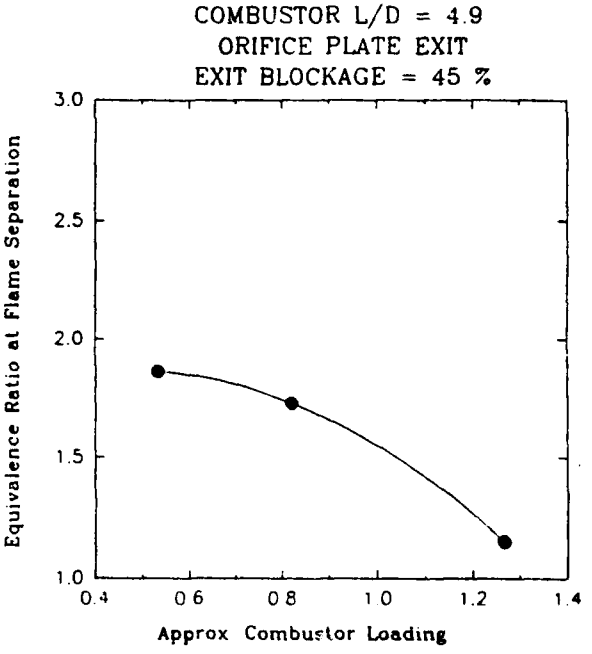

Fig. 10 Influence of Combustor Loading on Equivalence Ratio for Flame Separation at 45 Percent Exit Blockage

DIRECT EFFECTS ON LEAN BLOWOUT

It was observed for low values (about 0.18 $lb_m/(sec.ft.^3 atmos.^n)$ close to the flammability limits for propane/air mixtures at these conditions) of the loading parameter that the blowout equivalence ratio decreased linearly as the exit blockage by orifice plate was increased. This is shown in Figure 11, and is somewhat surprising since the lifted flame is positioned (Roquemore et al., 1991) in the regions where the mean flow is beginning to be accelerated due to the blockage (Figures 3 and 4), at least in isothermal flow. Heat release should increase the flow acceleration. The improvement in stability depended on the combustor L/D ratio; for a given blockage, the shorter the combustor the less stable it was and the greater its sensitivity to the exit blockage. For the 4.9 L/D combustor at this loading, the lean blowouts were virtually independent of exit blockage.

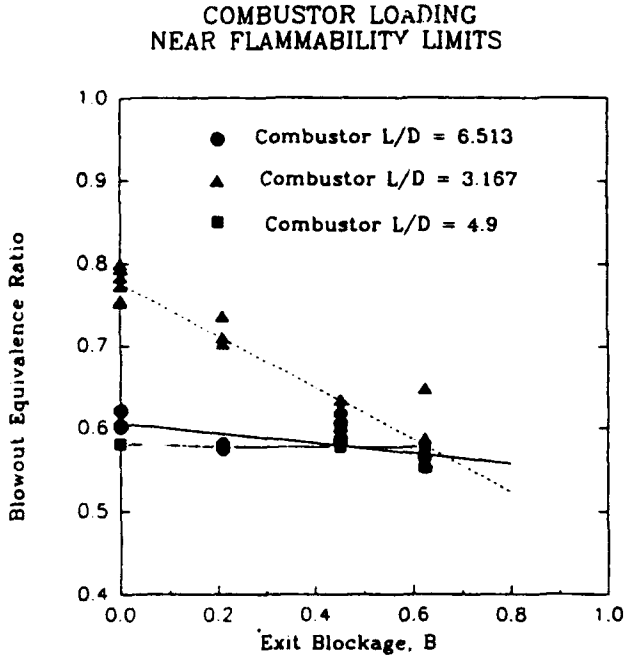

Fig. 11 Influence of Exit Blockage on Lean Blowout at Low Combustor Loading in Three Combustor Lengths

For a fixed exit orifice plate blockage of 45.1 percent at slightly higher loading parameter, the dependency on L/D is given in Figure 12, where it can be seen that an optimum L/D exists. Close to the flammability limits there is also a fairly strong sensitivity of blowout equivalence ratio to combustor loading parameter. The existence of the optimum combustor length for maximum stability close to the flammability limits (Lewis and von Elbe, 1961) can be attributed to the occurrence of acoustic coupling (organ-pipe resonance driving eddy shedding off the step at 55 Hertz) at large L/D (Heneghan et al., 1990), and outlet interference with flame holding at small L/D.

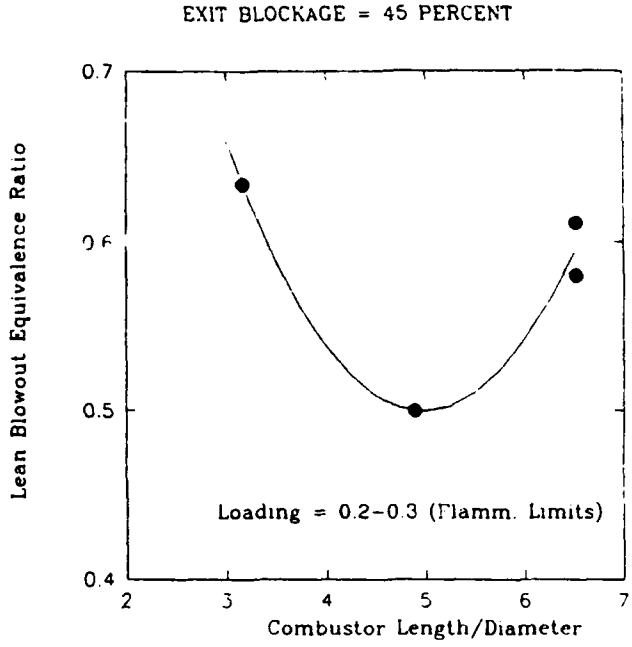

Fig. 12 Dependence of Lean Blowout at Low Loadings on Combustor Length with 45 Percent Exit Blockage

At 45.1 percent exit blockage the peak amplitude of the 55 Hz frequency signal measured inside the combustor by Kistler pressure transducers, was increased by a factor of 5.5 when the combustor L/D was increased from 3.167 to 6.513. For the 4.9 L/D combustor with 45.1 percent exit blockage (and the acoustic treatment described in Heneghan et al., 1990), the peak-to-peak amplitudes for low frequency oscillations (1-600 Hz) were less than 0.69 N/m^2 and for high frequency oscillations (1-5 KHz) the amplitudes were less than 6.9 N/m^2.

Figure 13 displays the sensitivity to exit blockage in the 4.9 L/D combustor operating at loadings (10 $lb_m/(sec.ft.^3 atmos.^n)$) near to the peak heat release rate condition (obtained with a combination of high airflow rates and injection of excess nitrogen as a diluent). Again, the blowout equivalence ratio decreases linearly with increasing blockage. However, when contrasted with the sensitivity to blockage for this combustor near the flammability limits (Figure 11), it is seen that blockage exerts a much more powerful influence on stability at this higher loading.

The general conclusion can be drawn that exit blockage improves the lean stability of the research combustor. The effectiveness of blockage in improving the stability in a combustor of given length, depends on the loading at which the combustor is operated. Of the three combustor lengths evaluated (and for operation at low loadings at least), the 4.9 L/D combustor has the best stability at any blockage level between 0 and 62 percent. Exit blockage reduces the rich stability of the research combustor, and the extent of this also depends on the combustor loading.

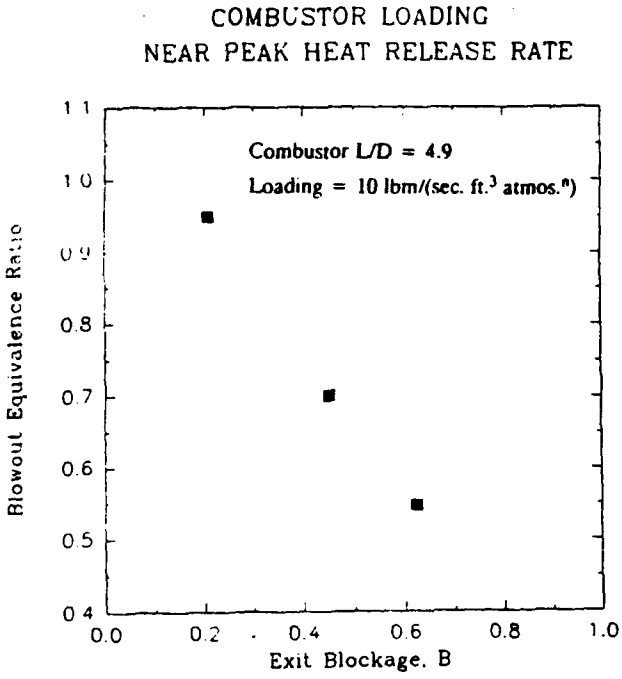

Fig. 13 Influence on Lean Blowout of Exit Blockage at High Combustor Loading

WALL TEMPERATURE BEHAVIOR

The wall temperatures for the combustor are needed to provide boundary condition information for subsequent computational fluid dynamic calculations to be made in attempts to model the lean blowout process. They can also provide by inference, additional information concerning development of major flow features in the combustor.

Wall temperatures are most conveniently expressed in nondimensional form, sometimes known as Metal Temperature Factor (MTF), and defined by,

$$MTF = \frac{T_s - T_{in}}{T_{ad,fl} - T_{in}}$$

where

T_s = wall temperature

$T_{ad,fl}$ = adiabatic flame temperature.

For premixed flames, MTF represents a normalized wall temperature, and is particularly useful in the present case therefore, because of the partial premixing that takes place when the flame is lifted.

Figure 14 compares at 44.5 mm downstream from the step and inside the step recirculation zone, actual thermocouple temperatures over a range of equivalence ratios against temperatures derived from the MTF trend with downstream distance. Data are provided for zero and 45.1 percent exit blockage in the 4.9 L/D combustor. The tests were made for a variety of jet velocity ratios and combustor flow functions. No effect of velocity ratio was apparent, and substantial increase in flow function resulted in only a negligible increase in MTF.

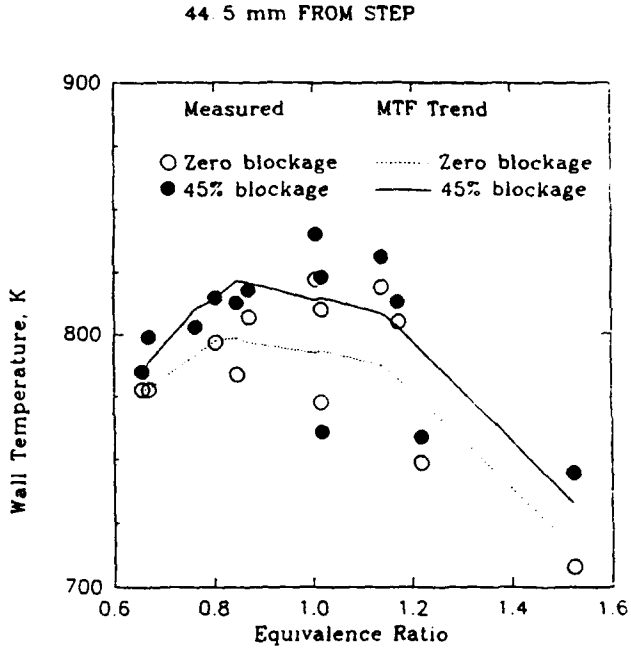

Fig. 14 Comparison of Actual Wall Temperatures with Smoothed Values Over a Range of Equivalence Ratios, Showing Influence of Exit Blockage

The figure shows that wall temperatures in the recirculation zone increase with combustor exit blockage by about 20 to 25 deg. K for 45.1 blockage. Peak temperatures occur at equivalence ratios in the range of 0.9 to 1.1. For the attached flame condition ($\phi \geq 1.05$), temperature levels are about 820K, and fall to about 780K as lean blowout is approached.

The form of MTF variation with equivalence ratio is shown in Figure 15 for a station 146 mm downstream from the step (still inside the recirculation zone). The behavior in the figure is typical of all axial stations along the combustor. MTF decreases with increasing equivalence ratio up to an equivalence ratio of about 0.95, and then becomes independent out to a value of 1.6. There is negligible effect of blockage on MTF at this station.

The "break" in the curve of Figure 15 may be interpreted as representing the flame-lift condition. The inferred equivalence ratios for flame-lift based on this break for different axial locations are shown in Figure 16 compared with the equivalence ratios for flame-lift based on direct observation (Figure 6). As might be anticipated, inferences based on data from downstream are in better agreement with direct observations. No effect of blockage is apparent on the inferred flame-lift, which does not conflict with direct observation in Figure 6.

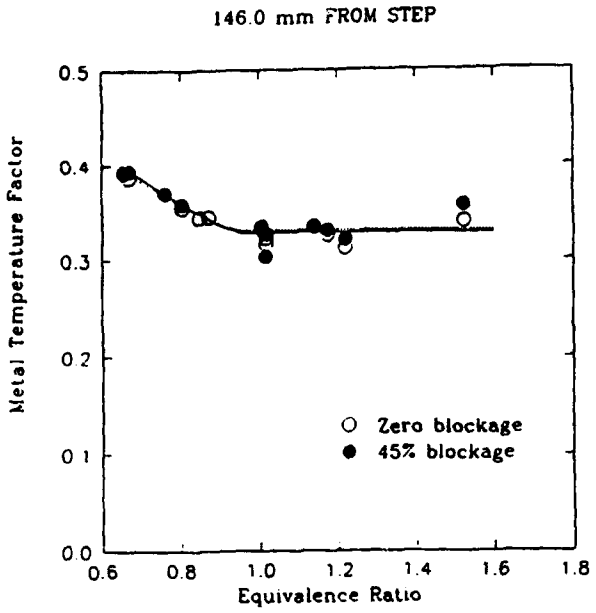

Fig. 15 Normalized Wall Temperatures at 126 mm from Step–Plane for Zero and 45 Percent Exit Blockage, Showing Influence of Equivalence Ratio

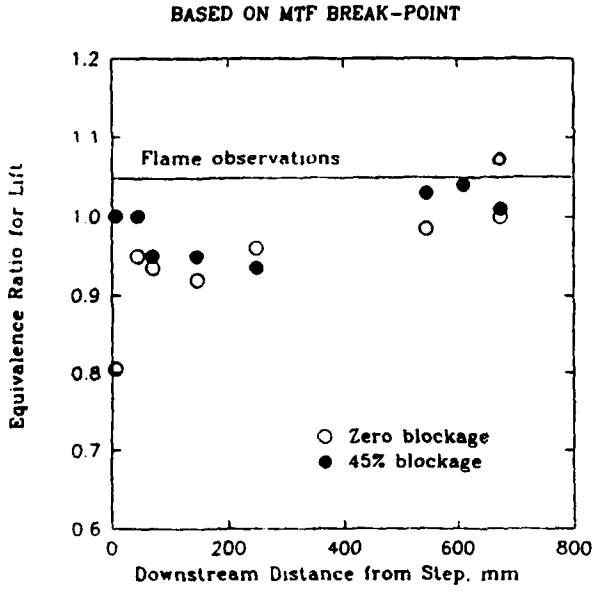

Fig. 16 Indicated Equivalence Ratios for Flame-Lift from Wall Temperatures, Compared with Direct Observations

The variations of the maximum value of MTF with equivalence ratio for 0, 45.1 and 62 percent geometric blockages are given in Figure 17; the flame condition – lifted or attached – is delineated based on Figure 6. The values of maximum MTF, and the positions at which they occur, were derived at each equivalence ratio from differentiation of curve fits to MTF versus axial distance information obtained from the curves in plots such as given in Figure 15.

Figure 17 indicates that maximum MTF reaches its minimum value at about the equivalence ratio for flame-lift. Exit blockage does not affect the value of maximum MTF, but maximum MTF does increase as lean blowout is approached.

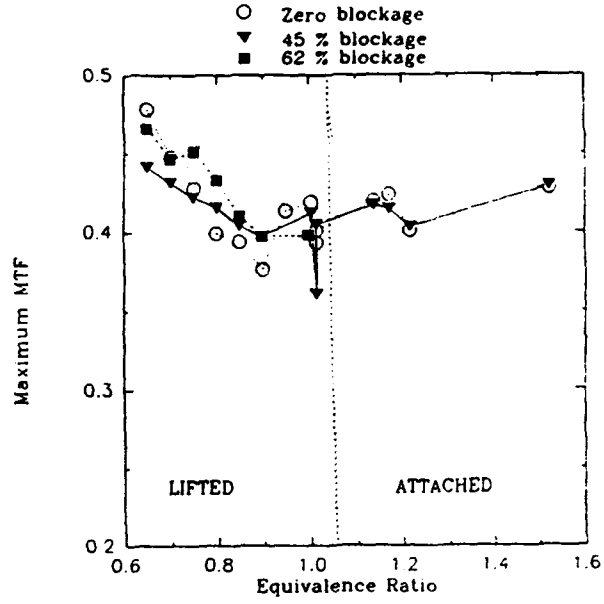

Fig. 17 Variations of Maximum Normalized Wall Temperatures for Lifted and Attached Flames at Several Values of Exit Blockage

When the position at which maximum MTF is reached is plotted in similar fashion in Figure 18, a strong effect of blockage is apparent for lifted flames; equivalence ratios for attached flames do not influence this position significantly. For the three blockages shown, the position of maximum MTF is roughly constant around 450 mm from the step for attached flames.

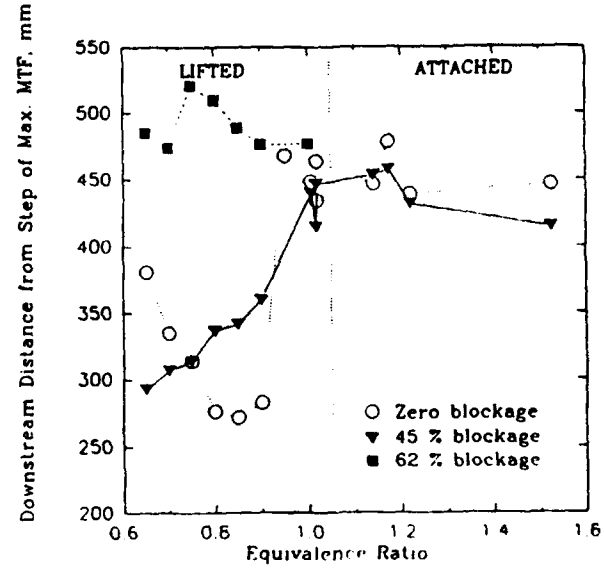

Fig. 18 Dependency of Position of Maximum Normalized Wall Temperature on Exit Blockage for Lifted and Attached Flames

When equivalence ratio is reduced so that a lifted flame is established, an unrestricted combustor exit results in the position of maximum MTF initially moving back toward the step. However, for an equivalence ratio of 0.9, the closest position to the step is reached at about 270 mm; therefore, as equivalence ratio is further lowered toward a lean blowout, the position again moves downstream as the flame-lift increases.

The addition of exit blockage introduces an additional recirculation zone (on the orifice plate upstream face) into the combustor, and the existence of this recirculation is how blockage exerts an influence on the position of maximum MTF. The position of maximum MTF is associated with the reattachment plane of the step recirculation zone since this is where the jet shear layers reach the combustor wall (Sturgess et al., 1991b). These jet shear layers are where the majority of the heat release takes place during combustion, whether or not the pilot flame is attached (Sturgess et al., 1991a). Movements of the position of maximum MTF therefore reflect, albeit in crude fashion, movements of the reattachment plane for the step recirculation zone. The lack of blockage-effect on the value of maximum MTF (Figure 17) indicates that heat release in the jet shear layers is not substantially changed by combustor exit blockage; however, the trajectory of these shear layers is (Figure 18), possibly due to flow acceleration as a result of the heat release. The behavior evident in Figure 18 for 45.1 and 62 percent blockage is the result of interactions between the step and orifice plate recirculation zones, due to heat release rate as equivalence ratio is varied, and modified by the two flame conditions.

With this flow model, the lifted-flame (partially premixed) behavior for maximum MTF in Figure 18 at zero exit blockage is consistent with the findings of Morrison et al. (1987), Pitz and Daily (1983), and Stevenson et al. (1982) for premixed flames that a step recirculation zone at fixed (turbulent) Reynolds number decreases in size with increasing equivalence ratio. The minimum distance occurring at an equivalence ratio of 0.9 suggests that pilot flame attachment is becoming evident before the directly-observed equivalence ratio of 1.05 (Figure 6). Examination of the intermittency of the pilot flame (Roquemore et al., 1991, and Chen, 1991) tends to confirm this suggestion.

WALL STATIC PRESSURES

For an atmospheric pressure discharge combustor with exit blockage, wall static pressures provide means for a convenient assessment of the extent of the additional recirculation zone set up on the orifice plate upstream face. With a free exit, the difference between ambient pressure and wall static pressure in the combustor reaches zero in the exit plane. However, when the exit is restricted, this difference reaches zero at some position inside the combustor (Heneghan et al., 1990). The position where this occurs marks the stagnation plane for the aft recirculation zone on the orifice plate.

In isothermal flow the wall static pressure at a given station is a function of the jet velocity ratio λ, and the inlet flow parameter, as can be seen for a station 44.5 mm downstream, in Figure 19. As Figure 20 demonstrates, when exit blockage is introduced, the dependency of wall static pressure on velocity ratio is suppressed. Combustion also suppresses the dependency on jet velocity ratio, even for a free exit. This is illustrated in Figure 21, where it is also shown that the flame condition does not exert an influence.

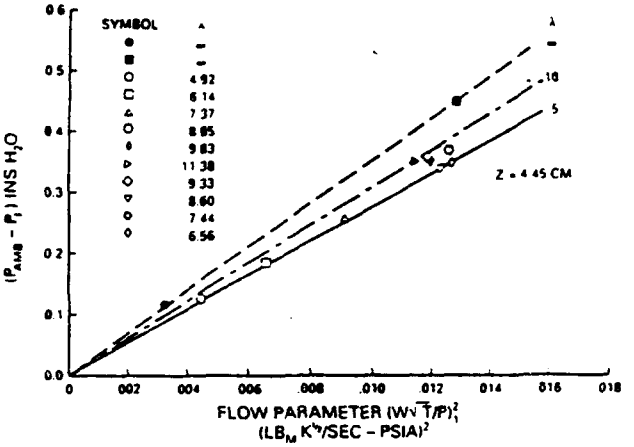

Fig. 19 Dependency of Wall Static Pressures in the Step Recirculation Zone on Inlet Flow Parameter and Jet Velocity Ratio in Isothermal Flow with a Free Exit

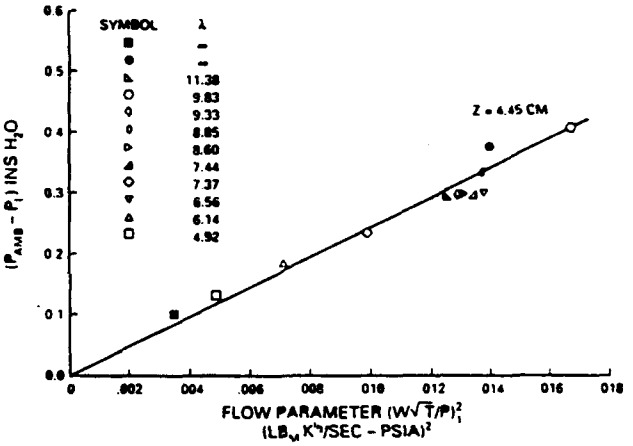

Fig. 20 Suppression of Dependency of Wall Static Pressure on Jet Velocity Ratio by Exit Blockage in Isothermal Flow

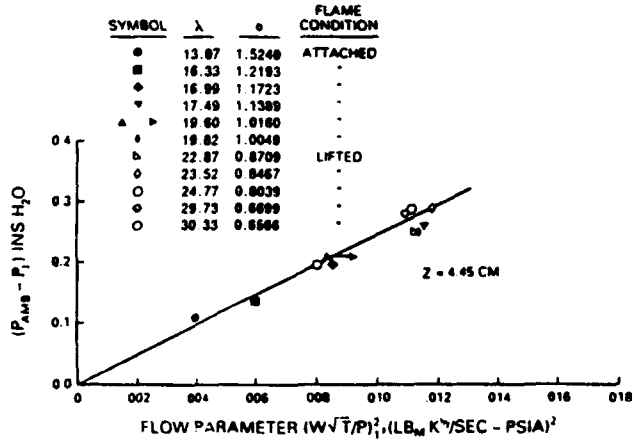

Fig. 21 Suppression of Dependency of Wall Static Pressure on Jet Velocity Ratio by Combustion with a Free Exit

Again using curve fits and differentiation, the axial positions along the combustor at which atmospheric pressure was attained, were found. Typical wall static pressure axial distributions are given in Figure 3 of Heneghan et al. (1990). Figure 22 shows that in isothermal flow this condition was reached at a constant 580 mm approximately, with 45.1 percent exit blockage, and was so regardless of inlet flow parameter or jet velocity ratio. With combustion and the same blockage, the position for atmospheric pressure was a strong function of equivalence ratio, as Figure 23 shows, where the leading-edge of the aft recirculation zone moves progressively forward in the combustor as equivalence ratio is reduced, independent of flame condition.

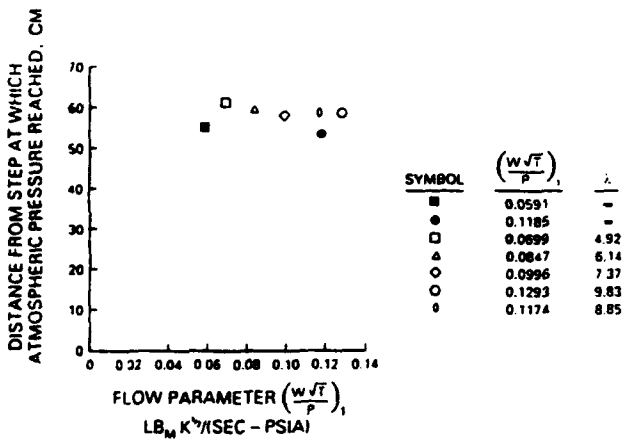

Fig. 22 Independence from Inlet Flow Parameter and Jet Velocity Ratio of Position Where Atmospheric Pressure Is Reached on the Combustor Wall, in Isothermal Flow with 45 Percent Exit Blockage

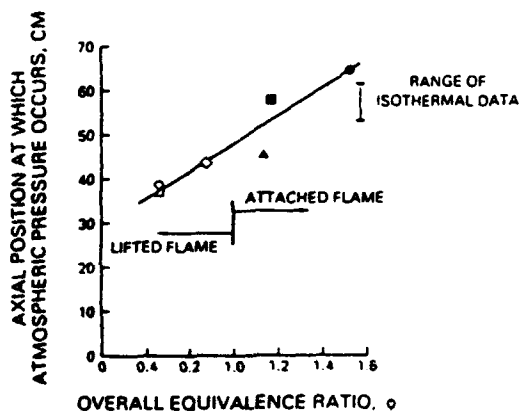

Fig. 23 Variation of Downstream Position Where Wall Static Pressure Reaches Atmospheric with Equivalence Ratio at 45 Percent Exit Blockage

At 62 percent blockage the position at which atmospheric pressure was attained was always greater than 600 mm from the step, and thus could not be accurately determined from the static tap positions available.

RELATIONSHIP BETWEEN RECIRCULATION ZONES

The information on the end of the step recirculation zone inferred from MTF data (Figure 18) can be combined with the information on the beginning of the orifice plate recirculation zone from the static pressure data (Figure 23) in order to examine the relationship between these two important flow features in the restricted-exit combustor.

Figure 24 shows a combination of Figures 18 and 23 for 45.1 percent exit blockage with combusting flow. It can be deduced that there is always positive separation between the end of the step recirculation zone and the beginning of the orifice plate recirculation zone for this blockage. Furthermore, for lifted flames, this separation is maintained at a constant distance of about 80 mm, so that direct interference never happens. For attached flames, the separation distance increases, as Figure 25 shows.

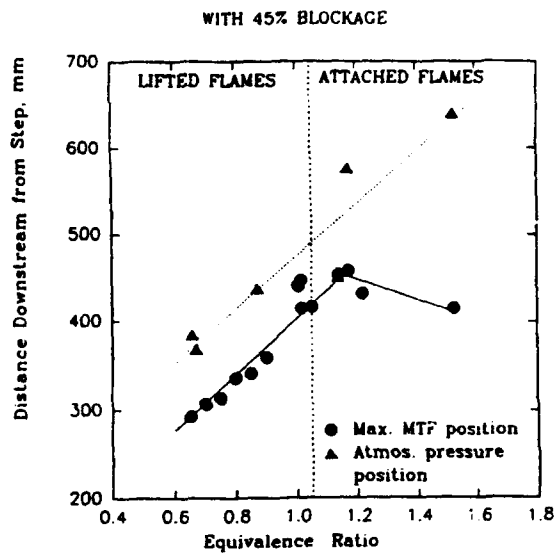

Fig. 24 Downstream Positions Where Atmospheric Pressure and Maximum Normalized Wall Temperature Are Attained as Equivalence Ratio Is Varied for Fixed Exit Blockage

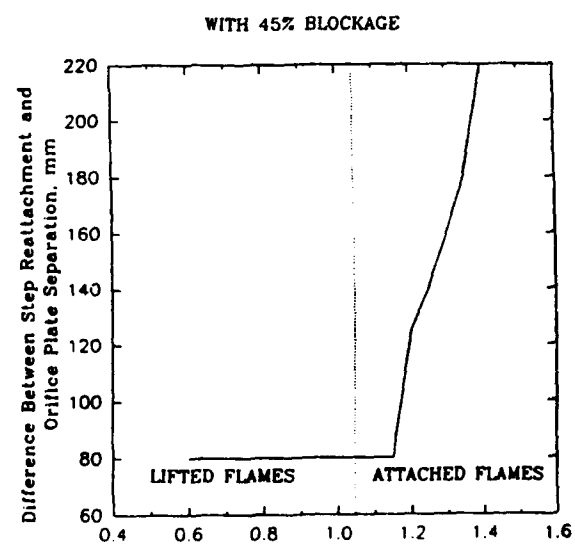

Fig. 25 Distance Between Recirculation Zones for Lifted and Attached Flames at Fixed Exit Blockage

For 62 percent blockage, it appears as though direct interference between zones does not occur either, despite the inferred position of the end of the step recirculation zone being further downstream at around 500 mm for all equivalence ratios (Figure 18).

GAS TEMPERATURE PROFILES

Limited gas temperature measurements were made using the CARS system. Profiles along the combustor centerline and, radially, close to the step, were taken at 0, 45.1 and 62 percent exit blockage by orifice plates in order to assess what blockage did to the all-important step recirculation zone. This was a quick preliminary look made prior to more extensive field-mapping of temperature to be reported separately.

The axial profiles of mean temperature along the combustor centerline at 45.1 percent exit blockage for lifted and attached flames are given in Figure 26, where the temperatures are presented as the ratio of actual temperature to the adiabatic flame temperature. The combustor loadings in both cases are in the range of 0.7 to 0.76 $lb_m/(sec.ft.^3atmos.^n)$, i.e., fairly near to the lean flammability limit. For both flames the temperature initially falls, and then increases again for distances greater than 100 mm from the step-plane. By consideration of Sturgess et al. (1991b), the increases in centerline mean temperature can be associated with the inner edge of the reacting jets shear layer reaching the centerline and thereby introducing sufficient oxidant for extensive chemical reaction to take place on the centerline. The initial distance in this profile can therefore be viewed as a conditional thermo-chemical potential core region. Note that the position of mean temperature increase is in the region where in isothermal flow the centerline mean axial velocity begins to accelerate with the 45.1 percent exit blockage (Figure 3). Also, for the attached flame the dimensionless mean temperature level is generally increased over that for the lifted flame.

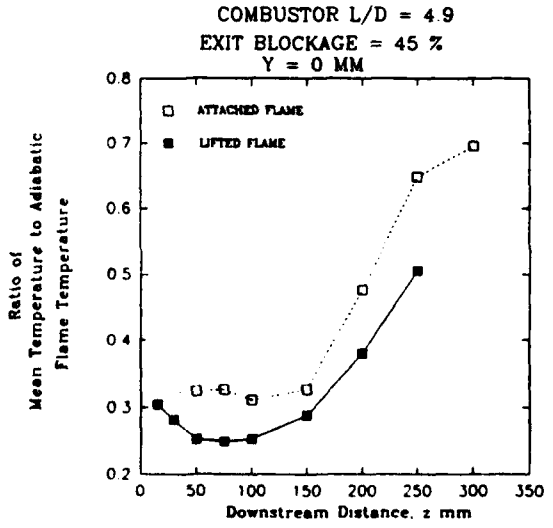

Fig. 26 Centerline Profiles of Dimensionless Mean Gas Temperature for Attached and Lifted Flames at Fixed Exit Blockage

Radial profiles of dimensionless mean temperature for the condition above are given in Figure 27 for a downstream station 5 mm from the step. Comparison of these profiles reveals the effect of the attached flame on mean temperature, and shows the pilot flame to be located at a radius of 17 to 20 mm. The probability distribution functions (p.d.f.) confirm this definition. This is somewhat consistent with the mean position of 24 mm radius for the attached flame determined at 10 mm downstream with thin filament pyrometry (TFP) (Roquemore et al., 1991). Again, the levels of dimensionless temperature are higher at all radial positions for the attached flame condition. The p.d.f.'s for the lifted flame condition agree with the measurements of the spontaneous OH emission given in Roquemore et al. (1991), that there is a finite probability of the pilot flame being present part of the time, even though the main flame is fully lifted and an anchored pilot flame is not directly observed. For both lifted and attached flames, the step recirculation zone provides a significant high-temperature reservoir for the combustion processes developing in the shear layers.

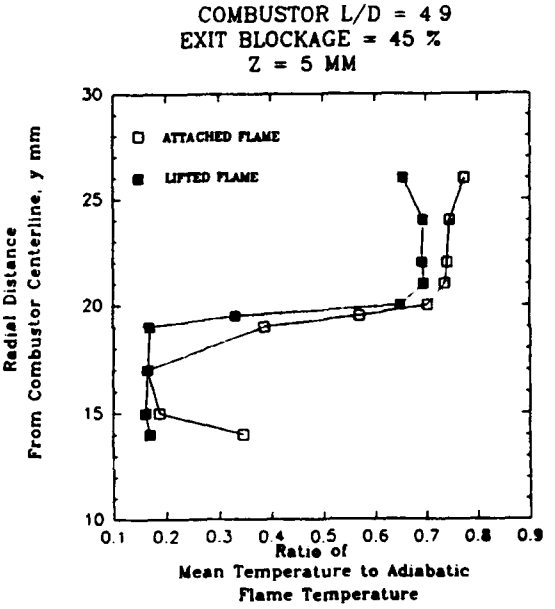

Fig. 27 Radial Profiles of Dimensionless Mean Gas Temperature in the Step Region for Attached and Lifted Flames at Fixed Exit Blockage

Note that both Figures 26 and 27 indicate an elevation of gas temperatures over the inlet conditions close to the confluence of the jets and around the region encompassing the small, central recirculation bubble (Sturgess et al., 1991b). Although not yet supported by strong direct evidence, it has been hypothesized (Sturgess et al., 1991a) that nonstationary flow interactions of the fuel and air jets with the central recirculation bubble result in additional radial mass transport of reactants. Such mass transport could account for early chemical reaction and hence, the observed elevated temperatures close to the orifice. The p.d.f. at a radius of 14 mm for an equivalence ratio of 1.36 at a combustor loading of 0.428 $lb_m/(sec.ft.^3atmos.^n)$ shows that there is an equal probability of the flame being present as there is of fluid at

inlet temperatures. This radius marks the position of the outer-edge of the fuel tube. For this temperature condition to be so, either direct flame or a hot gas ignition source from the step recirculation zone must be transported completely across the annular air-jet path (see Figure 1).

The addition of blockage increases the centerline mean temperatures for lifted flames at loadings fairly near to the lean flammability limit. The effect is particularly strong for distances closer to the confluence of the jets than 100 mm, as Figure 28 shows. The radial profiles of dimensionless mean temperature indicate that blockage slightly increases the temperature in the step recirculation zone.

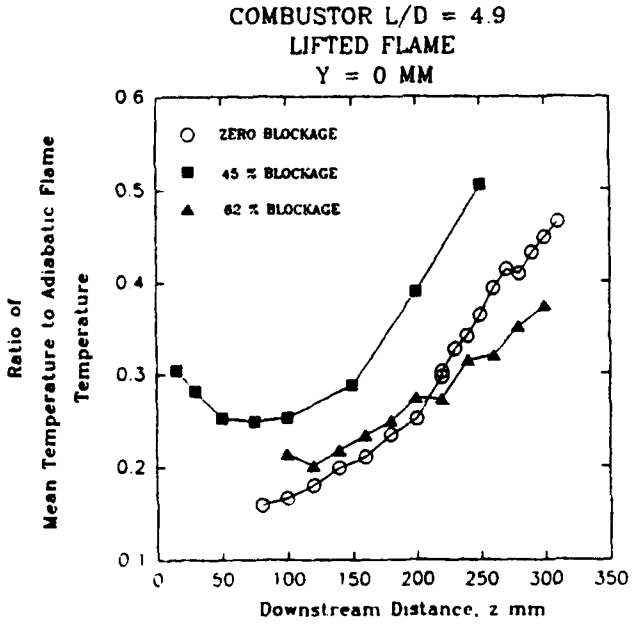

Fig. 28 Comparison of Centerline Profiles of Dimensionless Mean Gas Temperatures for Lifted Flames at Various Exit Blockages

The centerline profiles of the ratio of the RMS value of fluctuating temperature to mean temperature for 0, 45.1 and 62 percent exit blockage in the 4.9 L/D combustor are given in Figure 29. The equivalence ratios are such that the flames were all lifted, and the combustor loadings were 0.7 to 0.76 $lb_m/(sec.ft.^3 atmos.^n)$. The fluctuating temperatures superimposed on the mean temperatures are not significantly affected by exit blockage. What is noteworthy, however, is the dramatic increase in the fluctuating component for distances closer than 50 mm to the jet origins. This is associated in particular with the forward stagnation point of the small, central recirculation zone, which for isothermal flow is situated at about 14 mm from the origin.

Figure 30 presents radial profiles of the ratio of RMS temperature to mean temperature at 5 mm downstream from the step-plane for a range of exit blockage at the same operating conditions as for the previous figure, i.e., lifted flame at light loadings. Temperature fluctuations in the step recirculation zone are not much affected by the exit blockage. In sharp contrast, the existence of any blockage at all exerts a powerful suppressing effect on fluctuations in the jet shear layers.

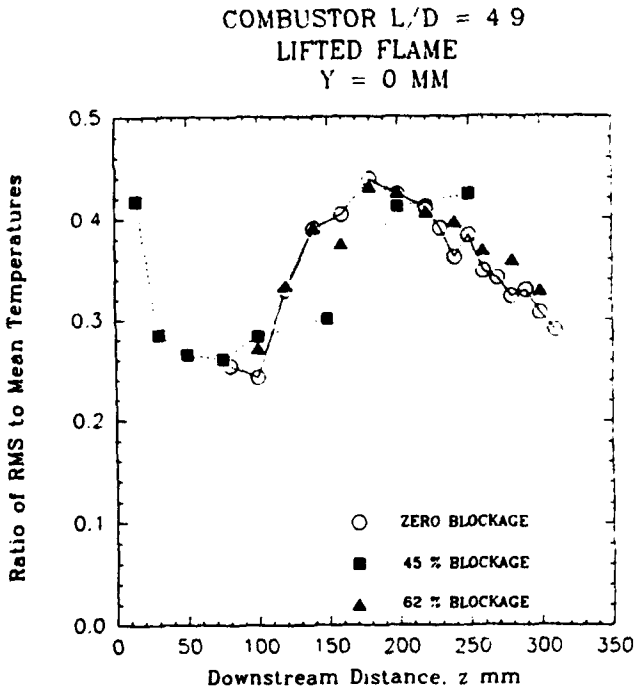

Fig. 29 Comparison of Centerline Profiles of Dimensionless Fluctuating Gas Temperatures for Lifted Flames at Various Exit Blockages

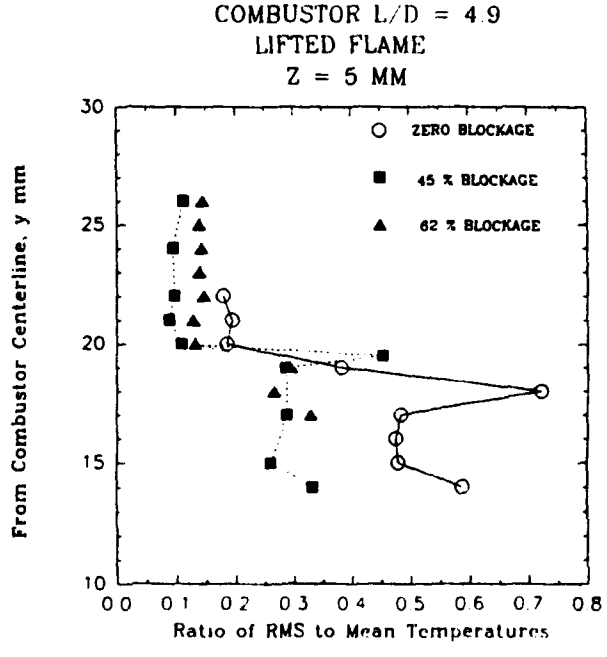

Fig. 30 Radial Profiles of Dimensionless Fluctuating Gas Temperatures in the Step Region for Lifted Flames at Various Exit Blockages

Whether the flame is lifted or attached, there are no changes in temperature fluctuations in the step recirculation zone at 5 mm downstream with 45.1 percent exit blockage. There appear to be some differences for the two flame conditions in the shear layers (possibly the pilot flame), but the present data are not sufficient to be sure.

DISCUSSION

The long-term intent for the research program, of which this effort is but a part, is to derive calculation procedures for lean blowout in gas turbine engine combustors. One of the calculation procedures being developed for this purpose is computational fluid dynamics (CFD). For viability, CFD should be able to provide a reasonable simulation of the real physical behavior involved in the lean blowout process. It is therefore required that significant flame events in the blowout process should be experimentally identified and characterized. The attached, separated and lifted flames and the influence of combustor geometry on the operational conditions under which these are encountered, hence form a significant part of the data base. The ability to calculate these characteristics will form a critical test of the efficacy of any CFD modeling of lean blowout.

The research combustor exhibits a distinct and repeatable flame pattern change as it blows out on the lean side (Figure 5). There are similarities in the flame changes for both rich and lean blowouts. A key element in these sequences of flame change is the loss of the thin, sheath-like pilot flame anchored at the outer diameter of the air jet. This pilot flame serves as a continuous ignition source for the main flame that then originates in the shear layers associated with the fuel and air jets, and the recirculation zones. For rich blowouts, loss of the pilot flame does not result in obvious changes in the main flame, either in position or character. It tends to remain concentrated in the shear layers. However, for lean blowouts, loss of the pilot flame causes the main flame to lift to a downstream position. This clearly allows significant premixing of reactants to occur, with the result that the main flame in its lifted position is more distributed across the width of the combustor. Blowout in the separated rich flame takes place suddenly; in the lifted lean flame, blowout is preceded by the onset of large-scale axial oscillations of the main flame about its mean position (Figure 5).

The flame events described are controlled by the operating equivalence ratio of the combustor (Figures 5 and 10). The equivalence ratios at which flame events occur are modified by the existence of back-pressure applied at the exit from the combustor (Figures 6 through 9 inclusive). The sensitivity of the event-equivalence ratios to the exit back-pressure depends on the combustor loading, and this sensitivity generally increases with the loading (Figures 8 and 10).

The application of exit back-pressure to the research combustor exerts a favorable influence on the lean blowout (Figure 11). At fixed combustor loading, the effect depends on the combustor length to diameter ratio. When acoustic effects and direct loss of the step recirculation zone (Figure 12) are eliminated through use of an appropriate combustor length, the changes in blowout due to exit blockage are sensitive to combustor loading (Figures 11 and 13). Predictably, they are strongest at high loadings approaching the peak heat release rate condition. At low combustor loadings, the improvement in stability due to blockage is consistent with a more persistent anchored flame (Figures 6 and 7), but conflicts with an earlier onset of large-scale axial movements of the lifted flame (Figure 8).

The presence of the outlet blockage changes the isothermal flow field in the combustor by causing acceleration of the mean axial velocities about the centerline (Figures 3 and 4), and by introducing an additional recirculation zone on the upstream face of the orifice plate placed at the combustor exit. Acceleration of the central flow is evident as close as 125 mm downstream from the step plane (Figure 3), or, at an L/D of 0.83 in the 4.9 L/D combustor at 45.1 percent blockage. This is upstream of the reattachment plane for the step recirculation, which is at about 2.82 L/D (Sturgess et al., 1990). With a free exit in isothermal flow, the central flow is decelerated as the fuel and air jets merge and expand into the combustor around the step recirculation zone. The net acceleration that results with exit blockage represents a modification of the shear layers, and thus, flame holding in these shear layers can be expected to be changed.

The wall static pressure measurements in the step recirculation zone show that combustion suppresses a sensitivity to jet velocity ratio that is apparent in isothermal flow (Figures 19 and 21); the addition of exit blockage in isothermal flow exercises a similar effect (Figure 20).

With combustion, it can be inferred from wall thermocouple measurements that the position of the step recirculation zone reattachment shifts according to the equivalence ratio (Figure 18). For lifted flames, the dependency on equivalence ratio is modified by the degree of outlet blockage (Figure 18). From wall static pressure tap measurements, the size of the orifice plate recirculation is inferred also to be influenced by combustion (Figure 23). For a lifted flame at a given blockage, the movements of these two stagnation planes with equivalence ratio is such that a constant separation between them exists (Figures 24 and 25), i.e., there is no direct interference. When the attached pilot flame condition is established, movement of the step recirculation zone reattachment essentially ceases (Figure 24). However, the orifice recirculation zone continues to decrease in size (Figure 24), with the result that the separation between stagnation planes is increased (Figure 25). Therefore, it is unlikely that the lean blowout improvement with exit blockage is associated with direct modification of the step recirculation zone.

The "quick-look" at mean gas temperature profiles shows the existence of the pilot flame for equivalence ratios when it is present (attached flame), and indicates slightly increased temperatures in the step recirculation zone and on the combustor centerline in the near-field. For lifted flames, exit blockage exerts its greatest effect in the near-field on the combustor centerline, particularly associated with the small, central recirculation bubble; there is little effect in the step recirculation zone. The CARS p.d.f.'s confirm earlier findings by OH emission and TFP measurements that the pilot flame is intermittently present even when direct observations indicate that it is lost and the main flame is lifted.

Fluctuating gas temperatures along the combustor centerline are insensitive to exit blockage (Figure 29); however, they once again confirm the strong dynamic nature of the flow associated with the central recirculation bubble that is generated by entrainment of the central fuel jet by the much stronger surrounding annular air jet (Sturgess et al., 1991b). In the near-field (at 5 mm) the radial profiles of fluctuating temperature suggest that exit blockage is a dampening effect; only slightly in the step recirculation, but much more strongly in the jet shear layers (Figure 30).

Back-pressuring the flame (by exit blockage in this case) exerts a powerful stabilizing effect on lean blowout, especially at the high combustor loadings that can represent critical operating conditions for military aircraft. Direct action of back-pressure on the step recirculation zone does not seem to take place. The back-pressure acts most strongly on the initial processes occurring in the jet shear layers by modifying their trajectories and turbulence characteristics. These initial processes emerge as being critical to the overall flame stabilization, whether the main flame is attached or lifted. Evidence is building (here and in earlier work) that dynamic behavior of the flow in the near-field can control the combustion process, perhaps through radical changes in radial mass transport.

The present results confirm that future attention should be directed at the pilot flame, the circumstances of its existence and its contribution to the main flame. The dynamic interactions of the central recirculation bubble with the jet shear layers and of the jet shear layers with the step recirculation zone must be explored in detail, and characterized if possible. It would be desirable if such future studies could include a mass transport experiment, and time-resolved flow visualization of the combustion in the shear layers.

CONCLUSIONS

1. Back-pressure by means of exit blockage does exert an effect on the lean blowout characteristics of a combustor. The effect is weakest at low combustor loadings near the flammability limits, and strongest at high combustor loadings near the peak heat release rate. Modification of the effect occurs with changes in combustor length to diameter ratio.

2. Direct interference effects of exit blockage on the step recirculation zone do not occur.

3. The major effects of exit blockage on lean blowout are due to changes in the fuel and air jet shear layers, and in the interaction of this shear layer with the step recirculation zone and with the central recirculation bubble. Dynamic processes appear to play a significant part in these interactions.

4. Future experimental work should concentrate on the near-field region, the dynamic interactions taking place there, and the circumstances governing the existence and role of the anchored flame.

5. The combustor exhibits consistent and well-characterized flame behavior that depends on equivalence ratio and exit blockage. The ability to represent this behavior will provide a stringent test of the realism of any numerical modeling (CFD) of this combustor.

ACKNOWLEDGEMENTS

The authors wish to acknowledge the contributions to this work from their colleagues at Wright-Patterson Air Force Base and Pratt & Whitney, and also, from Dr. P. Hedman, Brigham Young University, Provo, Utah. The University of Dayton work was supported by the U.S. Air Force Wright Laboratories, under Contract F33615-87-C-2767 (Contract Monitor Dr. W. M. Roquemore), and Pratt & Whitney was supported under Contract F33615-87-C-2822 (Contract Monitors 1st Lt. A. L. Lesmerises and Mr. D. Shouse). The authors thank the Air Force and Pratt & Whitney for permission to publish the results of this research.

REFERENCES

Chen, T. H., 1991, private communication of unpublished work.

Gupta, A. K., Lilley, D. G., and Syred, N., 1984, Swirl Flows, Abacus Press.

Heneghan, S. P., and Vangsness, M. D., 1990, "Instrument Noise and Weighting Factors in Data Analysis," *Experiments in Fluids*, Vol. 9, pp. 290-294.

Heneghan, S. P., and Vangsness, M. D., 1991, "Analysis of Slit Function Errors in Single-Shot Coherent Anti-Stokes Raman Spectroscopy (CARS) in Practical Combustors." *Reviews of Scientific Instruments*, Vol. 62, pp. 2093-2099.

Heneghan, S. P., Vangsness, M. D., Ballal, D. R., Lesmerises, A. L., and Sturgess, G. J., 1990, "Acoustic Characteristics of a Research Step Combustor," AIAA Paper No. AIAA-90-1851, (to appear in *Journal of Propulsion and Power*).

Heneghan, S. P., Vangsness, M. D., and Pan, J. C., 1991, "Simple Determination of the Slit Function in Single Shot CARS Thermometry," *Journal of Applied Physics*, Vol. 69, pp. 2692-2695.

Lefebvre, A. H., 1983, Gas Turbine Combustion, Hemisphere Publishing Corp., McGraw-Hill Book Company.

Lewis, B., and von Elbe, G., 1961, Combustion, Flames and Explosion of Gases, 2nd Edition, Academic Press.

Morrison, G. L., Tatterson, G. B., and Long, M. W., 1987, "A 3-D Laser Velocimeter Investigation of Turbulent, Incompressible Flow in an Axisymmetric Sudden Expansion," AIAA Paper No. AIAA-87-0119, AIAA 25th Aerospace Sciences Meeting, Reno, Nevada.

Pitz, R. W., and Daily, J. W., 1983, "Combustion in a Turbulent Mixing Layer Formed at a Rearward Facing Step," *AIAA Journal*, Vol. 21, No. 11, pp. 1565-1569.

Roquemore, W. M., Reddy, V. K., Hedman, P. O., Post, M. E., Chen, T. H., Goss, L. P., Trump, D., Vilimpoc, V., and Sturgess, G. J., 1991, "Experimental and Theoretical Studies in a Gas-Fueled Research Combustor," AIAA Paper No. AIAA-91-0639, presented at the 29th Aerospace Sciences Meeting, Reno, Nevada.

Stevenson, W. H., Thompson, H. D., Gold, R. D., and Craig, R. R., 1982, "Laser Velocimeter Measurements in Separated Flow with Combustion," Paper 11.5, presented at the International Symposium of Laser-Doppler Anemometry in Fluid Mechanics, Lisbon, Portugal.

Sturgess, G. J., Sloan, D. G., Lesmerises, A. L., Heneghan, S. P., and Ballal, D. R., 1990, "Design and Development of a Research Combustor for Lean Blowout Studies," ASME Paper 90-GT-143, (to appear in *Transactions of ASME, Journal of Engineering for Gas Turbines and Power*).

Sturgess, G. J., Sloan, D. G., Roquemore, W. M., Reddy, V. K., Shouse, D., Lesmerises, A. L., Ballal, D. R., Heneghan, S. P., Vangsness, M. D., and Hedman, P. O., 1991a, "Flame Stability and Lean Blowout - A Research Program Progress Report," *Proc. 16th ISABE*, Nottingham, England, pp. 372-384.

Sturgess, G. J., Heneghan, S. P., Vangsness, M. D., Ballal, D. R., and Lesmerises, A. L., 1991b, "Isothermal Flow Fields in a Research Combustor for Lean Blowout Studies," ASME Paper 91-GT-37, (to appear in *Transactions of ASME, Journal of Engineering for Gas Turbines and Power*).

Sturgess, G. J., Heneghan, S. P., Vangsness, M. D., Ballal, D. R., and Lesmerises, A. L., 1991c, "Lean Blowout in a Research Combustor at Simulated Low Pressures," ASME Paper 91-GT-359, (to appear in *Transactions of ASME, Journal of Engineering for Gas Turbines and Power*).

APPENDIX F

FLAME STABILITY AND LEAN BLOWOUT

BY

G. J. Sturgess and D. G. Sloan
Pratt & Whitney, East Hartford, Connecticut

W. M. Roquemore, V. K. Reddy, D. Schouse and A. L. Lesmerises
WRDC/POSF, Wright-Patterson Air Force Base, Ohio

D. R. Ballal, S. P. Heneghan and M. D. Vangsness
University of Dayton, Dayton, Ohio

P. O. Hedman
Brigham Young University, Provo, Utah

Published in The Proceedings of the Tenth International Symposium on Air Breathing Engines, Nottingham, U.K., pp. 372-384, September, 1991.

ISABE 91-7037

FLAME STABILITY AND LEAN BLOWOUT
A Research Program Progress Report

G. J. Sturgess and D. G. Sloan
Pratt & Whitney, East Hartford, Connecticut

W. M. Roquemore, V. K. Reddy, D. Schouse and A. L. Lesmerises
WRDC/POSF, Wright-Patterson Air Force Base, Ohio

D. R. Ballal, S. P. Heneghan and M. D. Vangsness
University of Dayton, Dayton, Ohio

P. O. Hedman
Brigham Young University, Provo, Utah

Abstract

A progress report is presented on a comprehensive research program aimed at improving the design and analysis capabilities for flame stability and lean blowout in the combustors of aircraft gas turbine engines. The motivation and aims of the program are reviewed, and the unusual approach adopted to address the research issues is outlined. The supporting experimental program and the test vehicles involved are described, together with some major results obtained to date. The modeling techniques that are being explored are summarized. Their potential and limitations are highlighted. Although much work remains yet to be done, the progress made thus far gives rise to reasonable optimism for achieving the program objectives.

Program Overview

Traditional gas turbine combustor design methodology has been based on empirical correlations, experience, scaling of successful designs, and extensive development testing. This approach has been amazingly successful. However, as the demands on the combustor have increased, the margin for error in achieving goals has been reduced. At the same time, the escalating costs of rig tests and experimental engines is limiting the amount of development work that can be carried out.

The weakness of the traditional approach is two-fold: First, empirical correlations, and the phenomenological models upon which they are based, provide limited insight into the fundamental physical and chemical processes that they represent. This fact makes radical departures from previous designs very risky. Second, and perhaps the greatest weakness, is that when things go wrong in a design the methodology is seldom capable of providing explanations or offering solutions to the problem.

Reasonably complete mathematical simulation of practical aerospace systems by means of computational fluid dynamics (CFD) has recently emerged as a modeling tool of considerable and ever-growing potential and power.[1] Although successful application of the technique as an engineering tool to complex internal flows has not yet advanced to anywhere near the same degree as for external flows, recent progress in the area has been rapid.[2,3] Although many improvements are still needed, CFD computer codes when incorporated in a design system, offer the potential benefit of a methodology that is predictive, confer increased understanding of complex coupled behavior, and promise a reduced reliance on expensive experimental tests.

In the United States of America, Government funding has been a powerful motivator for the development of CFD applied to the modeling of aerospace powerplants. In the combustor area, the U.S. Army Research Laboratories initiated and funded the first serious effort in 1975. In 1977 the U.S. Air Force launched the Combustion Model Evaluation (CME) program to develop advanced diagnostic techniques and to establish a technology base for the evaluation of combustion models. In parallel, U.S. industry initiated its own internally funded, exploratory programs[4]. By 1981, NASA's Lewis Research Center introduced the Hot Section Technology (HOST) program. A three-phase program, Phase I of this endeavor utilized published data to establish the accuracy and identify short-comings of the most popular CFD codes then current.[5-7] Some of the problems identified in Phase I were addressed in Phase II, which produced improvements in numerical accuracy[8] and computational speed, and added to the experimental database. Regrettably, the HOST program ended in 1987 before entering Phase III, where based on the preceding work, a new state-of-the-art CFD code was to have been developed. Consequently, CFD development remained with industry where efforts were wisely concentrated on converting the early codes into useful engineering tools through the introduction of extensive pre- and post-processing capabilities and, flexible boundary condition specification and complex geometry representation, together with solution procedure speed-up[9]. Progress in this area has been both rapid and impressive. However, the current CFD codes essentially retain the technical capabilities of the original generation of codes.

The gap in physical modeling resulting from the premature termination of HOST prompted the U.S. Air Force to restructure the CME program to focus on combustor technical modeling. In 1987 the Combustor Design Model Evaluation (CDME) program was established. The CDME is an effort to improve the available physical modeling such that the engineering-tool CFD codes can be upgraded to address the design of combustors for gas turbine engines in comprehensive fashion.

The program specific objective is "to bring about significant improvements in the design capabilities of

Copyright © 1991 by ISABE and AIAA. All rights reserved.

computer-based gas turbine models to advance the methodology for designing gas turbine combustors."

There are many areas of physical modeling related to gas turbine combustion that require improvement. However, of all of the combustor design requirements that must be satisfied, combustor stability is considered to be the most important since it directly concerns aircraft safety. Current modeling practice for combustor stability is phenomenological and design specific; the resulting data-correlations are such that when used for design purposes, they can result in volume uncertainties as much as 2:1. Furthermore, engine design trends towards high temperature rise combustors, together with renewed demands for low exhaust emissions of pollutants, are eroding available stability margins for fixed geometry combustors.[10] Even staged combustors (either fuel or air) can have stability difficulties at the staging point(s). Combustor stability therefore represents one suitable target for the CDME program.

Problem Background

The combustion stability limits in an aircraft gas turbine engine can typically be determined by four major factors. These factors are: the fundamental flame holding behavior of the combustor, acoustic coupling effects in the combustor, reactant supply limitations imposed by the engine systems (e.g. fuel atomization, fuel pump speed, fuel control settings, compressor vane scheduling, etc.), and, operating excursions due to dynamic interactions between the engine components (e.g. compressor stalls and surges, etc.). The present study is concerned only with the first of these.

The flame holding characteristics of the combustor are sometimes referred to as the blow-off limits. Stability in this context is defined as the range of operating fuel-to-air ratios within which a time-mean stationary flame can be maintained inside the combustor. Implied is the existence at any operating point (combustor loading) of two limiting fuel-to-air ratios, one involving excess fuel (rich) and the other involving excess air (lean) over the values to completely convert all the reactants. Blow-off at fuel-rich conditions is difficult to achieve under normal circumstances, except near the peak heat release rate condition. If encountered it commonly results in severe thermal damage to the turbine and possibly the combustor also. Of more practical interest is blow-off at fuel-lean conditions.

For the aircraft engine, combustor blow-off limits are encountered during low engine speeds at high altitudes over a range of flight Mach numbers. This is illustrated in Fig. 1 as a loss in the operating envelope. The shape and extent of the envelope loss depend on the flow characteristics of the engine at low speeds (windmilling flight or flight idle conditions normally), and on the design of the combustor. It is the task of the combustion engineer to design a combustor that will be stable for all required flight operating conditions. By that, all steady state engine operating points should lie inside an envelope defined by the combustor loading and the rich and lean fuel-to-air ratio range within which combustion can be sustained. This envelope should be extensive enough to encompass the under- and over-shoots associated with the different response rates to throttle movements of the fuel system and the rotating machinery; adequate allowance for safety margins should also be included. Fig. 2 illustrates these requirements.

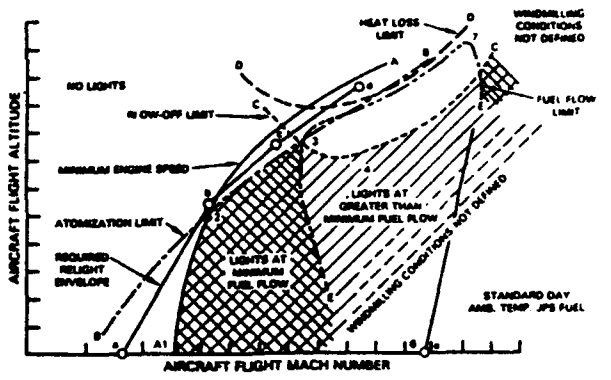

Fig. 1 Engine operating envelope determined by relight capability.

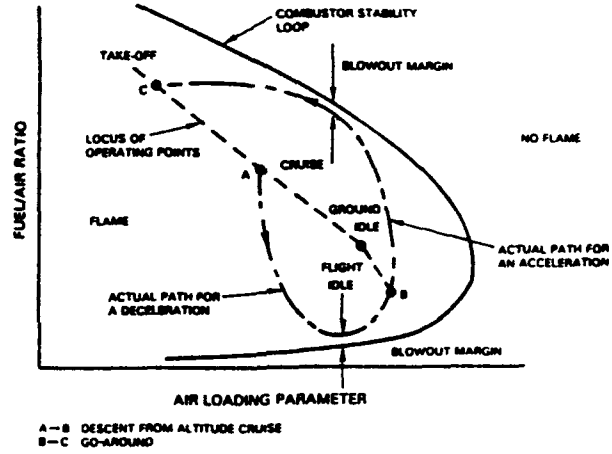

Fig. 2 Engine operations superimposed on a stability loop, showing how transients reduce stability margins.

Program Approach

The overall strategy adopted to address the program objective as applied to combustor stability, involved three distinct steps:

1. Provide by experimental means, an improved understanding of the physics involved in lean blowout.
2. Model the lean blowout process, and integrate the modeling with CFD codes.
3. Provide experimental databases against which the modeling is tested and calibrated.

The following procedure for implementing the strategy was devised: The total problem was divided into two phases that separated out liquid fuel preparation from the basic aerodynamics and combustion chemistry. If the initial phase, in which gaseous fuels were to be used, was unsuccessful then

the second phase for liquid fuels (JP8/JP5/Jet A) would not proceed.

Phase I, for which propane was selected as the prime gaseous fuel, consists of a fundamental element and an applied element. The fundamental element (Task 100) contains the design, development and testing of a research combustor, and the modeling development. The applied element (Task 200) contains the design, development and testing of a generic gas turbine combustor, and comparison of the Task 100 modeling against the Task 200 measurements.

To maximize the likelihood of success, the joint program utilizes the combined talents available from the U.S. Air Force Wright Research and Development Center (WRDC), the University of Dayton Research Institute (UDRI), Systems Research Laboratories Inc. (SRL), and Pratt & Whitney (P&W). The intent was to have P&W design the research combustor, provide the generic combustor, and develop the modeling, while WRDC and two on-site Air Force contractors, UDRI and SRL, conducted the experimental program proposed by P&W; overall direction was to be by the Air Force Contract Monitor and the P&W Program Manager. In practice, as the effort developed these responsibilities have become somewhat blurred, and individuals now enthusiastically contribute regardless of affiliation, functioning as part of an integrated team. Additional contributions are being made from the university community through the WRDC Summer Professor program.

Research Combustor

The purpose of the research combustor is to yield experimental information on the lean blowout process to assist in understanding the events taking place, and so guide in modeling them. To achieve this purpose in relevant fashion the research combustor should reproduce the essential flame holding characteristics of an aircraft gas turbine combustor. Fig. 3 illustrates the flow patterns observed in such a P&W annular combustor. Note the axial swirling jet of fuel and air associated with each fuel introduction, and the sudden expansion of these jets as they enter the primary zone to create local recirculation zones surrounding the jets. This action is assisted by the back-pressure provided through an array of radial air jets positioned at the end of the primary zone.

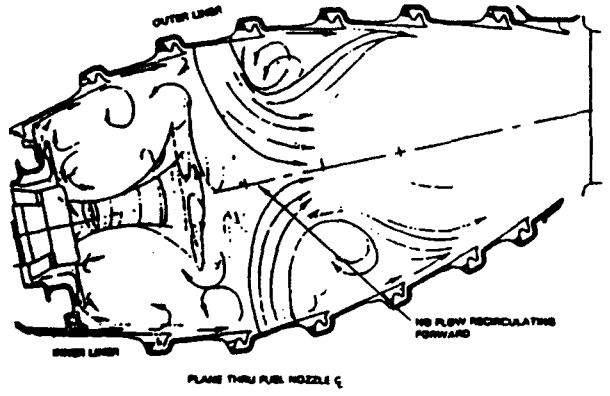

Fig. 3 Flow patterns in a combustor.

The Task 100 research combustor was designed[11] to reproduce the primary zone flow field of Fig. 3, but in simplified form. The design was also required to provide good optical access for flow visualization and use of laser diagnostics.

An axisymmetric configuration was adopted for the reactants supply, where a 29.7 mm inside diameter central fuel jet (gaseous propane) is concentrically mounted in a surrounding 40 mm diameter air jet. The jets are located centrally in a 150 mm nominal diameter duct forming the combustor body. A later modification will allow the introduction of controlled swirl into the annular air jet. A backward-facing step at the jet discharge plane closes the combustor body and completes the sudden expansion, giving a step height of 55 mm. The combustor has an overall length from step to exit of 735 mm, and the exit is restricted by an orifice plate of 45 percent blockage.

Optical access is provided in the initial 475 mm of the combustor, and results in the cross-section of flat quartz windows and vorticity-suppressing metal corner-pieces, shown in Fig. 4. The uncooled combustor is mounted vertically on a flow-conditioning unit, and the whole assembly is traversed vertically and horizontally through a cut-out in the fixed optical bench of the UDRI combustion laboratory at WRDC.

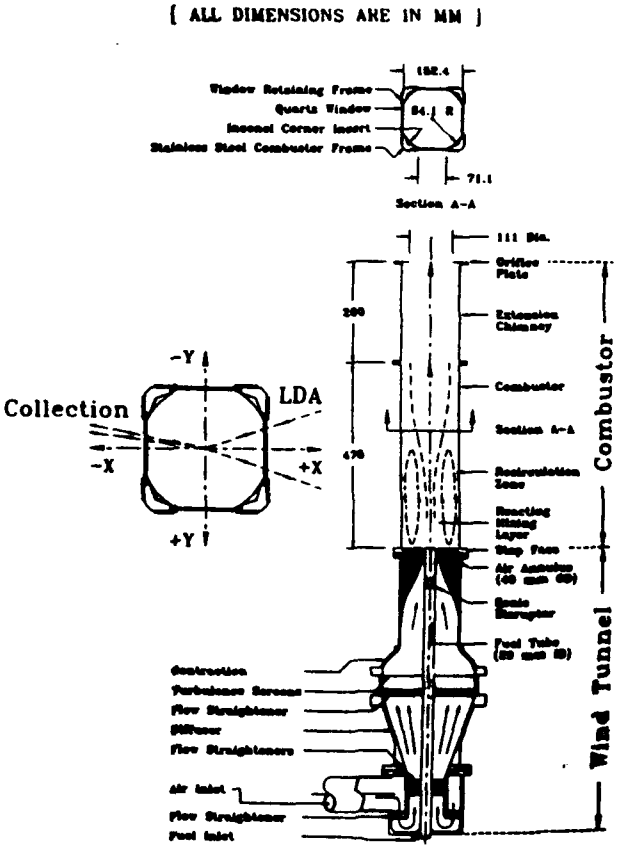

Fig. 4 Research combustor.

Combustion-induced acoustic oscillations can severely limit the operating ranges of some practical combustors, and

especially simple combustors of the present type. As was anticipated, initial reacting flow tests of the Task 100 combustor revealed some acoustic coupling that required redesign of the inlet flow conditioner, acoustic-closing of the fuel supply, and determined the configuration of the combustor outlet configuration.[13] These modifications essentially eliminated or so reduced the acoustic effects that there was no substantial effect on the lean blowout performance of the combustor.

When operated at a typical combustor loading and with jet velocity ratios corresponding to a fuel/air blowout condition at this loading, the isothermal (air/air) flow field measured in the combustor by laser-Döppler anemometer (LDA) revealed the presence of the desired major primary zone flow features evident in Fig 3, i.e. a jet shear layer system, an outer recirculation zone stabilized on the step and, a small, central recirculation zone generated by the momentum ratio of the jets.[12] Comparison of the measured jet time-mean and fluctuating velocity development with data in the literature revealed no evidence that the flat optical windows and their interfacing with the corner fillets introduced any adverse effects into the flow.

The Task 100 combustor was found[11] to operate with two flame configurations. When operated fuel-rich (overall equivalence ratios greater than unity) the flame is very stable and is anchored in the jet shear layers by a pilot flame that is attached to the step near the outer edge of the air supply tube. Fuel for this flame is recirculated from downstream by the step recirculation zone, and air for diffusion combustion is supplied by the air jet; ignition of this pilot flame is by hot gases from downstream that are also recirculated. As the bulk equivalence ratio is reduced the pilot flame becomes less stable, and eventually reaches a point where it is detached from the base region (lifts) and the entire flame structure becomes stabilized downstream of the shear layers due to loss of the pilot action. As a consequence of the flame-lift, a significant degree of partial premixing of the reactants then takes place upstream of the lifted flame position. When the equivalence ratio is further reduced the downstream flame stabilized by the recirculation zone becomes progressively less stable[13] in its lifted condition, and eventually blows out.

The piloting action of the flame in the jet shear layers by the attached flame at the step appears to be crucial to the stability of the combustor. Although the lifted flame condition itself is relatively stable[13], and an attached condition is readily recoverable from it by either increasing the fuel flow or reducing airflow, the beginning of the blowout process can clearly be associated with the loss of the attached flame. Successful calculation of the Task 100 combustor stability characteristics requires that the attached flame and its lift, be modeled.

Due to the stochastic nature of the flame and the integrating tendency of the human eye, visual observations of the attached flame at the step suggest that it is continuous and steady. It does not become obviously intermittent until the lift-condition is almost reached. In reality, careful study with optical diagnostics revealed that at any equivalence ratio the "attached" flame is alternatively lifted and then reattached; for rich conditions it is attached most of the time and for equivalence ratios near unity it is lifted most of the time. Precise determination of the equivalence ratio for lift was obtained by monitoring the signal intensity of the spontaneous OH u.v. emission from the attached flame at its attachment point.[14] As fuel flow at fixed airflow was reduced there was a general decrease in the OH emission down to an equivalence ratio of 1.05; further reductions in fuel flow caused little change in the signal until blowout. this equivalence ratio is in excellent agreement with visual observations on flame lift and characteristics.[11,12]

A study of the attached flame was made using a 14 μm SiC_4 thin-filament pyrometer (TFP) positioned at 1 cm above the step, to provide a time-sequence of the radial profile of nearly instantaneous relative temperature for an overall equivalence ratio of 1.56.[14] These profiles yield some additional information on the attached flame. From the temperature peak, a flame thickness of about 5 mm was obtained. The radial position of the temperature peak oscillates about a mean radius of 24 mm with a displacement about 4 mm. This displacement is in agreement with the approximate size of vortices in the flame, as 10 ns exposure images of laser induced fluorescence (LIF) emission of OH[14] reveal. For both attached and lifted flames, there is a strong temperature intermittency at this position, with frequencies less than 10 Hz. This frequency is only a fraction of the estimated frequency for shedding off the step of the entire recirculation zone.[13]

The OH images of the flame show that the attached flame structure at any given time is associated with local vortices shed from the inner edge of the combustor step. The flame surface is not circumferentially continuous but contains local holes that appear to be associated with the braid regions of the vortex train. For this reason the flame is not instantaneously symmetric, as Fig. 5 illustrates. When the flame is lifted and stabilized downstream, the instantaneous OH images reveal combustion takes place in a more distributed form via relatively large "packets" of reaction.

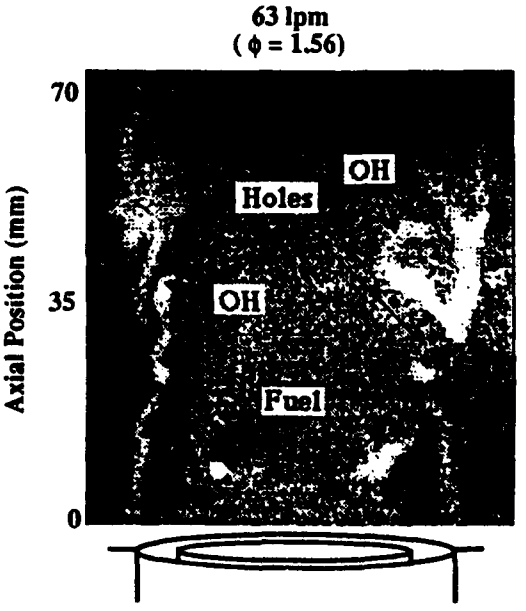

Fig. 5 Image of laser induced OH fluorescence for the attached flame with 63 lpm propane, 1000 lpm air, ϕ = 1.56.

In order to obtain a complete definition of the lean stability of the Task 100 combustor, operation at sub-atmospheric pressures is necessary. The UDRI laboratory at WRDC was only capable of operating at atmospheric pressure however, and was initially limited to propane flow rates less than 20 kg/hr. In order to overcome these limitations low pressure simulation was used.[15] Excess gaseous nitrogen was introduced into the air supply upstream of the combustor as a diluent to lower the concentration of reactants and to lower the reaction temperature by virtue of its heat capacity. These result in reduced reaction rates that are similar to those obtaining at true low pressures. A calibration for the technique was devised and verified. By this simulation the combustor was operated at equivalent pressures down to 0.1 atmosphere, with excess nitrogen to fuel mass ratios up to 9.

Fig. 6 displays the lean stability of the combustor in terms of the equivalence ratio at blowout, successfully correlated against a standard loading parameter LP, derived from chemical reaction rate theory but modified to include the effects of inert excess nitrogen, where,

$$LP = \dot{m}_{Tot} / (V P^{n}) \quad (1)$$

$$\dot{m}_{Tot} = \dot{m}_f + \dot{m}_a + \dot{m}_{N_2} \quad (2)$$

$$n = 2\phi_{LBO} / (1 + \dot{m}_{N_2} / \dot{m}_a) \quad (3)$$

where V is the combustor volume, P is the operating pressure, and $\dot{m}$ signifies mass flow rate with subscripts a, f and N_2 denoting air, fuel and excess nitrogen, respectively.

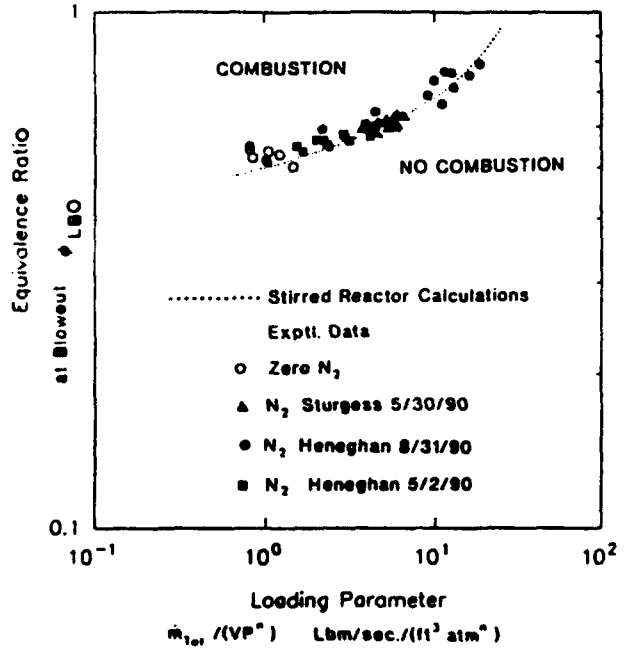

Fig. 6 Correlated blowout data for the research combustor, and comparison with the calculated well-stirred reactor blowout characteristic for the research combustor.

Work in the Task 100 research combustor is continuing using advanced laser and TFP diagnostics to elucidate the formation of the attached flame and the importance of the recirculation zone. Complete time-mean velocity and temperature fields within the combustor are also being obtained over a range of operating conditions, by means of LDA and CARS.

Generic Gas Turbine Combustor

The purpose of the generic gas turbine combustor (Task 200) is to provide an experimental database against which the lean blowout modeling might be tested and calibrated. This purpose places three major requirements on the design of the Task 200 combustor: First, that it be as close to a real aircraft gas turbine engine combustor as possible in terms of LBO performance and flow field. Second, that it be flexible enough to allow sufficient variation in relevant geometry and flow distribution to afford some investigation of the important primary zone design characteristics, such as equivalence ratio and residence time. Third, that sufficient optical access be provided so that laser diagnostics might yield details of important flow features.

Fig. 7 provides a schematic drawing of the Task 200 combustor cross-section. The configuration adopted is a four-injector, planar-section, simplified version of a conventional annular combustor. The anticipated flow field is similar to that shown in Fig. 3.

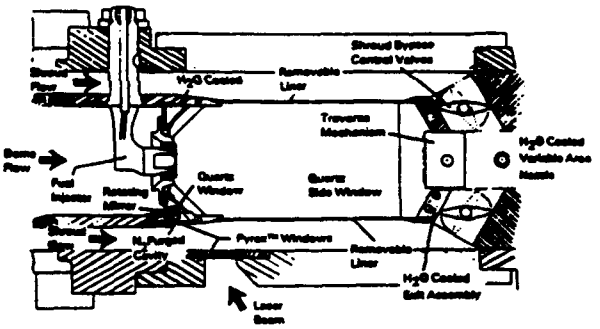

Fig. 7 Design features of generic combustor.

The fuel injectors and their combustor/dome interfaces are actual experimental engine hardware, with the injectors modified, calibrated and individually balanced to flow gaseous propane. The major dimensions of combustor dome height, length and injector spacing are based on those of the engine that supplied the injectors. Cooling air is introduced as a surface film at the dome/liner interfaces. The liners, upper and lower, are removable and may contain any desired pattern of air ports; they do not have any specific internal film cooling, but are provided with a thermal barrier coating and are convectively cooled by the shroud flows.

The current pattern of air ports in the liners is one successfully developed for an in-service engine. Careful *in situ* measurements were made of the discharge coefficients for the dome and liner air ports.

Two domes are available; one a plain bulkhead (also provided with thermal barrier coating), and the other a

vertically-symmetrical configuration shown in the figure, having filleted upper and lower corners. Ignition is by means of a hydrogen torch-ignitor.

Air is supplied to the dome and upper and lower shrouds by individually-metered supplies that are always isolated from each other by means of an upstream array of sonic venturis. At the exits from the combustor and shrouds are independent, water-cooled valves that control the bypass flows.

Fig. 8 shows the rig mounted in the test facility at WRDC. Flow is from left to right, and the rig exhausts from the facility via the circular duct to the right. Mounted about the test section may be seen the hardened LDA and CARS system.

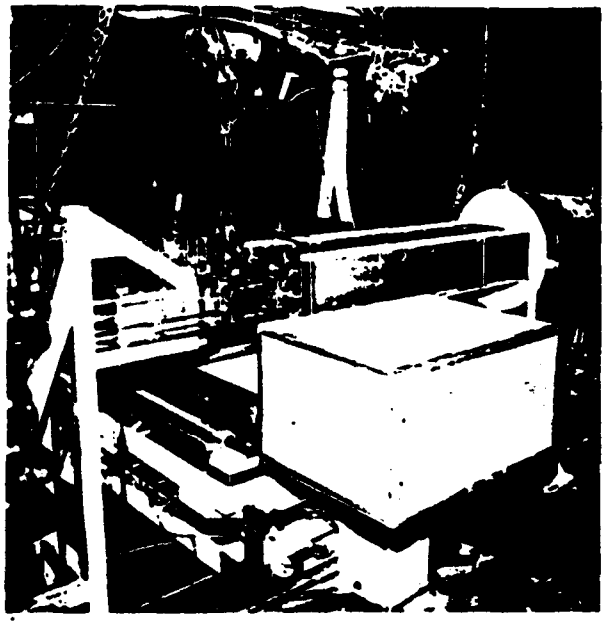

Fig. 8 Rig mounted in the test facility at WRDC.

Optical access to the combustor for visualization and laser diagnostics is provided primarily by the side-walls enclosing the four-injector section. These side-walls are of fused quartz, and are contained in water-cooled housings, fittings for which can be seen in Fig. 8. A further optical path is provided by windows in the base of the rig that allow laser beam access to a high-speed rotating mirror contained by the dome lower fillet-piece (this dome configuration only). Through selectively-opened slits in the dome, the rotating mirror can scan the combustor with vertical planar sheets of laser light for imaging purposes. For thermal protection, the mirror cavity is purged with a pressure-balanced flow of gaseous nitrogen. Additional means of optical access through the liners are being explored.

Considerable flexibility has been achieved in the design. The generic combustor rig is designed to be operated up to 65 psia, and the rig is provided with a gaseous nitrogen supply to also allow simulation of sub-atmospheric pressures, as with the Task 100 combustor. The fuels can be either propane or methane (Phase I). The amount of air that enters the combustor via the dome can be varied from 10 to 40 percent of the combustor total. Different transverse air jet patterns can be introduced by changing the removable liners, and two dome configurations (plain bulkhead and filleted) are available. Reasonable optical access has been achieved.

Testing in the Task 200 combustor has recently commenced, and Fig. 9 shows provisional LBO's at atmospheric pressure with the filleted dome passing 35 percent of the combustor airflow and using methane as fuel. The LBO equivalence ratios are correlated against the loading parameter described by Equations 1-3. Although the loading parameter range was extremely limited, the blowouts apparently evidence a characteristic that is indicative of flame holding provided by two burning zones.

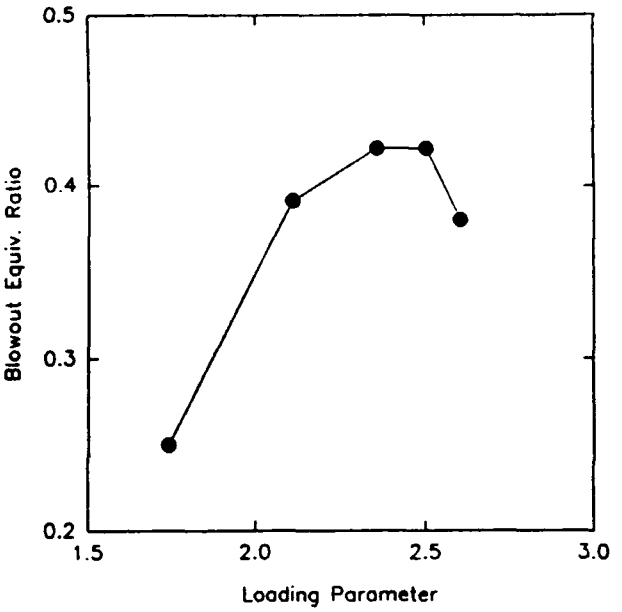

Fig. 9 Lean blowouts for generic combustor with methane.

Modeling Lean Blowout

As indicated above, lean blowout experimental data from a given combustor can be correlated in terms of the equivalence ratio at blowout and the reaction rate-based loading parameter defined by Equations 1-3. Fig. 10 gives examples of such data correlations for two practical gas turbine annular combustors; one is for a combustor using a long-stem bubble-cap vaporizer tube as a fuel injector[16], and the other is for a combustor using a strongly swirling prefilming airblast fuel injector. In both cases, the equivalence ratio is based on the total airflow through the combustor, and the volume used in the loading parameter is that of the complete combustor. In this instance, the apparent reaction order on pressure (Equation 3) is taken as 2.0, which is appropriate to stoichiometric mixtures. In addition to the differences in fuel injection and the differences in fuel distribution that resulted, the two combustors had completely different flow fields due to their different shapes and liner hole patterns.

Although the loading parameter adequately handles the range of inlet variables covered in the experiments, it can be seen that the two lean blowout characteristics are completely different. Note the similarity of the swirl-stabilized characteristic to the preliminary Task 200 combustor results in Fig. 9. As may be realized from Fig. 10, a completely general correlation for lean blowout in this simple form is not possible. Even attempts to correlate lean blowout data from a family of combustors having similar flow patterns and dimensional relationships but differing in scale and flow parameter, have not been especially successful.

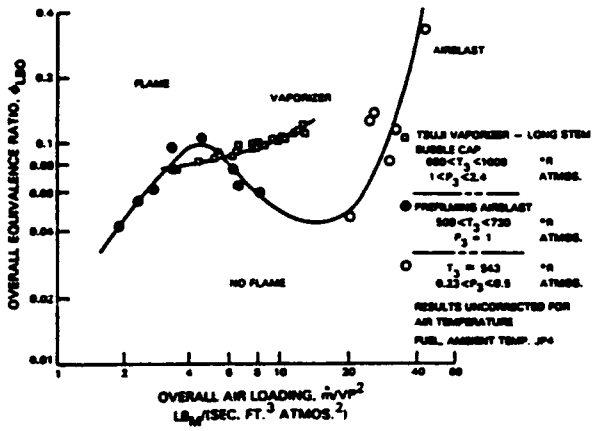

Fig. 10 Comparison of airblast atomizer and vaporizer-tube lean blowouts showing the existence of piloting action.

It becomes evident from the behavior of experimental lean blowout data that direct calculation offers the only possibility of making reliable *a priori* estimates of stability in gas turbine combustors. This difficult task becomes somewhat more tractable if CFD techniques can be used to define local characteristics in the combustor flow field.

Complete calculation of stability directly through CFD alone is not considered as a viable approach. Lean blowout is dominated by the kinetics of chemical reaction due to the low air pressures and temperatures where it is encountered. A CFD calculation would be required to incorporate in its combustion model a chemical reaction mechanism that yielded the correct heat release. For hydrocarbon fuels, very many reaction steps involving several individual species might be necessary to achieve this. A general transport equation of the form,

$$\frac{\partial}{\partial x_j}\left(\bar{\rho}\,\bar{u}_j\,\bar{m}_i - \Gamma_{eff}\,\frac{\partial \bar{m}_i}{\partial x_j}\right) = S_{\bar{m}_i} \qquad (4)$$

where i denotes chemical species, m_i is the mass fraction of i, and S_{mi} is a species source term, would need to be solved for each of the species. Even for reduced reaction mechanisms, the computational burden involved is presently unacceptable. Furthermore, since reaction rates are reduced as blowout is approached, laminar chemistry is not sufficient; the influences of turbulence on the reactions must be accounted for.

The approach adopted for the calculation of lean blowout is to uncouple the chemistry from the fluid dynamics, and to address each problem separately. This basic philosophy is applied at three levels of simplicity:

1. Phenomenological modeling based on a characteristic time approach, with CFD providing local flow properties.

2. Application of full chemistry via a stirred reactor network established on the basis of CFD analysis of the flow field.

3. Incorporation within the CFD calculation of stirred reactors at the sub-grid level, and using reactor extinction criteria based in the Level 1 approach.

Characteristic Time Models

As an example of the first level, a reaction-quenching model has been derived from the argument that propagation of flame will not take place when the rate of mixing between the small turbulent eddies of hot products and cool reactants is greater than the local chemical reaction rate. Similar arguments have been used by Lockwood and Megahed[17]. Derivation is not presented here for reasons of brevity, but the quenching criterion resulting is given as,

$$\frac{1.5\left(D + \frac{C_\mu}{\sigma_t}\,\frac{K^2}{\epsilon}\right)}{\nu\left(\frac{S_L}{(\epsilon\nu)^{1/4}} + 1\right)} > 1.0 \qquad (5)$$

where D is the laminar diffusion coefficient, K is the kinetic energy of turbulence, and ϵ is its rate of dissipation, C_μ is a constant, σ_t is a turbulent Schmidt number, and S_L is the laminar flame speed.

The quenching criterion requires turbulence parameters for evaluation. An isothermal flow CFD calculation provides this information at each grid node of the calculation domain. The quenching can then be examined on a point-by-point basis to see if any part of the flow field could support combustion. Two additional conditions must also be satisfied for stable combustion. First, in regions where the turbulence would not quench combustion, the local fuel/air mixtures must be inside the flammability limits for the fuel. Second, the local mean flow velocities should not exceed the turbulent burning velocity. Again, the CFD results enable these conditions to be evaluated.

In somewhat limited evaluations, Equation 5 showed promise in the Task 100 combustor of being successful in delineating between operating conditions where combustion was possible and where it was not.

Stirred Reactor Modeling

Representation of the combustor by an equivalent global stirred reactor network inexpensively enables full chemistry to be used in a calculation, so that stability can be

determined from thermo-chemistry considerations. In this approach, aerodynamic effects, such as turbulence quenching or acceleration of reaction, are removed from consideration. Fluid dynamics only enters via a CFD calculation from which the suitable reactor network is established.

To establish a good global reactor network, considerable and careful post-processing of the CFD solution is necessary. Flow structures existing in the fields must be identified, classified, and dimensionally defined. Local mass flow rates, including that recirculated where appropriate, must be assigned to each structure. For three-dimensional calculation domains, this is not a trivial task, and flow topology mapping techniques[18-20] can be used with profit.

Swithenbank[21] has presented a dissipation gradient approach for defining perfectly-stirred regions of combustors. This classification approach was successfully applied to the two-dimensional Task 100 research combustor[15]. Based on this analysis, the rapid mixing region of the combustor was established from CFD calculations as the volume contained within a surface contour containing 96 percent of the turbulence kinetic energy and 99 percent of its rate of dissipation, and over which the total dissipation gradient was not less than 10 times the minimum value recommended by Swithenbank. From within this rapid mixing region, a well-stirred reactor volume was then defined by super-imposing an additional space encompassing fuel/air mixtures falling inside the flammability limits for propane and air. The resulting reactor was 44 percent of the combustor volume, and corresponded reasonably well to the lifted flame observed in the real combustor.

Fig. 6 contains an LBO line representing the stirred reactor calculation of the Task 100 combustor. The Task 100 combustor was modeled as a single, perfectly-stirred reactor, defined as described above, with separate air and fuel inlets and a single discharge of products; there was no product recirculation. The agreement of the calculation with the measured data is extremely good.

A more complex reactor network is needed to represent the Task 200 combustor. As a temporary procedure and pending completion of the full topology post-processing technique in three dimensions, a provisional reactor network was established in order to explore the behavior of such a network over a range of combustor loadings as blowouts were approached. The network was set up by video taping the flow structures present in the combustor near blowout conditions (through the quartz side windows in the rig), and then tracing those images off the playback screen to determine their size and connectivity. Reactor classification of the sized structures was based on the color of the video images. Despite its crudity, this procedure was believed to be reasonably representative for the intended purpose. The major uncertainty was associated with the recirculated mass flow rates, which of course could not be obtained by these means, and were therefore made purely arbitrary and subject to parametric analysis.

The combustor modeled was the same as that yielding the provisional LBO data shown in Fig. 9, and used methane fuel in the filleted dome which passed 35 percent of the total combustor airflow. The reactor network consisted of six mixing, perfectly-stirred or plug-flow reactors in series, with recirculation from Reactor 3 to Reactor 1 via an additional perfectly-stirred reactor. Calculations were made at a number of airflow levels, and, for a flow distribution to the various reactors made according to the measured effective areas of the real combustor and the assigned reactor distribution. Atmospheric, sub-atmospheric and super-atmospheric pressures were used, and the resulting lean blowout equivalence ratios were correlated by the loading parameter (Equations 1-3). The equivalence ratios for LBO were based on the combustor total airflow, and the volume term used in the loading was the total for the complete combustor.

Fig. 11 shows the results of the provisional calculations. Compared to the Task 100 measurements and calculations, the Task 200 calculations show:

- A loading for peak heat release that is an order of magnitude smaller.
- A limiting LBO equivalence ratio that is almost one-fourth.

This broadening of the stability limits and reduction of loading for peak heat release is behavior that is typical of practical combustor performance compared to that of perfectly-stirred reactor performance[11].

The calculated lean stability for the Task 200 combustor is close to that indicated by the limited initial measurements in this combustor (Fig. 9). The agreement is not perfect, and this was not unexpected. Compared to the measured stability for other real combustors with liquid fuel (Fig. 10), the calculations show a reduction in limiting LBO equivalence ratio that is appropriate for the increased homogeneity associated with gaseous fuels.

The reactor network calculations for the Task 200 generic combustor exhibit some interesting behavior concerning changes in flame holding. This is where flame holding is passed from one part of the network to another at some point as fuel flow is reduced and as individual reactors in the network begin to go out. Depending on the loading and the equivalence ratio, flame can be held by reactors representing the central near-stagnation region existing at the confluence of the injector fuel/air swirling jet with the first row of transverse air jets (Fig. 3), by reactors representing the outer recirculation zones surrounding the fuel/air jet issuing from the injectors, or by reactors representing the array of transverse airjets in the central region of the combustor. This behavior mimics characteristics seen in some practical combustors, e.g., the swirl-stabilized combustor of Fig. 10.

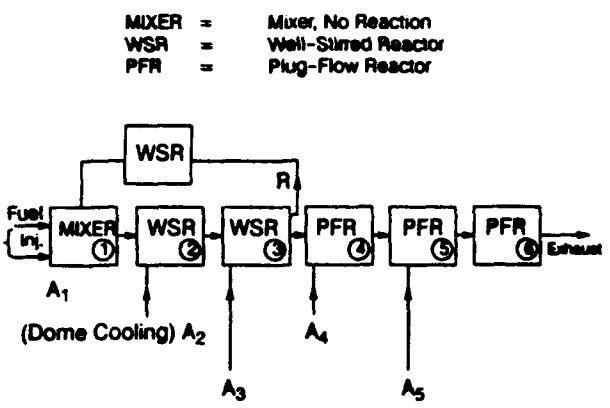

Total Combustor Airflow = Dome Flow + Non-Dome Flow

$\dot{m}_3 = A_1 + A_2 + A_3 + F$

F = Fuel; A = Air

$R = .5\,\dot{m}_3$

A_1 = .711 x Dome Flow

(Dome Cooling) A_2 = .289 x Dome Flow

A_3 = .164 x Non-Dome Flow (first row holes)

A_4 = .541 x Non-Dome Flow (second row holes)

A_5 = .295 x Non-Dome Flow (third row holes)

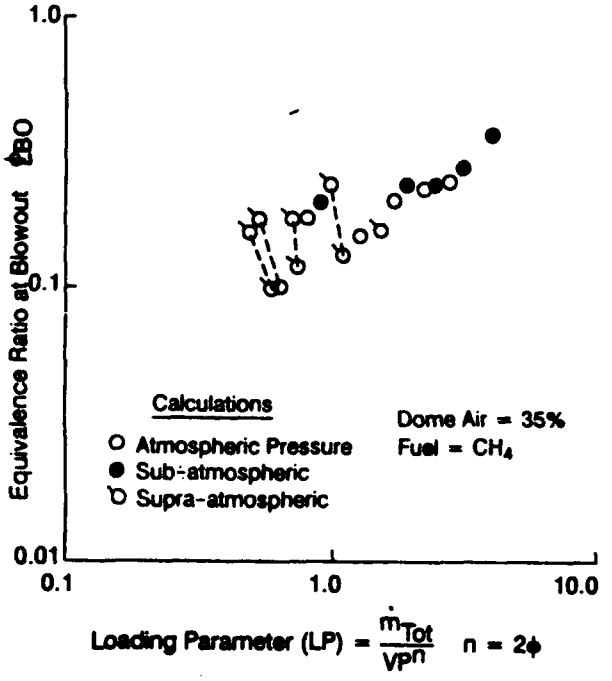

Fig. 11 Calculated stability for generic combustor.

The ordinary differential equations solved in the reactor code are numerically stiff equations. For this reason, the numerical solution procedures can be sensitive to high rates of change. Thus, if the fuel flow rate is reduced too rapidly during a reactor network LBO calculation, the calculation can indicate that the whole network is out at some point. However, at the same operating conditions but with a very gradual reduction in fuel flow rate, the indicated network outlet temperature might fall to very low levels as one reactor goes out, and then recover as the combustion efficiency in another reactor picks up and sustains the network for a further range of falling fuel flows and falling outlet temperatures. The behavior is similar in result to the actual flame behavior in some real combustors, where "pilot flames" can exist in addition to the main flame under some circumstances, but are very susceptible to being extinguished by a flow disturbance (acoustic, for example), a rapid engine throttle movement, or sometimes regions of intense turbulence.

Networks of stirred reactors, particularly when established from CFD calculations, appear to offer exciting possibilities for calculating limiting lean blowout performance. However, care might be needed in interpreting the results of such calculations since only the thermo-chemical limits to combustion can be determined.

Sub-Grid Scale Reactor Modeling

The Eddy Dissipation Concept (EDC) of Magnussen[22] is a general model for chemical reaction in turbulent flow. The EDC combustion model is based on the concept that the reactants are homogeneously mixed within the fine structures of turbulence. The microscales of the fine structures are related to the Kolmogorov eddies by a simplified spectral energy transfer analysis. With the basic postulate, the fine structures can be treated as well-stirred reactors. To evaluate the chemical reactions occurring within the reactors, it is necessary to know the reactor (fine-structure) volume, as well as the mass exchange rate between the reactors and the surrounding fluid. The model supplies a system of equations which describe the reaction process within the fine-structure reactors and then relates the microscale parameters to the ensemble-averaged, mean flow field. Since Kolmogorov length scales will always be much less than any CFD computational grid size, the modeling represents a sub-grid scale approach.

The procedure differs from the Characteristic Time approach and the Stirred Reactor modeling in that the individual reactor stability is tested within the CFD calculation, and not after it. The reactor definition equations, together with full chemical kinetic equations, can be solved at every node of a CFD computational grid applied to the combustor domain; this is done at every iteration of the solution procedure. Thus, the calculated flame position moves through the flow field as the solution develops.

Since application of the kinetics for a reasonably complete chemical reaction mechanism at every node of a very fine grid needed for flame resolution would impose a high cost on the calculation, reduced mechanisms might be used to mimic the essential features of the more complete mechanism. An alternative approach to using full or reduced chemical kinetics is to assume a one-step, irreversible reaction step and/or fast chemistry, and then use a local quenching criterion.

In order to examine the capabilities of the kinetics approach, a full reaction mechanism for propane/air combustion and consisting of 249 reversible steps involving

51 individual species, was compared to blowout and species data from three different perfectly-stirred reactor experiments in the literature. The performance of this full mechanism was not satisfactory in being able to predict the loading parameter at blowout. Given the poor performance of the full mechanism, it is unlikely that an adequate reduced mechanism for LBO can be obtained. Calibration of the reaction mechanism to fit experimental extinction data might be made, be the mechanism either a full or reduced one. This being so, a calibrated single-step mechanism (ultimate reduced mechanism) might do as well, and would certainly have a major computational cost advantage.

The efficacy of the calibrated, global, single-step reaction mechanism approach was tested by comparing the calibrated global mechanism of Kretschmer and Odgers[23] against the stirred reactor data of Clarke, et al.[24]. Although this does not represent an especially stringent test of the calibration, good predictions of LBO for both lean and rich mixtures resulted. These predictions were much better than those obtained with the multi-step reaction.

When the calibrated global mechanism of Reference 23 was incorporated as the kinetic mechanism in a perfectly-stirred reactor code for a further check, significant discrepancies were found between the calculated temperatures for large residence times and true equilibrium temperatures. These discrepancies resulted in correspondingly large errors in temperature and residence time near blowout, and adversely affected LBO calculations. Accordingly, the products of reaction in the mechanism were redefined to be the equilibrium product distribution so as to restore correct temperatures for long residence times. Minor adjustments were then made to the loading expression, and these involved replacing the fixed exponents on reactant concentrations and the pre-exponential factor by polynomials in equivalence ratio. The changes resulted in the PSR code duplicating the LBO performance of the original expression.

An extinction residence time can be expressed as,

$$\tau_{Ext} = (\rho / \dot{m}''')_{Ext} \qquad (6)$$

where $\dot{m}'''$ is the total inlet mass flow rate per unit volume of reactor. Thus, τ_{Ext} can be calculated solely as a function of the inlet temperature and equivalence ratio from the Kretschmer and Odgers' expression. Then, when the hydrodynamic residence time in the reactor is less than the extinction (chemical) time, reaction will occur. If the fine scales of turbulence represent perfectly stirred reactors, the hydrodynamic residence time in the fine scales can be related to the bulk fluid through the mass fraction of fine structures present in the flow.

This characteristic time approach to LBO within the EDC model was implemented with fast chemistry. To test the combustion modeling, CFD calculations of an attached flame condition at a very rich condition in the Task 100 research combustor were made.

The axisymmetric CFD calculations were made with the Pratt & Whitney two-dimensional PREACH code. There were three constraints applied on chemical reaction: first, the EDC combustion model using characteristic times, where the chemical extinction time was based on the Kretschmer and Odgers' stability model. Second, local mixtures had to be within independent flammability limits for combustion. The upper limit was fixed at an equivalence ratio of 2.0, while the lower limit was a function of temperature, and varied between 0.2 and 0.5 for propane/air mixtures. Third, the action of turbulence was brought in through flame speed. For scalar transport calculation, the turbulent Schmidt/Prandtl number was taken as a constant 0.5, appropriate for recirculating flows[4]. Combustor wall temperatures were specified on the basis of thermocouple measurements at attached flame conditions. On all solid surfaces, a wall deadspace model was applied to quench near-wall chemical reactions for a dimensionless distance of $y^+ \leq 100$. Flow inlet conditions were based on LDA measurements[12]. A grid of 77 x 57 for one-half of the combustor from the axis of symmetry was used; 15 cells were used in the fuel tube and 5 for the air annulus.

Fig. 12 displays regions in one-half of the combustor where chemical reaction is excluded; note that the axial and radial axes are not to the same scale. Combustion does not take place on the walls, nor in the central region until half a meter downstream from the combustor step plane; it is allowed in the step recirculation zones, however. The calculated isotherms are shown in Fig. 13.

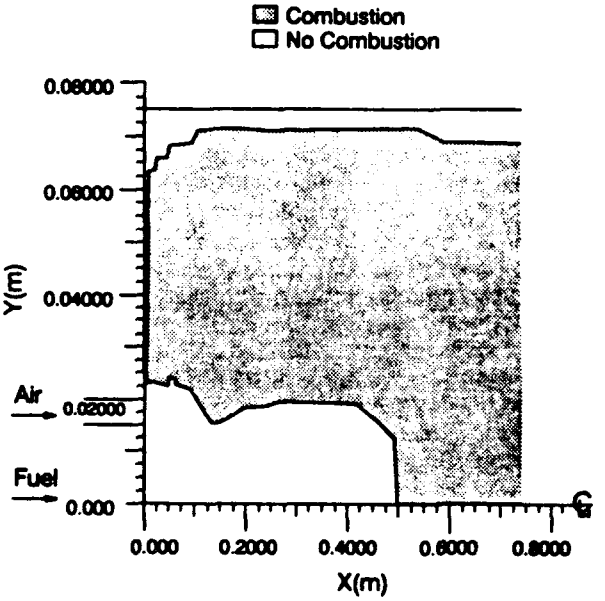

Fig. 12 Research combustor with regions where combustion is excluded by modeling.

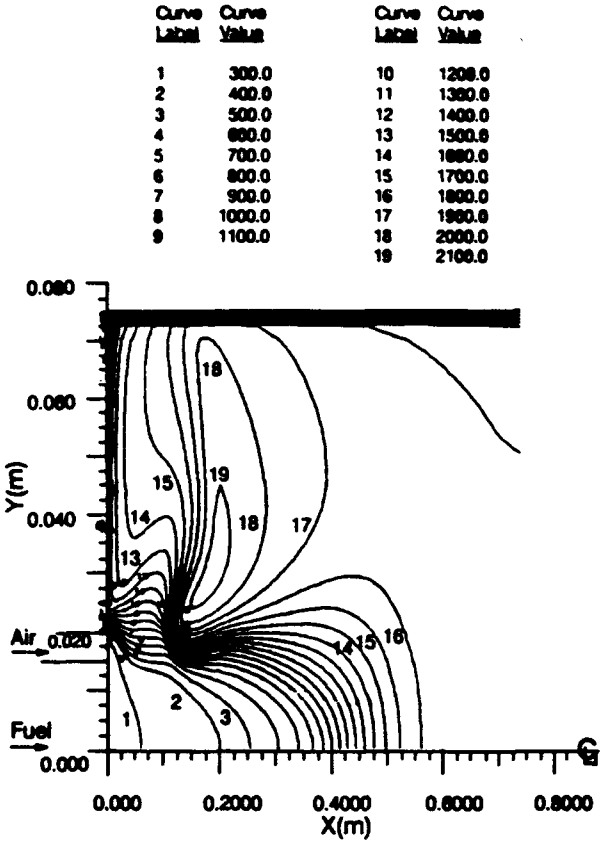

Fig. 13 Research combustor, showing calculated isotherms for attached flame conditions using Eddy Dissipation Concept modeling.

The calculated streamlines (not presented) show that the air jet and outer edge of the step recirculation zone initially converge on the combustor centerline before expanding radially. This gives a characteristic "waist" at about 6 cm from the jet confluence, as is observed by eye from the flames in the real combustor.

Analysis of the calculated results indicates that the stoichiometric contour (based on chemical reactions being reversed) crosses the step recirculation zone from the confluence of the jets and reaches the combustor wall about halfway between the step and the recirculation reattachment plane. Inferred from the temperatures, the main flame exists in the jet shear layers and originates about 10 cm from the step-plane, i.e., lifted. It is rather thick and follows the stoichiometric contour across the recirculation zone. There is good agreement between the inferred flame and the actual flame characteristics in the time-mean photographs, and in near-instantaneous pictures of laser-induced OH fluorescence where concentrated islands of reaction in the jet shear layers give an apparent sudden thickening of the instantaneous "flame region."

The recirculation zone is, in general, very hot with temperatures exceeding 1500K. Most of the fuel that enters the recirculation is consumed very quickly. Although there is some unreacted fuel, largely as a consequence of the deadspaces, the quantity being returned to the vicinity of the air jet as a result of recirculation remains outside the flammability limits. From the isotherms, there is no evidence of the attached pilot flame that is known to exist at these operating conditions.

The calculated characteristics for the Task 100 combustor using the EDC combustion model are very different from those that are calculated using the early generation "mixed is burned" eddy breakup model[25]. The current model does calculate the lifted flame condition and will blow out as fuel flow is reduced (although full calculation of the Task 100 combustor stability characteristic has yet to be made using this model). Although the calculations reproduce some of the observed flame characteristics of this combustor at these conditions, they are not successful in giving the all-important attached pilot flame.

Summary

An important feature of aircraft gas turbine engine combustor design has been identified that is in need of modeling improvements. This is lean blowout stability. A classical technical approach consisting of a fundamental experimental investigation, followed by modeling of the phenomena, and finally, generic test of the modeling, has been adopted in order to achieve the established goal of improving combustor design and prediction methodologies for lean blowout. The implementation of the technical approach is far from classical. Involving multiple contractors, it is not easy to manage, but is proving extremely fertile and exciting in ideas. The modeling practice used is a wholly pragmatic one where the current limitations imposed by computer technology and numerical methods have been circumvented by combining two individually successful and established techniques - CFD and stirred reactors - into integrated methods that are more powerful than their individual components alone. Although the program is far from complete, the work accomplished to date has already surfaced important questions, and indicates reasonable promise of engineering success.

The research combustor, a deceptively simple device, has been successfully developed to be a useful experimental tool with which to explore the physics of lean blowout over a wide range of combustor loadings. These loadings are achieved using simulation methods. Experiments with this combustor have identified the importance of recirculation zones to good stability. A key deficiency in the CFD modeling has been highlighted. This deficiency involves the accuracy of the turbulent mass transport calculation. It appears as though time-dependent mean flow interactions of the fuel jet with the centerline recirculation bubble could be resulting in periodic ejections of fuel across the air jet and directly into the step recirculation zone. This transport of fuel would be in addition to that entering the recirculation zone via the path around the recirculation taken by the fuel/air jet shear layers. Additional experimental work is planned to further explore this hypothesis. If this additional mechanism is indeed present, it cannot be modeled by the stationary state computer codes in engineering use today. The additional fuel so introduced, could account for the attached pilot flame that is observed.

The generic combustor is emerging as an extremely flexible tool to be used for studying primary zone design

variables that influence lean blowout. Many similarities of flame behavior with the research combustor can be seen.

Although much remains yet to be done, the potential of incorporating stirred reactor modeling with CFD methods, both the fully integrated approach when used in series, has been demonstrated.

Acknowledgements

The prime authors of this report (G. Sturgess, D. Ballal and W. Roquemore) wish to acknowledge the contributions of all the program researchers listed under the main title. The University of Dayton work was supported by the U.S. Air Force Wright Research and Development Center, Aero Propulsion and Power Laboratories, under Contract F33615-87-C-2767 (Contract Monitor Dr. W. M. Roquemore); Systems Research Laboratories was supported under Contract F33615-90-C-2033 (Contract Monitor Dr. W. M. Roquemore); and Pratt & Whitney was supported under Contract F33615-87-C-2822 (Contract Monitor 1st Lt. A. L. Lesmerises and currently, Mr. D. Schouse). Dr. P. Hedman was supported by the Air Force Office of Scientific Research (AFOSR) through a Summer Faculty Research Program. AFOSR also supported the research through direct funding to the Aero Propulsion and Power Laboratory.

References

1. Lord, W. K., Pickett, G. F., Sturgess G. J. and Weingold, H. D., "Applications of CFD Codes to the Design and Development of Propulsion Systems," *Proc. Symp. Supercomputing in Aerospace*, NASA Rept. CP 2454, NASA Ames Research Center, Moffett Field, California, March 10-12, 1987, pp. 139-148.

2. Shyy, W., Correa, S. M. and Braaten, M. E., "Computational Models for Gas Turbine Combustors," *Proc. ASME Symp. Calculations of Turbulent Reactive Flows*, ed. R. M. C. So, J. H. Whitelaw and H. C. Mongia, WAM, Anaheim, California, December 7-12, ASME AMD-Vol. 81, pp. 141-183.

3. Sturgess, G. J., "Calculation of Aerospace Propulsion Combustors: A View from Industry," ibid, pp. 185-231.

4. Syed, S. A. and Sturgess, G. J., "Validation Studies and Combustion Models for Aircraft Gas Turbine Combustors," *Proc. ASME Symp. Momentum and Heat Transfer Processes in Recirculating Flows*, ed. B. E. Launder and J. A. C. Humphrey, HTD-Vol. 13, WAM, Chicago, Illinois, November 16-21, 1980, pp. 71-89.

5. Kenworthy, M. J., Correa, S. M. and Burrus, D. L., Aerothermal Modeling, Phase I - Final Report, Vols. I and II, NASA Rept. CR-168296, November 1983.

6. Srinivasan, R., Reynolds, R., Ball, I., Berry, R., Johnson, K. and Mongia, H., Aerothermal Modeling Program Phase I - Final Report, Vols. I and II, NASA Rept. CR-168243, August 1983.

7. Sturgess, G. J., Aerothermal Modeling Phase I, Final Report, NASA Rept. CR-168202, May 1983.

8. Syed, S. A., Chiapetta, L. M. and Gosman, A. D., Error Reduction Program - Final Report, NASA Rept. CR-174776, January 11, 1985.

9. Ryder, R. C., "Massively Parallel TEACH-Type Code Using an Approximately Implicit Algorithm," *Proc. Symp. Recent Advances and Application in Computational Fluid Dynamics*, ed. O. Baysal, FED Vol. 103, ASME WAM, Dallas, Texas, November 25-30, 1990, pp. 67-73.

10. Bahr, D. W., "Technology for the Design of High Temperature Rise Combustors," Paper No. AIAA-85-1292, AIAA/SAE/ASME/ASEE 21st Joint Propulsion Conference, Monterey, California, July 8-10, 1985.

11. Sturgess, G. J., Sloan, D. G., Lesmerises, A. L., Heneghan, S. P. and Ballal, D. R., "Design and Development of a Research Combustor for Lean Blowout Studies," Paper No. 90-GT-143, ASME Gas Turbine and Aeroengine Congress and Exposition, Brussels, Belgium, June 11-14, 1990, (to be published in *Trans. ASME*).

12. Sturgess, G. J., Heneghan, S. P., Vangsness, M. D. and Ballal, D. R., "Isothermal Flow Fields in a Research Combustor for Lean Blowout Studies," Paper No. 91-GT-37, ASME Gas Turbine and Aeroengine Congress and Exposition, Orlando, Florida, June 3-6, 1991, (to be published in *Trans. ASME*).

13. Heneghan, S. P., Vangsness, M. D., Ballal, D. R., Lesmerises, A. L. and Sturgess, G. J., "Acoustic Characteristics of a Research Step Combustor," Paper No. AIAA-90-1851, presented at AIAA/SAE/ASME/ASEE 26th Joint Propulsion Conference, Orlando, Florida, July 16-18, 1990, (to be published in *J. Propulsion and Power*).

14. Roquemore, W. M., Reddy, V. K., Hedman, P. O., Post, M. E., Chen, T. H., Goss, L. P., Trump, D., Vilimpoc, V. and Sturgess, G. J., "Experimental and Theoretical Studies in a Gas-Fueled Research Combustor," Paper No. AIAA-91-0639, AIAA 29th Aerospace Sciences Meeting, Reno, Nevada, January 7-10, 1991.

15. Sturgess, G. J., Heneghan, S. P., Vangsness, M. D., Ballal, D. R. and Lesmerises, A. L., "Lean Blowout in a Research Combustor at Simulated Low Pressures," ASME Gas Turbine and Aeroengine Congress and Exposition, Orlando, Florida, June 3-6, 1991, (to be published in *Trans. ASME*).

16. Tsuji, S., "A Study on a Vaporizing Combustor for Gas Turbines," NASA Technical Translation, NASA TT F-13272, October 1970.

17. Lockwood, F. and Megahead, I. E. A., "Extinction of Turbulent Reacting Flows," *Combustion Science and Technology*, Vol. 19, 1978, pp. 77-80.

18. Helman, J. and Hesselink, L., "Representation and Display of Vector Field Topology in Fluid Flow Data Sets," *Computer*, Vol. 22, No. 8, August 1989, pp. 27–36.

19. Perry, A. E. and Chong, M. S., "A Description of Eddying Motions and Flow Patterns Using Critical-Point Concepts," *Annual Review of Fluid Mechanics*, Vol. 19, 1987, pp. 125–155.

20. Tobak, M. and Peake, D. J., "Topology of Three-Dimensional Separated Flows," *Annual Review of Fluid Mechanics*, Vol. 14, 1982, pp. 61–85.

21. Swithenbank, J., "Flame Stabilization in High Velocity Flow," Combustion Technology – Some Modern Developments, ed. H. B. Palmer and J. M. Beer, Academic Press, 1974, pp. 91–125.

22. Byggstoyl, S. and Magnussen, B. F., "A Model for Flame Extinction in Turbulent Flow," *Turbulent Shear Flows 4*, ed. L. J. S. Bradbury, F. Durst, B. E. Launder, F. W. Schmidt and J. H. Whitelaw, Springer-Verlag, Berlin, 1985.

23. Kretschmer, D. and Odgers, J., "Modeling of Gas Turbine Combustors – A Convenient Reaction Rate Expression," *Trans. ASME, J. Engineering for Power*, Vol. 94, July 1972, pp. 173–180.

24. Clarke, A. E., Morrison, A. J. and Odgers, J., "Combustion Stability in a Spherical Combustor," *7th Symposium (International) on Combustion*, Butterworths Scientific Publications, London, 1958, pp. 664–673.

25. Magnussen, B. F., "Heat Transfer in Gas Turbine Combustors – A Discussion of Mathematical Modeling of Combustion, Heat and Mass Transfer with Emphasis on Heat Transfer in Gas Turbine Combustors," AGARD Conference Preprint No. 390, Heat Transfer and Cooling in Gas Turbines, Paper No. 23, 1985.

APPENDIX G

TURBULENT COMBUSTION PROPERTIES BEHIND A CONFINED CONICAL STABILIZER

by

J. C. Pan, W. J. Schmoll, and D. R. Ballal
University of Dayton, Dayton, Ohio

Published in Transactions of ASME, Journal of Engineering for Gas Turbines & Power, Vol. 114, pp. 33-38, January 1992.

Turbulent Combustion Properties Behind a Confined Conical Stabilizer

J. C. PAN, W. J. SCHMOLL, and B. R. BALLAL
University of Dayton
Dayton Ohio, U.S.A.

Abstract

Turbulence properties were investigated in and around the recirculation zone produced by a 45° conical flame stabilizer of 25% blockage ratio confined in a pipe supplied with a turbulent premixed methane-air mixture at a Reynolds number of 5.7×10^4. A three-component LDA system was used for measuring mean velocities, turbulence intensities, Reynolds stresses, skewness, kurtosis, and turbulent kinetic energy.

It was found that wall confinement elongates the recirculation zone by accelerating the flow and narrows it by preventing mean streamline curvature. For confined flames, turbulence production is mainly due to shear stress-mean strain interaction. In the region of maximum recirculation zone width and around the stagnation point, the outer stretched flame resembles a normal mixing layer and gradient-diffusion closure for velocity holds. However, and in the absence of turbulent heat flux data, counter-gradient diffusion cannot be ruled out. Finally, and because of the suppression of mean streamline curvature by confinement, in combusting flow, the production of turbulence is only up to 33% of its damping due to dilatation and dissipation.

Nomenclature

a	= ratio of $(\overline{uv}/q)$
BR	= blockage ratio
C_P	= static pressure coefficient $(\Delta P/0.5\ \rho U_a^2)$
d	= base diameter of conical stabilizer
D_t	= turbulent eddy diffusivity
K	= kurtosis
L	= length of the recirculation zone
$\dot{m}$	= mass flow rate
P	= pressure
q	= turbulent kinetic energy (TKE)
r	= radial direction
R	= pipe radius
S	= skewness
T	= temperature
U, V	= mean velocities in axial and radial directions
u, v	= fluctuating velocities in axial and radial directions
$\overline{uv}$	= Reynolds shear stress
$\overline{uT}, \overline{vT}$	= axial and radial turbulent heat flux
W	= recirculation zone maximum width
x	= axial direction
ϕ	= equivalence ratio
ν	= kinematic viscosity
ψ	= mean stream function
θ	= cone apex angle
ρ	= density
τ	= heat release parameter

Superscripts

-	= mean value
'	= rms value

Subscripts

a	= annular flow
c,f	= combusting flow, flame
u, b	= unburned and burned
r	= reverse direction
t	= total, turbulent

Introduction

Bluff body flame holders are widely used in afterburners and other practical combustion systems to stabilize a flame. They produce a recirculation zone in the flowfield. This zone serves a triple purpose: (i) producing a region of low velocity, (ii) providing long residence time for the flame to propagate into the incoming fresh mixture, and (iii) serving as a source of continuous ignition

*Presented at the Gas Turbine and Aeroengine Congress and Exposition—June 11-14, 1990—Brussels, Belgium
This paper has been accepted for publication in the Transactions of the ASME
Discussion of it will be accepted at ASME Headquarters until September 30, 1990

for the incoming fuel-air mixture. Thus, a steady flame is stabilized and propagates downstream into the combustor.

Many different geometric shapes of bluff bodies such as a cylinder, cone, disk, vee-gutter, or sphere can be used as flame stabilizers. The recirculation zone produced by each bluff body is affected by its geometry (aerodynamic effect), the type of fuel and equivalence ratio (chemical effect), and its confinement (pressure-gradient effect) in the combustor. Thus, a complex aerodynamics-chemistry-pressure gradient interaction is present in reactive recirculatory flowfields. This fact, together with its existence in many practical combustor configurations, such as gas turbine combustors, dump combustors, and backward-facing step combustors, makes any investigation of this type of flowfield of considerable practical significance.

Numerous studies report measurements of mean and turbulent cold flow properties behind bluff bodies; for example, see a review paper by Griffin (1985). In contrast, very little information is available on the turbulent combustion properties behind bluff bodies. The work of Winterfeld (1965) describes effects of recirculation zone geometry on exchange coefficients and mean residence time, that of Ballal and Lefebvre (1979) discusses weak extinction limits, and that of Rao and Lefebvre (1982) analyzes flame blowout. Recently, Heitor and Whitelaw (1986), and Sivasegaram and Whitelaw (1987) have presented measurements of stability limit in a small gas turbine combustor, and discussed the suppression of combustion instability. Finally, Ballal et al. (1989) report data on turbulent flow properties, but in an *open* turbulent premixed flame.

In this paper, we provide turbulence properties in the practically more interesting case of a *confined* turbulent recirculatory flame. Measurements of turbulent velocity fluctuations such as mean and rms values, skewness and flatness factors, Reynolds shear stresses, and axial mean pressure gradients are reported with and without combustion. Then these data are interpreted to elucidate the recirculation zone structure, effects of flow confinement, and the role of combustion-generated turbulence.

Experimental Work

1 Test Facility. Figure 1 shows the test facility we used for these experiments. A machined stainless steel conical flame stabilizer of base diameter, d = 4.44 cms (1.75 in.), apex angle θ = 45°, and BR = 25% was mounted coaxially inside a pipe of 8-cm nominal dimension and which has cut-outs for four optical quality glass windows. This pipe is supplied with high velocity, premixed methane-air combustible mixture from a vertical combustion tunnel mounted on a three-axis traversing platform described by Ballal et al. (1987). A torch igniter was used to ignite the turbulent combustible mixture. Measurements of turbulence quantities and mean wall-static pressure were performed downstream of the confined conical stabilizer by using a three-component Laser Doppler Anemometer (LDA) and precision micromanometer respectively.

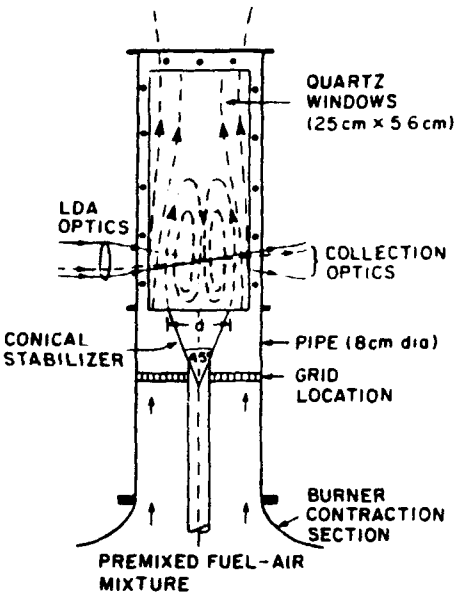

Fig. 1 Schematic diagram of the confined flame stabilizer test facility.

2 Test Condition. Zukoski and Marble (1955) have pointed out that the bluff body wake region becomes fully turbulent when $Re_d \geq 10^4$. Therefore, all our experiments were performed at U_a = 20 m/s or $Re_d = U_a d/\nu = 5.7 \times 10^4$, and approach turbulence level u'/U_a = 4%, and v'/U_a = 2.8%. Thus, conditions of fully developed turbulence existed in our recirculatory flowfield. Also, limitations posed by the test facility maximum fuel flowrate, capability of the LDA seed particle generator, and safety considerations related to flame flashback, all combined to restrict the maximum annular mixture velocity to the above stated value. Tests were performed at three different equivalence ratios, ϕ = 0.65, 0.80, and 1.0, of methane-air mixture, corresponding to T_f = 1755 K, 1996 K, and 2226 K respectively at room temperature and pressure. The measurement locations ranged in axial direction from x/d = 0.05 to 4.5 and in radial direction from r/d = -0.55 to + 0.55.

3 LDA Instrumentation. A three-component LDA system was used for all velocity measurements. Essentially, this instrument is an upgraded and refined version of the two-component LDA system used by Ballal et al. (1989) earlier. It uses the green (514.5 nm) and blue (488 nm) lines of a 15W, Argon-ion laser as a source. Two measurement channels of this LDA system are separated by polarization, whereas the third channel uses the blue beam. Principally, this instrument incorporates Bragg cell frequency shifting for measurements in a recirculatory flow, a unique three-channel coincidence circuit for rapid acquisition of valid data (a feature necessary for integrating LDA with CARS, Raman or Rayleigh spectroscopic techniques), software to filter spurious signals, for example, due to seed agglomeration, and a correction subroutine to account for the LDA signal biasing effect in combusting flows. The third channel optics of the LDA is set up normal to the two-channel optics, and the scattered signal is

collected in a forward direction 10° off-axis. A fluidized bed seeder is used to inject submicron sized Al_2O_3 seed particles into the flowing combustible mixture. The effective LDA measurement volume dimensions were 50 μm x 500 μm x 1000 μm. Scattered signals were detected by TSI Counter Processors (CP) and processed by our custom-designed software to yield intensity, shear stresses, higher moments (skewness and kurtosis), and pdfs. Typical sampling rates for LDA measurements exceeded 1 kHz for both isothermal and combusting flows. For a three-component system with a relatively small measurement volume, these sampling rates (particularly in combusting flows) were considered satisfactory.

4 **Error Analysis.** Both the fuel flow and airflow were monitored by separate TYLAN electronic flow control units to within 1%. Also, mass conservation balance in the plane of the bluff body base provided an additional cross-check against flowmeter readings. The primary source of error in LDA measurement is the statistical bias of the final measured velocity towards higher mass flux (velocity x density) when number-weighted averages are used to calculate stationary statistics. Chen and Lightman (1985) and Glass and Bilger (1978) have discussed bias correction schemes. After allowing for this bias, we estimated that for the single-stream seeding and relatively high-sampling rates of our experiments, the uncertainty in the measurement of mean velocity was 1%, for rms velocity 5%, and for skewness and flatness 7%. Near the flame front, where intermittency would be much higher, the uncertainty in rms velocity could be greater than 7%. The long-term repeatability of measurements was found to be within 5% for turbulence quantities.

Results and Discussion

Recently, it has been recognized that *chaotic* systems such as turbulent flows are extremely sensitive to inlet boundary conditions. Also, as suggested by Strahle and Lekoudis (1985), modeling codes require the specifications of inlet or starting conditions to initiate predictions of flow development downstream. Finally, the importance of inlet boundary conditions to numerical simulation of combustor flows is very elegantly demonstrated by Sturgess et al. (1983). For these reasons, we begin by providing turbulence properties in the inlet plane of the conical bluff body. Lack of space precludes us from presenting all our data. Therefore, only selected data that are relevant to the discussion of recirculation zone structure, effect of confinement, and combustion-generated turbulence are presented.

1 **Inlet Boundary Conditions.** Figures 2a and 2b show radial profiles of mean and turbulence quantities in the axial plane x/d = 0.05 (x = 2.25 mm) respectively. This plane is so close to the base of the bluff body that, as seen in Fig. 2a, the axial mean velocity is negligibly small in the recirculation zone (r/d < 0.5) and rises rapidly to U/U_a = 1 beyond r/d >0.5. Also, the axial turbulence intensity has value close to approach turbulence value of u'/U_a = 4%, but the radial turbulence intensity v'/U_a is significantly higher and dominates.

Figure 2b shows the radial profiles of Reynolds shear stress, skewness $S(= \overline{u^3}/(\overline{u^2})^{3/2})$ and kurtosis $K(= \overline{u^4}/(\overline{u^2})^2 - 3)$ of axial velocity fluctuations. The Reynolds shear stress reaches a maximum value in the mixing region around the conical stabilizer. Values of S and K were respectively *lower* than and *higher* than zero in the hot recirculatory flow, but tend to zero in the annular stream because of the small-scale structure of the incoming freestream turbulence. Note that for this confined flame, no narrow peaks or transient dips could be observed as was the case for the open flame (see Ballal et al. 1989, Figs. 3a and 3b).

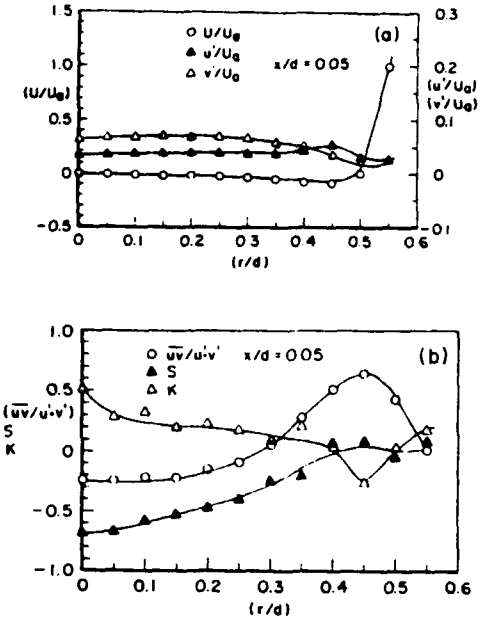

Fig. 2 Measurements of inlet boundary flow conditions at U_a = 20 m/s, ϕ = 0.65, and (x/d) = 0.05: (a) profiles of mean and rms turbulence velocities; (b) profiles of Reynolds shear stress, skewness, and kurtosis.

2 **Axial Pressure Distribution.** When the combustion process is confined, it accelerates the incoming isothermal flow and decreases wall static pressure. Figure 3 shows the measured axial wall pressure gradient dP/dx in our combustor for isothermal and combusting cases. A negative value of dP/dx suggests flow acceleration and this is found to be the case for combusting flows. For isothermal flow, deceleration sets in beyond x/d = 0.7 which corresponds to a minimum value of C_p or the location of maximum recirculation zone width. Finally, the maximum positive value of dP/dx is generally associated with the location of the rear stagnation point. Therefore, the data presented in Fig. 3 gives the recirculation zone length as 1.5d, 1.7d, and 1.6d for isothermal, confined lean-combusting (ϕ = 0.65), and confined stoichiometric-combusting (ϕ = 1) flows respectively.

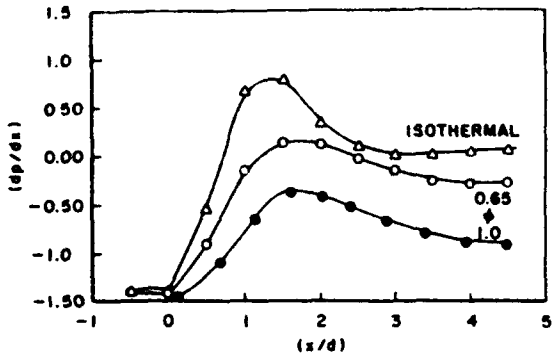

Fig. 3 Combustor wall pressure gradients at U_a = 10 m/s in confined isothermal and combusting flows.

3 Recirculation Zone Parameters. The size, shape, and mean flow structure of the recirculation zone may be determined by calculating the spatial distribution of the mean stream function ψ from the equation;

$$\psi = \int_0^r \rho U r\, dr \qquad (1)$$

Also, knowing the value of $C_{p,min}$, we can derive the maximum width W of the recirculation zone as:

$$W = R\,[1-\{(1-BR)/(1-C_{p,min})^{1/2}\}]^{1/2} \qquad (2)$$

From equation (1), the ratio of reverse to total mass flow rate $\dot{m}_r/\dot{m}_t$ was calculated. This ratio represents the recirculation strength. Figure 4 shows a sketch of the recirculation zone which appears similar to an ellipsoid of revolution. Table 1 lists the various recirculation zone parameters for confined cold flow, confined flame, and open flame respectively.

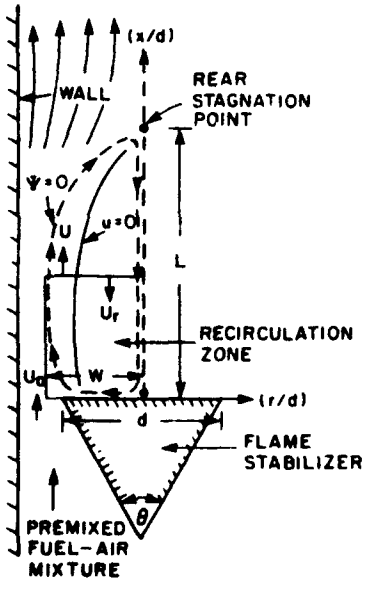

Fig. 4 Sketch of the recirculation zone in a confined combusting flow.

In Table 1, the recirculation zone is more elongated in combusting as opposed to isothermal flows. This is consistent with the findings of Winterfeld (1965). A physical explanation is that acceleration of flow throughout the combustor together with prevention of mean streamline curvature by the confining walls causes the flow to better overcome the adverse pressure gradients, thereby producing an elongated recirculation zone. On the other hand, confined combustion always produces a certain positive back pressure and this keeps the length of the recirculation zone somewhat shorter in confined than in open flames. Large mean streamline curvature and turbulent dilatation in open flames produce the widest recirculation zone. The recirculation strength of the cold confined flow is highest principally because of higher gas density, even though the reverse mean flow velocity is highest in confined flame. Finally, in an open flame, large streamline curvature more than compensates for any damping of turbulence by dilatation and generates larger axial and radial turbulence intensities and turbulent kinetic energy as compared to confined flows.

Table 1: Recirculation zone parameters.

Conical Stabilizer

$\theta = 45^\circ$, BR = 25%, ϕ = 0.65, $Re_d = 5.7 \times 10^4$

	Confined Cold Flow	Confined Flame	Open Flame
(L/d)	1.5	1.70	1.85
(W/d)	0.55	0.58	0.65
$(U_r/U_a)^*$	-0.24	-0.40	-0.30
$(\dot{m}_r/\dot{m}_t)$	0.20	0.13	0.10
(u'/U_a)	0.3	0.24	0.32
(v'/U_a)	0.26	0.17	0.28
(q_c/q)	1.0	0.64	1.12

* at x/d = 0.8, r/d = 0.3

4 Turbulence Properties. As illustrated in Fig. 4, the recirculation zone causes flame stretching in the axial plane corresponding to its maximum width and in the vicinity of the rear stagnation point. For our confined flame, these two locations are at x/d = 0.8 and 1.7 respectively. Therefore, we present and discuss data on turbulence properties at these locations.

(a) *Region of Maximum Recirculation Zone Width.* Figure 5a shows profiles of centerline mean and rms velocity fluctuations.

Note that the mean reverse velocity and axial turbulence intensity have maximum values in the axial plane corresponding to the first location of the flame stretch. At the stagnation point, $U/U_a = 0$ and both axial and radial turbulence intensities are significant as expected.

Figure 5b shows radial profiles of u'/U_a, u'/v', S, and K in the axial plane of maximum recirculation zone width, x/d = 0.8. It is observed that axial turbulence intensity is fairly constant within the recirculation zone and reaches a maximum value of 28% at r/d = 0.45, very close to the stretched flame surrounding the recirculation zone. Close to this location, the reactive flow has a highly skewed turbulence structure (note: S = 0.8 and K = -0.7), presumably due to the presence of a large scale eddy formed in the mixing layer around the highly strained flame region. Also, note that the axial turbulence intensity dominates in the flame region.

(b) *Stagnation Point Region.* The exact location of the stagnation point is very difficult to assess. This is a small region in which the flow direction is quickly reversed, the fluid parcels are stretched, and strong gradients of mean and turbulence quantities are present. A simple way to ascertain the location of the stagnation point is to seek a common location at which axial and radial velocity profiles cross and change sign. However, a more definitive way to establish the location of the stagnation point is to seek the maximum local value of u'/U. These criteria were combined to pinpoint the exact *mean* location of the stagnation point at x/d = 1.7 and r/d = 0.

Figures 6a and 6b show turbulence properties in the vicinity of the stagnation point. In Fig. 6a, positive axial velocity is found beyond r/d = 0.3. This suggests, and visual observations confirm, the necking down of the flame in the vicinity of the stagnation point. The axial turbulence intensity has a peak value of almost 25% at r/d = 0.3 in this second flame stretch region. Finally, and as would be expected, the Reynolds shear stresses change sign about half-way (at r/d = 0.15) between the centerline and the flame necking-down location.

Figure 6b illustrates the nature of turbulent flow in the vicinity of the stagnation point via plots of u'/v', S, and K. Inspection of (u'/v') data immediately reveals that marked anisotropy of turbulence prevails in the region around the stagnation point. Moreover, the radial turbulence component is dominant in the zone between the centerline and the flame necking-down region, i. e., r/d = 0 to 0.3. Also, peaks in skewness and kurtosis profiles are evident around r/d = 0.3. Such peaks can also arise due to flow unsteadiness, and spectral analysis may be required. Nevertheless, it is apparent that the turbulence structure is distorted in the combusting flow. This observation differs from the experiments of Starner and Bilger (1980) who found that the structure parameters were essentially the same for both isothermal and reacting flows for a jet diffusion flame with axial pressure gradient.

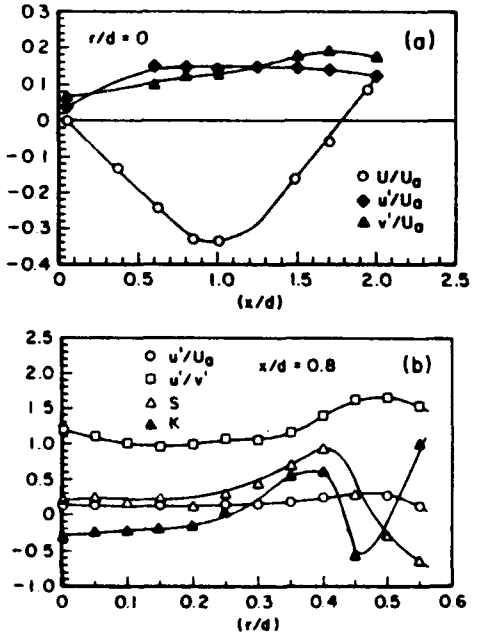

Fig. 5 Measurements of turbulence properties at U_a = 20 m/s, ϕ = 0.65, in the region of maximum recirculation zone width (x/d) = 0.8: (a) centerline profiles of mean and rms velocity fluctuations; (b) radial profiles of axial turbulence intensity, anisotropy, skewness, and kurtosis.

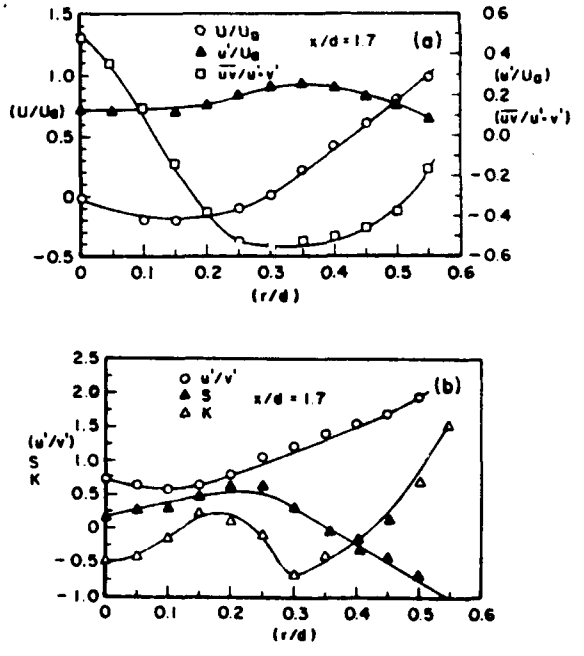

Fig. 6 Turbulence properties for U_a = 20 m/s, ϕ = 0.65, in the rear stagnation point region (x/d) = 1.7: (a) profiles of mean and rms velocities, and Reynolds shear stresses; (b) profiles of anisotropy, skewness, and kurtosis.

Further Discussion

In this section, we briefly discuss three issues: (i) the effect of wall confinement, (ii) the nature of flame reaction zone, and (iii) combustion-generated turbulence.

(i) *Influence of Wall Confinement.* A bluff body confined in a pipe not only produces a geometric blockage, but also an aerodynamic blockage corresponding to the deflection of the mean separation streamline from its trailing edge. Wall confinement prevents any significant deflection of mean flow streamlines and also produces flow acceleration to elongate the recirculation zone. Consequently, in confined flames, the production of TKE is by the interaction of Reynolds stress and shear strain, i. e., via the term $\overline{uv}\,\partial U/\partial r$, and therefore restricted to the shear layer surrounding the maximum width of the recirculation zone. If the wall confinement is removed, only turbulent dilatation and mean pressure gradients (i. e., normal and not Reynolds stresses) would contribute to TKE production. An increase in aerodynamic blockage (say by increasing geometric blockage) decreases the angles of the streamline at the baffle trailing edge. It also brings streamlines closer to the walls. Both these effects contribute to decreasing streamline curvature and, as shown by Winterfeld (1965), produce increased length and decreased width of the recirculation zone.

(ii) *Turbulent Flame Region.* It is important to examine the flame region surrounding the recirculation zone particularly in a confined flame. This is because this region produces both TKE and heat release. Accordingly, Fig. 7 shows plots of the ratio turbulent shear stress to kinetic energy, $a = \overline{uv}/q$, and values of $\delta U/\delta r$ at each location. It is observed that (a) both positive and negative values of Reynolds stresses can be found in the combusting recirculation zone, (b) values of coefficient a lie between -0.3 and 0.3; and therefore are close to values expected in "normal" shear layers as suggested by Bradshaw et al.(1967) and Harsha and Lee (1970), (c) in almost all of the flowfield, the Reynolds stresses (or a) have sign opposite to that of $\delta U/\delta r$, i. e., the conventional *gradient-diffusion* turbulence modeling which employs the eddy viscosity closure assumption $-\rho\overline{uv} = D_t\,\partial U/\partial r$ may be successful to the extent of predicting velocity flowfield.

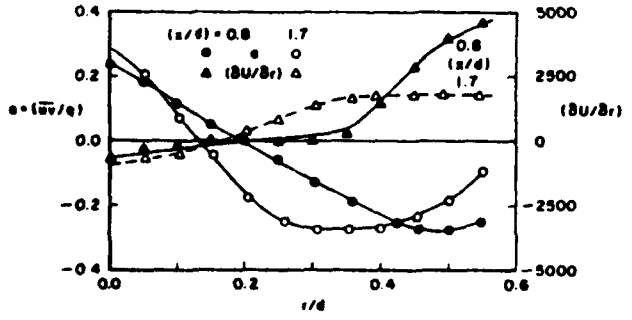

Fig. 7 Radial profiles of ($\overline{uv}$/q) and $\delta U/\delta r$ at U_a = 20 m/s, ϕ = 0.65, illustrating the validity of the gradient-diffusion relationship in turbulent combusting flows.

In confined turbulent reactive flow, Shepherd et al. (1982) have reported counter-gradient diffusion of turbulent heat fluxes. In confined flows involving significant heat release and large density fluctuations, counter-gradient diffusion arises because low density, fully burned products of combustion are preferentially accelerated by the pressure gradient in comparison with high density unburnt reactants. Thus, turbulent transport is influence by preferential diffusion in addition to conventional eddy diffusion. Now, in a confined recirculatory reactive flow, this situation is further complicated because the mean axial pressure gradient is favorable in the outer flame zone (r/d >0.5) but adverse inside the recirculation region (r/d < 0.5). Therefore, detailed measurements of turbulent heat fluxes $\overline{uT}$ and $\overline{vT}$, and mean temperature gradients $\partial T/\partial x$ and $\partial T/\partial r$ are required to examine this flowfield fully.

(iii) *Combustion-Generated Turbulence.* Combustion affects the turbulent flowfield in a variety of ways. Ballal (1988) has stated that turbulent dilatation and viscous dissipation processes suppress flame turbulence, whereas turbulent advection and shear-generated turbulence will augment flame turbulence. Depending upon which processes dominate, combustion will either produce additional so-called combustion-generated turbulence or damp existing isothermal turbulence.

Figure 8 shows radial variation of ratio (q_c/q) at two different axial locations. Clearly, the TKE is lower by as much as 70% in the combusting flow than in cold flow. This result suggests that a minimum shear-generated turbulence is produced because wall confinement prevents deflection of mean flow streamlines and produces extremely low streamline curvature. In the absence of this strong turbulent production mechanism, the processes of turbulent dilatation and viscous dissipation take over to significantly damp cold flow turbulence. We believe that an oblique flame of fast burning mixtures e. g., H_2 or stoichiometric combustion when confined in a duct may generate enough shear to overcome the damping of turbulence. In Fig. 8 note that where shear is prominent e. g., at r/d = 0.45, and 0.2 for x/d = 0.8 and 2 respectively, the TKE ratio does increase.

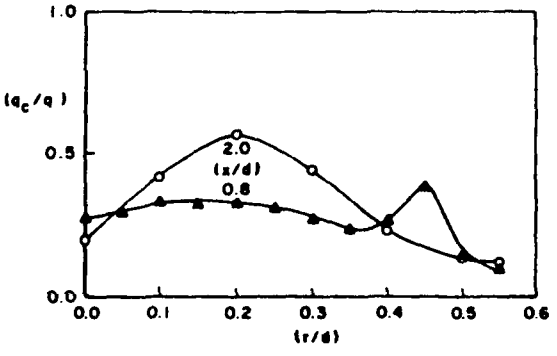

Fig. 8 Radial profiles of (q_c/q) at U_a = 10 m/s, ϕ = 0.65, illustrating the influence of combustion on turbulent kinetic energy in a confined recirculatory flow.

From his studies of combustion-generated turbulence, Ballal (1986) derived simple formulae to estimate the magnitudes of shear-generated turbulence, turbulence dilatation, viscous dissipation and turbulent advection. For the confined flame studied here, T_f = 1755 K and T_u = 295 K, so $\tau = (T_f - T_u)/T_u \approx 5.0$. So, we can calculate that the magnitude of suppression due to turbulent dilatation = 55% and that due to viscous dissipation = 24%, i. e., total suppression = 79%. However, in Fig. 8, at x/d = 0.8, the TKE in the combusting flow is lower by 70% in the recirculation zone (r/d < 0.4) and lower by 60% in the vicinity of the flame front. Thus, the total turbulence production (shear-generated turbulence + turbulent advection) in these two regions can be estimated to be about 9% and 19% respectively. Likewise, at x/d = 2, the total turbulence production is up to 26% downstream of the rear stagnation point. These estimates show that the ratio of production/suppression of turbulence varies between 12% to 33% in our fuel-lean (ϕ = 0.65) high-speed confined flame.

Concluding Remarks

The following observations summarize our studies of turbulent combustion properties:

(1) Combustor wall confinement elongates the recirculation zone by 13% over cold flow and narrows it by 12% over an open flame. Also, mean reverse flow velocity and hence also the recirculated mass flow increase by 30% over their corresponding values in open flame.

(2) Flame confinement prevents mean streamline curvature. In such flows, turbulence production is principally due to shear stress-mean strain interaction. In contrast, for open flames, normal stresses and dilatation dominate.

(3) Two regions of highly-strained flames; one in the axial plane of maximum recirculation zone width and other around the stagnation point are observed. A significant distortion of turbulent flow structure, as shown by high values of skewness and kurtosis, was evident in these regions.

(4) The flow enveloping the recirculation zone resembles a normal mixing layer, i. e., a = +0.3 to -0.3 and gradient-diffusion closure for velocity holds. However, and in the absence of turbulent heat flux data, counter-gradient diffusion cannot be ruled out.

(5) Finally, and principally due to suppression of mean streamline curvature by confinement, in combusting flow, the production of turbulence is only up to 33% of its damping due to dilatation and dissipation.

Acknowledgment

This research was sponsored by the U. S. Air Force, Wright Research and Development Center, Aero Propulsion and Power Laboratories, under Contract No. F33615-87-C-2767. The authors are indebted to Dr. W. M. Roquemore, the Air Force Technical Monitor, for his interest and helpful discussions during the course of this work.

References

Ballal, D. R., 1986, "Studies of Turbulent Flow-Flame Interaction," *AIAA Journal*, Vol. 24, pp. 1148-1154.

Ballal, D. R., Chen, T. H., and Schmoll, W. J., 1989, "Fluid Dynamics of a Conical Flame Stabilizer," ASME *Journal of Engineering for Gas Turbines and Power*, Vol. 111, pp. 97-102.

Ballal, D. R., and Lefebvre, A. H., 1979, "Weak Extinction Limits of Turbulent Flowing Mixtures," ASME *Journal of Engineering for Power*, Vol. 101, pp. 343-348

Ballal, D. R., Lightman, A. J., and Yaney, P. P., 1987, "Development of Test Facility and Optical Instrumentation for Turbulent Combustion Research," AIAA *Journal of Propulsion and Power*, Vol. 3, pp. 97-104.

Ballal, D. R., 1988, "Combustion-Generated Turbulence in Practical Combustors," AIAA *Journal of Propulsion and Power*, Vol. 4, pp. 123-134.

Bradshaw, P., Ferriss, D. H., and Atwell, N. P., 1967, "Calculation of Boundary Layer Development Using Turbulent Energy Equation," *Journal of Fluid Mechanics*, Vol. 28, pp. 593-616.

Chen, T. H. and Lightman, A. J., 1985, "Effects of Particle Arrival Statistics on Laser Anemometer Measurements," ASME-FED, Vol. 33, pp. 172-176.

Glass, M., and Bilger, R. W., 1978, "The Turbulent Jet Diffusion Flame in Coflowing Stream-Some Velocity Measurements," *Combustion Science and Technology*, Vol. 18, pp. 165-177

Griffin, O. M., 1985, "Vortex Shedding From Bluff Bodies in a Shear Flow: A Review," ASME *Journal of Fluids Engineering*, Vol. 107, pp. 298-306.

Harsha, P. T., and Lee, S. C., 1970, "Correlation Between Shear Stress and Turbulent Kinetic Energy," *AIAA Journal*, Vol. 8, pp. 1508-1512.

Heitor, M. V. and Whitelaw, J. H., 1986, "Velocity, Temperature, and Species Characteristics of the Flow in a Gas Turbine Combustor," *Combustion and Flame*, Vol. 64, pp. 1-32.

Rao, K. V. L., and Lefebvre, A. H., 1982, "Flame Blowoff Studies Using Large-Scale Flameholders," ASME *Journal of Engineering for Power*, Vol. 104, pp. 853-857.

Shepherd, I. G., Moss, J. B., and Bray, K. N. C., 1982, "Turbulent Transport in a Confined Premixed Flame," *Nineteenth Symposium*

(International) on Combustion, The Combustion Institute, pp. 423-431.

Sivasegaram, S. and Whitelaw, J. H., 1987, "Suppression of Oscillations in Confined Disk-Stabilized Flames," AIAA *Journal of Propulsion and Power*, Vol. 3, pp. 291-295.

Starner, S. H., and Bilger, R. W., 1980, "LDA Measurements in a Turbulent Diffusion Flame With Axial Pressure Gradients," *Combustion Science and Technology*, Vol. 21, pp. 259-270.

Strahle, W. C. and Lekoudis, S. G., 1985, "Evaluation of Data on Simple Turbulent Reacting Flows," Technical Report TR-85-0880, Air Force Office of Scientific Research, Bolling Air Force Base, Washington, D. C.

Sturgess, G. J., Syed, S. A., and McManus, K. R., 1983, "Importance of Inlet Boundary Conditions for Numerical Simulation of Combustion Flows," AIAA Paper No. 83-1263.

Winterfeld, G., 1965, "On Processes of Turbulent Exchange Behind Flame Holders," *Tenth Symposium (International) on Combustion*, The Combustion Institute, Pittsburgh, PA., pp. 1265-1275.

Zukoski, E. E. and Marble, F. E., 1955, "The Role of Wake Transition in the Process of Flame Stabilization on Bluff Bodies," AGARD *Combustion Researches and Reviews*, A. H. Lefebvre et al., ed., Butterworths Publishing Co., London, pp 167-180.

APPENDIX H

AERODYNAMICS OF BLUFF BODY STABILIZED CONFINED TURBULENT PREMIXED FLAMES

by

J. C. Pan, M. D. Vangsness, and D. R. Ballal
University of Dayton, Dayton, Ohio

Published in Transactions of ASME, Journal of Engineering for Gas Turbines & Power, Vol. 114, pp. 783-783, October 1992.

Aerodynamics of Bluff Body Stabilized Confined Turbulent Premixed Flames

J. C. PAN, M. D. VANGSNESS, and D. R. BALLAL
University of Dayton
Dayton, Ohio

Abstract

Detailed information on the influence of geometric and flow parameters on the structure and properties of recirculation zone in confined combusting flows is not available. In this paper, recirculation zone structure and turbulence properties of methane-air mixtures downstream of several conical flameholders were measured using LDA. These tests employed different blockage ratios (13% and 25%), cone angles (30, 45, 60, and 90 degrees), equivalence ratios (0.56, 0.65, 0.8, and 0.9), mean annular velocities (10, 15, and 20 m/s), and approach turbulence levels (2%, 17%, and 22%).

It was found that increasing the blockage ratio and cone angle affected the recirculation zone size and shape only slightly. Also, these parameters increased the shear stress and turbulent kinetic energy (TKE) moderately. Increasing the equivalence ratio or approach turbulence intensity produced a recirculation zone shape very similar to that found in the cold flow. TKE decreased due to turbulent dilatation produced by increased heat release. These observations are discussed from the viewpoint of their importance to practical design and combustion modeling.

Nomenclature

BR	= blockage ratio
C_p	= pressure coefficient ($\Delta p/0.5\ \rho U_a^2$)
d	= base diameter of conical stabilizer
I	= approach axial turbulence intensity
L_r	= length of the recirculation zone
p	= static pressure
q	= turbulent kinetic energy (TKE)
r	= radial direction
S	= flame burning velocity
T	= temperature
U, V	= mean velocities in axial and radial directions
u, v	= fluctuating velocities in axial and radial directions
$\overline{uv}$	= Reynolds shear stress
x	= axial direction
δ	= flame-front thickness
ℓ	= turbulence integral scale
ϕ	= equivalence ratio
ν	= kinematic viscosity
θ	= cone apex angle
ρ	= density
τ	= heat release parameter, $(T_f-T_u)/T_u$

Superscripts

—	= mean value
'	= rms value
"	= density-weighted value

Subscripts

a	= annular flow
f	= flame
l	= laminar
u	= unburned
t	= total, turbulent

Introduction

Bluff body flameholders are used in ramjet engines, afterburners, and many other combustion systems to maintain a steady flame in

Presented at the International Gas Turbine and Aeroengine Congress and Exposition
Orlando, FL June 3-6, 1991
This paper has been accepted for publication in the Transactions of the ASME
Discussion of it will be accepted at ASME Headquarters until September 30, 1991

a high-speed turbulent combustible mixture. The flame is stabilized by the recirculation zone formed in the wake of the bluff body. This recirculation zone provides long residence time and continuous ignition source for flame propagation into the incoming fresh mixture. Thus, the size, shape, and turbulence characteristics of the recirculation zone are crucial for flame stabilization.

The combustion performance of the afterburner depends upon the geometry and mixture characteristics of the flow. Flameholders, such as a cone or a vee gutter, introduce an area blockage in the afterburner pipe which creates pressure drop and recirculatory flow in the wake of the bluff body. The apex angle of the bluff body causes parallel streamlines of the incoming flow to curve and increase the aerodynamic width of the recirculation zone. Thus, blockage ratio (BR) and apex angle (θ) affect flameholding. Also, incoming mixture velocity (U) and turbulence intensity (I) influence flame holding by entraining the combustion zone with fresh mixture. Finally, a combination of air loading parameter (ALP) and mixture equivalence ratio (ϕ) determines the width of the combustion stability limits. In this manner, the five parameters BR, θ, U, I, and ϕ play an important role in the design and performance of practical afterburner flameholders.

Detailed information on the influence of geometric and flow parameters on the structure and properties of recirculation zone in confined combusting flows is scanty. Winterfeld (1965) studied combustion behind flameholders, but did not measure any turbulence properties. Rizk and Lefebvre (1986) investigated the influence of BR and θ, but only for isothermal flows. Heitor et al. (1988) examined velocity and scalar characteristics but mostly for a confined *disk-stabilized* flame, and Fujii and Eguchi (1981) provide a comparison of cold and reacting flow turbulence properties, also for a single flameholder only. As pointed out by Moreau et al. (1987), the available data provide only limited information about bluff-body flame stabilization.

In a previous paper, Pan et al.(1990) examined the turbulence properties of confined conical stabilizers in a combusting flow. Measurements of turbulent velocity fluctuations such as mean and rms values, skewness and flatness factors, Reynolds shear stresses, and axial mean pressure gradients were reported and data interpreted to elucidate recirculation zone structure, effects of flow confinement, and the role of combustion-generated turbulence. The objectives of this work were (i) to investigate the influence of geometric parameters BR and θ, and flow parameters U, I, and ϕ on the recirculation zone structure and the turbulence properties within and surrounding this zone, and (ii) to provide bench-mark quality data set for evaluating and refining computer models used for the design of bluff body flameholders in practical afterburners. The present work fills a long-overdue need for detailed information on the influence of parametric variations on recirculation zone structure and turbulence properties.

Experimental Work

1 Test Rig. Figure 1 shows the test rig employed for these experiments. Several stainless steel conical flame stabilizers were manufactured including two base diameters, d = 4.44 cm and 3.18 cm corresponding to the blockage ratios BR = 25% and 13% respectively, and four apex angles, θ = 30, 45, 60 and 90 degrees. Each stabilizer was mounted coaxially inside a 8 cm × 8 cm × 28.4 cm test section with rounded corners which has four 5.64 cm × 25.4 cm cut-outs for quartz windows. This test section was mounted on a vertical combustion tunnel with a three-axis traversing mechanism described by Ballal et al. (1987). Different turbulence grids could be inserted at 5.8 cm upstream of the base of the conical bluff body. Measurements of turbulence quantities and mean wall-static pressure were performed downstream of the confined conical flame stabilizer by using a two-component Laser Doppler Anemometer (LDA) and a precision micromanometer respectively.

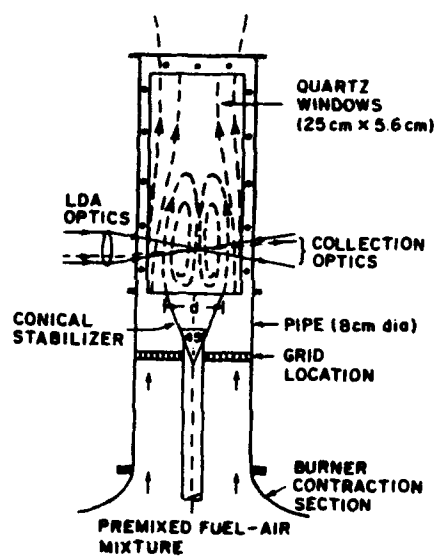

Fig. 1 Schematic diagram of the confined flame stabilizer test facility.

2 Flow Condition. In these experiments, premixed methane-air flames were studied. The mean annular velocities were 10, 15, and 20 m/s which covered a range of Reynolds number from Re_d = 3×10^4 to 6×10^4. Zukoski and Marble (1955) have pointed out that the bluff body wake region becomes fully turbulent when Re_d = $U_a d/\nu \geq 10^4$. Four different equivalence ratios, 0.56, 0.65, 0.8, 0.9 were tested, corresponding to adiabatic flame temperatures of 1590 K, 1755 K, 1990 K, and 2130 K respectively. The inlet turbulence intensity level was varied from 2% to 22% by using different grids.

3 LDA Instrumentation. A two-component LDA system was used for all velocity measurements. Essentially, this instrument uses polarization separation of the two channels and is an upgraded and refined version of the LDA system used by Ballal et al. (1989). The LDA system parameters are listed in Table 1.

Principally, this instrument incorporates Bragg cell frequency shifting for measurements in a recirculatory flow, a unique coincidence circuit for rapid acquisition of valid data, software to filter spurious signals, for example, due to seed agglomeration, and a correction subroutine to account for the LDA signal biasing effect in combusting flows. A fluidized bed seeder was used to inject submicron sized ZrO_2 seed particles into the flowing combustible mixture. Scattered signals were detected by TSI Counter Processors (CP) and processed by our custom-designed software which calculates intensity, shear stresses, higher moments (skewness and kurtosis), and pdfs. Typical sampling rates for LDA measurements exceeded 1 kHz for both isothermal and combusting flows.

4 Error Analysis. Both the fuel flow and airflow were monitored by separate electronic flow control units to ± 0.5% and ± 1.5% respectively. The combined error produced an uncertainty of ± 1.5% in equivalence ratio. The primary source of error in LDA measurement is the statistical bias of the final measured velocity towards higher mass flux (velocity x density) when number-weighted averages are used to calculate stationary statistics. Chen and Lightman (1985) and Glass and Bilger (1978) have discussed bias correction schemes. After allowing for this bias, we estimated that for the single-stream seeding and relatively high-sampling rates of our experiments, the uncertainty in the measurement of mean velocity was 1% and for rms velocity 5%. Near the flame front, where intermittency would be much higher, the uncertainty in rms velocity could be greater than 7%. The long-term repeatability of measurements was found to be within 5% for turbulence quantities.

Results and Discussion

Our turbulence measurements encompassed a large test matrix. All these data, which may be used for evaluating and refining models of turbulent combusting recirculatory flows, will be available in a separate report (Pan et al. 1990) . Lack of space precludes us from presenting all our data (for example, increasing mean velocity above 15 m/s did not reveal any significant changes in the recirculation zone and hence these results are not shown here). Therefore, only selected data that illustrate the influence of parametric variation on mean flow field and turbulence properties are presented and discussed below.

Table 1: 2-component LDA system parameters

15 W Argon-ion laser wavelength	514.5 nm
Laser beam e^{-2} size	1.58 mm
Input lens focal length	350 mm
Beam intersection half-angle	2.88 degrees
Fringe spacing	5.106 μm
LDA measuring spot size	175 μm × 1500μm
Signal collection angle	9.5 degrees forward
Collection lens focal length	400 mm
PMT pinhole aperture	200 μm
Net frequency shift	5 MHz
Seed particles	ZrO_2
Seed particle size	97% < 1 μm

1 Mean Flowfield.

Figures 2-4 show mean velocity and axial pressure coefficient for all the conical stabilizers tested. In general, the mean axial velocity characteristics of Figs. 2a-4a reveal the magnitude of maximum reverse velocity, length of the recirculation zone, and acceleration of products due to combustion downstream of the rear stagnation point. Likewise, the pressure coefficients plotted in Figs. 2b-4b show a minimum associated with the maximum width of the recirculation zone, a favorable pressure gradient corresponding to the acceleration of products, and cold-flow pressure recovery (Figs. 3b-4b) downstream of the recirculation zone. These trends for both combusting and cold flows are broadly in agreement with the past work of Ballal et al. (1989), Pan et al. (1990) and Heitor et al. (1988). However, these data reveal important influences of blockage ratio, cone angle, equivalence ratio, mean annular velocity, and incoming turbulence level on the mean flowfield. A discussion of these effects is facilitated by identifying three regions; (i) region 1 spans the axial distance between the base of the bluff body and the location of maximum recirculation zone width, (ii) region 2 covers the axial distance downstream up to rear stagnation point, and (iii) region 3 is downstream of the rare stagnation point.

(a) Blockage Ratio: Figures 2a-2b show the influence of approximately doubling the blockage ratio, BR on axial mean velocity and pressure coefficient in a combusting flow. In region 1, increase in BR decreases the pressure coefficient. For region 2, we observe a slight decrease in the recirculation zone length with increasing BR, an observation in line with the results of Winterfeld (1965) and Wright (1959). Finally, in region 3, the acceleration of the flow is relatively greater with higher BR. This occurs, presumably because of an increase in the dilatation due to a larger amount of heat released in this region.

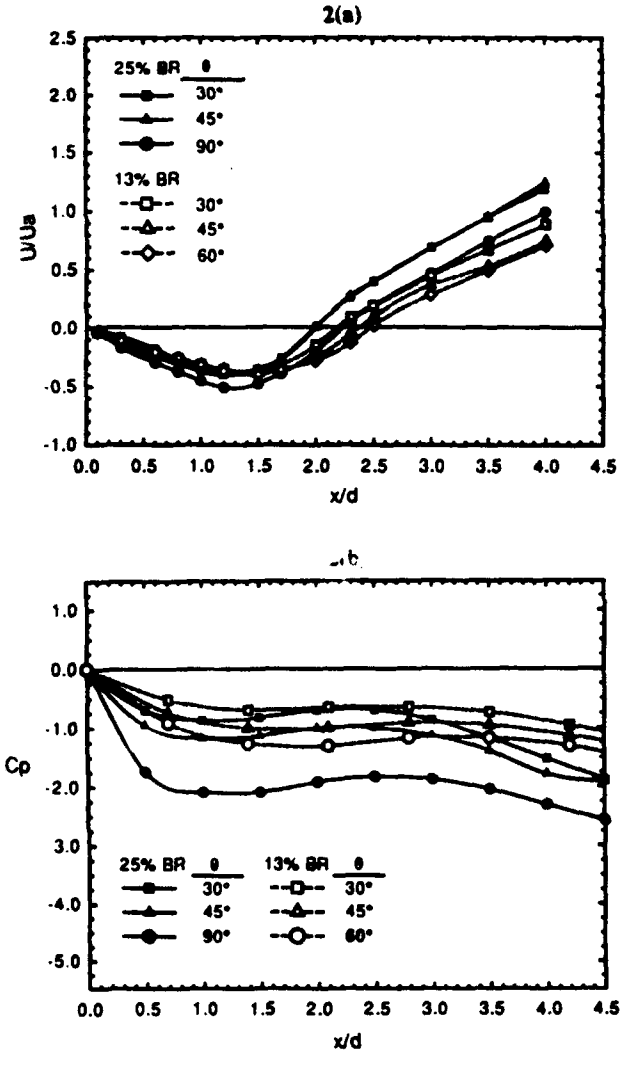

Fig. 2 Velocity and pressure coefficient characteristics plotted to illustrate the influence of blockage ratio and cone angle on mean flowfield. All measurements are in a confined combusting flow (ϕ = 0.65, U = 15 m/s): (a) centerline mean velocity, (b) axial pressure coefficient.

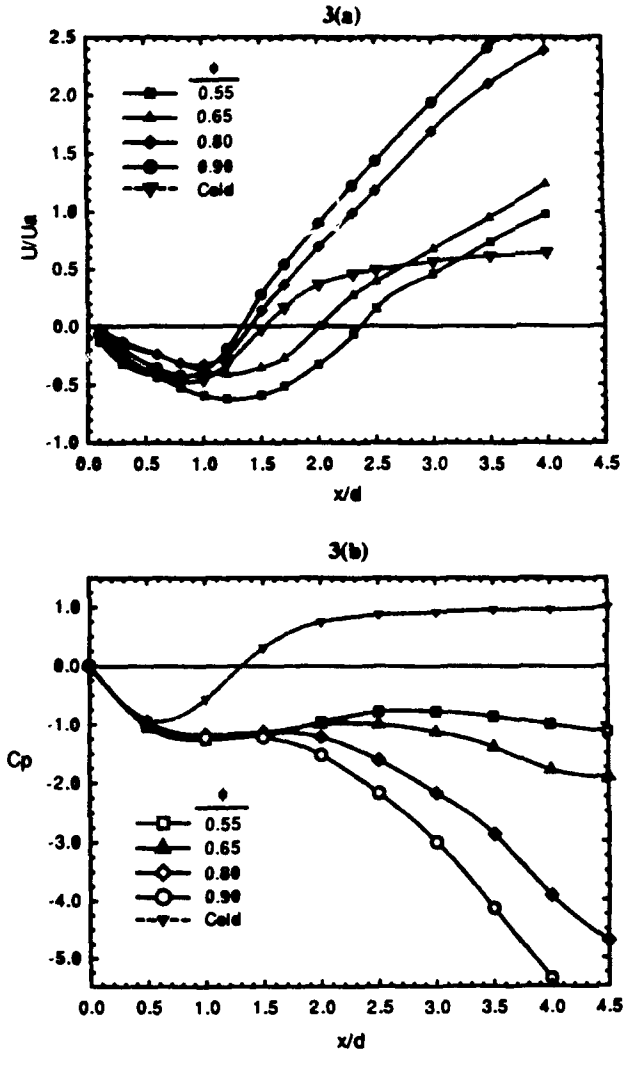

Fig. 3 Velocity and pressure coefficient characteristics plotted to illustrate the influence of equivalence ratio on mean flowfield. All measurements, except one, are in a confined combusting flow (BR = 25%, θ = 45 degrees, U = 15 m/s): (a) centerline mean velocity, (b) axial pressure coefficient.

(b) Cone Angle: The effects of cone angle on mean velocity and pressure coefficient are also demonstrated in Figs. 2a-2b. Increasing the cone angle increases the deflection of the mean separation streamline from the trailing edge of the bluff body. As Lefebvre (1983) has shown, in cold flow, this increases the aerodynamic blockage and hence also the recirculation zone width. In region 1 of the confined combusting flow, recirculation zone width increases due to increased streamline curvature. Also, in region 2, recirculation zone is elongated because wall confinement decreases streamline curvature. The net effect of these two changes is to produce a slightly larger recirculation zone volume and widen the flame stability limits. However, in confined flows, rigid walls accelerate the axial velocity in the vicinity of the flame and this may adversely affect flame stabilization with further increases in cone angle.

(c) Equivalence Ratio: Figures 3a-3b show the effects of equivalence ratio of the incoming fresh mixture, ϕ, on mean velocity and pressure coefficient. An increase in ϕ from 0.56 to 0.90 decreases the recirculation zone length dramatically from x/d = 2.35 to 1.32, i. e., slightly shorter than that found in the cold flow (x/d = 1.52). It also accelerates axial velocities in region 3 as clearly seen in Fig. 3b. Both these effects are a result of increasing heat release rates and higher turbulent flame propagation speed

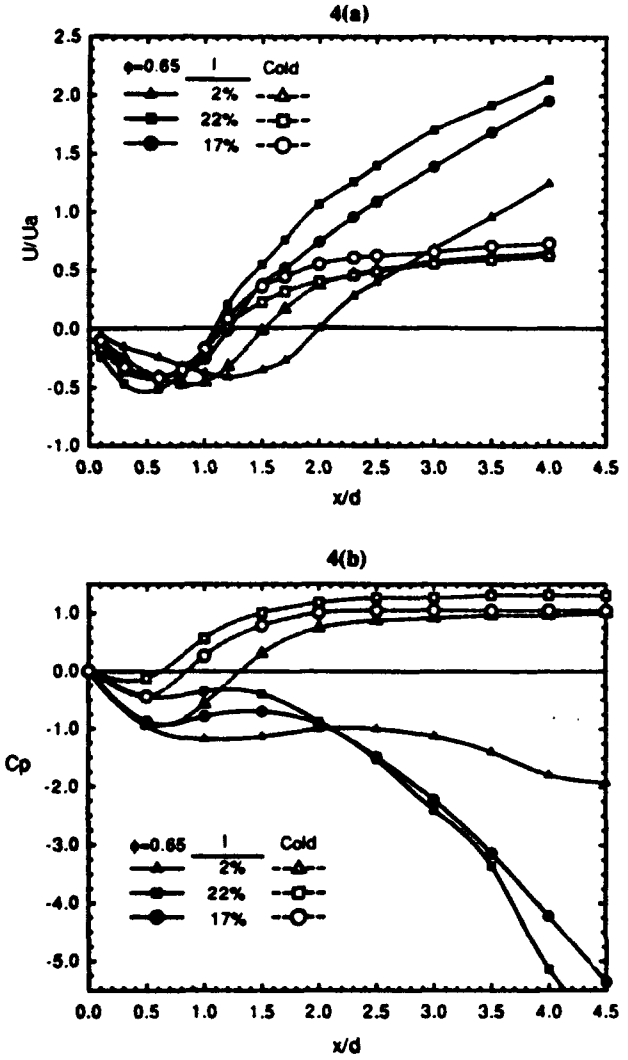

Fig. 4 Velocity and pressure coefficient characteristics plotted to illustrate the effects of approach turbulence intensity on mean flowfield. Comparisons between combusting (ϕ = 0.65) and cold flows are shown (BR = 25%, θ = 45 degrees, U_a = 15 m/s): (a) centerline mean velocity, (b) axial pressure coefficient.

(fast chemistry) brought about by increasing the equivalence ratio towards stoichiometry. This result clearly shows how compact the primary zone of a gas turbine combustor can be, provided it operates at or near stoichiometric equivalence ratios. It also demonstrates that for $\phi \leq 0.75$, combustion is kinetically controlled and requires a recirculation zone of size larger than that for cold flow to stabilize a flame.

(d) Approach Turbulence Intensity: Figures 4a-4b demonstrate the influence of increasing the approach mixture turbulence intensity, u'/U_a from 2% (no grid) to 17% (grid 7), to 22% (grid 3). In region 1, increase in turbulence shifts the location of maximum recirculation width upstream from x/d = 0.8 to 0.4. It also shortens the length of region 2 from x/d = 2 to 1.1, a value close to that for cold-flow. This dramatic change in the structure of the recirculation zone can be explained by recognizing that the turbulent burning velocity of the flame increases with an increase in the turbulence intensity; for example, Lefebvre (1983) gives $S_T/S_L = [1 + (u'/S_L)^2]^{0.5} \approx u'/S_L$ for large values of u'/S_L. Thus, a five-or six-fold increase in turbulent burning velocity dramatically reduces the size of the recirculation zone. In region 3, acceleration of products downstream of the recirculation zone continues. Similarities between the effects of increasing equivalence ratio and increasing turbulence intensity are very evident in Figs. 3 and 4.

2 Turbulence Flowfield

Figures 5-7 illustrate the turbulent combusting flowfield in and around recirculation zones, produced by different bluff bodies confined in the test section. Each figure has three parts:

(i) The recirculation zone structure sketched by the mean flow streamlines shows not only the width and length, but also the reverse velocity flowfield. The location of zero velocity (eye) region is also evident.

(ii) The contours of Reynolds shear stress ($\overline{uv}/u'v'$) illustrate regions of maximum shear stress and locations where the shear stress changes sign.

(iii) The TKE contours provide information on turbulence production due to normal stresses.

In general, strong turbulence activity is present around the periphery of the recirculation zone. This is because, in confined flames, the production of TKE is by the interaction of Reynolds stress and shear strain, i. e., via the term $\overline{uv}\,(\partial U/\partial r)$, and therefore generally restricted to the shear layer surrounding the maximum width of the recirculation zone. This observation is in agreement with the results of Pan et al. (1990).

It is also found that in these confined combusting flows, the locations of zero stress lines do not coincide with those of zero mean velocity gradient. This suggests that not only shear stresses (production term) but also normal stresses (dilatation term of the form $\overline{u'^2}\,(\partial U/\partial r)$) play an important role in modifying the turbulence flowfield. The influence of blockage ratio, cone angle, equivalence ratio, and inlet turbulence intensity on turbulence flowfield is now discussed.

(a) Blockage Ratio: A comparison between Figs. 5a and 5b reveals the effect of almost doubling the blockage ratio (but maintaining the same value of U_a = 15 m/s) on the recirculation zone structure and the surrounding flowfield. High blockage ratio nar-

rows the width of the annular gaseous jet surrounding the bluff body. Thus, the incoming fresh mixture behaves more as a *thin* annular jet than as a *thick* jet spreading into a dump combustor. As a consequence, in Fig. 5b, streamlines around the recirculation zone are crowded and mean velocity gradient increased, particularly in the narrow r/d = 0.45-0.55 region. Also, acceleration of gases produces a relatively thin flame at the trailing edge of the bluff body. However, further downstream, i. e., x/d > 1 (region 2), rapid entrainment leads to a thickened flame front.

The measurements of Reynolds shear stresses and TKE in Figs. 5a and 5b show that for a high value of blockage ratio, both shear stresses and TKE are spread throughout the recirculation zone (Fig.5b) rather than being confined to a narrow region surrounding it (Fig.5a). This may be a consequence of high spreading rate (0.14) of the boundary of thin annular jet as compared to 0.09 for the thick jet (see Ribeiro and Whitelaw, 1980).

(b) Cone Angle: A comparison between the results plotted in Figs. 5b and 5c demonstrates the influence of increasing the cone angle from 30 to 90 degrees. A larger cone angle produces a radially outward deflection of the separation streamline at the trailing-edge of the bluff body, effectively increasing its aerodynamic blockage. This causes pinching of the annular gaseous jet at the axial location of maximum recirculation zone width (x/d = 1). Upstream of this location, no significant effects of cone angle on shear stresses or TKE can be detected, because the shearing action is decreased. However, further downstream (i. e., in region 2), the TKE appears to be concentrated around the periphery of the recirculation zone. This is presumably because the slight elongation of the recirculation zone in this region shifts turbulence production radially outward, in the vicinity of the flame zone.

(c) Equivalence Ratio: Figures 6a and 6b show measurements of turbulence flowfield at $\phi = 0.56$ ($T_f = 1590$ K, $\tau = 4.5$) corresponding to lean extinction limit and at $\phi = 0.9$ ($T_f = 2130$ K, $\tau = 6.3$) close to stoichiometric combustion respectively. Dramatic changes in the mean flow structure of the recirculation zone are clearly evident, principally a decrease in the recirculation zone length to its cold flow value. Due to increased heat release rates and wall confinement of the flame, streamline curvature is smaller. Therefore, turbulent dilatation and *not* turbulent shear production is the dominant process in these experiments. Thus, TKE is significantly decreased at high equivalence ratios as evident in Fig. 6b.

Another effect of increasing the equivalence ratio is that it decreases chemical reaction time (S_L / δ_L) or increases the Damkohler number, $D = (\ell S_L / u' \delta_L)$. As Bray (1980) has stated and McDannel et al. (1982) have found, premixed flames of large Damkohler number produce strong scalar (temperature or density) fluctuations. Thus, and bearing in mind that the dilatation term dominates, Reynolds shear stresses are not altered significantly.

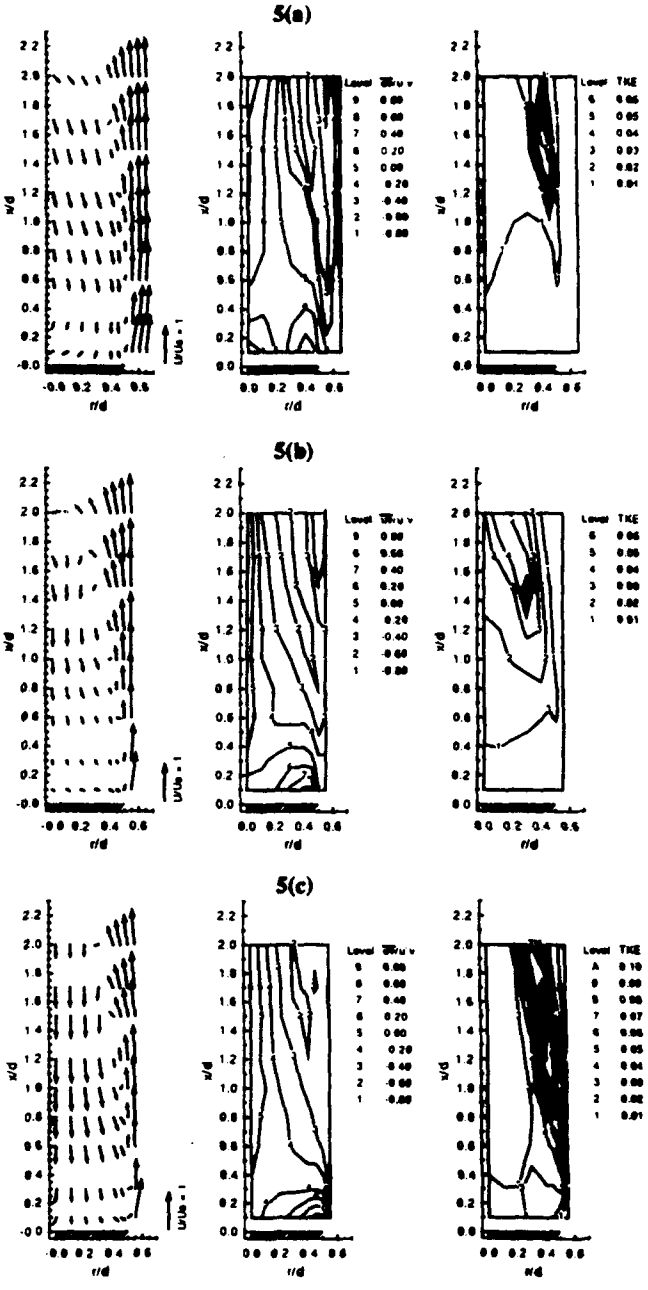

Fig. 5 Mean flow structure, Reynolds shear stresses, and turbulent kinetic energy plotted to illustrate the effects of blockage ratio and cone angle on turbulence flowfield. All measurements are in a confined combusting flow ($\phi = 0.65$, U_a = 15 m/s): (a) BR = 13%, θ = 30 degrees, (b) BR = 25%, θ = 30 degrees, (c) BR = 25%, θ = 90 degrees.

(d) Approach Turbulence Intensity: Figs. 5b, 7a and 7b illustrate the effect of increasing the approach turbulence intensity on the turbulence flowfield. As the approach turbulence intensity increases from 2% (Fig. 5b) to 17% (Fig. 7b) the recirculation zone

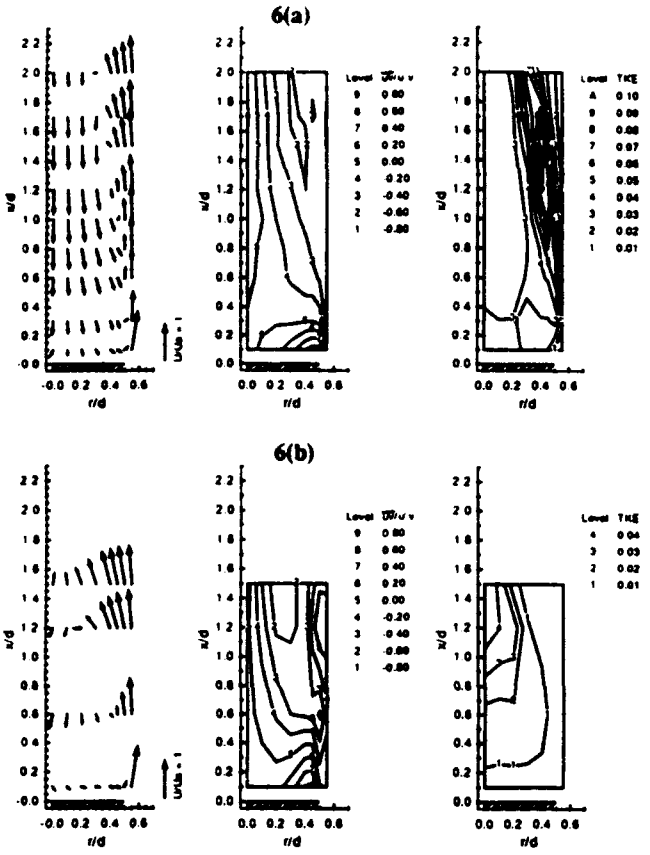

Fig. 6 Mean flow structure, Reynolds shear stresses, and turbulent kinetic energy plotted to illustrate the effects of equivalence ratio on turbulence flowfield. All measurements are in a confined combusting flow (BR = 25%, θ = 45 degrees, U_a = 15 m/s): (a) lean extinction limit, ϕ = 0.56 (b) near-stoichiometric combustion, ϕ = 0.90.

length decreases dramatically from x/d = 2 to x/d = 1.2. But, further increase in turbulence intensity to 22% (Fig. 7a) has an insignificant effect as compared to Fig. 7b. This dramatic shortening of the recirculation zone length shifts regions with strong concentration of both shear stress and TKE from the outer periphery of the recirculation zone to radially inward location around r/d = 0.2. The magnitude of shear stresses is about the same, but the TKE appears to be slightly higher for the high turbulence case (Fig. 7a).

Since the size of the combusting recirculation zone in Fig. 7b resembled that of the cold flow (see Ballal et al. 1989), measurements of cold turbulence flowfield were performed for grid 7. These are plotted in Fig. 7c for comparison with Fig. 7b. Although the mean recirculation zone structure, and to some extent the shear stresses, are identical, magnitude of TKE in cold flow is much higher than in combusting flow.

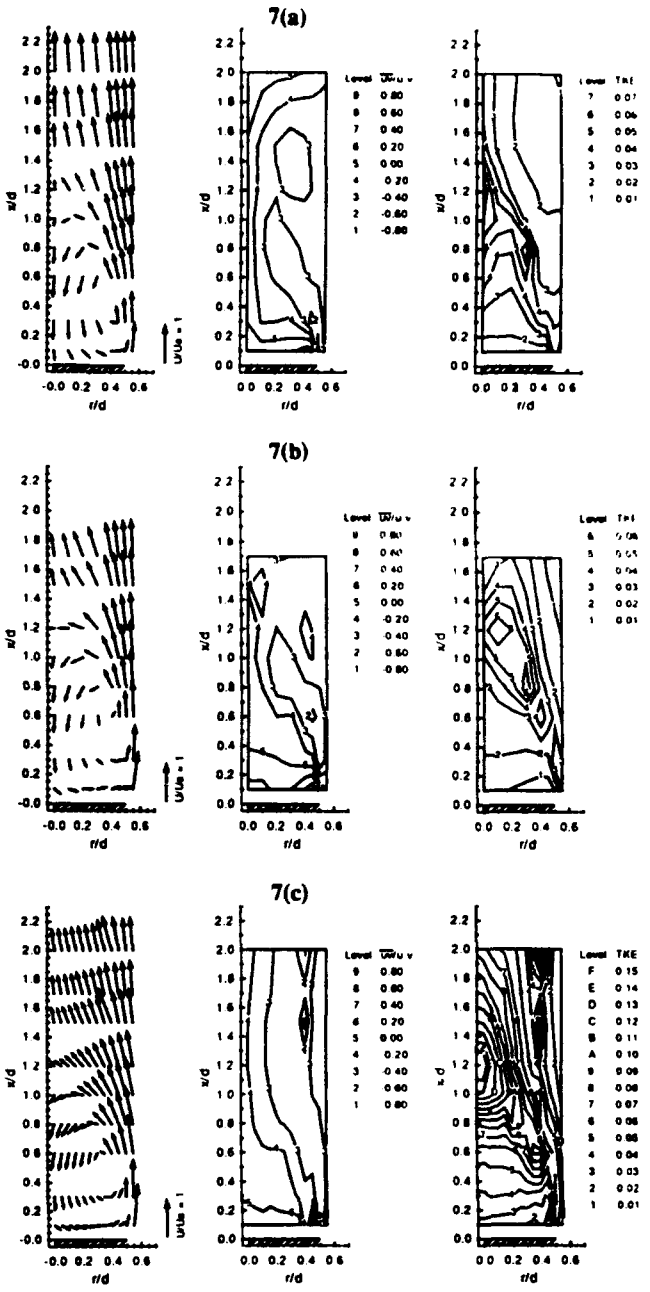

Fig. 7 Mean flow structure, Reynolds shear stresses, and turbulent kinetic energy plotted to illustrate the effects of approach turbulence intensity on turbulence flowfield. All measurements, except (c) below, are in a confined combusting flow (BR = 25%, θ = 45 degrees, ϕ = 0.65, U_a = 15 m/s): (a) approach turbulence intensity, I = 22%, (b) approach turbulence intensity, I = 17%, (c) confined cold flow, I = 17%.

The above observations can be explained by recognizing that increasing approach turbulence affects the flame and the

recirculation zone structure in two different ways. First, higher turbulence in the fresh mixture augments turbulent burning velocity. This increases heat release rates and hence also the turbulence dilatation which suppresses TKE in combusting flows. Second, higher turbulence decreases mixing time, increases entrainment between the fresh mixture and the flame, i. e., the flame loading is increased, and the flame front is thickened. Thus, combustion shifts from a mixing-controlled to a reaction-controlled process. As Bray (1980) has pointed out, scalar thermodynamic variables of temperature, density, and composition do not fluctuate relatively strongly in this type of thick flame.

Further Comments

Here, we briefly discuss recirculation zone structure and turbulence properties from the viewpoint of their importance to practical design and combustion modeling.

(i) Recirculation Zone Structure: In these experiments, we have observed that in turbulent confined combusting flows, increasing the blockage ratio or approach flow turbulence, and in the limit of fast chemistry, the recirculation zone size decreases to its value for fully developed, cold turbulent flow wake. Thus, in the limit of high Reynolds number, *mixing-controlled* combustion, the recirculation zone size can be predicted from the non-reactive turbulence modeling codes. In contrast, for *reaction-controlled* combustion, the recirculation zone is highly elongated. Intermediate between these two extremes, recirculation zone size and shape may vary with geometric (BR, θ), chemical (ϕ), and flow (U_a, I) parameters. Therefore, numerous past observations on the recirculation zone size and shape can be reconciled by developing a criteria for mixing- or reaction-controlled combustion in that particular experiment.

For the present, we observe that only ϕ and I have a strong effect on the recirculation zone structure in combusting flows. Although geometric (hardware) parameters, BR and θ undoubtedly influence cold flow results (see Heitor et al. 1988 and Rizk and Lefebvre 1986) and indeed have important practical role in the flameholder design (pressure loss, heat transfer, fuel injection considerations) they appear to be less important in defining the recirculation zone structure in combusting flows.

(ii) Turbulence Properties: We have noted that the geometric parameters BR and θ produce a moderate increase in the shear stress and TKE in either the interior or at the periphery of recirculation zone respectively. Increasing ϕ or I increases heat release and presumably this increases magnitude of both the shear-generated turbulence and the turbulence dilatation terms. However, dilatation predominates in the presence of wall confinement and small streamline curvature and the net result is a decrease in TKE in this combusting flow. Thus, in practical gas turbine combustors combustion may actually suppress TKE.

In the context of combustion modeling, another term of importance in a *confined combusting turbulent flow* is the source term $-\overline{u_i''}(\partial P/\partial x_i)$ from the conservation equation of turbulence stresses. The magnitude of this term would be important in regions where both $\overline{u_i''}$ and $(\partial P/\partial x_i)$ are large. Although no local measurements of $(\partial P/\partial x_i)$ in the combusting flow were possible, it is easy to visualize at least two distinct regions where the streamline curvature is high and the term $\overline{u_i''}(\partial P/\partial x_i)$ could become important. First, the stretched flame region surrounding the recirculation zone at the location of its maximum width would provide a source of turbulence. Second, the highly-curved region in the vicinity of the rear stagnation point represents yet another region of turbulence production.

Conclusions

Detailed measurements of the mean and turbulent combusting flowfield were performed in the wake and downstream region of several conical flameholders confined in a test section. The following conclusions were drawn on the influence of blockage ratio, cone angle, equivalence ratio, and approach turbulence intensity on recirculation zone structure and turbulence properties in and surrounding flowfield.

(1) Increasing the blockage ratio slightly decreases the recirculation zone length and produces a moderate increase in the shear stress and TKE in either the interior or at the periphery of recirculation zone respectively.

(2) Increasing the cone angle produces a slightly larger recirculation zone volume and moderately augments TKE production, downstream of the axial plane of maximum recirculation zone width.

(3) Increasing the equivalence ratio from its lean extinction limit to near-stoichiometry decreases the recirculation zone length to one-half its original value and very close to its value in the cold flow. TKE is drastically decreased due to suppression of turbulence by dilatation.

(4) Increasing the approach turbulence intensity drastically shortens the recirculation zone length close to its value in the cold flow. The distribution of both shear stresses and TKE shifts from the outer periphery of the recirculation zone to radially inward locations.

Finally, recirculation zone structure and turbulence properties of the flow are discussed from the viewpoint of their importance to practical design and combustion modeling.

Acknowledgment

This work was supported by the U. S. Air Force, Wright Research and Development Center, Aero Propulsion and Power Laboratories, Ohio, under Contract No. F33615-87-C-2767. The authors are grateful to Dr. W. M. Roquemore, the Air Force Technical Monitor, for his interest and helpful discussions during the course of this work.

References

Ballal, D. R., 1986, "Studies of Turbulent Flow-Flame Interaction," *AIAA Journal*, Vol. 24, pp. 1148-1154.

Ballal, D. R., Chen, T. H., and Schmoll, W. J., 1989, "Fluid Dynamics of a Conical Flame Stabilizer," ASME *Journal of Engineering for Gas Turbines and Power*, Vol. 111, pp. 97-102.

Ballal, D. R., Lightman, A. J., and Yaney, P. P., 1987, "Development of Test Facility and Optical Instrumentation for Turbulent Combustion Research," AIAA *Journal of Propulsion and Power*, Vol. 3, pp. 97-104.

Bray, K. N. C., 1980, "Turbulent Flows With Premixed Reactants," In *Turbulent Reacting Flows*, Edts. P. A. Libby and F. A. Williams, pp. 115-183, Springer Verlag, New York, NY.

Chen, T. H. and Lightman, A. J., 1985, "Effects of Particle Arrival Statistics on Laser Anemometer Measurements," ASME-FED, Vol. 33, pp. 172-176.

Fujii, S. and Eguchi, K., 1981, "A Comparison of Cold and Reacting Flows Around a Bluff-Body Flame Stabilizer," ASME, *Journal of Fluids Engineering*, Vol. 103, pp. 328-334.

Glass, M., and Bilger, R. W., 1978, "The Turbulent Jet Diffusion Flame in Coflowing Stream-Some Velocity Measurements," *Combustion Science and Technology*, Vol. 18, pp. 165-177

Heitor, M. V., Taylor, A.M. K. P., and Whitelaw, J. H., 1988, "Velocity and Scalar Characteristics of Turbulent Premixed Flames Stabilized on Confined Axisymmetric Baffles," *Combustion Science and Technology*, Vol. 62, pp. 97-126.

Lefebvre, A. H., 1983, *Gas Turbine Combustion*, Hemisphere Publishing, New York, NY, pp. 179-220.

McDannel, M. D., Peterson, P. R., and Samuelsen, G. S., 1982, "Species Concentration and Temperature Measurements in a Lean Premixed Flow Stabilized by a Reverse Jet," *Combustion Science and Technology*, Vol. 28, pp.211-220.

Moreau, P., Labbe, J., Dupoirieux, F., and Borghi, R., 1987, "Experimental and Numerical Study of a Turbulent Recirculation Zone With Combustion," *Turbulent Shear Flows*, Vol. 5, pp. 337-346, Springer Verlag, New York.

Pan, J. C., Schmoll, W. J., and Ballal, D. R., 1990, "Turbulent Combustion Properties Behind a Confined Conical Stabilizer," ASME Paper 90-GT-51, To appear in *Journal of Engineering for Gas Turbine and Power*.

Pan, J. C. and Ballal, D. R., 1990, "Turbulent Combustion Properties of Premixed Flames Stabilized Behind a Conical Bluff Body-Data Sets," Report in Preparation.

Ribeiro, M. M. and Whitelaw, J. H., 1980, "The Structure of Turbulent Jets," *Proceedings of The Royal Society*, London, Vol. A370, pp. 769-775.

Rizk, N. K., and Lefebvre, A. H., 1986, "The Relationship Between Flame Stability and Drag of Bluff-Body Flameholders," AIAA *Journal of Propulsion*, Vol. 2, pp. 361-365.

Winterfeld, G., 1965, "On Processes of Turbulent Exchange Behind Flameholders," *Tenth Symposium (International) on Combustion*, The Combustion Institute, Pittsburgh, PA, pp. 1265-1275.

Wright, F. H., 1959, "Bluff-Body Flame Stabilization-The Blockage Effects," *Combustion and Flame*, Vol. 26, pp. 319-328.

Zukoski, E. E. and Marble, F. E., 1955, "The Role of Wake Transition in the Process of Flame Stabilization on Bluff Bodies," AGARD *Combustion Researches and Reviews*, A. H. Lefebvre et al., ed., Butterworths Publishing Co., London, pp 167-180.

APPENDIX I

SCALAR MEASUREMENTS IN BLUFF BODY STABILIZED FLAMES USING CARS DIAGNOSTICS

by

J. C. Pan, M. D. Vangsness, S. P. Heneghan, and D. R. Ballal
University of Dayton, Dayton, Ohio

Published as ASME Paper No. 91-GT-302. To Appear in Transactions of ASME, Journal of Engineering for Gas Turbines & Power.

Scalar Measurements in Bluff Body Stabilized Flames using Cars Diagnostics

J. C. PAN, M. D. VANGSNESS, S. P. HENEGHAN, and D. R. BALLAL
University of Dayton
Dayton, Ohio

Abstract

Measurements of mean and rms temperature fluctuations were performed in confined turbulent premixed methane-air flames, stabilized on a conical flameholder. A CARS system was used for these measurements. These tests employed flameholders of different blockage ratios (13% and 25%), and mixtures with different equivalence ratios (0.56, 0.65, 0.8, and 0.9) and approach turbulence intensity (2%, 17%, and 22%).

It was found that the recirculation zone closely resembles a perfectly well-stirred reactor. Blockage ratio, equivalence ratio, or approach turbulence intensity did not alter the scalar field. The turbulent flame structure enveloping the recirculation zone comprises: (i) an ignition/thin flame region in the vicinity of the flameholder base, (ii) a reacting shear layer region of large-scale coherent structures, and (iii) a thick flame region where entrainment is the dominant mechanism. Finally, analysis suggests that the scalar gradient-diffusion relationship is valid and areas of non-gradient diffusion, if any, are probably small.

Nomenclature

BR	= blockage ratio
C	= reaction progress variable $(T-T_u)/(T_f-T_u)$
C_t	= rms temperature $(T_{rms})/(T_f-T_u)$
d	= base diameter of conical stabilizer
I	= approach axial turbulence intensity (u'/U_a)
L_r	= length of the recirculation zone
r	= radial direction
T	= temperature
U, V	= mean velocities in axial and radial directions
u, v	= fluctuating velocities in axial and radial directions
x	= axial direction
δ	= flame thickness
ϕ	= equivalence ratio
ν	= kinematic viscosity

Superscripts

—	= mean value
'	= rms value

Subscripts

a	= annular flow
f	= flame
u	= unburned
t	= total, turbulent

Introduction

In designing afterburner systems and ramjet combustors, provision must be made to initiate and sustain effective flameholding in highly turbulent combustible mixtures. A bluff body is commonly used to create a recirculation zone. This zone exchanges mass and momentum with the flame surrounding it and also provides the necessary heat flux to ignite the incoming reactants. In this type of flowfield, the magnitude and nature of the scalar transport depend upon mean temperature gradients, temperature fluctuations, velocity-temperature correlations, and properties of the premixed reactants such as equivalence ratio and burning velocity. Also, knowledge of scalar transport allows accurate computation of mean reaction rate and therefore heat release, flame stability, and production of unburned hydrocarbons (UHC) and NO_x.

Presented at the International Gas Turbine and Aeroengine Congress and Exposition
Orlando, FL June 3-6, 1991

Many years ago Longwell et al. (1953) proposed that the recirculation zone may be viewed as a perfectly-stirred reactor. However, in practical combustors, the situation of perfect homogeneity does not exist. To simulate the practical combustion process more closely, Swithenbank et al. (1980) and Pratt (1980) proposed models of "partially-stirred reactor" and "imperfect micromixing". To evaluate these models and to understand the mechanism of flame stabilization require data on turbulent scalar properties.

Measurement of flame temperature in highly turbulent, confined, recirculatory flows is an extremely difficult task. Comparatively few results are available in the literature. Lewis and Moss (1979), Shephard and Moss (1982), and Shephard et al. (1982) reported heat flux measurements in a weakly sheared unconfined and confined premixed flames. Heitor et al. (1987, 1988) measured temperature fluctuations in disk-stabilized open and confined flames. Sivasegaram and Whitelaw (1983) and Taylor and Whitelaw (1980) have presented temperature data in a step-stabilized premixed flame, and in an axisymmetric combustor respectively.

Almost all the temperature measurement reported above employed either uncompensated or compensated fine-wire thermocouples. Hence, these measurements suffer from many deficiencies as follows: (i) uncertainty in mean and rms temperatures of 120 K or more due to large wire-size (e. g., Shephard and Moss (1982) and Shephard et al., 1982), (ii) uncompensated thermocouple or one with a large time constant (100 ms or more) of the compensation circuit introduces errors in pdf measurements (e. g., Lewis and Moss 1979), (iii) uncertainty in radiation correction, catalytic effects of coatings, and heat loss to thermocouple prongs can result in the underestimation of temperature by 150 K or more (e. g., Heitor et al. 1987), (iv) flow disturbances produced by inserting the thermocouple within the flame can significantly alter the flame structure, e. g., thermocouple can act as a flameholder.

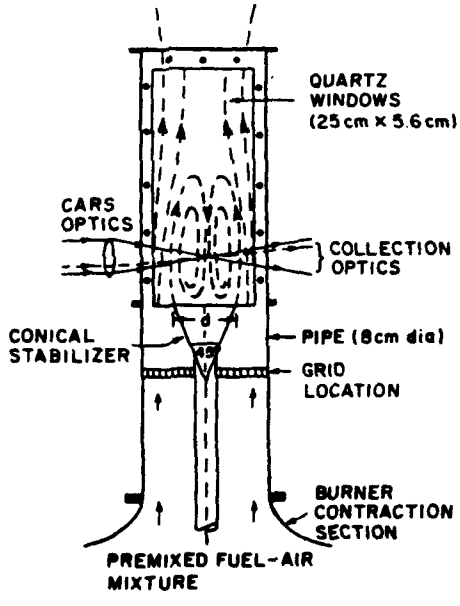

Fig. 1 Schematic diagram of the confined flame stabilizer test facility.

To overcome the uncertainties of thermocouple temperature measurements, we employed a Coherent Anti-Stokes Raman Spectroscopy (CARS) system. This system offers several advantages such as non-intrusive probing, high spatial and temporal resolution, good accessibility to confined flames, insensitivity to soot and particulates, and good reproducibility.

The objectives of our work were to (i) measure temperature fluctuations in and around a confined recirculation zone, (ii) study the influence of blockage ratio, equivalence ratio, and approach turbulence intensity on the scalar distribution within and around the recirculation zone, and (iii) develop an understanding of the turbulent flame structure surrounding the recirculation zone.

Experimental Work

1 **Test Rig.** Figure 1 shows the test rig employed for these experiments. Several stainless steel conical flame stabilizers were manufactured including two base diameters, d = 4.44 cm and 3.18 cm corresponding to the blockage ratios BR = 25% and 13% respectively. Each stabilizer was mounted coaxially inside an 8 cm × 8 cm × 28.4 cm test section with rounded corners which has four 5.64 cm × 25.4 cm cut-outs for quartz windows. This test section was mounted on a vertical combustion tunnel with a three-axis traversing mechanism. Different turbulence grids could be inserted at 5.8 cm upstream of the base of the conical bluff body. Measurements of turbulence quantities and mean wall-static pressure, which are reported by Pan et al. (1990, 1991), were performed by using a two-component Laser Doppler Anemometer (LDA) and a precision micromanometer respectively. A CARS system was used to perform independent temperature measurements.

2 **Test Condition.** In these experiments, premixed methane-air flames were studied. The mean annular velocity was 15 m/s and the Reynolds number varied between $Re_d = 3 \times 10^4$ to 4.2×10^4. Zukoski and Marble (1955) have pointed out that the bluff body wake region becomes fully turbulent when $Re_d = U_a d/\nu \geq 10^4$. Four different equivalence ratios, 0.56, 0.65, 0.8, 0.9 were tested, corresponding to adiabatic flame temperatures of 1590 K, 1755 K, 1990 K, and 2130 K respectively. The inlet turbulence intensity level was varied from 2% to 22% by using different grids.

3 **CARS System.** The CARS optics layout is shown in Fig. 2. The laser source is provided by a Nd:YAG pulse laser with 10 ns time resolution. The frequency-doubled source green beam (532 nm) is equally divided into four parts. Two of these serve as the pump beams, while the other two pump a dye laser oscillator and amplifier. The dye laser is tuned to provide a red broad-band Stokes beam (110 FWHM) centered at 607 nm. The red Stokes beam and the two green pump beams are then focused together by a 25-cm focal length lens in a BOXCARS configuration. A 25-μm-x-250-μm measuring spot size is achieved. The CARS signal is collected by a Spex 1702 spectrometer, 1024 element DARSS camera, and Tracor-Northern multichannel analyzer. The raw data are processed by a MODCOMP minicomputer.

From the raw data, the temperatures are determined by comparing the actual nitrogen spectra to the calculated spectra, using a least square fit. The calculation of a nitrogen CARS spectrum requires knowledge of the instrument slit function. This slit function is normally determined at a known temperature and then assumed to be the applicable function at all temperatures, independent of the optical path which varies with density or temperature gradients. However, the constant slit function assumption can lead to serious error in temperature determination. Heneghan et al. (1991) have developed a simple method of determining the slit function from the collected data at the actual temperature and turbulence level by applying the principle of local thermodynamic equilibrium. In general, the mean temperature is measured for two different curve-fit weighting schemes and two different slit widths. The actual mean temperature and slit width are calculated by finding the intersection of the two lines (T vs. slit width at constant weighting). This method yields improvement in the precision of the CARS measurement.

4 **Error Analysis.** Both fuel flow and air flow were monitored by separate electronic flow control units to within ± 0.5% and ± 1.5% respectively. The combined error produced an uncertainty of ± 1.5% in equivalence ratio, or ± 30 K in temperature. Usually, 500 samples were taken for each CARS measurement to ensure that the error in the rms temperature was less than 10 K, while 1500 samples were taken in the flame region where the rms values were expected to be large. As shown by Heneghan and Vangsness (1990), the rms temperature is susceptible to CARS instrument noise. However, in combusting flow, the temperature fluctuations are much greater than the instrument noise and thus the measurement precision (reproducibility) is good. Overall, we estimated the CARS mean temperature measurement accuracy to be within 50 K, while the precision is well within 20 K. Unlike the LDA, CARS temperature measurements are time-averaged, without density biasing effects.

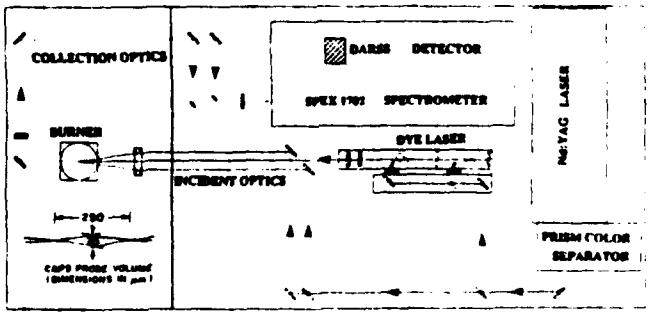

Fig. 2 Arrangement of the CARS system optics.

Results and Discussion

In this section we present and discuss three principal features of the temperature field, namely (i) influence of parametric variations on the temperature field, (ii) nature of temperature pdfs, and (iii) structure of the turbulent reacting shear layer. All the temperature data were made non-dimensional and plotted in the form of reaction progress variable C and C_t which are relevant in developing theories of premixed turbulent combustion (for example, see Bray, 1980). In all the figures, the approach turbulence intensity I = 2% unless otherwise stated.

1 **Influence of Parametric Variations.** Figures 3a-b show axial and radial distributions of the reaction progress variable C and C_t for BR = 25% and 13% respectively. In Figs. 3a-b, we observe that within the recirculation zone (r/d < 0.5) and near the metal base of the bluff body (x/d = 0.1), C = 0.90-0.87. Further downstream, the mean temperature within the recirculation zone is lower than the adiabatic flame temperature by approximately 5%. Also, the rms temperature fluctuation is around 5% and constant throughout. These results suggest that the recirculation zone (i) loses about 5% (or less) heat to the environment, (ii) loses approximately 5%-8% heat to the metal base of the bluff body, and (iii) is almost, but not perfectly well-stirred. These observations are also generally valid for the rest of the data presented in Figs. 4 and 5. Now, effects of parametric variations on scalar field are discussed.

(a) Blockage Ratio: Figures 3a-b show the influence of approximately doubling the blockage ratio on mean and rms temperature fluctuations. It is observed that the blockage ratio does not affect either the mean or the rms temperature. Since Pan et al. (1991) have reported no significant change in the size of the recirculation zone, it is clear that the flame position, and therefore the scalar field, remain unaltered. In practical afterburner systems, the blockage ratio mainly influences the drag of the bluff body. For the same annular velocity, a large bluff body confined in a combustor has less mass flow of reactants taking part in combustion. This increases residence time for complete combustion, but also decreases the total heat released downstream of the recirculation zone. Clearly, combustor pressure loss, reactant mass flow,

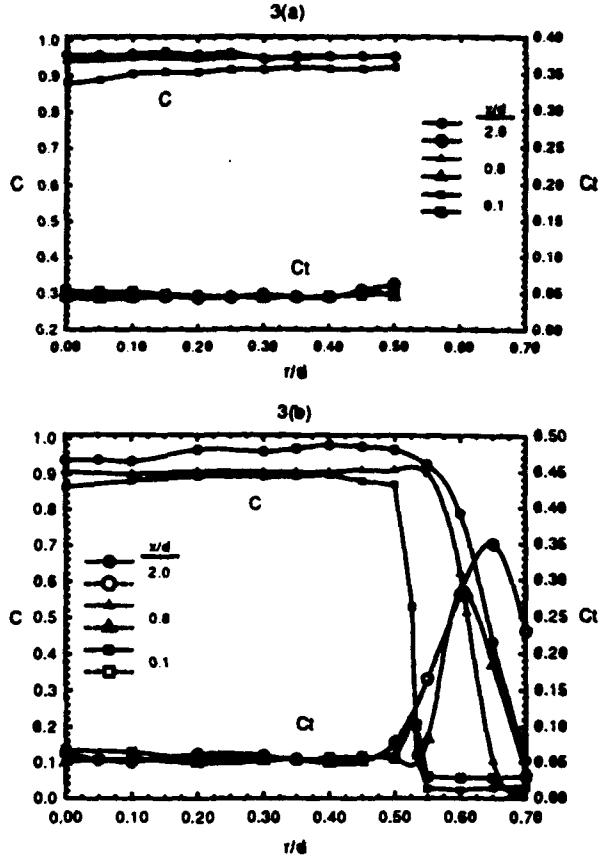

Fig. 3 Radial profiles of non-dimensional mean temperature (reaction progress variable) and rms temperature plotted to illustrate the influence of blockage ratio on scalar fluctuations. These measurements are for a 45 degree conical-body, at U_a = 15 m/s and ϕ = 0.65, (a) BR = 25%, L_r/d = 2, (b) BR = 13%, L_r/d = 2.37.

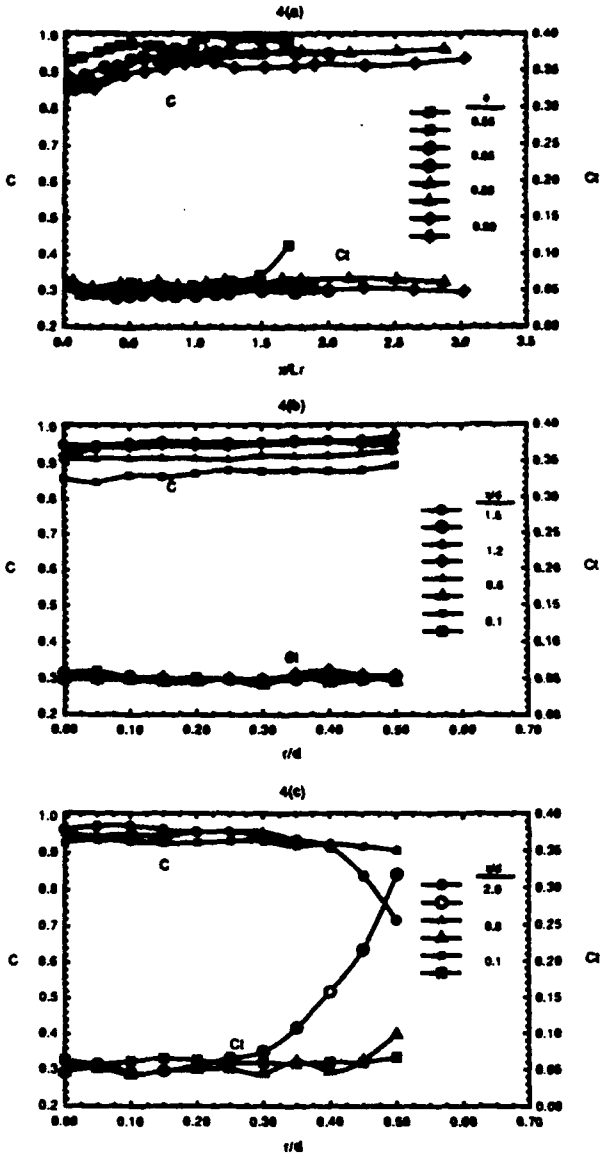

Fig. 4 Axial and radial profiles of non-dimensional mean temperature (reaction progress variable) and rms temperature plotted to illustrate the influence of equivalence ratio on scalar fluctuations. These measurements are for a 45 degree conical-body, BR = 25%, U_a = 15 m/s, (a) centerline profiles (b) radial profiles for ϕ = 0.8, L_r/d = 1.4, (c) radial profiles for ϕ = 0.56, L_r/d = 2.37.

and combustor size are just some of the factors that determine a suitable value of the blockage ratio for use in a given practical application.

(b) Equivalence Ratio: Figures 4a-c illustrate the effects of equivalence ratio on mean and rms temperatures. In Fig. 4a, the centerline temperatures are plotted. These data show that the rms temperature fluctuation is nearly constant at 5%, but the mean temperature within the recirculation zone gradually increases with downstream distance. Also the reaction progress variable C increases with decreasing equivalence ratio from 0.90 to 0.56. At least two factors contribute to this trend: (i) a decrease in the heat loss to the metal base of the bluff body with decreasing temperature difference from 1870 K to 1500 K, and (ii) a complete conversion of entrained reactants to hot products within the recirculation zone.

In Figs. 4b-c radial temperature profiles are shown for various axial planes. The results of Fig. 4b are almost identical to those of Fig. 3a and the same explanations are valid here also. Figure 4c illustrates the results of experiments at the lean extinction limit of methane-air mixture. Specifically, we observe a rapid growth in the temperature fluctuations (C_t rises from 5% to 30%) for r/d ≥ 0.3 and x/d = 2, i. e., upstream of the rear stagnation

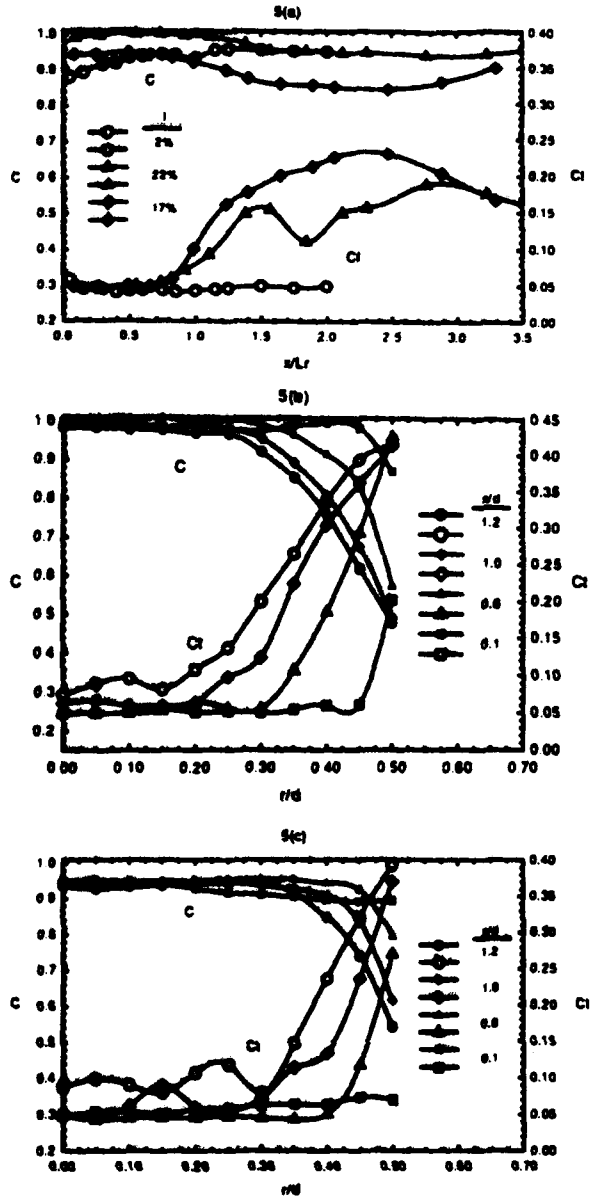

Fig. 5 Axial and radial profiles of non-dimensional mean temperature (reaction progress variable) and rms temperature plotted to illustrate the influence of approach turbulence intensity on scalar fluctuations. These measurements are for a 45 degree conical-body, BR = 25%, U_a = 15 m/s, and ϕ = 0.65, (a) centerline profiles (b) radial profiles for I = 22%, L_r/d = 1.1, (c) radial profiles for I = 17%, L_r/d = 1.3.

point. Also, the centerline plot in Fig. 4a suggests a growing temperature fluctuation downstream of the rear stagnation point for the lean extinction limit.

In summary, increasing the equivalence ratio (i) strongly affects the size (and specifically the length) of the recirculation zone and this modifies the velocity flowfield (Pan et al. 1991), but (ii)

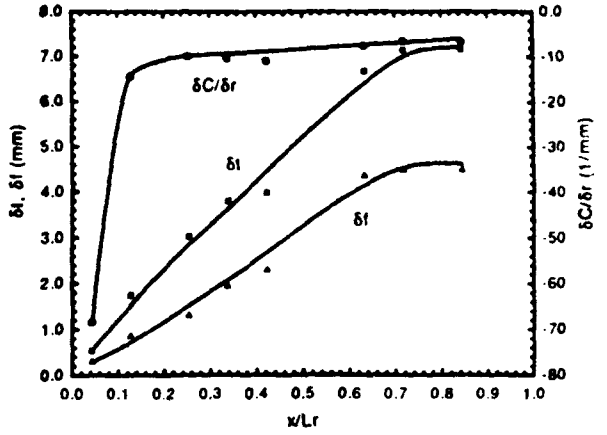

Fig. 6 Temperature gradient and thickness of the turbulent flame structure for a 45 degree conical-body at U_a = 15 m/s, ϕ = 0.65, and BR = 13%.

the scalar field is not altered in any dramatic manner for a stable flame, except through changes in the magnitude of heat losses stated above. However, at the lean extinction limit, the turbulent burning velocity of the flame is not fast enough to consume the reactants completely. This allows entrainment of fresh or partially burned reactants into the region around the stagnation point and increases the scalar fluctuations.

(c) Approach Turbulence Intensity: Figures 5a-c demonstrate the influence of increasing the approach turbulence intensity from 2% to 17% to 22%. In Fig. 5a, centerline axial distribution of temperature is shown. Within the length of the recirculation zone ($x/L_r \leq 1$), increasing the approach turbulence intensity increases mean temperature but does not change rms temperature fluctuations. This can be explained by noting that Pan et al. (1991) have reported a dramatic decrease in the size, and hence also the surface area, of the recirculation zone with increasing reactant turbulence intensity and this must contribute to reducing the heat loss from the recirculation zone. Further downstream of the rear-stagnation point ($x/L_r \geq 1$), increasing turbulence reduces mean temperature and increases rms temperature fluctuations, both the result of accelerated exchange of mass and heat transfer between cold reactants and hot products.

Figures 5b-c show radial profiles of mean and rms temperatures. It should be noted that within the recirculation zone ($r/d \leq 0.3$) values of C and C_t remain fairly constant. However, outside the zone ($r/d > 0.3$), the mean value gradually falls and the rms value rapidly increases within the vicinity of the flame. Clearly, increasing the turbulence level of the reactants increases both the heat transfer between cold and hot gases (which decreases mean temperature) and turbulent burning velocity of the flame (which increases temperature fluctuations). Again, these results appear consistent with the heat loss arguments invoked earlier.

2 **Temperature Pdfs.** From the radial temperature profiles of Figs. 3-5, we can calculate the mean temperature gradient ($\partial C/\partial r$) and the flame thickness δ. Two types of flame thickness were defined: (i) total thickness, δ_t spanning the value C = 0-1, and (ii) flame front thickness, δ_f corresponding to the range C = 0.5-1 (note: C = 0.5 implies that combustion products are present half the time and reactants are present the rest of the time at this location, i. e., this represents the mean flame position).

Figure 6 shows plots of ($\partial C/\partial r$), δ_t, and δ_f for a bluff body with BR = 13%, over the axial distance covering the length of the recirculation zone. It is observed that the radial temperature gradient ($\partial C/\partial r$), which is negative throughout, rises steeply within x/L_r = 0-0.12 (corresponding to δ_t = 0.54 mm and δ_f = 0.29 mm) and then maintains a fairly constant value. This result shows that the ignition of reactants and the establishment of the flame by the heat flux transported from the recirculation zone are achieved within 12% of the length of the recirculation zone. Also, the flame front is extremely thin (< 1 mm). Downstream of this ignition/thin flame region, the mean temperature gradient remains fairly flat but the flame thickness continues to increase eventually to δ_t = 7.1 mm and δ_f = 4.5 mm. This suggests that entrainment is the dominant mechanism in this region and it is responsible for producing the thick flame front.

Figures 7a-e show typical CARS temperature pdfs measured in the reacting shear layer around the bluff body at three different axial locations, (i) within the ignition zone, x/d = 0.1, (ii) near the vortex center, x/d = 0.8, and (iii) within the thick flame region, x/d = 1.5. These data are for a 45 degree conical-body, BR = 13%, U_a = 15 m/s, and ϕ = 0.65.

In Figs. 7a-b, the two radial locations differ from one another by only 0.2 mm. These results show only one skewed peak in each pdf; (i) in Fig. 7a, the peak corresponds to the product gas temperature of 1070 K (C ~ 0.5) on the hot side, and (ii) in Fig. 7b, the peak corresponds to the reactant temperature of 470 K on the cold side. This dramatic shift in the pdf confirms that the flame front is extremely thin at this axial location.

The temperature pdf shown in Fig. 7c shows a bimodal distribution with approximately equal weighting on each of the cold and hot peaks (C ~ 0.5). The cold gas peak is centered corresponding to gas temperatures in the preheat zone, somewhat higher than

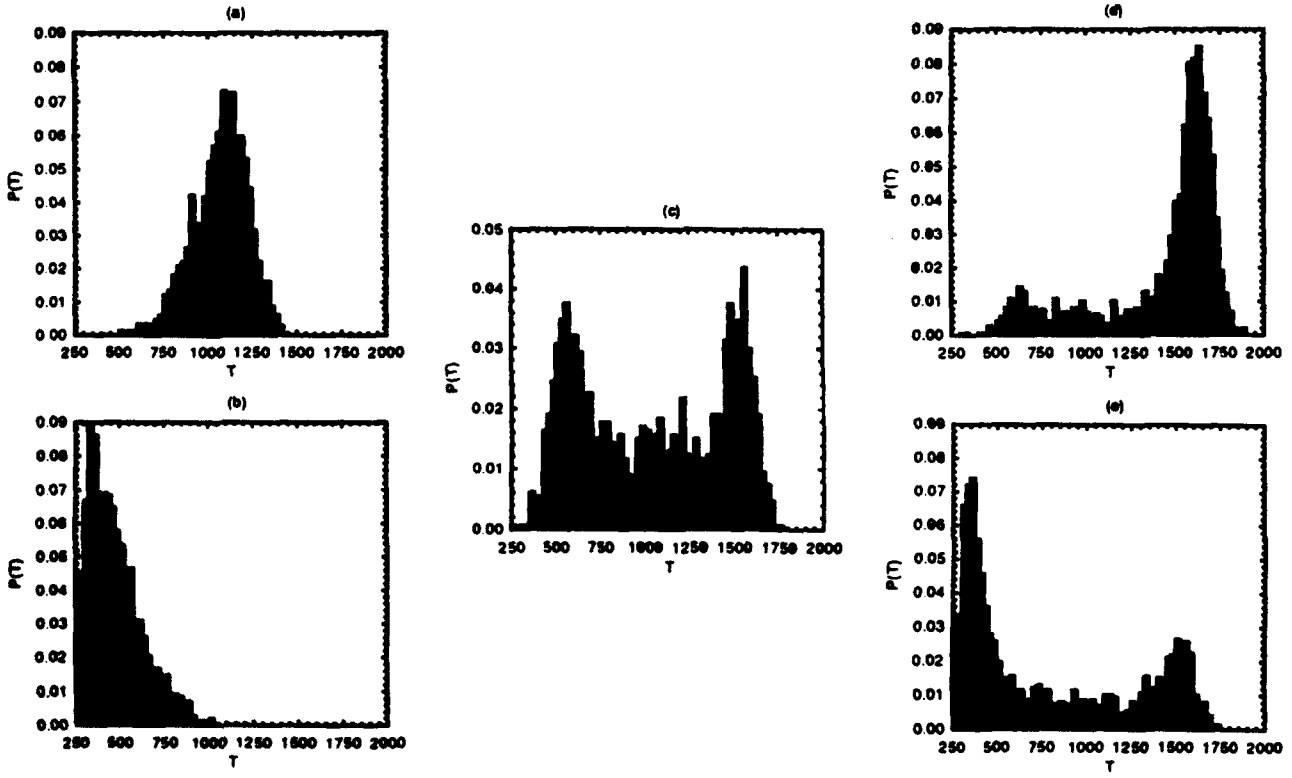

Fig. 7 CARS temperature pdfs measured in the reacting shear layer for a 45 degree conical-body, BR = 13%, U_a = 15 m/s, ϕ = 0.65, and L_r/d = 2.37, (a) x/d =0.1, r/d = 0.526, T = 1070 ± 155 K, C = 0.53, (b) x/d = 0.1, r/d = 0.532, T = 470 ± 149 K, C = 0.12, (c) x/d = 0.8, r/d = 0.61, T = 1047 ± 410 K, C = 0.51, (d) x/d = 1.5, r/d = 0.60, T = 1440 ± 339 K, C = 0.78, (e) x/d = 1.5, r/d = 0.65, T = 795 ± 477 K, C = 0.34.

the room temperature and the hot gas peak is centered near the adiabatic flame temperature. The bimodal nature of the scalar pdf indicates the presence of large-scale coherent structures within the reacting shear layer. As Spalding (1976) has suggested, these structures form as folds around the flame edge, and then grow in size downstream, entraining reactants and products and thickening the reacting shear layer.

Finally, Figs. 7d-e show temperature pdfs within the thick flame region separated radially by 1.6 mm. Both pdfs show a skewed-bimodal type of distribution with one dominant peak. The hot gas peak found in Fig. 7d is much higher than the one found in Fig. 7e, while the cold gas peak of Fig. 7e is very close to the room temperature. A finite probability of intermediate temperatures also exists in both the temperature pdfs which suggests the presence of gas in the partially burned-unburned state. Thus, the flame front structure is extremely complex comprising large-scale structures, entrainment, and stretching produced due to the necking-down of mean streamlines in the vicinity of the rear stagnation point. In such instances, the Bray-Moss-Libby model (Bray, 1980) which describes the statistics of the thin flame front, cannot be applied.

3 **Turbulent Flame Structure.** From the above experimental observations, a model of the turbulent flame structure enveloping the recirculation zone was developed. A schematic diagram of this model is shown in Fig. 8 and it is described below.

Turbulent combustion in the reacting shear layer is a *three-stage* preheat-ignition-propagation process. Near the base of the bluff body and along its edge, the flowing reactants are preheated and ignited by the heat flux transported radially outward from the recirculation zone. Within the region x/L_r = 0-0.12, ignition of the incoming reactants takes place and a thin flame that conforms to the "fast-chemistry" assumptions sits slightly oblique to the oncoming reactants. This type of flame can be successfully modeled by the Bray-Moss-Libby theory (Bray, 1980).

Downstream of this ignition-thin flame region, ($x/L_r > 0.12$), the temperature remains either fairly constant or decreases slightly, i. e., $\partial C/\partial r \leq 0$. This suggests that no radial heat flux is transported, and only entrainment of reactants and products is taking place downstream. In this region, large-scale coherent structures begin to grow within the reacting shear layer. These structures form as folds around the flame edge and then grow in size downstream, producing a convoluted reaction zone with many isolated pockets of hot product and cold reactant gas. These coherent bodies of gas are squeezed and stretched during their travel through the flame and the entrainment process causes their growth downstream thereby thickening the flame.

Further downstream, and in the vicinity of the rear stagnation point, the flame front is thick (≈ 4.5 mm) and mass entrainment of fresh reactants is the dominant mechanism at work. In this region,

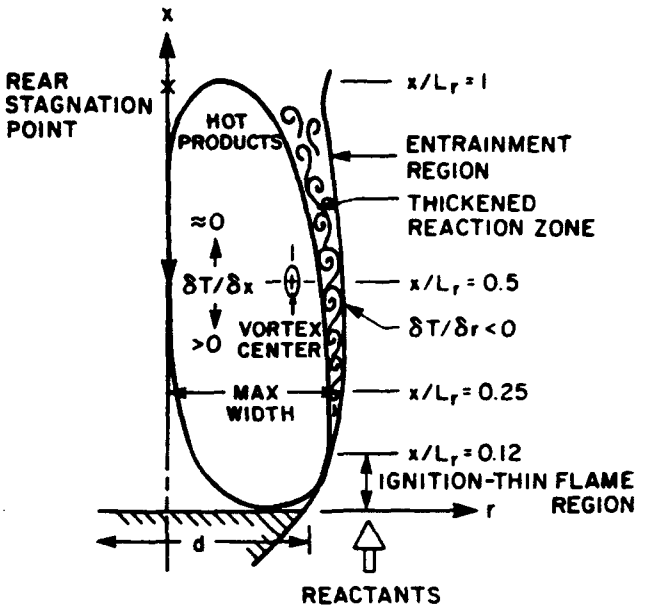

Fig. 8 Schematic diagram illustrating the turbulent flame structure enveloping the recirculation zone.

large temperature fluctuations (C_t = 25%-35%) are measured as observed in Figs. 3b, 4c, and 5b-c. Such fluctuations may acoustically couple with a sufficiently long duct and produce combustion instability or *rumble* in practical combustors. Clearly, the relatively simple statistical description of the wrinkled thin flame front is inadequate here. Rather, the "eddy-entrainment, combustion-in-depth" process of Ballal and Lefebvre (1974) is at work. Thus, the instantaneous region of combustion is distributed throughout the time average of the combustion zone rather than being confined to a thin wrinkled laminar flame. Also, since an intermediate state of gas exists, neither the perfect-stirred reactor theory of Longwell et al. (1953) nor the characteristic time theory of Zukoski and Marble (1955) can fully describe the bluff body flame stabilization mechanism accurately. More work is required to examine these issues in detail.

Finally, within the reverse flow region of the recirculation zone, the axial heat flux is directed towards the bluff body because hot products ($T > 0$) are moving axially towards the bluff body (u = -ve) and cold reactants are moving axially downstream, i. e., the axial heat flux $\overline{uT}$ is negative. In this same region, the axial temperature gradient $\partial C/\partial x$ is generally positive as evident from Figs. 4a and 5a. These observations support the scalar gradient-diffusion relationship of the form $-\overline{uT} = D_h (\partial C/\partial x)$. Outside of the recirculation zone ($r/d > 0.5$) and within the flame, hot products ($T > 0$) are moving axially downstream (+ u), i. e. the axial heat flux $\overline{uT}$ is positive and the axial temperature gradient $\partial C/\partial x$ is ≤ 0. Again this lends credence to the validity of the above scalar

gradient-diffusion relationship. Now, the radial heat flux $\overline{vT}$ is always positive because reactants are preheated and ignited by the heat flux transported radially outward from the recirculation zone. Also, Fig. 6 shows that $\partial C/\partial r$ is negative throughout. Therefore, it appears that the conventional scalar gradient-diffusion relationship of the form $\overline{vT} = - D_h (\partial T/\partial r)$ is valid in this type of reactive flowfield.

Our above arguments suggesting the validity of the scalar gradient-diffusion relationship are in conflict with the scalar measurements of Shephard et al. (1982) in confined premixed flames, those of Heitor et al. (1987) in open baffle-stabilized flames, and the analysis of Libby and Bray (1981). These authors found counter-gradient diffusion effects. However, they used thermocouples with relatively large-wire sizes and it is possible that their measurements of flame temperature could have suffered from relatively large experimental uncertainties or errors discussed earlier. On the other hand, direct, laser-diagnostics-based, non-intrusive measurements of axial and radial turbulent heat fluxes are required in the future to examine in an unambiguous manner if counter-gradient diffusion exists within these type of flows. Currently, the LDA-CARS systems are being integrated in our laboratory for meeting this goal.

Conclusions

Using a CARS system, mean and rms temperatures were measured within and outside the recirculation zone produced by a conical flameholder confined in a test section and supplied with turbulent premixed methane-air mixtures. The following conclusions emerged.

(1) Measurements reveal that the recirculation zone loses about 5% heat to outside and about 5-8% heat to the flameholder base. Also, low rms temperatures (~ 5%) suggest that a perfectly well-stirred reactor description of the recirculation zone is very close to valid.

(2) Blockage ratio does not affect either the mean or rms temperature fluctuations. Increasing the equivalence ratio or approach turbulence intensity increases heat losses from the recirculation zone, but does not alter the scalar field in any dramatic way.

(3) Near the flameholder base, temperature pdfs reveal an extremely thin flame front. Downstream of this, temperature pdf is bimodal and suggests the presence of large-scale coherent structures within the reacting shear layer. Further downstream, a thick flame consisting of partially burned-unburned gas states develops.

(4) The turbulent flame structure enveloping the recirculation zone comprises an ignition/thin flame region, a reacting shear layer which has large-scale coherent structure, and finally, a thick flame region where entrainment is the dominant mechanism. Analysis suggests that the gradient-diffusion relationship is valid and areas of non-gradient diffusion, if any, are probably small.

Acknowledgment

This work was supported by the U. S. Air Force, Wright Research and Development Center, Aero Propulsion and Power Laboratories, Ohio, under Contract No. F33615-87-C-2767. The authors are grateful to Dr. W. M. Roquemore, the Air Force Technical Monitor, for his interest and helpful discussions during the course of this work.

References

Ballal, D. R. and Lefebvre, A. H., 1974, "The Structure and Propagation of Turbulent Flames," *Proceedings of the Royal Society*, London, Vol. A344, pp. 217-234.

Bray, K. N. C., 1980, "Turbulent Flows With Premixed Reactants," In *Turbulent Reacting Flows*, Edts. P. A. Libby and F. A. Williams, pp. 115-183, Springer Verlag, New York, NY.

Heitor, M. V., Taylor, A. M. K. P., and Whitelaw, J. H., 1987, "The Interaction of Turbulence and Pressure Gradients in a Baffle-Stabilized Premixed Flame," *Journal of Fluid Mechanics*, Vol. 181, pp. 387-413.

Heitor, M. V., Taylor, A. M. K. P., and Whitelaw, J. H., 1988, "Velocity and Scalar Characteristics of Turbulent Premixed Flames Stabilized on Confined Axisymmetric Baffles," *Combustion Science and Technology*, Vol. 62, pp. 97-126.

Heneghan, S. P. and Vangsness, M. D., 1990, "Instrument Noise and Weighting Factors in Data Analysis," *Experiments in Fluids*, Vol. 9, pp. 290-294.

Heneghan, S. P., Vangsness, M. D., and Pan, J. C., 1991, "Simple Determination of the Slit Function in Single Shot CARS Thermometry," To appear in *Journal of Applied Physics*.

Lewis, K. J. and Moss, J. B., 1979, "Time Resolved Scalar Measurements in a Confined Turbulent Premixed Flames," *Seventeenth Symposium (International) on Combustion*, The Combustion Institute, Pittsburgh, PA, pp. 267-275.

Libby, P. A. and Bray, K. N. C., 1981, "Countergradient Diffusion in Premixed Flames," *AIAA Journal*, Vol. 19, 205-213.

Longwell, J. P., Frost, E. E., and Weiss, M. A., 1953, "Flame Stability in Bluff-Body Recirculation Zones," *Industrial and Engineering Chemistry*, Vol. 47, No.8, pp. 1634-1643.

Pan, J. C., Schmoll, W. J., and Ballal, D. R., 1990, "Turbulent Combustion Properties Behind a Confined Conical Stabilizer," ASME Paper 90-GT-51, To appear in ASME *Journal of Engineering for Gas Turbine and Power*.

Pan, J. C., Vangsness, M. D. and Ballal, D. R., 1991, "Aerodynamics of Bluff Body Stabilized Confined Turbulent Premixed Flames," ASME Paper 91-GT-00, Submitted to ASME *Journal of Engineering for Gas Turbine and Power*.

Pratt, D. T., 1980, "Coalescence/Dispersion Modeling of Gas Turbine Combustors," in *Gas Turbine Combustor Design Problems*, Edt., A. H. Lefebvre, Hemisphere Publishing, New York, NY, pp. 315-334.

Shephard, I. G. and Moss, J. B., 1982, "Measurements of Conditioned Velocities in a Turbulent Premixed Flame," *AIAA Journal*, Vol. 20, pp. 566-573.

Shephard, I. G., Moss, J. B. and Bray, K. N. C., 1982, "Turbulent Transport in a Confined Premixed Flame," *Nineteenth Symposium (International) on Combustion*, The Combustion Institute, Pittsburgh, PA, pp. 423-431.

Sivasegaram, S. and Whitelaw, J. H., 1983, "Temperature Characteristics of Turbulent Premixed Flames," *Experiments in Fluids*, Vol. 1, pp.161-170.

Spalding, D. B., 1976, "Development of the Eddy-Breakup Model of Turbulent Combustion," *Sixteenth Symposium (International) on Combustion*, The Combustion Institute, Pittsburgh, PA, pp. 1657-1662.

Swithenbank, J., Turan, A., and Felton, P. G., 1980, "Three-Dimensional, Two-Phase Modeling of Gas Turbine Combustors," in *Gas Turbine Combustor Design Problems*, Edt., A. H. Lefebvre, Hemisphere Publishing, New York, NY, pp. 249-314.

Taylor, A. M. K. P. and Whitelaw, J. H., 1980, "Velocity and Temperature Measurements in a Premixed Flame With an Axisymmetric Combustor," *AGARD CP-281*, Paper No. 14.

Zukoski, E. E. and Marble, F. E., 1955, "The Role of Wake Transition in the Process of Flame Stabilization on Bluff Bodies," *AGARD Combustion Researches and Reviews*, A. H. Lefebvre et al., ed., Butterworths Publishing Co., London, pp 167-180.

APPENDIX J

CHEMISTRY AND TURBULENCE EFFECTS IN BLUFF-BODY STABILIZED FLAMES

by

J. C. Pan and D. R. Ballal
University of Dayton, Dayton, Ohio

Published as AIAA Paper No. 92-0771. To Appear in AIAA Journal of Propulsion.

Chemistry and Turbulence Effects in Bluff-Body Stabilized Flames

J. C. Pan† and D. R. Ballal
University of Dayton, Dayton, OH
(†Now at Phillips Laboratory, Edwards Air Force Base, CA)

Abstract

The effects of chemistry and approach turbulence intensity were studied for confined, turbulent, and premixed bluff-body stabilized methane-air flames. These experiments employed different blockage ratios (13% and 25%), equivalence ratios (0.56, 0.65, 0.8, and 0.9), and approach turbulence levels (2% and 22%). A two-component LDA was used for the velocity measurements and a CARS system performed all the temperature measurements.

It was found that both faster chemistry (i.e., increasing equivalence ratio) and increasing the approach turbulence dramatically decreased the recirculation zone size. Also, TKE was decreased due to dilatation. Both, slower chemistry (near lean extinction limit) and higher turbulence produced a rapid growth in temperature fluctuations. A flame model was developed comprising an ignition-thin flame region, a large-scale reacting shear layer, and finally, a thick flame region where entrainment is the dominant mechanism. This flame model was used to explain the lean blowout (finite chemistry effect) and the turbulent flame propagation on the basis of previously established criteria.

Nomenclature

BR	= blockage ratio
C	= mean reaction progress variable $(T-T_u)/(T_f-T_u)$
C_t	= rms reaction progress variable (T_{rms}/T_f-T_u)
d	= base diameter of conical stabilizer
I	= approach axial turbulence intensity
L_r	= length of the recirculation zone
m	= mass flow
p	= static pressure
q	= turbulent kinetic energy (TKE)
Re	= Reynolds number
Re_λ	= turbulent Reynolds number ($= u'\lambda/\nu$)
r	= radial direction
S	= flame burning velocity
T	= temperature
t	= time
U, V	= mean velocities- axial, radial directions
u, v	= fluctuating velocities-axial, radial directions
$\overline{uv}$	= Reynolds shear stress
x	= axial direction
δ	= flame-front thickness
ℓ	= turbulence integral scale
λ	= turbulence microscale
η	= Kolmogoroff scale
ϕ	= equivalence ratio
ν	= kinematic viscosity
θ	= cone apex angle
τ	= heat release parameter, (T_f-T_u/T_u)

Superscripts

----	= mean value
'	= rms value
"	= density-weighted value

Subscripts

a	= annular flow
f	= flame
L	= laminar
u	= unburned
t	= total, turbulent

Copyright © 1992 by authors. Published by the American Institute of Aeronautics and Astronautics, Inc., by permission.

1. Introduction

In ramjet engines, jet afterburners, and gas turbine combustors, recirculation of combustion products is used to stabilize the combustion process. In these types of combustion systems, intense turbulent mixing is present due to large fluctuations in temperature, composition, and density. Also, because of the non-linearity of the chemical kinetics terms, chemistry effects become important and controlling. Thus, from a practical viewpoint, there exists an important need to study the effects of chemistry and turbulence in confined recirculatory combusting flows.

A dump combustor and a bluff-body combustor are the two most common means of generating recirculatory combusting flows. Recently, one of us reported the chemistry [1] and the turbulence [2] effects in a dump combustor. In this paper, we have investigated these two effects for confined bluff-body stabilized flames. Our combustor, which is supplied with premixed fuel-air mixture, has a centrally-located conical bluff-body. This introduces an area blockage which produces pressure drop, and creates recirculation in its wake. The chemistry effects are simulated by varying the equivalence ratio of the incoming mixture from its value at the lean flammability limit to its stoichiometric value. The turbulence

effects are produced by inserting turbulence grids upstream of the base of the conical bluff-body and thereby changing the level of turbulence intensity and scale in the plane of the base.

Using the above experimental configuration, we have made detailed velocity and temperature measurements within and around the recirculation zone. From these data, the structure and behavior of the recirculatory flowfield is assessed and the effects of chemistry and turbulence level on flame stabilization are discussed.

2. Experimental Work

Test Rig: Figure 1 shows the test rig employed for these experiments. Several stainless steel conical flame stabilizers were manufactured including two base diameters, d = 4.44 cm and 3.18 cm corresponding to the blockage ratios BR = 25% and 13% respectively. Each stabilizer was mounted coaxially inside a 8 cm × 8 cm × 28.4 cm test section with rounded corners which has four 5.64 cm × 25.4 cm cut-outs for quartz windows. This test section was mounted on a vertical combustion tunnel with a three-axis traversing mechanism described by Ballal et al. [3]. Different turbulence grids could be inserted at 5.8 cm upstream of the base of the conical bluff body. Measurements of turbulence quantities and mean wall-static pressure were performed downstream of the confined conical flame stabilizer by using a two-component Laser Doppler Anemometer (LDA) and a precision micromanometer respectively.

Flow Condition: In these experiments, premixed methane-air flames were studied. The mean annular velocities were 10, 15, and 20 m/s which covered a range of Reynolds number from $Re_d = 3\times10^4$ to 6×10^4. Zukoski and Marble [4] have pointed out that the bluff body wake region becomes fully turbulent when $Re_d = U_a d/\nu \geq 10^4$. Four different equivalence ratios, 0.56, 0.65, 0.8, 0.9 were tested, corresponding to adiabatic flame temperatures of 1590 K, 1755 K, 1990 K, and 2130 K respectively. The inlet turbulence intensity level was varied from 2% to 22% by using different grids.

LDA Instrumentation: A two-component LDA system was used for all velocity measurements. Essentially, this instrument uses polarization separation of the two channels and is an upgraded and refined version of the LDA system used by Ballal et al. [5].

Principally, this instrument incorporates Bragg cell frequency shifting (5 MHz) for measurements in a recirculatory flow, a unique coincidence circuit for rapid acquisition of valid data, software to filter spurious signals, for example, due to seed agglomeration, and a correction subroutine to account for the LDA signal biasing effect in combusting flows. A fluidized bed seeder was used to inject submicron sized ZrO_2 seed particles into the flowing combustible mixture. Forward scattered signals were collected 9.5-degrees off axis, and detected by TSI Counter Processors (CP), and processed by our

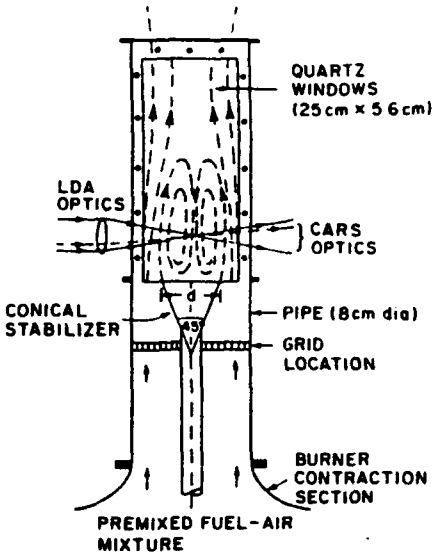

Fig. 1: Schematic diagram of the confined flame stabilizer test facility.

custom-designed software which calculates intensity, shear stresses, higher moments (skewness and kurtosis), and pdfs. The LDA ellipsoidal probe volume size was 175 μm × 1500 μm, fringe spacing was 5 μm, and typical sampling rates exceeded 1 kHz for both isothermal and combusting flows.

CARS System: The CARS optics layout is described in detail by Pan et al. [6]. Essentially, the laser source is provided by a Nd:YAG pulse laser with 10 ns time resolution. The frequency-doubled source green beam (532 nm) is equally divided into four parts. Two of these serve as the pump beams, while the other two pump a dye laser oscillator and amplifier. The dye laser is tuned to provide a red broad-band Stokes beam (110 FWHM) centered at 607 nm. The red Stokes beam and the two green pump beams are then focused together by a 25-cm focal length lens in a "BOXCARS" configuration. A 25-μm-x-250-μm measuring spot size is achieved. The CARS signal is collected by a Spex 1702 spectrometer, 1024 element DARSS camera, and Tracor-Northern multichannel analyzer. The raw data are processed by a MODCOMP minicomputer.

From the raw data, the temperatures are determined by comparing the actual nitrogen spectra to the calculated spectra, using the least square fit. The calculation of a nitrogen CARS spectrum requires knowledge of the instrument slit function. Heneghan et al. [7] have developed a simple method of determining the slit function from the collected data at the actual temperature and turbulence level by applying the principle of local thermodynamic equilibrium. This method improves the precision of the CARS measurement.

Error Analysis: Both the fuel flow and airflow were monitored by separate electronic flow control units to ± 0.5% and ± 1.5% respectively. The combined error produced an uncertainty of ± 1.5% in equivalence ratio or ± 30 K in

temperature. The primary source of error in LDA measurement is the statistical bias of the final measured velocity towards higher mass flux (velocity x density) when number-weighted averages are used to calculate stationary statistics. Chen and Lightman [8] and Glass and Bilger [9] have discussed bias correction schemes. After allowing for this bias, we estimated that the uncertainty in the measurement of mean velocity was 1% and for rms velocity 5%. Near the flame front, where intermittency would be much higher, the uncertainty in rms velocity could be greater than 7%. The long-term repeatability of measurements was found to be within 5% for turbulence quantities.

Usually, 500 samples were taken for each CARS measurement to ensure that the error in rms temperature was less than 10 K, while 1500 samples were taken in the flame region where the rms values were expected to be large. As shown by Heneghan and Vangsness [10], the CARS mean temperature measurement accuracy was within 50 K, while the precision is well within 20 K. Unlike the LDA, CARS temperature measurements are time-averaged, without the density biasing effects.

3. Results

Our turbulence measurements encompassed a large test matrix and are available in a separate report by Pan et al. [11]. Only selected data that illustrate the influence of parametric variation on chemistry and turbulence are presented and discussed below.

Chemistry Effects: Figures 2a and 2b demonstrate (moving from left to right) the effects of equivalence ratio of the incoming fresh mixture, ϕ, on mean velocity, Reynolds shear stresses, and turbulent kinetic energy respectively. In Fig. 2a, measurements of turbulence flowfield at $\phi = 0.56$ ($T_f = 1590$ K, $\tau = 4.5$) corresponding to lean extinction limit are shown, while Fig. 2b plots data for $\phi = 0.9$ ($T_f = 2130$ K, $\tau = 6.3$) close to stoichiometric combustion respectively. The mean recirculation zone structure shows width, length, and the reverse velocity flowfield; the contours of Reynolds shear stress ($\overline{uv}/U_a^2$) illustrate regions of maximum shear stress and locations where the shear stress changes sign, and the TKE contours provide information on turbulence production due to normal stresses.

We observe that an increase in ϕ from 0.56 to 0.90 decreases the recirculation zone length dramatically from x/d = 2.35 to 1.32, i. e., slightly shorter than that found in the cold flow (x/d = 1.52). It also accelerates axial mean velocities downstream of the rear stagnation point as clearly seen in Fig. 2b. Both these effects are a result of increasing heat release rates and fast chemistry brought about by increasing the equivalence ratio towards stoichiometry. This result indicates how compact the size of the primary zone of a gas turbine combustor can be, provided it operates at or near stoichiometric equivalence ratios. Detailed examination of our data indicate

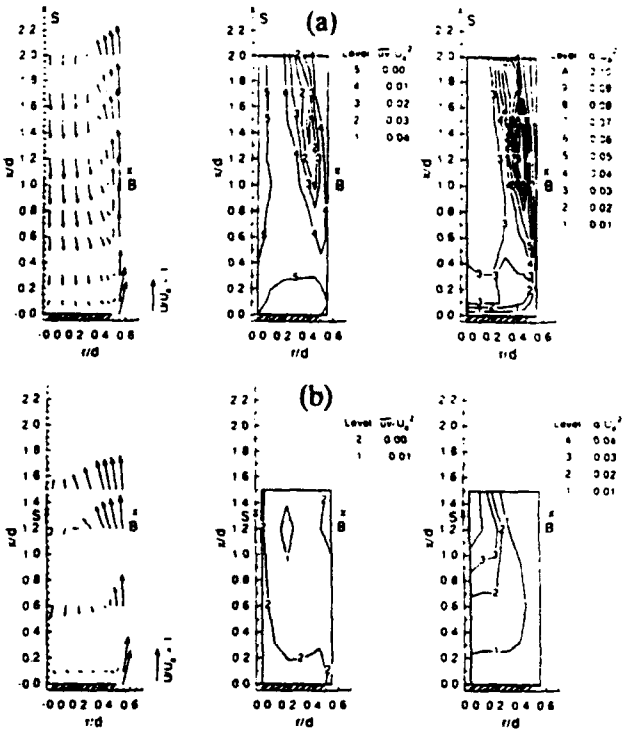

Fig. 2: Mean flow structure, Reynolds shear stresses, and turbulent kinetic energy plotted to illustrate the chemistry effects in a confined combusting flow (BR = 25%, θ = 45 degrees, U_a = 15 m/s): (a) lean extinction limit, ϕ = 0.56 (b) near-stoichiometric combustion, ϕ = 0.90.

that for $\phi \leq 0.75$, combustion is *kinetically controlled* and requires a recirculation zone of size larger than that for cold flow to stabilize a flame. Also, due to increased heat release rates and wall confinement of the flame, streamline curvature is smaller. Therefore, turbulent dilatation is the dominant process in these experiments. Consequently, as evident in Fig. 2b, both Reynolds shear stresses and TKE decrease at high equivalence ratios.

Another effect of increasing the equivalence ratio is that it decreases chemical reaction time (S_L / δ_L) or decreases the Damkohler number, $D_a = (\ell S_L / u' \delta_L)$. As Bray [12] has stated and McDannel et al. [13] have found, premixed flames of lower Damkohler number produce strong scalar (temperature or density) fluctuations. Therefore, Figs. 3a and 3b illustrate the effects of equivalence ratio on mean and rms temperatures. In Fig. 3a, the centerline temperatures are plotted. These data show that the rms temperature fluctuation is pretty near constant at 5%, but the mean temperature gradually increases with downstream distance. At least two factors contribute to this trend: (i) a constant heat loss to the metal base of the bluff body, and (ii) a relative increase in the thickness of the flame front which, as Bray [12] has pointed out, may decrease the level of scalar fluctuations within the flame and inhibit heat transport between hot products and cold reactants.

In Figs. 3b and 3c, radial temperature profiles are shown for various axial planes. Figure 3c illustrates a dramatic

growth in the temperature fluctuations (C_t rises from 5% to 30%) for r/d ≥ 0.3 and x/d = 2, i. e., upstream of the rear stagnation point. This occurs because the rapid necking-down of the outer flow streamlines in the vicinity of the rear stagnation point brings cold reactants rushing towards hot products flowing through the center portion of the combustor.

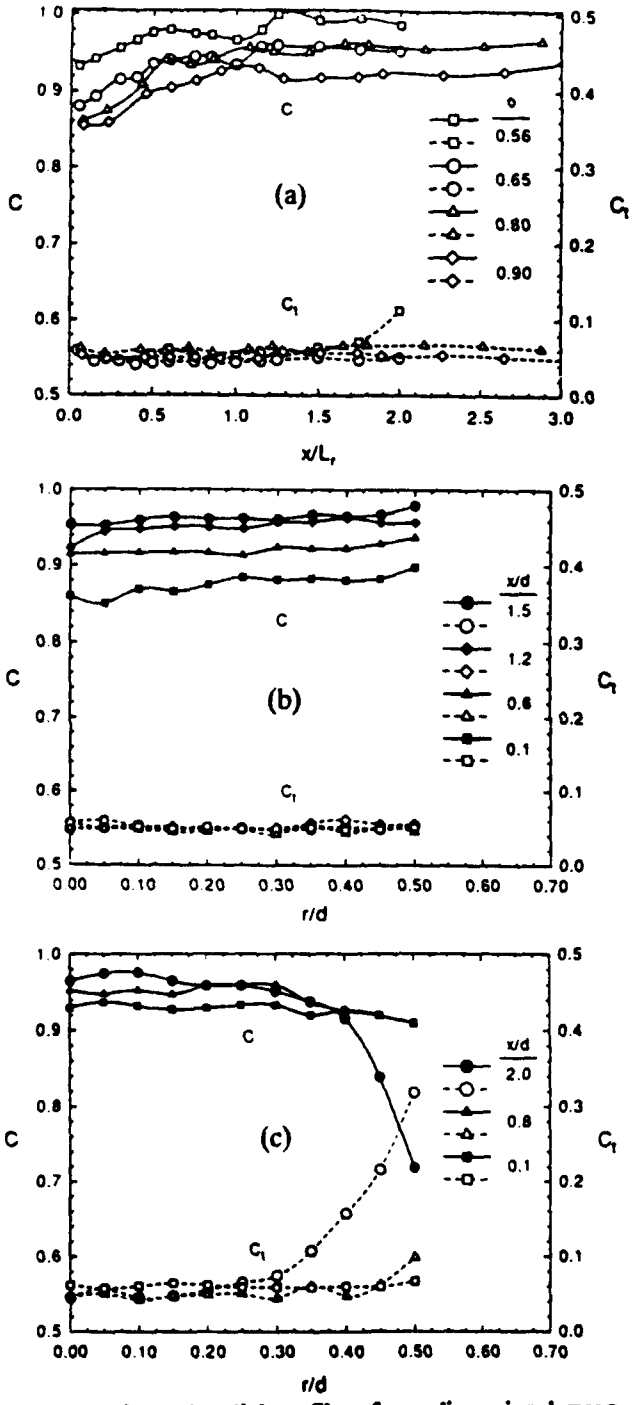

Fig. 3: Axial and radial profiles of non-dimensional mean temperature (reaction progress variable) and rms temperature plotted to illustrate the influence of chemistry on scalar fluctuations. (BR = 25%, θ = 45 degrees, U_a = 15 m/s): (a) centerline profiles, (b) radial profiles for ϕ = 0.8, (c) radial profiles for ϕ = 0.56.

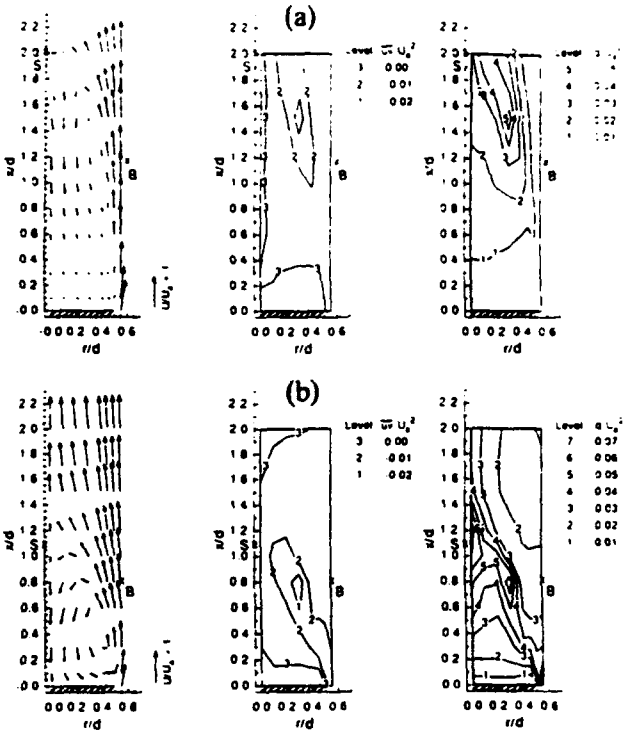

Fig.4: Mean flow structure, Reynolds shear stresses, and turbulent kinetic energy plotted to illustrate the effects of approach turbulence intensity in a confined combusting flow (BR = 25%, θ = 45 degrees, ϕ = 0.65, U_a = 15 m/s): (a) low turbulence, I = 2%, (b) high turbulence, I = 22%

Turbulence Effects: Figures 4a-4b demonstrate the influence of increasing the approach mixture turbulence intensity, u'/U_a from 2% (no grid) to 22% (grid 3). As the approach turbulence intensity increases from 2% (Fig. 4a) to 22% (Fig. 4b) the recirculation zone length decreases dramatically from x/d = 2 to x/d = 1.2. Also, the location of maximum recirculation width shifts upstream from x/d ~ 0.8 to 0.4. This dramatic change in the structure of the recirculation zone can be explained by recognizing that the turbulent burning velocity of the flame increases with an increase in the turbulence intensity; for example, Lefebvre [14] gives $S_T/S_L = [1+(u'/S_L)^2]^{0.5} \sim u'/S_L$ for large values of u'/S_L. Thus, a five-to six-fold increase in turbulent burning velocity dramatically reduces the size of the recirculation zone. Similarities between the effects of increasing equivalence ratio and increasing turbulence intensity are very evident in Figs. 2 and 4. Also, as evident in Fig. 4b, the dramatic shortening of the recirculation zone length shifts regions with strong concentration of both shear stress and TKE from the outer periphery of the recirculation zone to radially inward location around r/d = 0.2. The magnitude of shear stresses is about the same, but the TKE appears to be higher and concentrated in the region around the maximum width of the recirculation zone (Fig. 4b). This is because, in confined flames, the production of TKE is by the interaction of Reynolds stress and shear strain, i. e., via the term $\overline{uv}\,(\partial U/\partial r)$, and the flame is stretched around the maximum width of the recirculation zone.

Our detailed inspection of the data also showed that in these confined combusting flows, the locations of zero stress lines do not coincide with those of zero mean velocity gradient. This suggests that not only shear stresses (production term) but also normal stresses (dilatation term of the form $\overline{u'^2}$ $(\partial U/\partial r)$) play an important role in modifying the turbulence flowfield.

Figures 5a and 5b demonstrate the influence of increasing the approach turbulence intensity from 2% to 22% on mean and rms temperature fluctuations. In Fig. 5a, centerline axial distribution of temperature is shown. It is found that downstream of the rear-stagnation point ($x/L_r \geq 1$), increasing turbulence intensity decreases mean temperature somewhat and increases rms temperature fluctuations. Figures 5b shows radial profiles of mean and rms temperatures at high approach turbulence intensity. It should be noted that within the recirculation zone ($r/d \leq 0.3$) values of C and C_f remain fairly constant. However, outside the zone ($r/d > 0.3$), the mean value gradually falls and the rms value rapidly increases within the vicinity of the flame.

4. Discussion

Flame Model: From the temperature profiles of Figs. 3 and 5, we can calculate the mean temperature gradient $(\partial C/\partial r)$ and the flame thickness δ corresponding to the mean flame position, $C = 0.5$. Figure 6 shows plots of $(\partial C/\partial r)$ and δ for a bluff body with BR = 13%, over the axial distance covering the length of the recirculation zone. It is observed that the radial temperature gradient $(\partial C/\partial r)$, which is negative throughout, rises steeply within $x/L_r = 0$-0.16 (note: $\delta = 0.29$ mm at $x/d = 0.1$) and then maintains a fairly constant value. This result shows that the ignition of reactants and the establishment of the flame by the heat flux transported from the recirculation zone are achieved within 16% of the length of the recirculation zone. Downstream of this ignition-thin flame region, the mean temperature gradient remains fairly flat but the flame thickness continues to increase eventually to $\delta = 4.5$ mm as a result of fresh-mixture entrainment. This picture of, initially a thin and later a thick flame front, enveloping the recirculation zone was confirmed by CARS temperature pdf data of Pan et al. [11] and is sketched in Fig. 7.

In Fig. 7, we observe that the turbulent combustion in the reacting shear layer is a *three-stage* preheat-ignition-propagation process. Near the base of the bluff body and along its edge, the flowing reactants are preheated and ignited by the heat flux transported radially outward from the recirculation zone. A thin flame that conforms to the "fast-chemistry" assumptions sits slightly oblique to the oncoming reactants. Downstream, the temperature remains either fairly constant or decreases slightly, i. e., $\partial C/\partial r \leq 0$. In this region, large-scale coherent structures begin to grow within the reacting shear layer. These coherent bodies of gas are squeezed and stretched during their travel through the flame and the entrainment process causes their growth downstream thereby

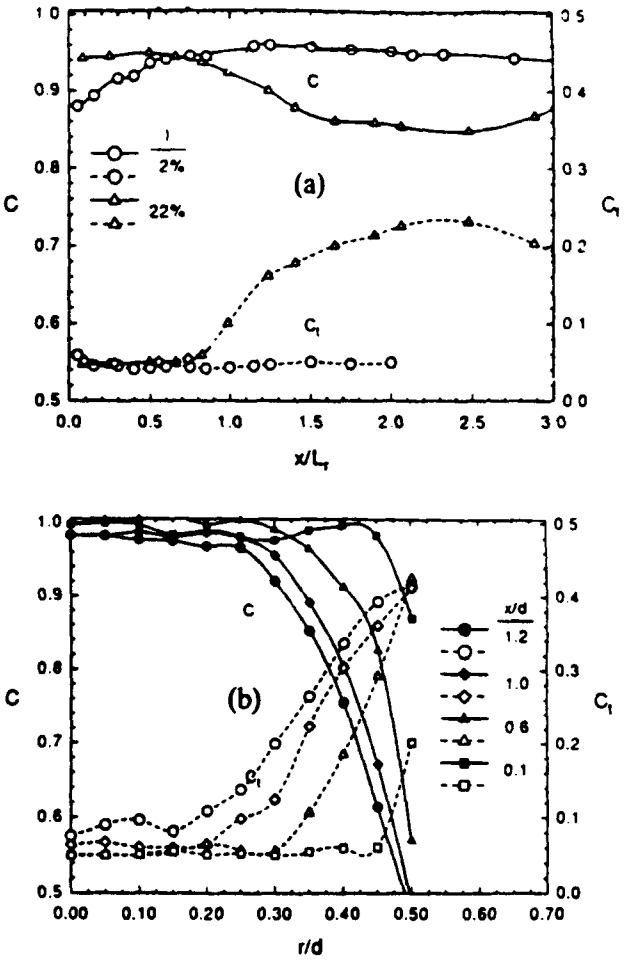

Fig. 5: Axial and radial profiles of non-dimensional mean temperature (reaction progress variable) and rms temperature plotted to illustrate the influence of approach turbulence intensity on scalar fluctuations. (BR = 25%, θ = 45 degrees, ϕ = 0.65, and U_a = 15 m/s): (a) centerline profiles, (b) radial profiles for I = 22%.

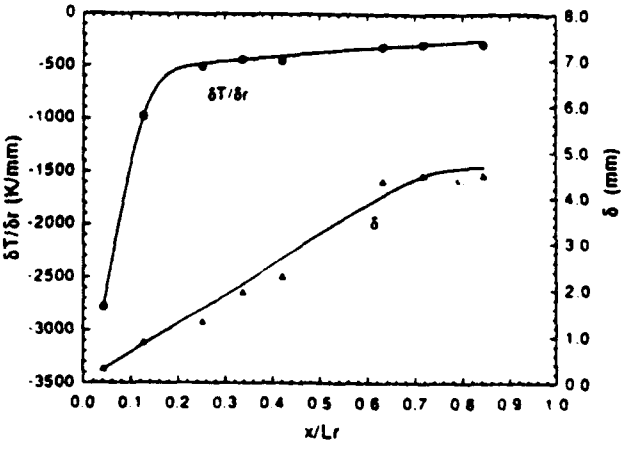

Fig. 6: Temperature gradient and turbulent flame thickness.

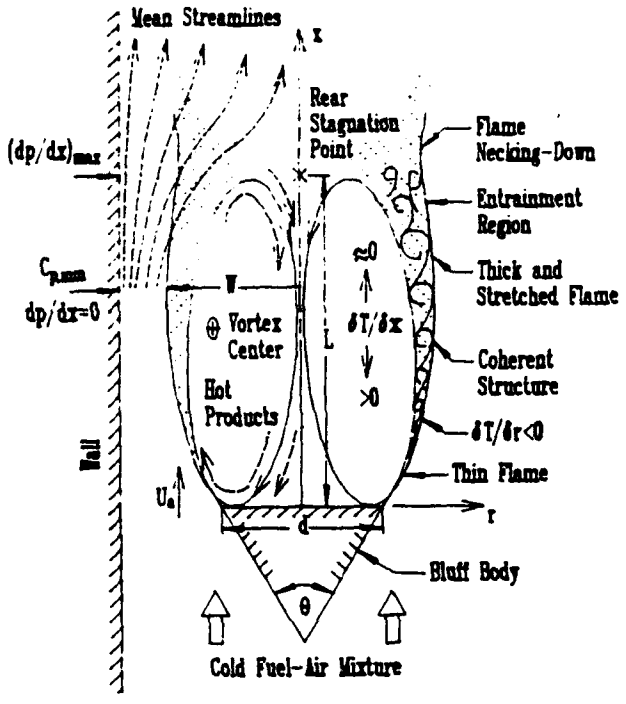

Fig. 7: Schematic diagram illustrating the turbulent flame structure enveloping the recirculation zone.

thickening the flame. Finally, in the vicinity of the rear stagnation point, the flame front is thick (δ = 4.5 mm) and mass entrainment of fresh reactants is the dominant mechanism at work. In this region, large temperature fluctuations (C_t = 25%-35%) are measured as observed in Figs. 3c and 5b.

Lean Blowout: Table 1 shows the effects of equivalence ratio on the calculated reverse mass flow within the recirculation zone and the pressure gradient $(dP/dx)_{max}$. Notice that as the equivalence ratio decreases, the magnitude of the adverse pressure gradient increases. This change in pressure gradient augments entrainment and increases reverse mass flow in a linear fashion as shown in Figure 8.

Table 1: Effects of equivalence ratio on reverse mass flow and mean pressure gradient: (45° cone, d = 4.44 cm, BR = 25%, and U_a = 15 m/s).

ϕ	T_{ad} (K)	L_r/d	W/d	m_r/m_t (%)	$(dP/dx)_{max}$ (psi/in)
Cold	298	1.52	0.61	7.13	0.49
0.56	1590	2.36	0.64	1.86	0.14
0.65	1755	2.00	0.63	1.20	0.07
0.80	2000	1.40	0.63	0.60	0.00
0.90	2130	1.32	0.63	0.55	-0.04

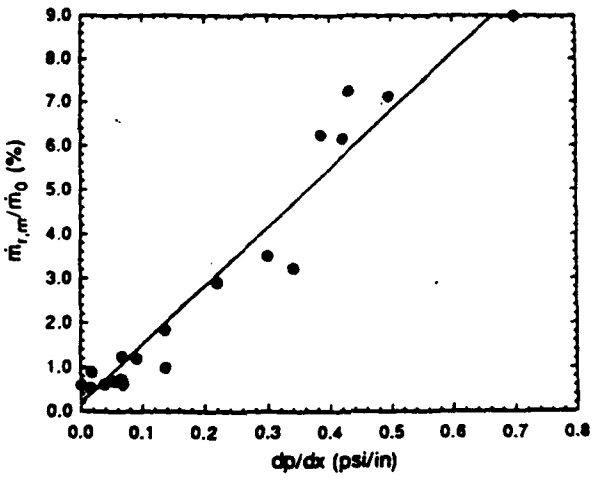

Fig. 8: Relationship between reverse mass flow and mean axial pressure gradient.

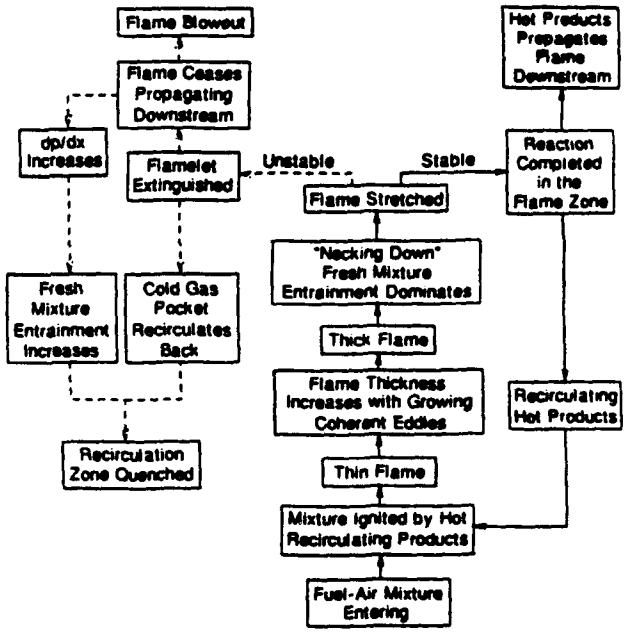

Fig. 9: Flow chart illustrating the mechanism of flame stabilization and lean blowout.

Figure 9 illustrates the sequence of events leading to lean blowout. Excess entrainment of cold reactants in the thick flame region causes flamelet extinction which increases the magnitude of the adverse pressure gradient downstream of the rear stagnation point. This, in turn, increases the entrainment of the cold reactant mixture, reduces the recirculation zone size towards the cold-flow value and quenches the flame in the preheat-ignition region.

Turbulent Flame Propagation: It is interesting to examine the propagation of the outer turbulent flame on the basis of the three-region model of premixed flame developed by Ballal and Lafebvre [15] and the criteria developed by Williams[16], Fig. 10.5). To do this, we computed values of (u'/S_L) and (η/δ) at $(x/L_r) = 0.08$, 0.40, and 1.00 corresponding to the approximate mid-point location of ignition, (recirculation zone) maximum width, and rear stagnation point regions respectively. Table 2 shows the computed results obtained by assuming that $\lambda = (10\ \nu t)^{0.5}$ and $\eta = 0.5\,\lambda/(Re_\lambda)^{0.5}$ from Hinze [17].

Results presented in Table 2 confirm the present experimental observations that for the low (2%) approach turbulence intensity; (i) the ignition region I corresponds to the thin-flame region, and (ii) downstream of this region corresponds to the thick flame region. For high (22%) turbulence case, the computations suggest the presence of a thick flame front throughout, whereas experiments show the development of a thin flame in the ignition region followed by a thick flame downstream. Thus, computations only partially confirm the experimental observations. The reason for this is that the thin-flame and the coherent-eddy development regions do not entrain reactant or product mass very efficiently. The thin-flame transport is dominated by molecular diffusion and Dimotakis and Brown [18] have shown that coherent eddies hold freshly entrained fluid intact for a long time until small-scale turbulence develops. Thus, only in the vicinity of the rear stagnation point do the processes of entrainment and thick-flame development become feasible.

5. Conclusions

The effects of (finite-rate) chemistry and approach turbulence intensity have been investigated for a bluff-body stabilized turbulent flame. The following conclusions emerged.

(1) Faster chemistry (i.e., increasing equivalence ratio from its lean extinction limit to near-stoichiometry) decreases the recirculation zone length to one-half its original value. Also, TKE is drastically decreased due to suppression of turbulence by dilatation. Slower chemistry (near lean extinction limit) produces a rapid growth in temperature fluctuations just upstream of the rear stagnation point.

(2) Increasing the approach turbulence intensity drastically shortens the recirculation zone length close to its value in the cold flow. The distribution of both shear stresses and TKE shifts from the outer periphery of the recirculation zone to radially inward locations. Finally, higher turbulence increases rms temperature fluctuations.

(3) The flame model comprises an ignition-thin flame region, a reacting shear layer which has large-scale coherent structure, and finally, a thick flame region where entrainment is the dominant mechanism.

Table 2: Turbulence parameters characterizing flame propagation [15, 16]: (45° cone, d = 4.44 cm, BR = 25%, $\phi = 0.56$, and $U_a = 15$ m/s).

x/L_r	u'/S_L	Re_λ	η(mm)	δ/η	Remarks
Approach turbulence = 2%					
0.08	3.0	15	0.10	3	Thin-Flame
0.40	2.0	13	0.14	17	Thick-Flame
1.00	1.2	10	0.20	23	Thick-Flame
Approach turbulence = 22%					
0.08	33	160	0.03	10	Thick-Flame
0.40	22	143	0.04	55	
1.00	13	110	0.06	75	

(4) Lean blowout (finite chemistry effect) occurs because excess entrainment of cold reactants in the thick flame region causes flamelet extinction and increases the adverse pressure gradient. This, in turn, increases the entrainment of the cold reactant mixture and quenches the flame in the preheat-ignition region.

(5) Examination of turbulent flame propagation on the basis of previously established criteria reveal many similarities between experimental observations and predictions with respect to the existence of thin and thick flame regions.

6. Acknowledgment

This work was supported by the U. S. Air Force, Wright Laboratory, Aero Propulsion and Power Directorate, Wright-Patterson Air Force Base, Ohio, under Contract No. F33615-87-C-2767 with Dr. W. M. Roquemore serving as the Air Force Technical Monitor.

7. References

1. Sturgess, G. J., Heneghan, S. P., Vangsness, M. D., Ballal, D. R., and Lesmerises, A. L., " Lean Blowout in a Research Combustor at Simulated Low Pressures," ASME Paper No. 91-GT-359, To appear in *Transactions of ASME, Journal of Engineering for Gas Turbines and Power*, 1992.

2. Sturgess, G. J., Heneghan, S. P., Vangsness, M. D., Ballal, D. R., and Lesmerises, A. L., "Isothermal Flowfields in a Research Combustor for Lean Blowout Studies," ASME Paper No. 91-GT-37, To appear in *Transactions of ASME, Journal of Engineering for Gas Turbines and Power*, 1992.

3. Ballal, D. R., Lightman, A. J., and Yaney, P. P., "Development of Test Facility and Optical Instrumentation for Turbulent Combustion Research," AIAA *Journal of Propulsion and Power*, Vol. 3, pp. 97-104, 1987.

4. Zukoski, E. E. and Marble, F. E., "The Role of Wake Transition in the Process of Flame Stabilization on Bluff Bodies," AGARD *Combustion Researches and Reviews*, A. H. Lefebvre et al., ed., Butterworths Publishing Co., London, pp 167-180, 1955.

5. Ballal, D. R., Chen, T. H., and Schmoll, W. J., "Fluid Dynamics of a Conical Flame Stabilizer," ASME *Journal of Engineering for Gas Turbines and Power*, Vol. 111, pp. 97-102, 1989.

6. Pan, J. C., Vangsness, M. D., Heneghan, S. P., and Ballal, D. R., "Scalar Measurements in Bluff Body Stabilized Flames Using CARS Diagnostics," ASME Paper No. 91-GT-302, 1991.

7. Heneghan, S. P., Vangsness, M. D., and Pan, J. C., "Simple Determination of the Slit Function in Single Shot CARS Thermometry," *Journal of Applied Physics*, Vol. 69, pp. 2692-2693, 1991.

8. Chen, T. H. and Lightman, A. J., "Effects of Particle Arrival Statistics on Laser Anemometer Measurements," ASME-FED, Vol. 33, pp. 172-176, 1985.

9. Glass, M., and Bilger, R. W., "The Turbulent Jet Diffusion Flame in Coflowing Stream-Some Velocity Measurements," *Combustion Science and Technology*, Vol. 18, pp. 165-177, 1978.

10. Heneghan, S. P. and Vangsness, M. D., "Analysis of Slit Function Errors in Single-Shot CARS," *Reviews of Scientific Instruments*, Vol. 62, pp. 2093-2099, 1991.

11. J. C. Pan, "Laser Diagnostic Studies of Confined Turbulent Premixed Flames Stabilized by Conical Bluff Bodies," *Ph. D. Thesis*, University of Dayton, Dayton, OH, July 1991.

12. Bray, K. N. C., "Turbulent Flows With Premixed Reactants," In *Turbulent Reacting Flows*, Edts. P. A. Libby and F. A. Williams, pp. 115-183, Springer Verlag, New York, NY, 1980.

13. McDannel, M. D., Peterson, P. R., and Samuelsen, G. S., "Species Concentration and Temperature Measurements in a Lean Premixed Flow Stabilized by a Reverse Jet," *Combustion Science and Technology*, Vol. 28, pp.211-220, 1982.

14. Lefebvre, A. H., *Gas Turbine Combustion*, Hemisphere Publishing, New York, NY, pp. 179-220, 1983.

15. Ballal, D. R. and Lefebvre, A. H., "The Structure and Propagation of Turbulent Flames," *Proceedings of the Royal Society*, London, Vol. A344, pp. 217-234, 1975.

16. Williams, F. A., *Combustion Theory*, The Benjamin/Cummings Publishing Company, Menlo Park, CA, pp. 412, 1985.

17. Hinze, J. O., *Turbulence*, McGraw Hill Inc., New York, NY, 1975.

18. Dimotakis, P. E., and Brown, G. L., "The Mixing Layer at High Reynolds Number: Large-Structure Dynamics and Entrainment," *Journal of Fluid Mechanics*, Vol. 78, pp. 535-560, 1976.

APPENDIX K

LIFTING CRITERIA OF JET DIFFUSION FLAMES

by

Fumiaki Takahashi and W. John Schmoll
University of Dayton, Ohio

Published in Twenty-Third Symposium (International) on Combustion, The Combustion Institute, pp. 677-683, 1990.

Twenty-Third Symposium (International) on Combustion/The Combustion Institute, 1990/pp. 677–683

LIFTING CRITERIA OF JET DIFFUSION FLAMES

FUMIAKI TAKAHASHI AND W. JOHN SCHMOLL
University of Dayton
Research Institute
300 College Park
Dayton, Ohio 45469-0001

The lifting mechanisms of methane/air coflow jet diffusion flames have been studied based on the three-component laser-Doppler velocimetry measurement with conditional seeding under near-limit conditions. Three distinct types of flame lifting behaviors were observed, i.e., (1) the lifting according to the flame-base stability mechanism previously proposed, (2) the lifting following the local extinction of the flame zone near the break-point, occasionally associated with metastable split flames, and (3) the lifting following the longitudinal oscillatory movement of the flame base. The first type was observed for a fuel tube lip thickness less than the minimum quenching distance of the methane/air mixture; the latter two types for a greater lip thickness. The conditional LDV measurement has revealed that the local extinction occurs as a result of the interaction between shear-generated large-scale vortices and the flame zone, which is formed in the intermittent boundary region of the turbulent jet fluid and the engulfed external fluid. The abrupt changes in the flow pattern in the recirculation zone in the fuel-tube wake, when approaching to the lifting limit, suggest that the unstable flame-base movement is presumably due to the lean-limit extinction of the reactions in the flame-holding zone. Four major lifting criteria are proposed based on the present observations and a literature survey, and a critical assessment is made to clarify the effects of burner configurations and fuel types.

Introduction

The flame stability limits essentially define operational boundaries of a combustion system. The critical conditions at the stability limits are highly dependent on geometric and flow configurations and to some extent types of fuels as well. Although various stability phenomena of jet diffusion flames have been studied in a variety of burner systems for over four decades since early investigators,[1-3] the lifting mechanisms of burner-rim-*attached* flames have received less attention as compared to recently-renewed attention to the blowout criteria of *lifted* flames.[4-7] Thus, there still exists some confusion as to the causes of lifting phenomena.

It has long been speculated[8] that there must be a flame velocity in the premixed zone near the flame base, which causes the combustion process to propagate downwards against the gas stream, thus preventing lifting. By using extensive experimental results[9-13] on the flame stability and structure, including the laser-Doppler measurement,[12] for various types of fuels, this hypothesis has been extended to a more concrete lifting mechanism[12,13] based on a balance between the entrained-stream velocity and the local maximum burning velocity at the flame base. Although there is a different view[14] of the limit, however, that lifting is resulted from flame extinction due to high strain on the flame, it is questionable whether this concept is applicable to the very end of the diffusion flame, i.e., the flame base.

By using methane flames, Eickoff et al.[4] concluded that lifting is caused by the flame extinction due to the interference of a vortical motion with the flame front at several jet diameters downstream. Coats and Zhao[15] followed this conclusion and reported distinct lifting behaviors between tube and nozzle burners. On the other hand, Gollahalli et al.[16] and Shekarchi et al.[17] used propane and reported that lifting is a laminar flame process at the flame base, supporting the previous observations by Takahashi et al.[12] Recent results by Chen and Goss[14] revealed different lifting behaviors between methane and propane flames. The local flame extinction has been known[4,14,17-22] to occur, primarily for hydrogen flames, due to the excess transport rate compared to the reaction rate at the transition point to turbulent flame.[20] The local extinction occasionally leads to split flames, i.e., a small near-burner-rim flame and a lifted-like flame downstream.[17-22] The occurrence of the local extinction and split

flames is dependent on the burner port lip thickness,[19] diameter,[18,22] shape[15,17] whether a contour nozzle or straight tube, and the fuel type.[14]

The principal purpose of this study is to gain better understanding on the critical conditions for lifting, to classify various lifting behaviors into several criteria based on the present and previous results by the authors and the literature survey, and to make a critical assessment on the effect of each experimental parameter on the physical mechanisms responsible for lifting.

Experimental Techniques

Methane (>98%) was injected vertically upward from a straight fuel tube (9.45 mm i.d. × 806 mm length) with different lip thickness (δ = 0.2, 1.2, and 2.4 mm) together with coflowing air issuing from a concentric annulus channel constituted of the fuel tube and an outer air tube (26.92 mm i.d.) into a low-speed (fixed at 0.5 m/s) general air stream in a combustion chimney (150 × 150 mm square cross-section with rounded corners, 483 mm length). The outer wall of the fuel tubes with lip thicknesses of 0.2 and 1.2 mm are tapered at a half cone angle of 2 degrees with respect to the burner axis.

The flame stability limits were measured by increasing the fuel flow rate gradually under a fixed annular air flow rate until the burner-rim-attached flame lifted typically several tube diameters above the burner tube (lift) or the *attached* flame extinguished (blowoff). A tailor-made three-component laser-Doppler velocimeter used is described in detail elsewhere.[23]

Results and Discussion

Stability Limits:

Figure 1 shows the stability limits of jet diffusion flames formed on the fuel tubes with various lip thicknesses. For both the sharp-edged (δ = 0.2 mm) and moderate (1.2 mm) lip thicknesses, the critical mean jet velocity at lifting (U_{jc}) with no coflowing annular air was approximately 22 m/s (Reynolds number, Re_j = 12500) and maintained constant over a very low mean annular air velocity range (U_a < 0.12 m/s). In this range, the intensity of the blue flame emission vanished locally near a breakpoint (z = 10–20 mm) where the laminar flame turned to "turbulent" (wrinkled laminar) flame. This region eventually became a hole in the flame zone (the local extinction). As the quenched area expanded all around the flame cross-section, the whole flame lifted. The metastable split flame was observed just prior to lifting. By contrast, at higher annular air velocities beyond this range, the flame base lifted

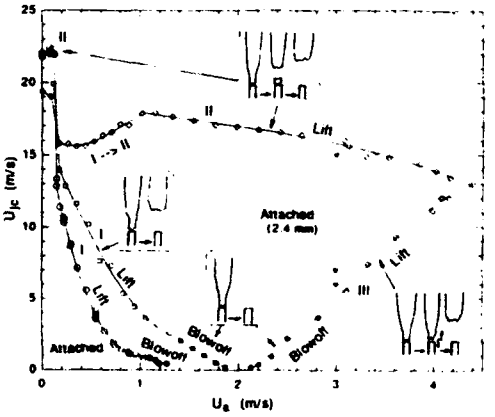

FIG. 1. Effect of lip thickness on the stability limits of methane/air coflow jet diffusion flames. Lip thickness: O●, 0.2 mm; □■, 1.2 mm; ◇◆, 2.4 mm. Open: lift, filled: blowoff. ▼, Experimental conditions for the LDV measurement.

abruptly without the local extinction, similar to the results reported previously.[9,12,13] These distinct flame stability behaviors observed can be categorized into two types, i.e., the lifting controlled by the flame base (Type I) and the lifting controlled by the local extinction at the breakpoint (Type II). The critical mean jet velocity decreased markedly as the annular air velocity was increased, similar to coflow hydrogen flames studied previously.[22] The flame stability behavior for δ = 1.2 mm was similar to that for 0.2 mm except for the expanded burner-rim-attached region. For higher annular air and lower critical mean jet velocities, the flame blew off abruptly instead of lifting, because no stable lifted-flame conditon was realized downstream due to excess dilution of the fuel by air.

In contrast to these thin lip thicknesses, dramatic changes in the stability behavior were observed for δ = 2.4 mm. At zero annular air velocity, the critical mean jet velocity was approximately 19 m/s. The local extinction was observed as well just prior to lifting (Type II) for U_a < 0.12 m/s, although the split flame was not recognized. The attached-flame region expanded markedly. In the range of 0.12 < U_a < 1.9 m/s, the flame base lifted abruptly (Type I), but the local extinction lifting (Type II) reappeared at higher annular air velocities (U_a > 1.9 m/s). It is notable that at U_a > 2.1 m/s, there appeared a lower branch of the stability limit curve. Apparently, this flame stability behavior is controlled by the flame-base holding in the thick-walled fuel-tube wake, different from the two types described, and is categorized as Type III. The lower branch was obtained by increasing the annular air velocity instead of the jet velocity.

Type I: Flame Base Stability Lifting:

Type I is the lifting behavior most commonly observed for thin-walled fuel tubes and controlled by the flame base. Since the physical mechanism for Type I has extensively been studied previously,[9,12,13] we will not pursue it further in this paper. The lifting mechanism proposed[12,13] is based on a balance between the entrained-stream velocity at the flame base and the local maximum (laminar) burning velocity obtainable when mixing the jet and oxidizing fluids. Here, the effects on the local burning velocity of both the lowered temperature at the flame base and the density ratio of unburned to burned gases should be considered. The basis of the stability model is the finding[10] that there exists a small laminar flame in the vicinity of the flame base even at the lifting limit and the main body of the flame is fully turbulent.

Type II: Local Flame Extinction Lifting:

To understand in more detail the critical condition for Type II lifting caused by the breakpoint flame extinction, the laser-Doppler velocimetry measurement was made in the near-exit region of the flame for $\delta = 2.4$ mm under near-lifting conditions ($U_j = 15$ m/s, $Re_j = 8440$; $U_a = 3$ m/s; see Fig. 1). The fully-developed turbulent pipe-flow was ejected from the fuel tube. Figures 2–5 show the radial profiles of the axial (U) and radial (V) mean (time-averaged) velocity components, the kinetic energy of turbulence ($q = (\overline{u'^2} + \overline{v'^2} + \overline{w'^2})/2$), and the Reynolds shear stress at three different heights from the jet exit. The locations of the (average) visible flame zone, measured visually by using a cathetometer, are included in the figures as well. The conditional data sampling[24] was made by seeding particles into only the fuel jet or only the coflow air. The axial mean velocity profiles (Fig. 2) show the spreading of both the jet and turbulent mixing layer where the particles from the jet or coflow exist intermittently. The laminar flame base was anchored in the immediate wake of the fuel tube at $z = 0.9$ mm. At $z = 5$ mm, the flame base was still laminar, residing in the outside of the turbulent shear layer of the jet. As the jet spread downstream ($z = 15$, 25 mm), the (average) visible flame zone entered into the boundary region of the intermittent layer and became thicker, indicating the transition to turbulent flame. The conditioned data show that the fluid elements from the jet are faster than those from the coflow on the average. The radial mean velocity component profiles (Fig. 3) show more striking features, revealing that the fluid elements from the jet are flowing outward on the average and for those from the coflow they are vice versa, even near the flame zone, suggesting the existence of large-scale vortical motion. This result

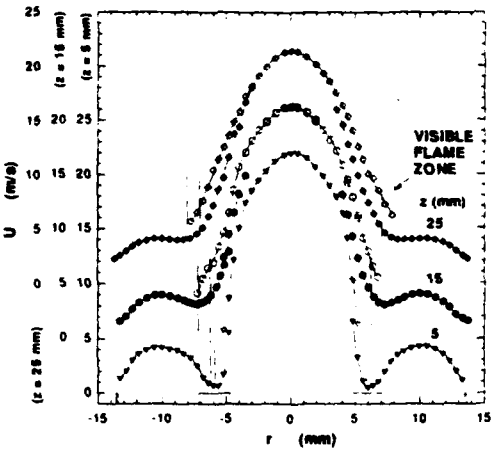

FIG. 2. Radial profile of the axial mean velocity component in a near-lifting (Type II) flame. $U_j = 15$ m/s, $U_a = 3$ m/s. ▽▼, $z = 5$ mm; ○●, $z = 15$ mm; ◇◆, $z = 25$ mm. Open: conditioned on jet seed; filled: annulus air seed.

appears to be consistent with the physical picture of large-scale turbulent structure in the shear layer.[6,7] The profiles of the turbulent kinetic energy (Fig. 4) and the Reynolds shear stress (Fig. 5) show sharp peaks which are coincident with locations of the high-shear (high U-gradient) region (see Fig. 2). Therefore, the production of the turbulent kinetic energy is through the term of a product of the Reynolds stress and the shear strain. At the

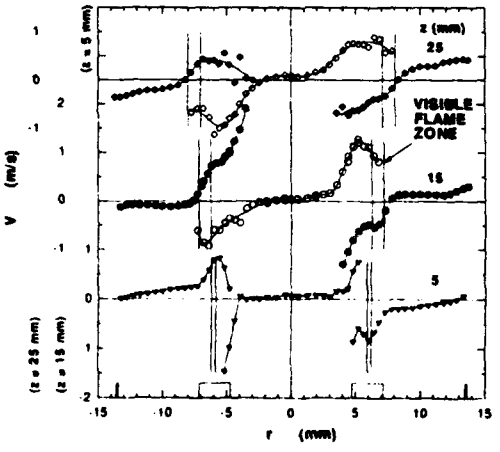

FIG. 3. Radial profile of the radial mean velocity component in a near-lifting (Type II) flame. $U_j = 15$ m/s, $U_a = 3$ m/s. ▽▼, $z = 5$ mm; ○●, $z = 15$ mm; ◇◆, $z = 25$ mm. Open: conditioned on jet seed; filled: annulus air seed.

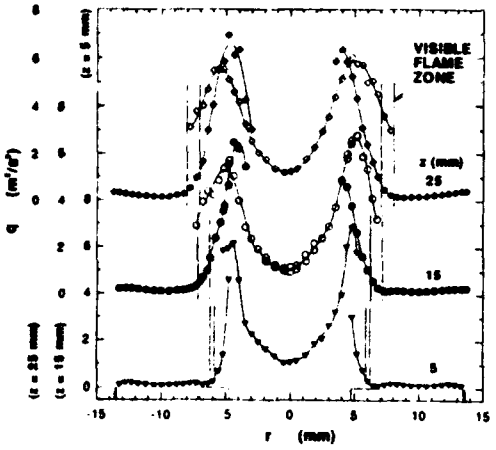

FIG. 4. Radial profile of the turbulent kinetic energy in a near-lifting (Type II) flame. U_j = 15 m/s, U_a = 3 m/s. ▽▼, z = 5 mm; ○●, z = 15 mm; ◇◆, z = 25 mm. Open: conditioned on jet seed; filled: annulus air seed.

edges of the intermittent boundary region where the visible flame zone resides, the intermittency of the turbulent jet fluid vanishes, and thus it is a relatively rare event that the jet fluid element reaches to the flame-zone location. The jet fluid elements have several times higher turbulent kinetic energy than those of co-flow near the visible flame zone (Fig. 4) and must consist of nearly pure fuel at these

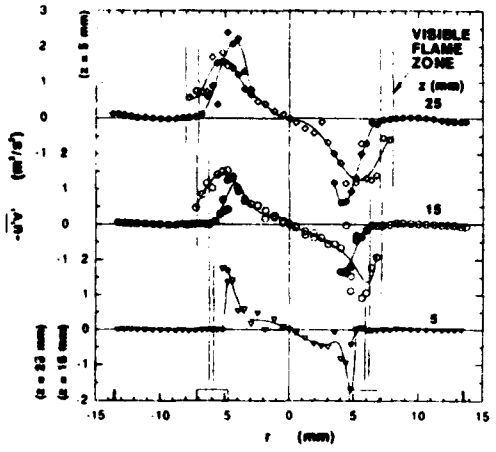

FIG. 5. Radial profile of the Reynolds sear stress in a near-lifting (Type II) flame. U_j = 15 m/s, U_a = 3 m/s. ▽▼, z = 5 mm, ○●, z = 15 mm, ◇◆, z = 25 mm. Open: conditioned on jet seed, filled: annulus air seed.

heights (z/d < 3). Therefore, when the large-scale vortex of the jet fluid is ejected radially, the flame zone must be quenched locally as the instantaneous flame surface is forced to shift outward due to the high fuel concentration and stretched out due to the engulfment motion of the large-scale vortices and perhaps the small-scale (pipe-flow) turbulence of the jet fluid itself.

Type III: Lean-Limit Extinction Lifting:

To investigate Type III lifting, the LDV measurement was made in the immediate wake of the thick-walled fuel tube at two different mean jet velocities (see Fig. 1) just before (U_j = 7 m/s) and after (U_j = 6 m/s) the unstable flame-base movement started, as approaching to the stability limit by decreasing U_j. Figure 6 shows the velocity vector fields in the flame stabilizing region. At U_j = 7 m/s (Fig. 6a), the laminar flame base was anchored at the rear end of the recirculation zone in the wake at z = 1.1 mm, where the axial mean velocity vanished. The fuel molecules must diffuse radially towards the flame zone and into the recirculation zone where premixed-type combustion reactions must be taking place. The diffusion flame base must be connected to the hot recirculation zone. Thus, the flame formed on the thick-walled fuel tube is much more stable as compared to the thinner tubes. The mechanism of Type III lifting can be speculated as follows. As the annular air velocity is increased at a fixed fuel jet velocity, the flux of air coming into the recirculation zone must increase due to the increased convective velocity, while the fuel flux remains unchanged. Thus the local equivalence ratio in the zone must decrease. Consequently, the picture of flame holding described above must be broken as the reactions in the recirculation zone cease by approaching the lean flammability limit. As a result, the flame base becomes unstable locally along the fuel tube exit circle, thereby locally oscillating up and down (in the range of 1 < z < 3.7 mm; see Fig. 6b), eventually leading to lifting. The flow pattern in the wake changed significantly (see Fig. 6b); the recirculation zone was elongated lengthwise (z: from 1.2 to 1.8 mm) and the highest point where reverse flow occurred increased as well. In the case where the flame base moved to the upper position (see Fig. 6b), the flow pattern around the flame base is similar to that in the near-limit flame formed on the sharp-edged fuel tube,[12,25] but the axial mean velocity component entrained into the flame base at this height (~0.5 m/s) is much larger than the critical value for methane flames formed on a sharp-edged tube (~ 0.23 m/s).[11,25] Therefore, if the flame base moves up to this height (~ 4 mm) all along the tube lip circle, the whole flame must lift typically several jet

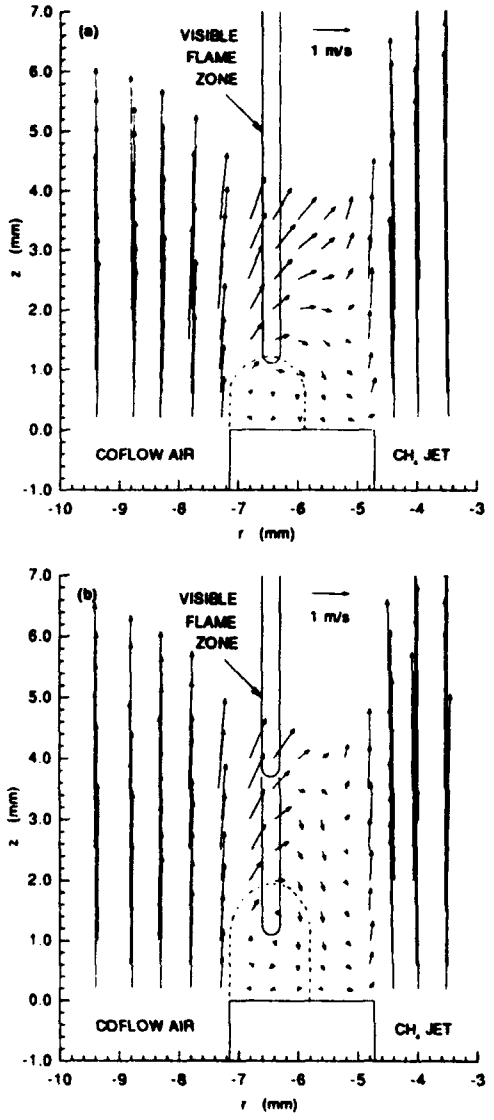

FIG. 6. Velocity vector fields in the stabilizing region of near-lifting (Type III) flames. U_o = 3 m/s. (a) U_f = 7 m/s. (b) U_f = 6 m/s.

diameters downstream to form a turbulent flame base.

Lifting Criteria:

The various flame stability behaviors observed in this study may be used as a frame work to classify various observations fragmentarily reported in the literature into several lifting criteria and to examine the experimental conditions for each criterion. Table I shows a summary of the lifting criteria and experimental configurations including present observations and the results found in previous reports. The flame-base stability lifting (Type I(a)) has been studied most extensively, and the lifting mechanism has been proposed.[12,13]

Type I(a) has been observed in both tube and nozzle burners for a wide range of burner diameters, a variety of fuels, but mostly for thin lip thicknesses. The recent observations on the lifting of methane flame due to "invasion"[15] of the laminar flame base by pipe-flow turbulence in the central gas jet may be categorized as a variation of the flame-base stability lifting (Type I(b)), since the disturbances caused by the pipe flow turbulence must break the stabilization balance at the flame base. This anomalous lifting appears to be due to properties of methane, which leads to higher tendency to lift, i.e., low reaction rate and high stoichiometric concentration (9.5 vol.%), which shifts the flame zone in closer proximity to the shear layer, thereby making it more susceptible to the pipe-flow disturbances.

The breakpoint extinction lifting behaviors (Type II) can be further classified into three subcategories depending on the fate of the split flame resulted from the local extinction: a) the local extinction causes flame lifting immediately, b) the local extinction leads to a stable split flame, and then the blowoff of the rim flame results in the lifting, and c) the lifted part of the stable split flame blows out first, thus leaving a residual rim flame, which then blows off. Type II(a) has been observed only for methane flames, probably because of the same reasons described for Type I(b). Type II(a) has been seen if the flame-base stability is secured at either very low coflow air velocities (<0.17 m/s) for the chamfered nozzles and thin-lip tubes or high coflow velocities (<1.9 m/s) for a thick-lip (2.4 mm) tube. Type II(b) has been reported for various fules; Type II(c) for hydrogen only except for city gas in a high temperature air flow. High reaction rate of hydrogen enabled to sustain the rim flame. The lean-limit extinction lifting (Type III) occurs for thick-walled tubes for both methane and hydrogen.

The lip thickness of the fuel tube is a critical factor in terms of whether Type I or Types II and III occurs. The critical lip thickness for these behaviors appears to be comparable to the minimum quenching distance of each fuel/air mixture (hydrogen, 0.6 mm;[30] methane, 2 mm;[31] propane, 1.7 mm)[31] as it relates to the minimum mixture volume required for sustaining premixed combustion in the recirculation zone.

An additional lifting phenomenon (Type IV) is the one for the aerated flames observed by Vranos et al.[19] This type of flames is non-luminous small flame formed in the immediate downstream of the fuel tube exit under the conditions of very high coflow

TABLE 1
Lifting criteria and experimental configurations

Lifting Criterion	Shape[a]	d (mm)	δ (mm)	U_e (m/s)[b]	Fuel Type	References
I. Flame-Base Stability	T	4.57	?	0?	C_4H_{10}	1
a) Imbalance between entrainment velocity and burning velocity	T	8.5	0.5	V	C_4H_{10}	3
	T	0.2–19.7	Sharp-edge	V	H_2, CH_4, C_2H_2, C_2H_4 C_3H_8, C_4H_{10}, City gas	18, 26, 27
	T	4.19–4.27	0.07–0.39	V	H_2	19
	T	0.43–5.98	0.03–0.12	V: 0–37	H_2, H_2/N_2, H_2/Ar, H_2/He C_2H_2, C_2H_2/N_2, CH_4	9, 12, 13, 26, 29
	T	9.45	0.2, 1.2	V: 0–2	CH_4	This study
	T + N	4.67	0.8	0	C_3H_8	17
	O	0.33–1.32	?	0?	C_2H_4	2
	N	8.74	?	0	C_3H_8	16
	N	5	Chamfered	0.15	C_3H_8	14
b) Pipe-flow turbulence disturbances	T	6	Chamfered	0.17	CH_4	15
II. Local Flame Extinction at Breakpoint	T	9.45	0.2, 1.2, 2.4	V: 0–4.5	CH_4	This study
a) Local extinction immediately followed by lifting	N	5	Chamfered	0.15	CH_4	14
	N	5	?	0?	CH_4	4
	N	6	Chamfered	0.17	CH_4	15
b) Local extinction to stable split flame then rim flame blowoff (lifting)	T	1.70–8.17	0.68–1.06	$U_j < U_e < 4U_j$	H_2	19
	T	4.67	0.8	0	C_3H_8	17
	T	0.60	0.03	0	H_2	22
	N	6	?	0?	H_2/Natural gas	21
c) Local extinction to stable split flame, lifted-part blowout, then residual flame blowoff	T	1.7–8.17	0.71–1.06	$U_e < U_j$	H_2	19
	T	1	0.5	V: 5–40	H_2, City gas ($T_e > 620$ K)	20
	T	0.21	Sharp-edge	0	H_2	18
III. Lean-Limit Extinction in Tube Wake	T	1.7–8.17	0.71–1.06	$U_e > 5U_j$	H_2	19
	T	9.45	2.4	V: 2–4.5	CH_4	This Study
IV. Aerated Flame Extinction	T	1.70–8.17	0.07–1.06	$U_e > 50\ U_j$	H_2	19

[a]T: tube, N: nozzle, O: orifice.
[b]V: varied

air velocity and very low fuel jet velocity. It can be speculated that a recirculation zone is formed in the immediate wake of the fuel tube exit including the near-axis region where combustion reactions occur in a well-mixed manner. Therefore, the flame lifting must be caused by increasing the fuel jet velocity such that the jet penetrates and breaks the recirculation zone, thus ceasing the reactions.

Conclusions

The current observations and the literature survey of the stability behaviors of jet diffusion flames have lead to four major lifting criteria and several sub-categories, depending on the burner port geometry, flow conditions, and fuel types. Type I: the lifting controlled by the flame base due to (a) the imbalance between the entrained-stream velocity and the local maximum burning velocity and (b) the flow field disturbances by pipe-flow turbulence. Type II: the lifting controlled by (a) the local flame extinction at the breakpoint due to the high strain on the flame by the shear-generated large-scale vortices, (b) subsequent blowoff of the rim-part of the split flame, or (c) blowout of the lifted part. Type III: the lifting controlled by the flame holding in the immediate wake of a thick-lip fuel tube. Type IV: the lifting of aerated wake flames. The present results of the LDV measurement shed light on Types II(a) and III. Further studies are desirable to determine in detail the physical processes and the critical conditions for each lifting criterion.

Acknowledgments

This work was supported by U.S. Air Force, Wright Research and Development Center, Aero Propulsion and Power Laboratory, Ohio, under Contract No. F33615-87-C-2767 with W.M. Roquemore as the Technical Monitor and D.R. Ballal as the Principal Investigator.

REFERENCES

1. Wohl, K., Kapp, N. M., and Gazley, C.: Third Symposium (International) on Combustion, p. 3, The Combustion Institute, 1949.
2. Scholefield, D. A., and Garside, J. E.: Third Symposium (International) on Combustion, p. 102, The Combustion Institute, 1949.
3. Barr, J.: Fourth Symposium (International) on Combustion, p. 765, The Combustion Institute, 1953.
4. Eickhoff, H., Lenze, B., and Leuckel, W.: Twentieth Symposium (International) on Combustion, p. 311, The Combustion Institute, 1985.
5. Pitts, W. M.: Twenty-Second Symposium (International) on Combustion, p. 809, The Combustion Institute, 1989.
6. Dahm, W. J. A., and Dibble, R. W.: Twenty-Second Symposium (International) on Combustion, p. 801, The Combustion Institute, 1989.
7. Miake-Lye, R. C., and Hammer, J. A.: Twenty-Second Symposium (International) on Combustion, p. 817, The Combustion Institute, 1989.
8. Gaydon, A. G., and Wolfhard, H. G.: Flames, Their Structure, Radiation and Temperature, 4th ed., p. 39, Chapman and Hall, London, 1979.
9. Takahashi, F., Mizomoto, M., and Ikai, S.: Hydrogen Energy Progress (T. N. Verziroglu, Ed.), p. 1165, Pergamon Press, 1980.
10. Takahashi, F., Mizomoto, M., and Ikai, S.: Comb. Flame 48, 85 (1982).
11. Takahashi, F., Mizomoto, M., and Ikai, S.: J. Heat Transfer 110, 182 (1988).
12. Takahashi, F., Mizomoto, M., Ikai, S., and Futaki, N.: Twentieth Symposium (International) on Combustion, p. 295, The Combustion Institute, 1985.
13. Takahashi, F.: Studies of the Transition to Turbulence and the Flame Stability of Jet Diffusion Flames, Dr. Eng. thesis, Keio University, Tokyo, Japan, 1982.
14. Chen, T. H., and Goss, L. P.: Flame Lifting and Flame/Flow Interactions of Jet Diffusion Flames, AIAA Paper No. 89-0156, 1989.
15. Coats, C. M., and Zhao, H.: Twenty-Second Symposium (International) on Combustion, p. 685, The Combustion Institute, 1989.
16. Gollahalli, S. R., Savas, O., Huang, R. F., and Rodriques Azara, J. L.: Twenty-First Symposium (International) on Combustion, p. 1463, The Combustion Institute, 1988.
17. Shekarchi, S., Savas, O., and Gollahalli, S. R.: Comb. Flame 73, 221 (1988).
18. Hattori, H.: Trans. JSME 30, 320 (1964).
19. Vranos, A., Taback, E. D., and Shipman, C. W.: Comb. Flame 12, 253 (1968).
20. Takeno, T., and Kotani, Y.: Acta Astronaut. 2, 999 (1975).
21. Hall, L., Horch, K., and Gunther, R.: Brennst. Warme Kraft 32, 26 (1980).
22. Takahashi, F., Mizomoto, M., Ikai, S., and Tsuruyama, K.: Stability Limits of Hydrogen/Air Coflow Jet Diffusion Flames, AIAA Paper No. 90-0034, 1990.
23. Takahashi, F., Schmoll, W. J., and Vangsness, M. D.: Exp. Fluids, submitted (1991).
24. Dibble, R. W., Hartmann, V., Schefer, R. W., and Kollman, W.: Exp. Fluid 5, 103 (1987).
25. Robson K., and Wilson, M. J. G.: Comb. Flame 13, 626 (1969).
26. Hattori, H.: Trans. JSME 30, 298 (1964).
27. Hattori, H.: Trans. JSME 30, 310 (1964).
28. Takahashi, F., Mizomoto, M., and Ikai, S.: The Jet Turbulence and the Flame Stability of Diffusion Flames, paper presented at the Thirteenth Symposium (Japanese) on Combustion, Tokyo, Japan, December 1975.
29. Tsuruyama, K.: A Study on the Stability of Jet Diffusion Flames, M. Eng. thesis, Keio University, Yokohama, Japan, 1980.
30. Drell, I. L., and Belles, F. E.: Survey of Hydrogen Combustion Properties, NACA Rept. 1383, 1958.
31. Anon.: Basic Consideration in the Combustion of Hydrocarbon Fuels with Air, NACA Rept. 1300, 1957.

APPENDIX I.

EFFECTS OF SWIRL ON THE STABILITY AND TURBULENT STRUCTURE OF JET DIFFUSION FLAMES

by

F. Takahashi, W. J. Schmoll, and M. D. Vangsness
University of Dayton, Dayton, Ohio

Published as AIAA Paper No. 90-0036, 1990.

EFFECTS OF SWIRL ON THE STABILITY AND TURBULENT STRUCTURE OF JET DIFFUSION FLAMES

F. Takahashi,* W.J. Schmoll,** and M.D. Vangsness**

University of Dayton, Dayton, Ohio

Abstract

The lifting stability and turbulent flow characteristics have been studied in swirling coflow jet diffusion flames by using a three-component laser-Doppler velocimeter with conditional seeding. Methane was ejected from a fuel tube with swirling co-annular air into a low-speed coflowing air stream in a combustion chimney. For a lip thickness less than the minimum quenching distance of the methane/air mixture, an increase in the annular air velocity decreased markedly the critical mean jet velocity at lifting, although strong swirl enhanced the flame stability significantly. For a larger lip thickness, however, the impact of swirl on the stability limit was relatively weak, because the recirculation zone in the wake of the fuel tube and the local flame extinction were predominant in determining the flame stability. Three major lifting criteria are proposed. The conditioned velocity data under the near-lifting condition revealed that large-scale vortices with the highly distorted turbulent structure and high turbulent kinetic energy exist adjacent to the flame zone in the intermittent boundary region of the jet and the entrained external fluids. The local extinction and subsequent lifting appear to occur as a result of the flame stretch due to the engulfment motion of the large-scale vortices of the fuel-rich jet fluid.

Introduction

Swirl has been widely used in various combustion systems such as gas turbine engines and industrial furnaces to enhance the flame stabilization, fuel-air mixing, and combustion intensity. Despite numerous studies[1-12] of the effect of swirl on various aspects of combustion aerodynamics, mechanisms of various flame stability phenomena (e.g., lift, dropback, and blowout) and the impact of swirl on the turbulent properties of flames have not been clearly understood. Although the stability phenomena of non-swirling jet diffusion flames, blowout in particular, have recently received growing attention as they relate to the turbulent flame structure of the lifted flame base, only few results have been reported[13-15] to date on the stability of swirling jet diffusion flames. In general, swirl promotes efficient turbulent mixing and combustion. However, recent studies[16-19] have shown a counter effect of swirl as well, i.e., retardation of turbulent mixing and combustion under certain conditions. Further, recent development of numerical modeling of turbulent combustion, e.g., the probability density functions (pdf) method[20-22] in particular, has made it possible to apply models to more complex combustion systems such as swirling, turbulent nonpremixed flames. Therefore, revealing the effect of swirl on various stability phenomena and their controlling mechanisms as well as producing bench-mark experimental data on turbulent properties under nonpremixed combustion conditions are of essential importance in developing turbulent combustion models which eventually lead to successful developmental efforts in advanced combustor designing. This paper reports the results of the stability limits of swirling and non-swirling coflow jet diffusion flames and the mean and fluctuating velocity properties obtained by using the three-component laser-Doppler velocimetry technique with conditional seeding.

Experimental Techniques

Figure 1 shows a schematic of the configuration of the combustor system used. The burner consists of a fuel tube (9.45 mm i.d. x 806 mm length; stainless steel) and a concentric air tube (26.92 mm i.d. x 769 mm length; stainless steel) through which annular coflowing air flows, centered in a vertical combustion chimney (150 x 150 mm square cross-section with 85-mm-radius rounded corners x 483 mm length) in which low-speed (~0.5 m/s) external coflowing air flows. Three fuel tubes with different exit lip thicknesses (0.2, 1.2, and 2.4 mm) were used. The outer wall of the former two fuel tubes and the air tube are tapered at a half cone angle of 2 degrees with respect to the burner axis. A helical vane swirler unit is placed in the annular channel between the fuel and air tubes at 96 mm upstream from the burner tube exit. Table 1 shows the design data of four swirler units and a straight vane unit used. The combustion chimney has quartz windows (76 x 457 mm) on all sides to permit visual observations and laser diagnostics.

* Research Engineer, Research Institute, Member AIAA
** Associate Research Physicist, Research Institute

Copyright (c) 1990 by Fumiaki Takahashi. Published by the American Institute of Aeronautics and Astronautics, Inc. with permission.

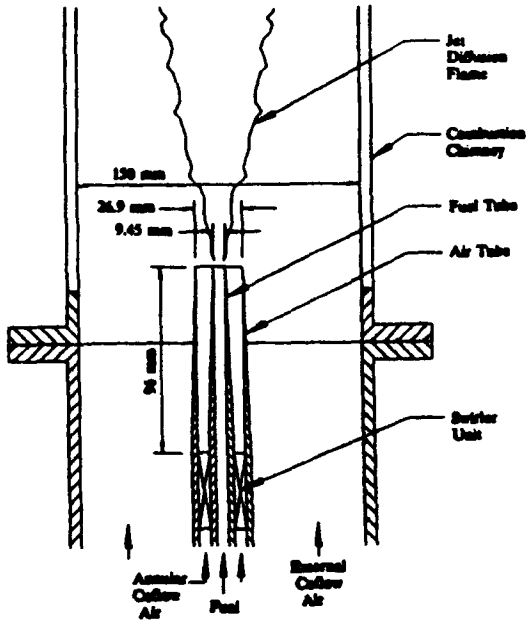

Fig. 1 Burner system configuration.

Table 1 Swirler unit design data

Vane helix angle (°)	Number of vanes	Axial vane length (mm)	Geometric swirl number
0	10	26.9	0
15	10	31.8	0.21
30	8	26.9	0.45
45	6	26.9	0.78
60	4	26.9	1.34

The flame stability limits were measured as follows. Under a fixed annular air flow rate, the fuel (methane >98%) flow rate was increased gradually until the burner-rim attached flame lifted several diameters above the burner (lift) or just extinguished (blowoff). Under certain conditions, the annular air flow rate was increased instead of the fuel flow rate.

A tailor-made three-component laser-Doppler velocimeter system consists of a three-beam two-component (vertical and radial) set using a 514.5 nm line of an argon ion laser (Spectra Physics, 18W) with a component separation based on the polarization principle and a two-beam third-component (tangential) set using a 488.0 nm line of the argon ion laser with separation by color. The axis of the third component laser beams is perpendicular to that of the first and second components, and thus the size of the measurement volume is minimized (approximately 125 x 250 μm diameter in the directions of the first two and third components, respectively). Counter-type signal processors (TSI 1990C) and a tailor-made coincidence electronics circuit and a computer input/output interface module were used. The data acquisition and processing were performed by using a minicomputer (MODCOMP Classic 32/85) and a microcomputer. The number of LDV data acquired at each location was 4096, and a portion (typically ~2%) of the data was filtered out further by the use of a computer program based on the 3-sigma (standard deviation) method and a software coincidence test. Submicron-size Z_rO_2 (Zircar Products, Type ZOP, crystallite size: 0.02-0.03 μm, agglomerate size distribution: <0.1 μm, 30%; <0.3 μm, 50%; <0.5 μm, 72%; <0.7 μm, 85%; <1 μm, 97%, surface area: 30-45 m^2/g) was used as seeding particles for scattering. The particles were sieved and dried in an oven at 120 C for at least 24h prior to the experiment. A novel particle seeder utilizing a fluidized bed with swirl-inducing jets and a pneumatic vibrator was developed to achieve a good control over the seeding rate.

Results and Discussion

Stability Limits

Sharp-edged Fuel Tube Figure 2 shows the critical mean jet velocity at the stability limit (U_{jc}) of methane/air coflow jet diffusion flames formed on a sharp-edged (0.2 mm lip thickness) fuel tube as a function of the mean annular coflow air velocity (U_a) for various swirler vane angles. At zero annular air velocity, the critical mean jet velocity was approximately 22 m/s and maintained nearly constant over a very low mean annular air velocity range (U_a<0.12 m/s). The flame behavior in this range is similar to that in non-swirling cases reported elsewhere.[23] The flame lifting occurred following the instability at the breakpoint region (z=10-20 mm) for the laminar-to-turbulent-flame transition, associated with vanishing intensity of the blue flame emission, which eventually turned into a hole in the flame zone. As the hole expanded all around the flame cross-section, the metastable split flame was observed just prior to lifting. At higher mean annular air velocities, no split flame was observed, and the critical mean jet velocity decreased markedly, similar to hydrogen flame studied previously.[24] The physical mechanism responsible for the lifting in this range must be base on the imbalance between the entrained-stream velocity at the flame base and the local maximum burning velocity obtainable when mixing the jet and oxidizing fluids, as described in more detail elsewhere.[23,25] For a 15-degree swirler, there is essentially no difference in the critical mean jet velocity compared to the non-swirling case over a whole range of the mean annular air velocity. For 30-degree and 45-degree swirlers, some enhancement in the flame stability is seen in the range U_a>0.6 m/s.

The most striking effect of swirl appeared for a 60-degree swirler. As the mean annular air velocity ex-

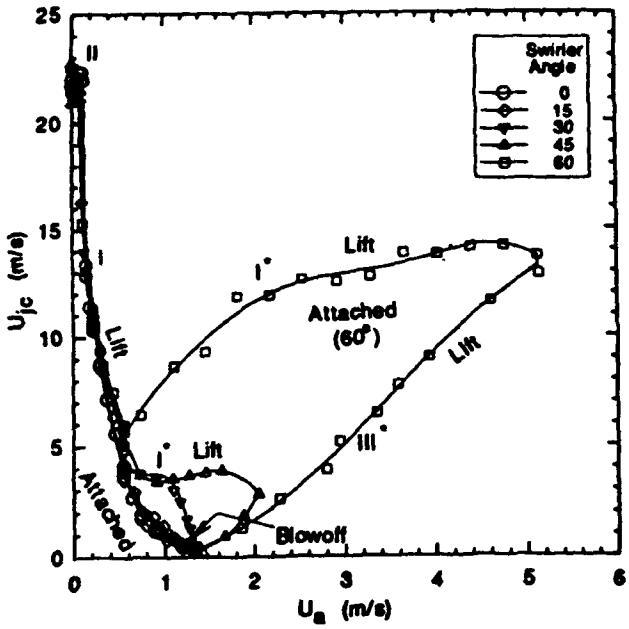

Fig. 2 Effect of swirl on the stability limit of methane-air coflow jet diffusion flames. Lip thickness: 0.2 mm.

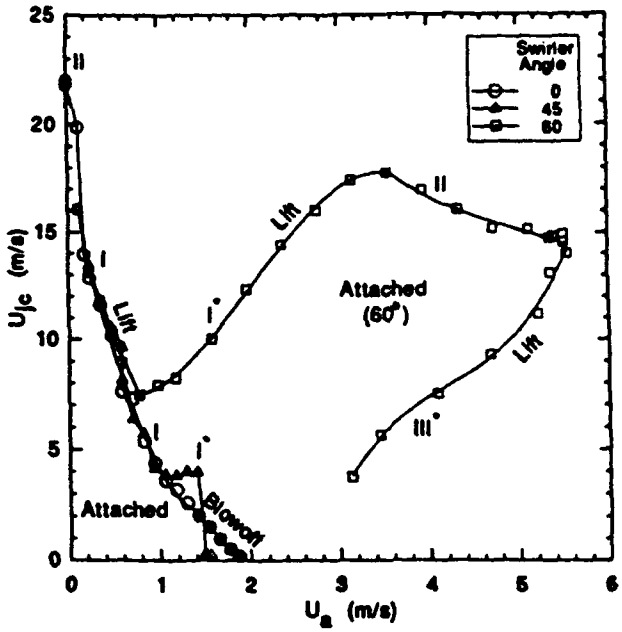

Fig. 3 Effect of swirl on the stability limit of methane-air coflow jet diffusion flame. Lip thickness: 1.2 mm.

ceeded 0.6 m/s, the critical mean jet velocity started to increase, expanding the burner-rim-attached region significantly. It is noticed that there existed a lower branch at the mean annular air velocity over 1.5 m/s. The lower branch was obtained by increasing the annular air velocity instead of the jet velocity. Some characteristic changes in the flame appearance were noticed for the 60-degree swirler. In the range of approximately $U_a>1.8$ m/s and $U_j<9.8$ m/s, the near-burner region (height form the jet exit, $z<30$ mm) of the flame became fatter in its shape and yellow in color due to the soot formation, indicating the formation of a recirculation zone due to swirl in the form of a toroidal vortex. As a result, the flow pattern and temperature distribution must be changed dramatically. The high temperature fuel rich condition and longer residence time in the recirculation zone must be favorable for the fuel pyrolysis which leads to the soot formation. As a result of strong swirl, the angle of spread of the jet must increase, increasing entrainment and thereby causing faster decay of the velocity with height from the jet exit. Therefore, the enhancement of the flame stability must be due to changes in the flow pattern and the lowered entrainment velocity in the flame stabilizing region, i.e., the flame base. Since both the fuel and air velocities increase along the lower branch, the critical conditions at the limit may probably relate to the local equivalence ratio at the flame base.

Medium-thick Fuel Tube Figure 3 shows the lifting limit of methane/air coflow jet diffusion flames formed on a fuel tube with a moderate lip thickness (1.2 mm) for three different swirler angles tested including a straight vane. The general trend of the flame stability behavior is the same as that for sharp-edged fuel tube described above, although the magnitude of the critical mean jet velocity is generally larger in the thicker-lip case. Similarly to the sharp-edged tube, the critical mean jet velocity with no annular air was approximately 22 m/s and maintained nearly constant over a very low mean annular air velocity range ($U_a<0.12$ m/s), in which the local extinction was observed followed by lifting. The critical mean jet velocity dropped beyond this range, but the slope of the critical mean jet velocity was smaller than that of the sharp-edged tubes, and thus the rim-attached region was expanded slightly. This result may be due to slight changes in the flow pattern and the entrainment velocity in the vicinity of the flame base due to the broadened wake of the fuel tube. Again, significant enhancement in the stability limit was observed for the 60-degree swirler. In the mean annular air velocity range of $3.7<U_a<5.1$ m/s after the critical mean jet velocity curve passed a peak, a distinct difference was noticed in the behavior of the flame just prior to lifting. In this range, the local flame extinction re-appeared just before lifting, triggering lifting. Apparently, the physical mechanism for the flame detachment in this region must be the same as that for the flames in the very low annular air velocity range (<0.12 m/s).

Flat-end Fuel Tube Figure 4 shows the stability limit for a fuel tube with a large lip thickness (2.4 mm) for four swirler angles including a straight vane. In contrast with the flame stability behavior for small lip thicknesses, marked changes were observed for the thick-lip fuel tube, as described elsewhere[23] for non-swirling conditions. The general trend in the stability limit curves is similar for all swirler angles, although the region of the burner-rim attached flame expanded as the swirler angle was increased. Similarly to the smaller lip thicknesses

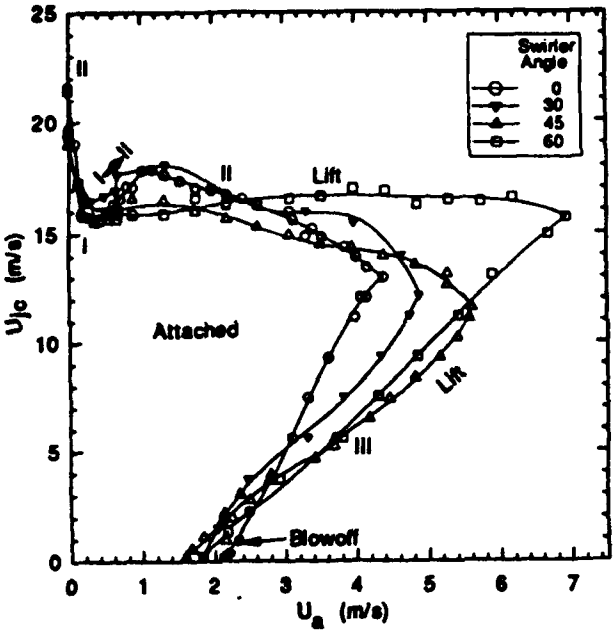

Fig. 4 Effect of swirl on the stability limit of methane-air coflow jet diffusion flames. Lip thickness: 2.4 mm.

described above, the critical mean jet velocities at lifting without the annular air flow were 19-21 m/s., and the local flame extinction led to lifting. The locally quenched flame for the thick fuel tube was less stable, and therefore the split flame was not recognized. Also, as the mean annular air velocity exceeded ~0.1 m/s, the flame lifted abruptly due to the instability at the flame base, and the critical mean jet velocity decreased markedly at first but was less sensitive to the mean annular air velocity afterwards. The local extinction re-appeared at higher annular air velocity (U_a>1.9 m/s). For all swirler angles, there existed a lower branch of the stability curve in U_a>1.6 m/s. The lower branch was obtained by increasing the annular air velocity instead of the jet velocity. At low critical jet velocities (<4 m/s), the flame blew off instead of lifting under non-swirling conditions, or for 40-degree and 60-degree swirlers a small, vibrating, aerated flame was formed just above the fuel tube due to the recirculation zone.

Lifting Criteria As described for non-swirling flames,[23] the lifting stability behaviors observed can be categorized into several criteria in terms of where and how the flame instability first starts. For non-swirling flames three criteria were found, i.e., the lifting controlled by the flame base (Type I), the lifting controlled by the local extinction at the breakpoint (Type II), and the lifting controlled by the flame holding in the wake (Type III). Types of the lifting criteria are indicated in the stability diagrams shown in Figs. 2-3. For swirling flames , the above three criteria plus variations of Types I and III (indicated as I* and III* , respectively) were observed. Type I lifting was primarily observed for a lip thickness less than the minimum quenching distance of the methane/air mixture (2 mm[26]). It appears to be controlled by the flame base according to the same physical mechanism previously proposed[25] for free jet diffusion flames formed on a sharp-edged fuel tube in still air. Types II and III were observed for a greater lip thickness. Type II was associated with the local extinction, which seems to be caused by the flame stretch due to the large-scale vortices as described in more detail in the next section. Type III appears to be caused by the lean-limit extinction in the recirculation zone in the wake of the fuel tube and by loosing the flame holding at the flame base.

Type I* is based on the same physical mechanism with Type I, but it is the case where the formation of a toroidal vortex recirculation zone due to strong swirl alters the flow field in the vicinity of the flame base and in turn enhances the flame stability significantly. Type III* is a lifting criterion observed at the lower branch of the stability limit of strongly swirling flames on a small lip thickness. For a swirling flame on a thick tube Types III* appears to be combined with Type III. Since the lower branch of the stability limit curves for the thin fuel tubes (0.2 and 1.2 mm lip thickness) was close to that of the thick tube (2.4 mm), and the critical mean jet velocity at the lower branch increased with the mean annular velocity, the critical conditions at the limit for all lip thicknesses seem to be controlled by the ratio of fuel and oxygen fluxes coming into the flame stabilizing region and in turn the local equivalence ratio. For thick tubes a recirculation zone formed in the tube wake where the flame base is anchored is predominant in controlling the flame stability, and for thin tubes the flame base itself is the stability controlling region.

Mean and Turbulent Flow Structure

To investigate in detail the local extinction and subsequent lifting phenomena (Type II), the three-component laser-Doppler velocimetry measurement was made near the breakpoint of a swirling jet diffusion flame for a 45-degree swirler angle under the near-lifting condition. The conditional data sampling[27,28] was made by seeding particles into only the fuel jet or annular coflowing air. Figure 5 shows the radial profiles of the axial (U), radial (V), and tangential (W) mean (time-average) velocity components. The locations of the (average) visible flame zone, measured by using a cathetometer, and the burner rim are included in the figure as well. The conditioned data on the axial mean velocity profile (Fig. 5a) shows the region where the jet and entrained external fluids exist intermittently and that the fluid elements from the jet are faster on the average than those from the coflow as was reported by previous workers. The visible flame zone is located in the boundary region of the intermittent layer.[27,28] It is noticed that in the visible flame zone the velocity gradient of the axial mean velocity component for the jet fluid elements is higher than that for the external fluid elements. The profile of the radial mean velocity component (Fig. 5b), revealed striking features that the jet fluid elements are moving outward radially on the average, whereas the external fluid elements are vice versa, even near the visible flame zone. The tangential mean velocity com-

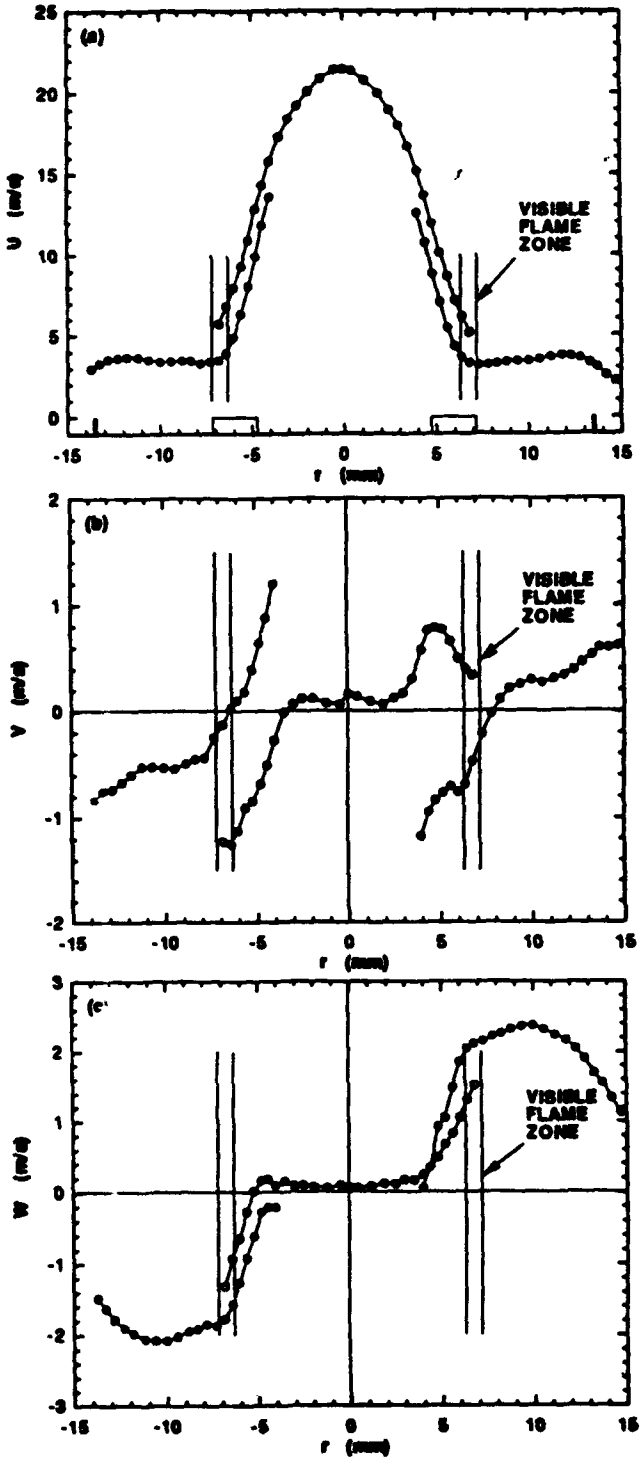

Fig. 5 Radial profiles of (a) axial, (b) radial, and (c) tangential mean velocity components in a swirling methane-air coflow jet diffusion flame. U_j=15 m/s, U_a=3 m/s, z=15 mm.

ponent profile data (Fig. 5c) shows that the tangential momentum in the annular coflowing air penetrated into the jet boundary region on the fuel side of the visible flame zone and that the external fluid elements have

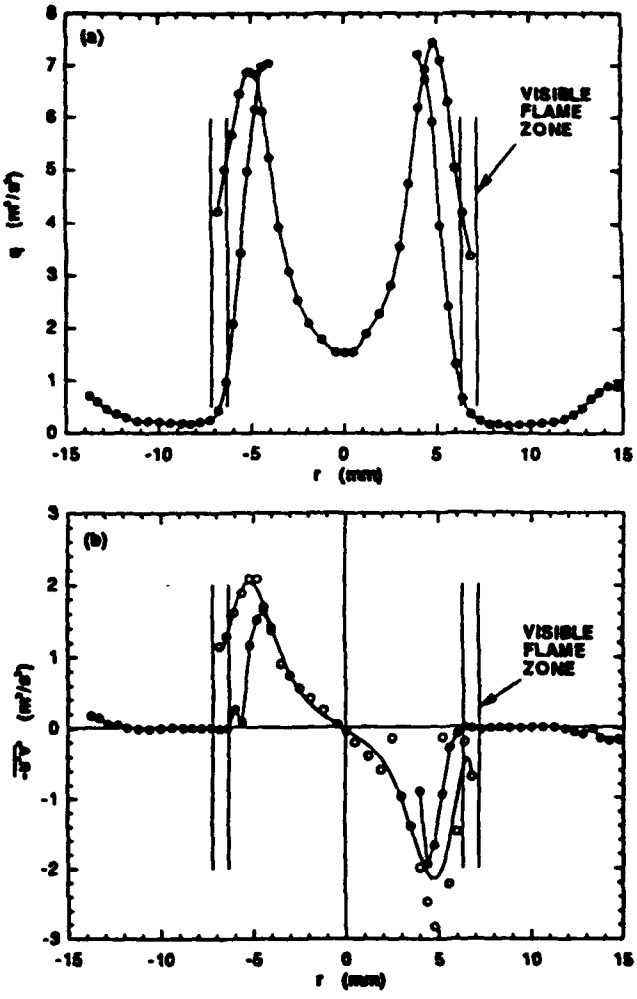

Fig. 6 Radial profiles of (a) turbulent kinetic energy and (b) Reynolds shear stress in a swirling methane-air coflow jet diffusion flame. U_j=15 m/s, U_a=3 m/s. z=15 mm.

higher velocity than those of the jet fluid. The velocity differences between the jet and external fluid elements in axial, radial, and tangential component were approximately 2.5 m/s, 1.2 m/s, and 0.6 m/s, respectively. This result clearly shows the existence of large-scale vortex structure in the intermittent layer.

Figure 6 shows the radial profiles of the kinetic energy of turbulence ($q=(\overline{u'^2}+\overline{v'^2}+\overline{w'^2})/2$ where u', v' and w' are the axial, radial, and tangential fluctuation velocity components) and the Reynolds stress ($-\overline{u'v'}$). The peak values of the relative intensities of turbulence (the root mean squares of u', v', and w'; not shown) were 13%, 7%, and 9%, respectively, and the peaks coincided with those of the turbulent kinetic energy. Other components of the Reynolds shear stresses ($-\overline{v'w'}$ and $-\overline{u'w'}$; not shown) were much smaller than $-\overline{u'v'}$. The peak values of the turbulent kinetic energy and the Reynolds shear stress in the swirling flame shown here were larger (approximately 15% and 35%, respectively) than those in

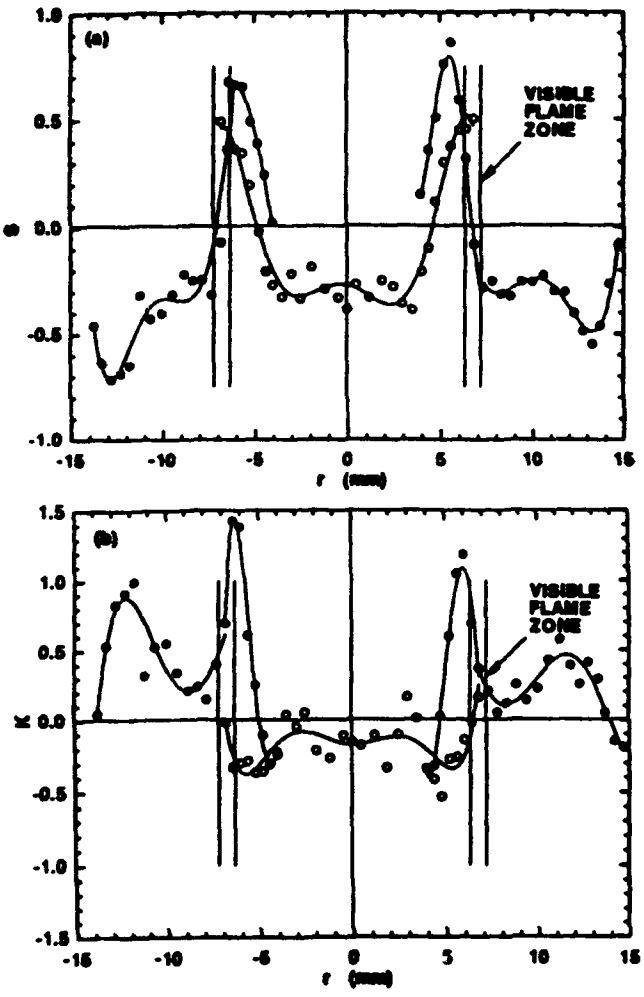

Fig. 7 Radial profiles of (a) skewness and (b) kurtosis of the axial velocity fluctuation in a swirling methane-air coflow jet diffusion flame. U_j=15 m/s, U_a=3 m/s. z=15 mm.

a non-swirling flame[23] due to a contribution by tangential velocity fluctuation. The peaks of the turbulent kinetic energy coincided with those of the Reynolds shear stress, located in the high-shear layer where the axial mean velocity gradient reached the maximum (see Fig. 5a) on the fuel side of the visible flame zone. Therefore, the production of the turbulent kinetic energy is through the term of a product of the Reynolds shear stress and the shear strain. Noticed in Figs. 6a and 6b that as the shear-generated turbulence, indicated by the peaks in the turbulent kinetic energy profile for the jet fluid element, diffuses toward the flame zone, the turbulent activities of the entrained external fluid element increased inwardly. It should be noted that both the turbulent kinetic energy and the Reynolds shear stress of the jet fluid elements were several times larger than those of entrained external fluid elements in the visible flame zone.

Figure 7 shows the radial profiles of skewness ($S=\overline{u^3}/(\overline{u^2})^{3/2}$) and kurtosis ($K=\overline{u^4}/(\overline{u^2})^2-3$) of axial velocity fluctuation. For a Gaussian pdf distribution associated with random small-scale fluctuations, S=0 and K=0. The peak values of S=0.5-0.8 for both the jet and external fluid elements and K=1.3 for the external fluid element were observed at the inner edge of the visible flame zone. This result shows the presence of highly distorted turbulent structure adjacent to the flame zone due to the presence of large-scale vortices generated in the intermittent region and highly skewed in the high-temperature near-flame region. The large-scale vortices thus carried the fuel toward the flame zone. Near the edge of the boundary region of the intermittent layer (approximately coincident with the end points of the data conditioned on jet seeding), the intermittency factor must vanish, and therefore, it must be relatively rare event that the jet fluid element reaches to the location of the visible flame zone. However, if the large-scale vortices of the jet fluid elements (nearly pure fuel at this height) approach closely to the instantaneous flame zone, it may be locally quenched by high strain due to the relative movement of the instantaneous flame zone and adjacent fluid induced by the engulfment motion and the high fuel concentration of the large-scale vortices.

Conclusions

The significant enhancement of the lifting stability of methane/air coflow jet diffusion flames by swirl is restricted to the case of strong swirl which creates a toroidal recirculation zone, which alters the flow field in the flame stabilizing zone. This effect is remarkable in particular for a lip thickness of the fuel tube less than the minimum quenching distance of the fuel/air mixture. For a larger lip thickness, the impact of swirl is relatively weak because the recirculation zone in the fuel tube wake and the local flame extinction are predominant in determining the flame stability. Three major lifting criteria, common with non-swirling flames, and two variations peculiar to swirling flames are proposed herein. The LDV measurement with conditional seeding in the breakpoint region of a near-limit swirling flame have revealed the turbulence-flame interaction which leads to the local extinction followed by lifting. Further experiments particularly on the measurements of scalar fields are desirable to clarify in more detail the flame-turbulence interaction with regard to the physical mechanisms responsible for the flame stability phenomena.

Acknowledgements

This work was supported by the U.S. Air Force, Wright Research and Development Center, Aero Propulsion and Power Laboratory, Ohio, under Contract No. F33615-87-C-2767 with W.M. Roquemore serving as the Technical Monitor and D.R. Ballal as the Principal Investigator. The authors wish to thank Dr. M.S. Anand of Allison Gas Turbine Division of General Motors, Messrs. E. Dudis (deceased), F. Timko, C.M. Reeves, Lt. A.L. Lesmerises for assistance in designing and fabrication of the burner system.

References

1. Chigier, N.A., and Beer, J.M.: *Combustion Aerodynamics*, Applied Science Publishing, London, 1972.
2. Osgerly, I.T.: *AIAA J.* 12, 743 (1974).
3. Syred, N., and Beer, J.M.: *Combust. Flame* 23, 143 (1974).
4. Chigier, N.A., and Dvorak, K.: *Fifteenth Symposium (International) on Combustion*, p.573, The Combustion Institute, 1975.
5. Leuckel, W., and Fricker, N.: *J. Inst. Fuel* 49, 103 (1976)
6. Lilley, D.G.: *AIAA J.* 15, 1063 (1977)..
7. Gupta, A.K., Beer, J.M., and Swithenbank, J.: *Sixteenth Symposium (International) on Combustion*, p.79, The Combustion Institute, 1977.
8. Edelman, R.B., and Harsha, P.T.: *Combust. Sci. Tech.* 4, 1 (1978).
9. LaRue, J.C., Samuelsen, G.S., and Seiler, E.T.: *Twentieth Symposium (International) on Combustion*, p.277, The Combustion Institute, 1985.
10. Tangirala, V., Chen, R.H., and Driscoll, J.F.: *Combust. Sci. Tech.* 51, 75 (1987).
11. Tangirala, V., and Driscoll, J.F.: *Combust. Sci. Tech.* 60, 143 (1988).
12. Chen, R.H., Driscoll, J.F.: *Twenty-Second Symposium (International) on Combustion*, p.531, The Combustion Institute, 1989.
13. Rawe, R., and Kremer, H.: *Eighteen Symposium (International) on Combustion*, p.667, The Combustion Institute, 1981.
14. Yuasa, S.: *Combust. Flame* 66, 181 (1986).
15. Feikema, D., Chen, R.H., and Driscoll, J.F.: AIAA Paper No. 89-0158, 1989.
16. Emmons, H.W., and Ying, S.J.: *Eleventh Symposium (International) on Combustion*, The Combustion Institute, p.475, 1967.
17. Chigier, NA., Beer, J.M., Grecov, D., and Bassindale, K.: *Combust. Flame* 14, 175 (1970).
18. Beer, J.M., and Chigier, N.A.: *Combust. Flame* 16, 39 (1971).
19. Takagi, T., Okamoto, T., Taji, M., and Nakasuji, Y.: *Twentieth Symposium (International) on Combustion*, p.251, The Combustion Institute, 1985.
20. Pope, S.B.: *Twentieth Symposium (International) on Combustion*, p.403, The Combustion Institute, 1985.
21. Pope, S.B.: *Progress Energy Combust. Sci.* 11, 119 (1985).
22. Anand, M.S., Pope, S.B., and Mongia, H.C.: U.S.-France Joint Workshop on Turbulent Reactive Flows, Rouen, France, July 1987.
23. Takahashi, F., and Schmoll, W.J.: *Twenty-Third Symposium (International) on Combustion*, The Combustion Institute, 1990 (submitted).
24. Takahashi, F., Mizomoto, M., Ikai, S., and Tsuruyama, K.: *Stability Limits of Hydrogen/Air Coflow Jet Diffusion Flames.* AIAA Paper No. 90-0034, 1990.
25. Takahashi, F., Mizomoto, M., Ikai, S., and Futaki, N.: *Twentieth Symposium (International) on Combustion*, p.295, The Combustion Institute, 1985.
26. Annon.: *Basic Consideration in the Combustion of Hydrocarbon Fuels with Air*, NACA Rept. 1300, 1957.
27. Dibble, R.W., Hartmann, V., Schefer, R.W., and Kollman, W.: *Exp. in Fluids* 5, 103 (1987).
28. Stepowski, D., and Cabot, G.: *Twenty-Second Symposium (International) on Combustion*, p.619, The Combustion Institute, 1989.

APPENDIX M

NEAR-FIELD TURBULENT STRUCTURES AND LOCAL EXTINCTION OF JET DIFFUSION FLAMES

by

Fumiaki Takahashi
University of Dayton, Dayton, Ohio

Larry P. Goss
Systems Research Laboratories, Dayton, Ohio

Published in Twenty-Fourth Symposium (International) on Combustion, The Combustion Institute, in Press.

NEAR-FIELD TURBULENT STRUCTURES AND THE LOCAL EXTINCTION OF JET DIFFUSION FLAMES

Fumiaki Takahashi
University of Dayton

Larry P. Goss
Systems Research Laboratories

The aerodynamic structure of turbulent jet diffusion flames of methane stabilized on a thick-walled fuel tube in coflowing air has been studied by using laser-Doppler velocimetry and Mie scattering techniques to elucidate the local flame extinction and subsequent lifting phenomena. Instantaneous planar flow visualization and real-time line measurements revealed large-scale vortical structures, constituting the intermittent mixing layer, and sporadic radial mass ejection from the jet-fluid core. By seeding the jet and coflow separately in the LDV measurement, conditioned joint probability-density functions (pdf's) of the axial and radial velocity components and their statistical moments, i.e., the conditioned (zone) averages, root-mean-square fluctuations, skewnesses, kurtoses, and Reynolds shear stress, were determined. The unconditioned pdf and, in turn, the statistical moments were obtained from the conditioned pdf's and intermittency of the jet fluid. The jet-fluid parcels had a higher mean axial velocity than that of the external-fluid parcels and a positive mean radial velocity in contrast to a negative value for the external-fluid parcels. These differences are responsible, to a great extent, for creating highly-distorted turbulent structures in the intermittent layer adjacent to the flame zone. Since diffusion processes require significantly longer time than convective processes associated with the large-scale vortices and the radial mass ejection, the radial location of the flame zone is insensitive, at least in the near-jet field, to the high-frequency jet-fluid concentration fluctuation in the core. As a result, the ejected jet fluid, or the large-scale vortex itself, can reach the flame-zone location without disturbing the concentration field, thereby locally quenching the already strained diffusion flame.

INTRODUCTION

Although various phenomena in jet diffusion flames have been studied since early days in combustion research, there remain certain aspects of the subject that need further investigation. The flame stabilization phenomena, e.g., liftoff and blowout, are of both fundamental and practical interest. It has recently[1] been clarified that there exist several distinct lifting mechanisms for jet diffusion flames, depending on the burner and flow configurations and the fuel type. In many cases, the flame stabilization and the detachment from the burner rim are controlled by local conditions near the flame base[2,3] (Type I in Ref. 1). The Type I case is likely to happen particularly if the lip thickness of the fuel tube or nozzle is small. However, if the flame base is stabilized securely on the burner rim by using, for example, a thick-lip fuel tube, the flame zone will be quenched locally at typically a few jet diameters downstream where the laminar flame zone becomes turbulent (i.e., breakpoint). For hydrogen[4-7] or propane[9] flames, the local extinction leads to formation of a stable split flame, i.e., a combination of a small laminar flame in the vicinity of the burner rim and a turbulent lifted-like flame downstream (Types II(b) and II(c) in Ref. 1). However, for methane flames,[1,3,9-11] the local extinction causes lifting of the flame almost immediately (Type II(a) in Ref.1). Takeno and Kotani[5] postulated that, for hydrogen flames, the local extinction is a result of the excess transport rate as compared to the reaction rate at the transition point of turbulent flames. More recently, the event when inner vortices interfere with the flame front was captured in methane flames by using instantaneous schlieren[9] or laser-sheet flow visualization[12,10] techniques. Eickhoff et al.[9] speculated that the diffusion flame was quenched because too much heat was diffused by the small scale turbulence superimposed in these vortices. Unfortunately, detailed flame structure data related to the local flame extinction phenomena are only slowly becoming available.

Turbulent diffusion flames are described in most cases as being composed of wrinkled, moving, laminar sheets of reaction, i.e., flamelets.[13,15] The concept of local flamelet extinctions due to high strain rate has been applied to the base of turbulent lifted flames to determine the liftoff height and blowout conditions.[16] Extinction processes have initially been considered to occur within small-scale turbulent structures.[16,17] More recent work[18-22] has suggested that large-scale structures are responsible for extinction. Since the flame zone is located generally outside of the large-scale vortex structure in burner-rim-attached turbulent jet diffusion flames, the large-scale vortex structure must play a major role also in the local extinction phenomena near the breakpoint. Unlike the lifted turbulent flame base, the transition region of attached flames is more stationary and continuous, and there is no complication due to the fuel-air premixing prior to combustion. Therefore, the near-jet field of rim-attached turbulent jet diffusion flames provide a unique, well-defined diffusion flame structure suitable to the study of dynamic turbulence-flame interactions. The major objective of this study is to gain a better understanding of the mechanisms of local extinction and subsequent lifting phenomena (Type II(a) in Ref 1).

EXPERIMENTAL TECHNIQUES

The experimental apparatus and the LDV system have been described in detail elsewhere.[11] The burner consists of a thick-walled, flat-end fuel tube (9.45 mm i.d., 2.4 mm lip thickness) and a concentric air tube (26.92 mm i.d.) through which annulus coflow air flows, centered in a low-speed (~0.5 m/s) general air stream in a vertical combustion chimney. Methane (>98%) was used as the fuel. Submicron Z_rO_2 particles were used for the LDV measurement.

The details of the instantaneous (10 ns) planar flow visualization and the real-time line measurements have been reported elsewhere.[10,12,23,24] For planar visualization, Mie

scattering from TiO_2 particles, formed from the reaction of seeded $TiCl_4$ vapor and water vapor in the combustion products, are visualized at right angles to a sheet of laser light (~0.25 mm thickness) from a pulsed Nd:YAG laser (Quanta-Ray DCR-3; frequency doubled, 532 nm, ~250 mJ). For the real-time line measurements, the output from an Argon ion laser (Spectra Physics 2000; multiline, 1-3W) is focused to a line above the burner. TiO_2 particles are preformed and introduced into the fuel tube. The scattered light is collimated by a f/2.5 lens and directed toward a multi-faceted rotating mirror wheel which sweeps the collimated light from the flame through a f/2 focusing lens onto a 50 μm aperture. The scattered light exiting the aperture is then detected by a photomultiplier, the output of which is amplified and digitized at a high rate. The digitization of the scattered light is synchronized with the rotation of the mirror by monitoring the reflection of a HeNe laser beam with a silicon diode detector, thereby triggering a 512 clock burst which is sent to the digitizer. A delay circuit is used to temporally adjust the clock burst to the sweep of the scattered light to ensure the correct signal is digitized. A transient recorder (Lecroy TR8818) with ECL memory is used to digitize the data with 8 bit resolution. For the experiments reported in this paper, the rotational speed of the multi-faceted mirror was 500 rpm which with 10 facets translates into 5000 sweeps per second. Each individual sweep was digitized at a rate of 8 MHz. The effective spatial resolution of the experiment was measured to be 75 μm/pixel, where a pixel is defined as one digitized channel or 1/512th of a single sweep.

RESULTS AND DISCUSSION

Mie Scattering Measurements

Figure 1 shows instantaneous planar flow visualization photographs. At a low mean jet velocity (Fig. 1a), the boundary between the $TiCl_4$-laden jet fluid and the combustion

products is clearly marked by TiO_2 particles as smooth green streaks up to the height from the jet exit, z~30 mm. It should be noted, however, that the flow inside the fuel tube is turbulent, as the Reynolds number ($Re_j=U_j\ d/\ \nu_j$=3380; d, the jet diameter; ν_j, the kinematic viscosity of the fuel) exceeds a critical value (~2300), and that the pipe flow turbulence is confined inside the visualized boundary. Notice that the blue visible flame zone is well separated (2-3 mm) from the visualized boundary. The instability of the boundary and the subsequent roll-up process, forming large-scale vortices, are seen downstream (z>30 mm) until yellow luminous flame cover the inside structure. Although the behavior of this breakpoint to turbulence has been studied[5,25] extensively by using schlieren photography, the detailed flow structure such as visualized here has never been revealed.

Figure 1b is a moderate velocity case, where $TiCl_4$ vapor is introduced into both the jet and annulus air to show the entrainment pattern. Due to the continuous radiation from the particles entrained into the flame zone, the color of the flame is no longer natural. It is notable that mixing on the air-side of the flame zone takes place also intermittently by large-scale vortices created in the shear layer of the annulus air jet. Many fine streaks engulfed into the inner large-scale vortices are seen. The observations augment further the recent view of entrainment based on the large-scale structures,[19,26,27] which differs significantly from a classic view based on the time-averaged flow pattern.

At a high mean jet velocity (Figs. 1c and 1d) near the critical mean jet velocity at lifting (U_{jc}=16.5~17 m/s at U_a=3 m/s),[1,11] more turbulent activities are observed. The large-scale vortices grow in the intermittent mixing layer. Although the large structures are not as orderly, or coherent, as observed in low-speed nozzle jet flames,[12,24] symmetric evolution of the vortices is evident as shown in Figs. 1c and 1d. At other times, it appears as though the large structures are more helical, as observed also in the far field,[26] or less

orderly. The blue flame zone is locally quenched momentarily in the range $10<z<60$ mm. It is noticed in the closed-up view (Fig. 1d), that the blue flame zone is essentially stationary despite the violent movement of the jet-fluid in the core region. The large-scale vortices are very close to the flame zone (0~1.5 mm), and smaller-scale radial mass ejection from the jet-fluid core extruding beyond the flame zone can be seen in the figure.

Figure 2 shows real-time traces of Mie scattering intensities along a line for the high velocity case. The radial movement of the boundary of the jet and external fluids increases toward downstream as a result of the growth of the large-scale structure. At the highest position (Fig. 2c), lower frequency movement associated with the slowed large-scale structures is more noticeable, and the external fluid reaches the centerline region occasionally. The images such as shown in Fig.2 were then processed such that each pixel had a binary value determined by comparing to a threshold value (typically set at ~50% of the maximum value of the average scattering intensity along a line). The processed binary image directly relates to an intermittency function[13,28,29] defined as a stochastic function having a value $I(z,r,t)=1$ in the jet fluid and $I(z,r,t)=0$ in the external fluid. The intermittency ($\overline{I}(z,r)$), i.e., the mean value of the intermittency function, represents the fraction of time that the jet fluid is present at the position in question. The crossing frequency (f_c), i.e., the number of crossings from the jet to external fluid per unit time then can be determined. Figure 3 shows the intermittency and crossing frequency obtained from the binary images. The radial locations of the visible flame zone, measured by using a stationary telescope and by moving the burner with the translational stage (5 μm precision), and the burner rim location are also included. In all cases, f_c peaked at $\overline{I}=0.5$, as expected. As U_j was increased (Figs. 3a and 3b), the intermittent mixing layer spread outwards due to transition to turbulent jet-external fluid mixing as observed in Fig. 1, approaching to a closer proximity of the thickened visible flame zone. At $U_j \sim U_{jc}$ (Figs. 3c and 3d), the radial

location where f_c peaked remained the same at different heights ($5<z<50$ mm), and the mixing layer spread on both sides. Although the line Mie scattering measurement was made up to z=125 mm, only the results in the potential core zone, where $\overline{I}$=1 at the centerline, were presented here. The crossing frequency for $\overline{I}$=0.5 ($f_{c1/2}$) provides a crude estimate for the scale of the large-scale turbulent structure which accompany intermittency.[29] The length between crossings is given by $U_{1/2}/f_{c1/2}$, where $U_{1/2}$ is the local mean axial velocity at $r=r_{1/2}$ where $\overline{I}$=0.5. A typical scale of the large eddies (l) can be calculated by taking half that length as $l=0.5U_{1/2}/f_{c1/2}$. Table 1 summarizes characteristics of the large-scale vortical structure.

LDV Measurements

Since a LDV instrument measures the velocities of individual seed particles to obtain the probability distribution of velocity components, there exist various statistical bias problems. To clarify limits of velocity bias due to non-uniform seeding, particles were added only to the fuel jet or annulus coflow air at a time, following previous investigators.[30] This technique is found to be useful not only to provide information related to bias problems but also details concerning the turbulent structure. Figure 4 shows the radial profiles of the conditioned means and root-mean-square (rms) fluctuations of the axial and radial velocity components and Reynolds shear stress. The unconditioned profiles in the figure will be discussed later. The innermost annulus-seed data point and the outermost jet-seed data point, where the particle arrival rate becomes extremely low, are consistent with the distribution of $\overline{I}$ (Fig. 3a).

In the mixing layer, the jet fluid parcels had a higher mean axial velocity than that of the external fluid parcels (Fig. 4a). The radial profiles of the mean radial velocity

component (Fig. 4b) revealed a rather striking feature, namely, that the jet fluid parcels were moving outwardly on the average, whereas the external fluid parcels were moving inwardly. These results were uniquely captured by conditional sampling and demonstrate the intermittent mixing process due to large-scale vortices, the occasional radial jet fluid ejection, and the engulfment of the external fluid into the large-scale structure.

The rms fluctuations of the axial and radial velocity components of the jet fluid (Figs. 4c and 4d) were generally larger than those of the external fluid, as expected because the jet fluid issuing from the fuel tube was a high-velocity turbulent flow and the external fluid in the mixing layer consisted of high-temperature combustion products with a high viscosity and a lower velocity. Further, the rms axial fluctuation was everywhere larger than that of the radial component, i.e., anisotropic. The Reynolds shear stress (Fig. 4e) of the external fluid was nearly zero on the air-side of the flame, displaying no active contribution to the turbulent transport.

Figure 5 shows the radial profiles of the radial gradients of the mean axial and radial velocity components and the skewness and kurtosis of the axial velocity component. The peaks of the Reynolds shear stress and the rms's (and therefore, turbulent kinetic energy) of the jet fluid coincided approximately with the points where the magnitude of the gradient of the mean axial velocity was maximum. This result is indicative of the gradient-type momentum diffusion in turbulent transport processes of small-scale eddies superimposed with the large structure and of the production of the turbulent kinetic energy through the product of the Reynolds shear stress and strain.

The unconditioned joint probability-density function (pdf) of the axial and radial velocity components $P(u,v;\ z,r)$ is determined from the pdf's conditioned on the jet fluid $P_j(u,v;\ z,r)$ and the external fluid originated from annulus-air $P_a(u,v;\ z,r)$ and the intermittency $(\bar{I}\,(z,r))$ as[13,28]

$$P(u,v;\, z,r) = [1 - \bar{I}(z,r)]P_a(u,v;\, z,r) + \bar{I}(z,r)P_j(u,v;\, z,r).$$

The unconditioned statistical moments then can be retrieved from the unconditioned pdf as shown in Figs. 4 and 5. It is noteworthy that because the conditioned (zone) averages are used to determine conditioned moments and the zone averages are different for the jet and external fluids, the unconditioned values, except for the time-averaged means, cannot be obtained simply by taking a weighted average of the conditioned values and the intermittency. This conventional method[28] is valid only if the time average is used for determining conditioned moments, and it is feasible for time-series measurements for which the time average is readily available. Figure 6 shows an example of the conditioned and unconditioned pdf's with contour plots. The pdf's conditioned on the jet fluid (Fig. 6a) and the external fluid (Fig. 6b) are broadly spread due to high rms values and shows a positive correlation ($\overline{u'v'}$~1.5 m^2/s^2; Fig.4e), typical of the shear layer, and the external fluid's pdf is more skewed (S_u~1; Fig. 5c). More importantly, due to the differences in the zone averages between the jet and external fluids, the unconditioned pdf (Fig. 6c) becomes more elongated shape, thus creating a large correlation $\overline{u'v'}$ (~2.7 m^2/s^2; Fig. 4e). This effect is even more apparent in the vicinity of the flame zone, where the unconditioned higher moments show highly-distorted turbulent structure (Figs. 5c and 5d).

Local Flame Extinction

In general, the extinction of laminar diffusion flames occurs due to nonequilibrium effects as a result of decreased Damkö hler number, i.e., the ratio of the local diffusion time to chemical reaction time. The critical strain rate (velocity gradient) beyond which the flame cannot be stabilized has been reported[31,32] for methane as 350-500 s^{-1}. It is remarkable that, in Fig. 5b, the radial velocity gradient of the mean radial velocity

component of the approach flow (external fluid) into the flame zone increases with increasing U_j and reaches approximately 500 s^{-1} at the near extinction condition (U_j=15 m/s). Although the actual value may fluctuate since the mean velocity was used here, the high velocity gradient means a thin diffusion layer and low Damkö hler number, and thus the flame zone is highly strained.

An important observation made by the planar flow visualization is that the blue flame zone in the near-jet region is essentially stationary despite the violent movement of the inner large-scale vortices. This indicates that the concentration field near the flame zone is insensitive to the high frequency variations in the core region. The characteristic fluctuation time associated with the axial convection of the large-scale structure can be estimated as $\tau_l=1/f_{c1/2}$~0.8 ms (U_j=15 m/s and z=15 mm; Table 1). The radial jet-fluid mass ejection must need even shorter time compared to τ_l, to reach the flame zone from the core. If the mass ejection velocity (v_m) is assumed to be the maximum mean radial velocity component of the jet fluid (1.2 m/s; Fig. 4b) plus three times maximum rms value (1.8 m/s; Fig. 4d), the characteristic time for the radial mass ejection would be, $\tau_m = \delta_d/v_m$~0.2 ms. Here, the diffusion layer thickness (δ_d) is ~1.5 mm, since $r_{1/2}$~5.5 mm (Table 1), and the outer edge of the visible flame zone is r~7 mm. The fuel molecules must diffuse from the jet-fluid core to the flame zone. By using the diffusion coefficient of methane at 1500K (D~0.7 cm^2/s) the characteristic diffusion time would be, $\tau_d=(\delta_d)^2/D$~30 ms. The diffusion process requires an order of magnitude longer time than the jet-fluid core fluctuations. Thus, there is not enough time to re-establish the concentration field in response to variations in the core and the flame zone location remains stationary. Therefore, the radial mass ejection or the large-scale vortex itself can reach the flame zone location without causing significant disturbances in the concentration field, and thus, the diffusion flame is

locally quenched by simply displacing the stoichiometric fuel-air mass flux field with nearly-pure fuel. This condition is eased downstream as the convective velocities decrease and the flame zone shifts radially away from the jet-fluid core. As a result, τ_l would increase faster than the increase in τ_d. Therefore, the local extinction occurs only in the mid-range of the near-jet region ($10<z<60$ mm).

CONCLUSIONS

The Mie scattering and LDV measurements in the near-field region of methane/air coflow turbulent jet diffusion flames provided a physical insight into the local extinction and subsequent lifting phenomena. The diffusion process needs at least an order of magnitude longer time compared to the concentration fluctuation time associated with the large-scale vortices in the core region and the radial jet-fluid mass ejection. As a result, the flame zone location is insensitive to the high-frequency inner fluctuation, and the fuel packets can reach the already strained flame zone and locally extinguish it. Due to the differences in the zone average velocities between the jet and external fluids, highly-distorted turbulent structures are created in the vicinity of the flame zone. Further, unconditioned quantities must be retrieved from the unconditioned pdf, rather than taking weighted averages from conditioned quantities and the intermittency.

ACKNOWLEDGEMENT

This work was supported by the U.S. Air Force, Wright Laboratory, Aero Propulsion and Power Directorate, Ohio, under Contract No. F33615-87-C-2767. Special appreciation is given to Drs. W.M. Roquemore (AF Technical Monitor) and D.R. Ballal for their support and helpful comments, Prof. T. Takeno for stimulating discussions, Messrs. W.J. Schmoll, G.L. Switzer, D.D. Trump, and B. Sarka for their assistance in conducting experiments.

REFERENCES

1. Takahashi, F., and Schmoll, W.J.: *Twenty-Third Symposium (International) on Combustion*, p.677, The Combustion Institute, 1991.
2. Takahashi, F., Mizomoto, M., Ikai, S., and Futaki, N.: *Twentieth Symposium (International) on Combustion*, p.295, The Combustion Institute, 1984.
3. Coats, C.M., and Zhao, H.: *Twenty-Second Symposium (International) on Combustion*, p.685, The Combustion Institute, 1989.
4. Vranos, A., Taback, E.D., and Shipman, C.W.: *Combust. Flame* 12, 253 (1968).
5. Takeno, T., and Kotani, Y.: *Acta Astronaut.* 2, 999 (1975).
6. Hall, L., Horch, K., and Günther, R.: *Brennst. Wärme Kraft* 32, 26 (1980).
7. Takahashi, F., Mizomoto, M., Ikai, S., and Tsuruyama, K.: *Stability Limits of Hydrogen/Air Coflow Jet Diffusion Flames*. AIAA Paper No. 90-0034, 1990.
8. Shekarchi, S., Savas, Ö, and Gollahalli, S.R.: *Combust. Flame* 73, 221 (1988).
9. Eickhoff, H., Lenze, B., and Leuckel, W.: *Twentieth Symposium (International) on Combustion*, p.311, The Combustion Institute, 1985.
10. Chen,T.H., and Goss, L.P.: *Combust. Sci. Technol.* 79, 311 (1991).
11. Takahashi, F., Schmoll, W.J., and Vangsness, M.D. 1990: *Effects of swirl on the stability and turbulent structure of jet diffusion flames*. AIAA Paper No. 90-0036.
12. Roquemore, W.M., Chen, L.-D., Goss, L.P., and Lynn, W.F.: *Turbulent Reactive Flows* (R. Borghi and S.N.B. Murthy, Ed.), p.49, Springer-Verlag, 1989.
13. Williams, F.A.: *Combustion Theory*, 2nd ed., Benjamin/Cummings, 1985.
14. Peters, N.: *Twenty-First Symposium (International) on Combustion*, p.1231, The Combustion Institute, 1988.
15. Bilger, R.W.: *Twenty-Second Symposium (International) on Combustion*, p.475, The Combustion Institute, 1989.
16. Peters, N., and Williams, F.A.: *AIAA J.* 21, 423 (1983).

17. Byggstøyl, S., and Magnussen, B.F.: *Turbulent Shear Flow* 4 (L.J.S. Bradbury et al. Eds.), p381, Springer, 1985.

18. Broadwell, J.E., Dahm, W.J.A., and Mungal, M.G.: *Twentieth Symposium (International) on Combustion*, p.303, The Combustion Institute, 1984.

19. Dahm, W.J.A., and Dibble, R.W.: *Twenty-Second Symposium (International) on Combustion*, p.801, The Combustion Institute, 1989.

20. Miake-Lye, R.C., and Hammer, J.A.: *Twenty-Second Symposium (International) on Combustion*, p.817, The Combustion Institute, 1989.

21. Pitts, W.M.: *Twenty-Second Symposium (International) on Combustion*, p.809, The Combustion Institute, 1989.

22. Pitts, W.M.: *Twenty-Third Symposium (International) on Combustion*, p.661, The Combustion Institute, 1991.

23. Vilimpoc, V., and Goss, L.P.: *Twenty-Second Symposium (International) on Combustion*, p.1907, The Combustion Institute, 1989.

24. Roquemore, W.M., Goss, L.P., Lynn, W.F., and Chen, L.-D.: Structure of Jet Diffusion Flames. Paper presented at the Central States/The Combustion Institute Meeting, May 1987.

25. Takahashi, F., Mizomoto, M., and Ikai, S.: *Combust. Flame* 48, 85 (1982).

26. Mungal, M.G., and O'Neil, J.M.: *Combust. Flame* 78, 377 (1989).

27. Broadwell, J.E., and Mungal, M.G.: *Phys. Fluids* A 3, 1193 (1991).

28. Libby, P.A., and Williams, F.A.: Turbulent Reacting Flows, p.21, Springer-Verlag, 1980.

29. Libby, P.A., Chigier, N., and LaRue, J.C.: *Prog. Energy Combust. Sci.* 8, 203 (1982).

30. Dibble, R.W., Hartman, V., Schefer, R.W., and Kollman, W.: *Exp. Fluids* 5, 103 (1987).

31. Tsuji, H.: *Prog. Energy Combust. Sci.* 8, 93 (1982).

32. Chelliah, H.K., Law, C.K., Ueda, T., Smooke, M.D., and Williams, F.A.: *Twenty-Third Symposium (International) on Combustion*, The Combustion Institute, in press, 1991.

Table 1 Characteristics of Large Structures

U_j (m/s)	z (mm)	$r_{1/2}$ (mm)	$U_{1/2}$ (m/s)	$f_{c1/2}$ (Hz)	l (mm)
6	15	5.0	5.1	704	3.6
10	15	5.3	7.0	1100	3.2
15	5	5.5	3.6[a,b]	1130	1.6
15	15	5.5	9.1	1330	3.4
15	25	5.3	12.1[a]	1230	4.9
15	50	5.4	---	1190	---

[a] Ref. [1]
[b] Extrapolated

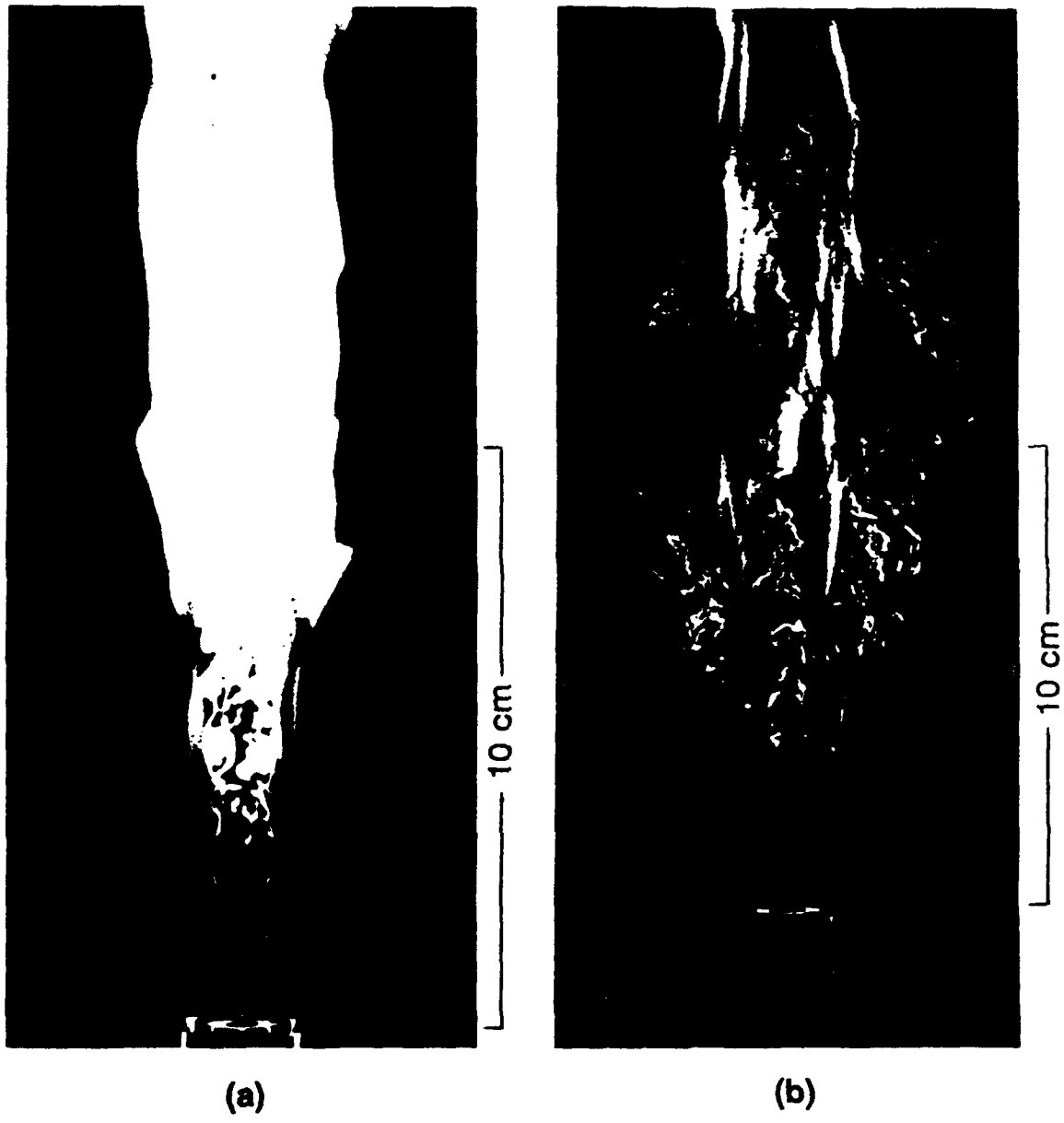

Figure 1 Instantaneous (10 ns) laser-sheet reactive Mie scattering images superimposed with time-exposure direct photographs of methane/air coflow jet diffusion flames. Scattering particles (TiO_2) were formed from seeded $TiCl_4$ and water vapor in the combustion products. U_a=3 m/s. (a) Jet seed, exposure 1/60 s, U_j=6 m/s (Re_j=3380). (b) Jet and annulus air seed, exposure 1/250 s, U_j=10 m/s (Re_j=5630). (c) Jet seed, exposure 1/60 s, U_j=15 m/s (Re_j=8460). (d) Jet seed, exposure 1/125 s, U_j=15 m/s.

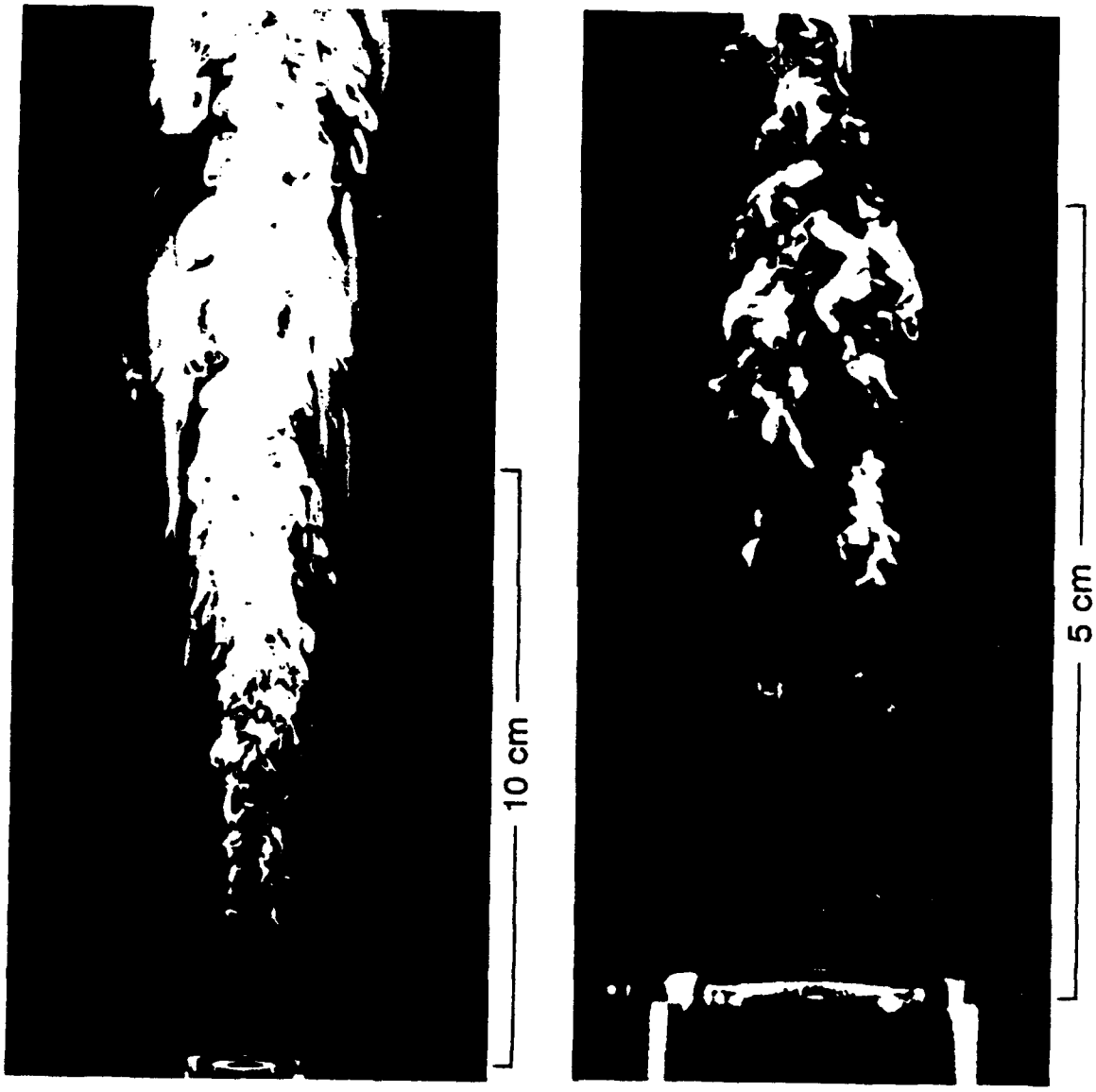

Figure 1. Continued

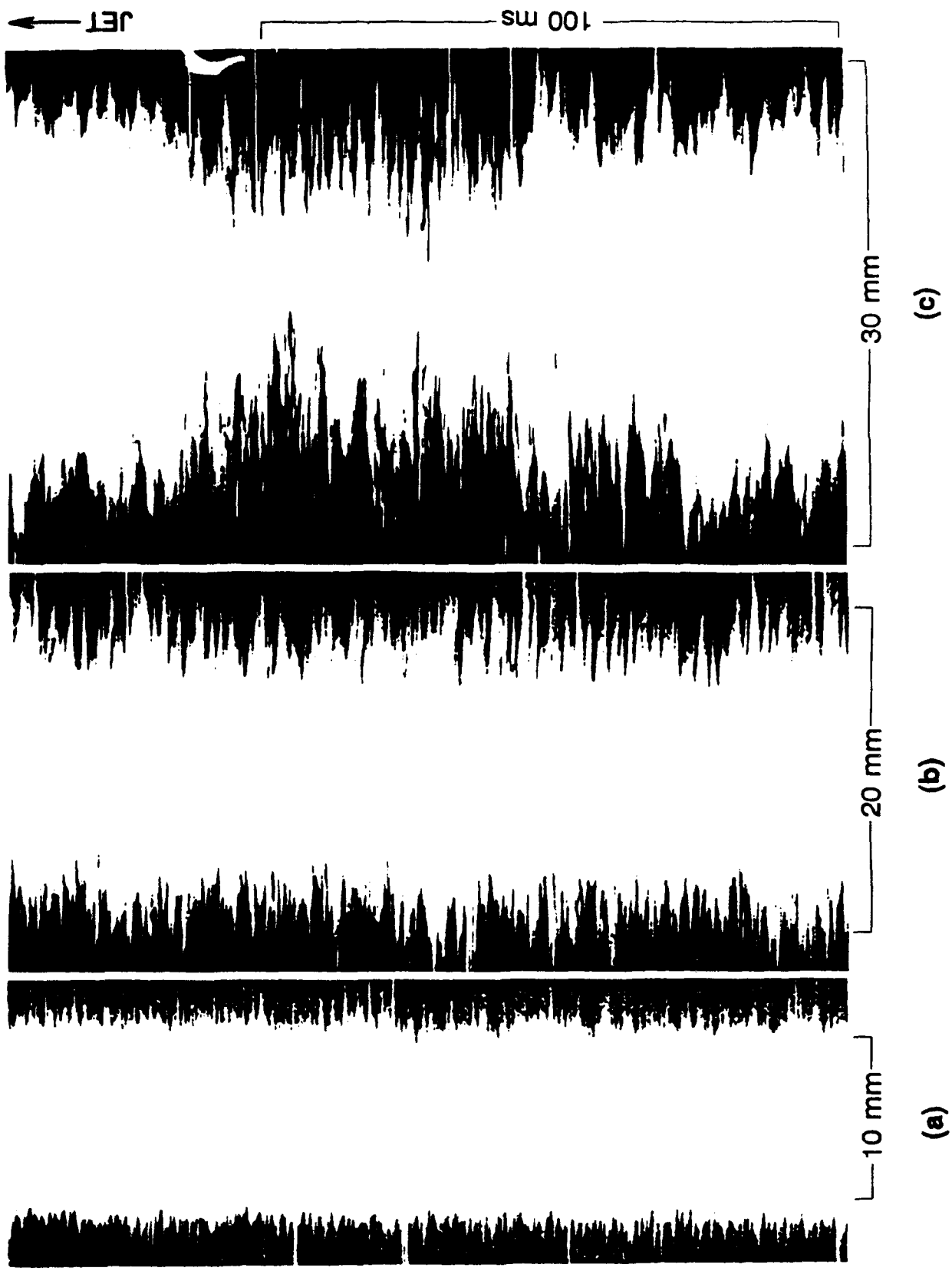

Figure 2 Real-time traces of Mie scattering intensities along a line in methane/air coflow jet diffusion flames. Scattering particles (TiO_2) were preformed from $TiCl_4$ and water vapor prior to the fuel tube inlet. U_j=15 m/s, U_a=3 m/s. (a) z=15 mm, (b) z=50 mm, (c) z=100 mm.

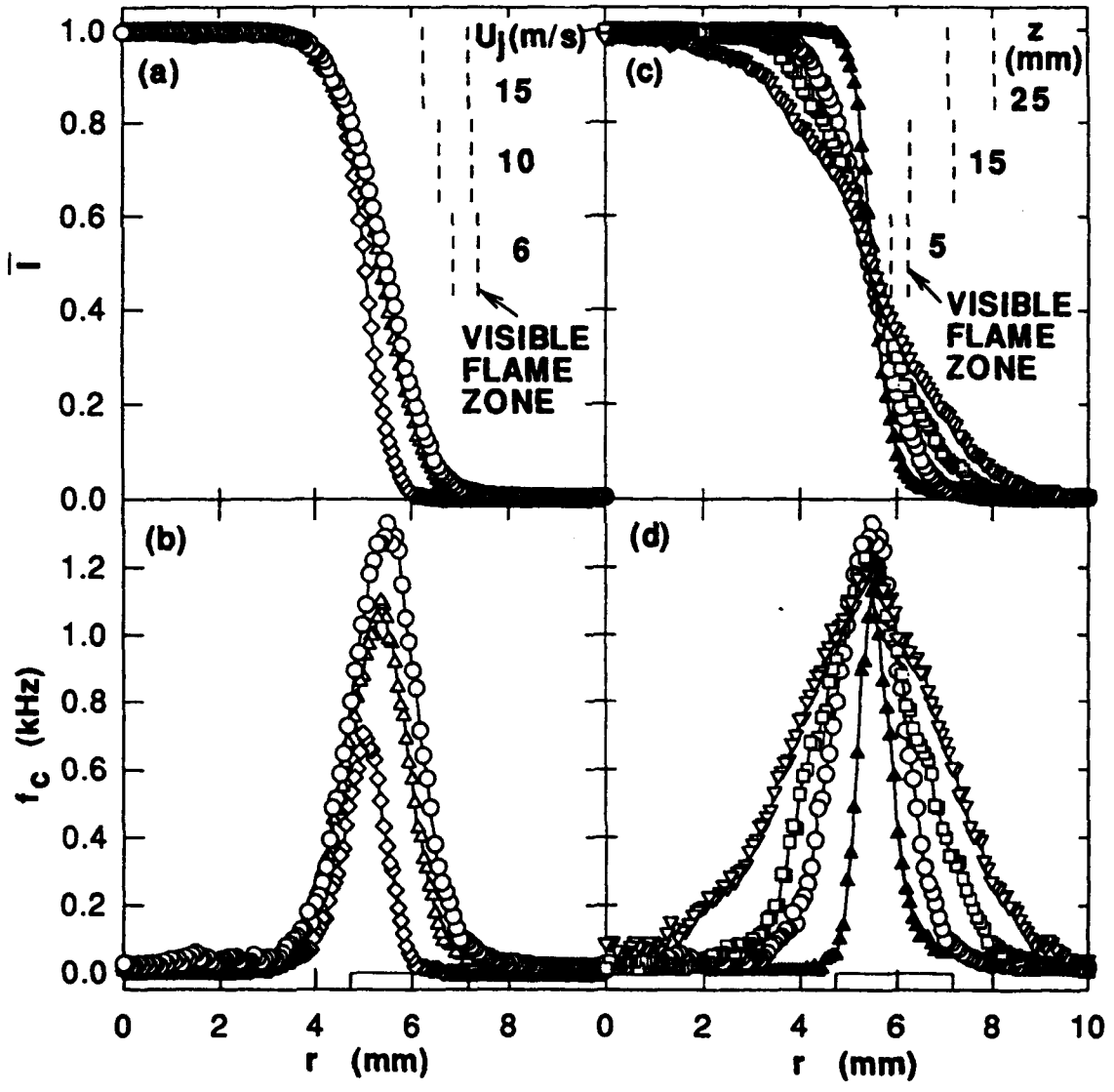

Figure 3 Radial profiles of the intermittency and crossing frequency of the jet fluid in a methane/air coflow jet diffusion flame. U_a=3 m/s. (a)(b) z=15 mm. ◇, U_j=6 m/s; △, U_j=10 m/s; ○, U_j=15 m/s. (c)(d) U_j=15 m/s. ▲, z=5 mm; ○, z=15 mm; □, z=25 mm; ▽, z=50 mm.

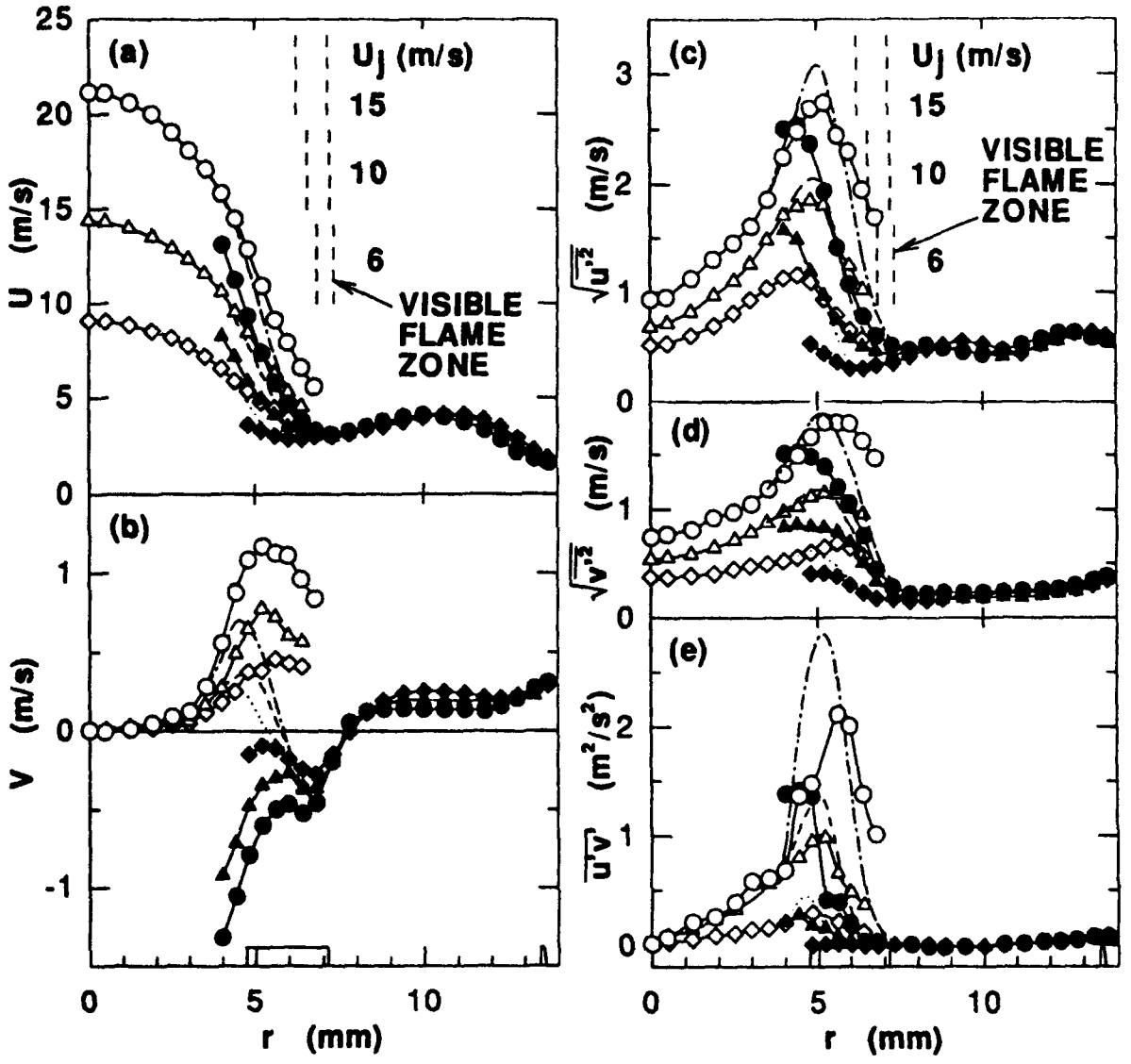

Figure 4 Radial profiles of (a) the mean axial and (b) radial velocity components, (c) the root-mean-square fluctuation velocity of axial and (d) radial components, and (e) Reynolds shear stress in methane/air coflow jet diffusion flames. U_a=3 m/s. z=15 mm. ◇ ◆, U_j=6 m/s ; △ ▲, U_j=10 m/s ; ○ ●, U_j=15 m/s. Open: conditioned on jet seed; filled: conditioned on annulus-air seed. ·····, – – –, –·–·–, Unconditioned.

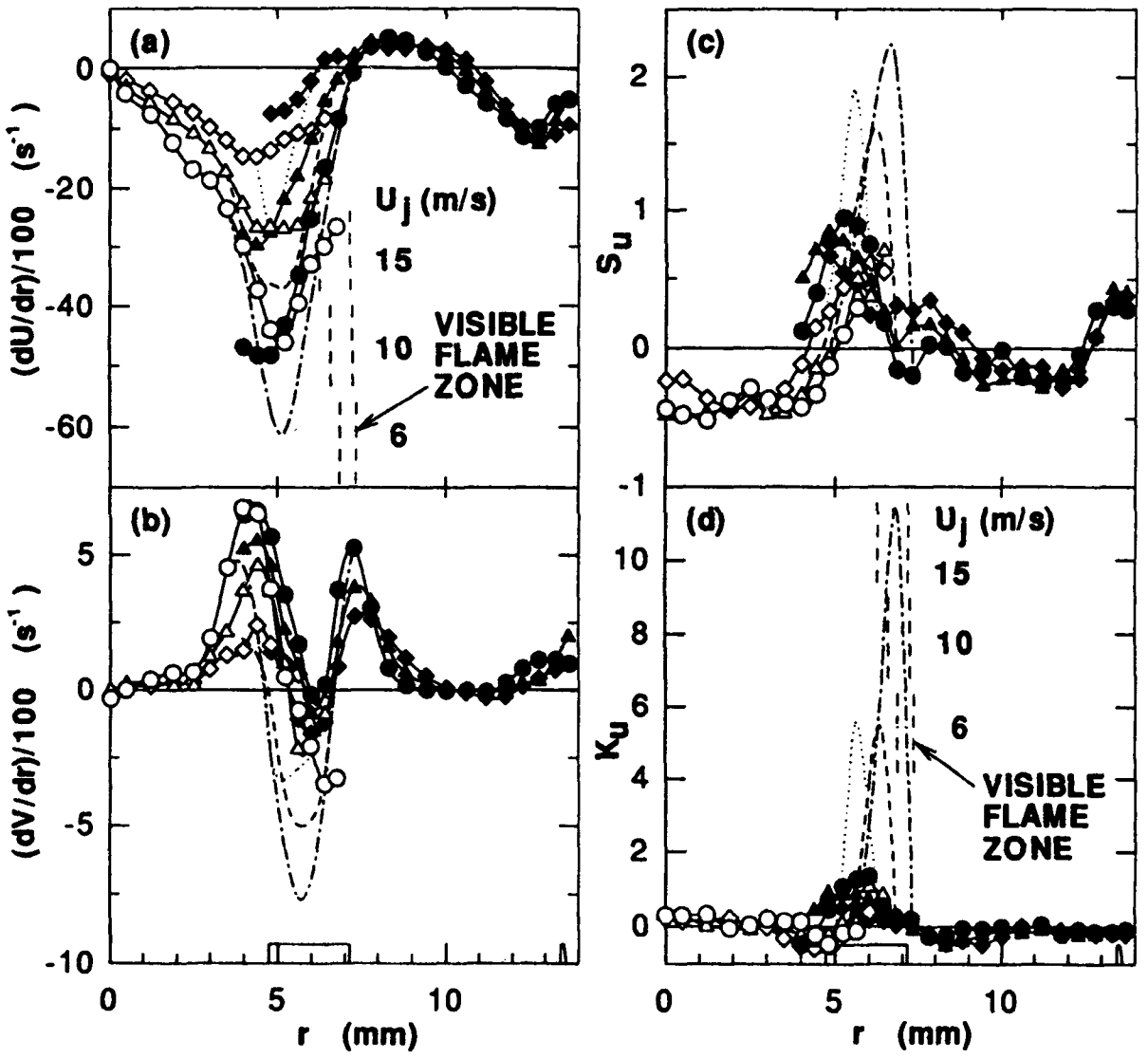

Figure 5 Radial profiles of (a) the gradients of the mean axial and (b) radial velocity components and (c) skewness and (d) kurtosis of the axial velocity component in methane/air coflow jet diffusion flames. U_a=3 m/s, z=15 mm. ◇ ◆, U_j=6 m/s ; △ ▲, U_j=10 m/s ; ○ ●, U_j=15 m/s. Open: conditioned on jet seed; filled: conditioned on annulus-air seed. ·····, – – –, –·–·–, Unconditioned.

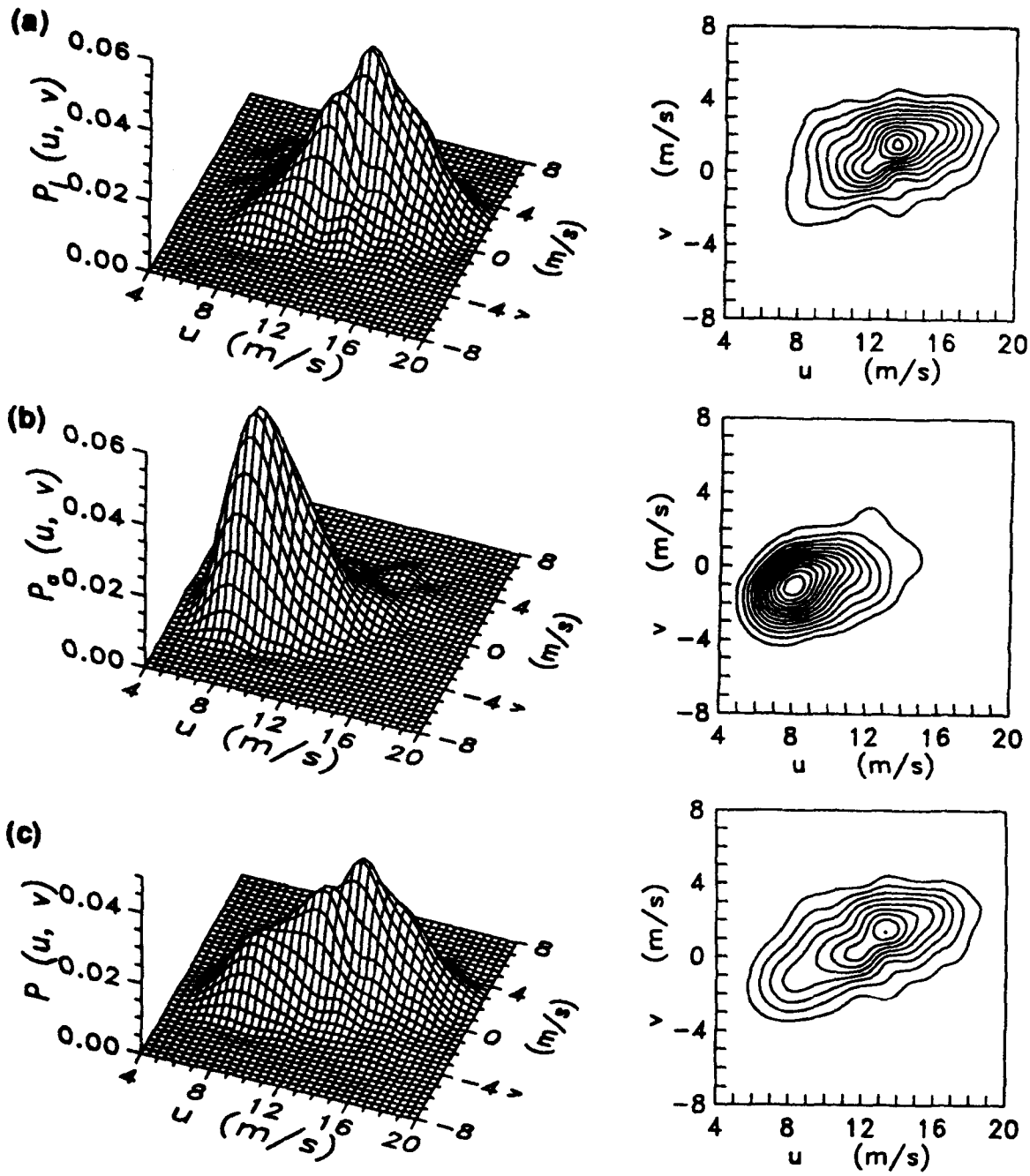

Figure 6 Joint pdf's of the axial and radial velocity components in a methane/air coflow jet diffusion flame and their contour plots. U_j=15 m/s, U_a=3 m/s, z=15 mm, r=4.8 mm. $\bar{I}$ = 0.77. Contour interval: every 0.004 from 0.004. (a) Conditioned on jet seed, (b) conditioned on annulus-air seed, (c) unconditioned.

APPENDIX N

HEAT TRANSFER IN HIGH TURBULENCE FLOWS-A 2D PLANAR WALL JET

by

R. B. Rivir, W. T. Troha
Wright Laboratories, Wright-Patterson Air Force Base, Ohio

W. A. Eckerle
Cummins Engine Company Inc., Columbus, Indiana

W. J. Schmoll
University of Dayton, Dayton, Ohio

Paper #8
AGARD 80th PEP Symposium
Heat Transfer and Colling in Gas Turbines
Antalya, Turkey
12-16 October 1992

HEAT TRANSFER IN HIGH TURBULENCE FLOWS - A 2D PLANAR WALL JET

R. B. Rivir
W. T. Troha
Aero Propulsion and Power Directorate, Wright Laboratories
Wright Patterson Air Force Base, Ohio, 45433-6563

W. A. Eckerle
Cummins Engine Company Inc.
Columbus, Indiana

W. J. Schmoll
University of Dayton Research Institute
Dayton, Ohio

SUMMARY

The accurate prediction of turbine heat transfer remains beyond our current capabilities. To investigate this condition, non conventional turbulence generation techniques have been employed to explore the impact of high turbulence or unsteadiness on heat transfer. The heat transfer from a 2D planar wall jet will be compared with an axi-symmetric wall jet with twice the turbulence scale and more turbulent kinetic energy - with an increased heat transfer shown by the planar configuration. The resulting comparisons of wall jet augmented heat transfer to engine turbine blade heat transfer is quite favorable.

LIST OF SYMBOLS

A	constant
C_p	specific heat at constant pressure, W-s/kg-°C
h	heat transfer coefficient, W/m²-°C
h'	nozzle height, cm
l	nozzle length, cm
Pr	Prandtl number = $\mu C_p/k$
R_{x}	Reynolds number = $\rho U x/\mu$, $\rho U \theta/\mu$
S_t	Stanton number = $h/(U\rho C_p)$
S_{t_o}	Stanton number for fully turbulent flat plate
T_u	x component of turbulence intensity = u'/ U
U	local x mean velocity, m/s
U_{max}	maximum mean x velocity, m/s
u	rms fluctuating component of x velocity, m/s
u'	non dimensional velocity defined by equation 1
V	local y mean velocity, m/s
v	rms fluctuating component of y velocity, m/s
W	local w mean velocity, m/s
w	rms fluctuating component of w velocity, m/s
w	span location from jet centerline, cm
x	distance from wall jet nozzle exit, cm
Y_{max}	y distance from wall to U_{max}, cm
y	y distance from wall, cm
y'	non dimensional distance from wall, equation 1
δ	boundary layer thickness, cm
Λ	integral scale of turbulence, cm
θ	momentum thickness, cm

1. INTRODUCTION

The near wall turbulence level for a fully turbulent flat plate boundary layer is typically 10-12% in the flow direction after the boundary layer has developed some age. This maximum occurs in buffer or transition region between the linear and the log law of the wall regions of the boundary layer. The turbulence then falls off to the free stream value. Film cooling flows exhibit similar characteristics with a maximum of 15-20% occurring farther away from the wall (Rivir et al. 1987) in the profile, as the blowing ratio increases, and then decays to the free stream value. Until very recently heat transfer and film cooling data for turbine designs were obtained with very low values of free stream turbulence (0.5-2%). The entering free stream turbulence level for a turbine rotor, although not comprehensively documented under engine conditions, has been measured by Binder et al. (1985) for cold flow due to the stator wakes. The level of turbulence was shown to approach 20% on the pressure surface and 10% on the suction surface. The issue to be addressed is what happens to the heat transfer when there is a 10-20% unsteadiness level in the free stream which then interacts with the naturally occurring wall or film cooling generated levels of 10-20%.

Under estimating the turbine blade surface temperature by 10% can result in a significant loss in lifetime for that component. This kind of accuracy in heat transfer can only be approached for very simple, well behaved, 2D boundary layers. Current heat transfer data bases for turbine blades and vanes are

obtained from experiments which include flat plates, linear cascades, large scale rotating cascades, light piston tubes, blow down tunnels, shock tubes, and engines. The fully turbulent flat plate boundary layer can be accurately (with in a few %) predicted by the empirical relationship of Kays and Crawford (1980), or 2D boundary layer codes such as STAN5 or Texstan, which have evolved from the Patankar Spaulding formulation. These codes typically invoke mixing length, κε, or other forms of turbulence models. When the free stream turbulence levels were increased to 4-6% by the use of up stream grids, systematic increases up to 10% above the predicted fully turbulent values of heat transfer were observed by Blair (1981). The addition of pressure gradient or acceleration combined with the 4-6% turbulence resulted in a further underestimate in the prediction of the heat transfer of 2D boundary layer codes, such as STAN5, by 30% (MacArthur 1985), as illustrated in Figure 1. Transition length from laminar to turbulent heat transfer is also slightly under predicted in length with Reynolds number by these 2D codes, again as illustrated in Figure 1.

In linear cascades, heat transfer measurements predicted with similar 2D codes show that transition and transition length are poorly predicted on both suction and pressure surfaces. In addition the absolute level of heat transfer on the pressure surface was under estimated by 50%. Figure 2 from Wittig et al. (1985) has been annotated to indicate the typical discrepancies with calculated values of heat transfer for the linear cascades. This is a combustion driven tunnel which uses grid generated turbulence to simulate wakes of the up stream stator. These calculations use a low Reynolds number κε turbulence model which is known to over predict heat transfer for some cases. Consigny and Richards (1982) tend to show the resulting VKI linear cascade effort heat transfer results, along with many others, to be bounded between the fully turbulent flat plate and the laminar flat plate case - based on the chord and the cascade exit Reynolds number. Locally these heat transfer measurements can exceed the fully turbulent flat plate values as indicated by Arts et al. (1992) in the same facility. The heat transfer in linear cascades is reasonably well predicted by the simple laminar and fully turbulent flat plate for many but not all cases. The additional complexity of an annular cascade does not appreciably affect the heat transfer prediction discrepancies.

The next level of complexity, addition of rotation and upstream stators, becomes more difficult to predict and explain the observed heat transfer due to the interaction of several unsteady flows are added to low levels of up stream turbulence. These experiments include transient experiments such as shock tubes (Calspan) and light piston tubes (MIT, Oxford, and RAE Pystock). Bayley and Priddy(1981) showed an increase of 2 to 4 times over steady state heat transfer values when a rotating bar investigated frequency effect (at a constant scale of turbulence) on the steady heat transfer value in a linear cascade. Rae et al., 1986 (Calspan) presents predictions for both a 2D and a 3D vane/rotor combination with an inlet turbulence of 5% of an unknown length scale. The 3D case is particularly difficult to rationalize with a 100% discrepancy on the vane surfaces and near experimental values on the rotor. In a low speed, large scale, multi-stage experiment, Sharma, et al. (1992) has observed excellent predictions of heat transfer on the rotor and then a large under prediction on the 2nd stator. This observation exceeds the fully turbulent flat plate value of heat transfer, as illustrated in Figure 3. Additional unpredicted behavior that is not captured by 2D or 3D Euler or Navier Stokes solvers are observed at the stagnation point as well as on the pressure and suction surfaces. Transition and transition length again are not predictable. There are numerous cases where the heat transfer exceeds the steady flow fully turbulent flat plate values such as Blair (1981), Bayley and Priddy (1981), Wittig et al. (1985), Rae, et al. (1986), and Sharma et al. (1992).

The examination of engine data, which now includes the combustor upstream, shows observed increases over the fully turbulent flat plate from over 3 times on the pressure and stagnation surfaces to 2 times on the suction surfaces, as shown in figure 4. Non steady Navier-Stokes calculations are now being made for these flows including the effects of the stator on the rotor for multi-stage geometries. Although these calculations show improvements they fail to come close to engine results. It is these cases which exhibit heat transfer above the fully turbulent flat plate predictions which are of interest for the non conventional turbulence or unsteady flow evaluation.

There have been several efforts underway to explore non conventional turbulence generators, and to establish the relationships between heat transfer, turbulence, turbulence length scale and the higher levels of heat transfer that occur in the actual engine. These turbulence generators have included free jets, wall jets, jets in cross flow, rotating bars, moving walls with grids, and blown grids. Grid generated turbulence has been able to produce only 6-8% levels in the final period of decay at scale sizes comparable to the boundary layer thickness or the blade passage size. In addition to the axial turbulence level, the appropriate nonisotropic turbulence decay rate (du'/dx) and turbulence scales (Λ/δ) are issues which have not been satisfactorily resolved in attempts to simulate the unsteady effects in the turbine hot section. A number of non conventional turbulence generators have been investigated over the years to achieve high turbulence levels at appropriate scales. In 1985, Maciejewski, Moffat, Han, and Rivir began looking at the importance of higher free stream turbulence levels. These turbulence levels were comparable or greater than the near wall levels. Moffat and Maciejewski investigated turbulence levels of 26-48% at Reynolds numbers of $2\text{-}5\text{x}10^4$ with a flat plate in a free axi-symmetric jet. This represented an augmentation of the fully turbulent flat plate heat transfer of 350%. Han, Rivir and later others (MacMullin et al. 1986) investigated turbulence levels of 2-20% with axi-symmetric and planar wall jets at Reynolds numbers of $1\text{x}10^5$ to $8\text{x}10^4$. The resulting heat transfer was observed to be up to 200% of the fully turbulent flat plate. McCarthy (1989) used a box with one wall a constant heat flux surface and the same 2D planar free jet which had been used in the wall jet studies. This resulted in an augmentation of 20 - 60% in the heat transfer. Young et al. (1991) used blown grids to generate turbulence levels of 5-20%. Ames (1990) used wall jets and jets in cross flow to simulate a combustor at turbulence levels of 5-20%. This resulted in a 30% augmentation in heat transfer over the fully turbulent level. The results of these efforts are compared in Figure 5. The heat transfer results have been shown to be similar to engine results even though the simulations provided by these alternate sources are not direct. Figure 4 shows the axi-symmetric and planar wall jet heat transfer results in engine coordinates.

2. DESCRIPTION OF THE 2D WALL JET EXPERIMENT

This effort presents three component LV measurements and begins to address the scale effect for a non conventional turbulence generator with a planar wall jet. An axi-symmetric wall jet which was used previously for high turbulence heat transfer investigations is described in MacMullin et al. (1987).

The same constant heat flux heat transfer surface was employed as described in the 1987 work with new foil and thermocouples. The axi-symmetric 20.32 cm ASME nozzle was replaced with a short radius ASME planar nozzle; 6.67 by 49.53 cm (l/h´=7.43) with a 0.64 cm lip thickness. In the settling chamber a 20/1 length to diameter flow straightener, with 75 mesh screens on either side, was added to reduce the exit core flow axial turbulence level from 5% in the 1987 work to 2%. A three component TSI off axis LV and traverse have been employed to obtain velocity, turbulence, and Reynolds stress profiles in the present work. A half angle of 15 degrees was required between component beams for other experiments with limited optical access. This reduces the accuracy of all components slightly over the recommended 20 degree half angle. The LV beam position accuracy was ±.00025 cm. The optics used produced a measurement ellipsoid of 25 microns diameter by 3 mm in length in the span wise direction. The axial turbulence scales are the order of several cm and the vertical scales the order of mm in the near wall regions. Nearly all the turbulent energy is below 3,000 Hertz for these flows, so the spatial resolution of the measurement volume is quite good except for the span wise direction. The LV measurements were made with-in a nominal coincidence window of 10 micro seconds. A small (10 degree) angle to the heat transfer surface was employed to allow wall measurements to be obtained. The LV axial and vertical mean and turbulent measurements were checked against single element hot wire measurements in the axi-symmetric wall jet and in the TSI 0.64 cm diameter calibration jet. The mean velocities agreed quite well. The u´ measurement in the calibrator free jet fell with in ±0.5 to 1% of the hot wire up to turbulence intensities of 10%; and were lower than the hot wire by 2% for turbulence intensities of 10 to 20%.

Single element hot wire measurements were employed to obtain the axial and vertical turbulence scales using a HP 3562 dynamic signal analyzer which provided the frequency spectrum and then inverted the spectrum with a FFT to provide the auto correlation function which was normalized and multiplied by the local mean velocity to provide the integral scale. This technique was compared against a direct auto correlation which was used in our 1987 axi-symmetric wall jet work and the 32,000 sample spectrum, an FFT, and an auto correlation calculation of Ames (1990) with favorable results - all three measurements gave the same value within 30% at the same time on the same flow. The vertical scale was obtained by rotating the single element wire to the span wise direction, with out moving the traverse, and repeating the measurement. The vertical scale measurement is sensitive to both the vertical and the span wise components. The vertical scale implication then needs to be considered to be representative of both near the wall rather than the vertical component alone. The measurements presented in this paper will be for the short radius ASME planar nozzle.

Heat transfer measurements were made at 7 stations with the same techniqueues described in MacMullin et al. (1987) axi-symmetric wall jet work. The x/h´ locations for the planar wall jet measurements become 7.69, 15.24, 26.28, 30.10, 37.48, 44.95 , and 52.95.

3. PLANAR WALL JET RESULTS

The original purpose of this planar wall jet effort was to provide a 2D flow with a smaller scale at the same x Reynolds numbers as the axial wall jet. Although the width to height dimension of this wall jet (7.43) make it a marginal 2D source by planar wall jet standards (Launder and Rodi,1981), there are two significant observations applicable to all planar wall jet measurements which should be made. The Reynolds number of this wall jet was chosen to provide heat transfer measurements in the x Reynolds number range for turbine blades. This places these measurements an order of magnitude above wall jet studies in the literature. The velocity profiles for these measurements (and also those of the axi-symmetric wall jet) are all locally similar in velocity profiles for all reported heat transfer and velocity profiles. These centerline velocity profiles give an axial jet decay which approaches that of Wygnasiki et al. (1991) at his highest Reynolds number flow of 19,000. These measurements then imply a high Reynolds number limit for wall jet spread which is independent of wall jet pressure ratio for this intermediate range of x/h´. Secondly, these mean velocity profiles have been analyzed in law of the wall coordinates by Narayanan et al. 1992) with the assumption of a constant Karman constant in the law of the wall relation:

$$u^+ = A + 2.44 \ln y^+ \qquad (1)$$

This relation was shown to be valid for all fully developed planar wall jets with the constant A dependent only on the axial turbulence in a simple linear relationship. This same relationship was also observed to be valid for a turbulent flat plate boundary layer when the maximum near wall axial turbulence intensity is used for the turbulence intensity. The LV wall jet profiles presented in this paper were used to obtain this result.

The center line velocity and velocity fluctuation profiles are presented in Figures 7 and 8 at each heat transfer measurement station. The velocity profiles are locally similar as previously pointed out, but are otherwise as one would expect for a planar wall jet. The rms fluctuations are nearly constant across the wall layer in the axial direction. This contrasts to profiles at much larger x/h´ locations normally quoted by planar wall jet efforts in which the shear layer has eroded the wall layer. A law of the wall plot at x/h´ = 52.95 is shown in figure 9, where the log region extending over a 1,000. This extremely large log region made an accurate assessment of the constants in the law of the wall region in contrast to regions of 50-100 in other planar wall jet studies. The span wise distribution of x hot wire measured velocities and rms velocities are shown in Figure 10.

The normalized Reynolds stresses $u'v'$, $v'w'$, $u'w'$, u'^2, v'^2, and w'^2, are shown in Figure 11. The u´ and v´ components are well behaved, however the span wise components of w´ all take on very large values as the wall is approached. The span wise components were shown to be very significant contributors to increases in shear stress in Johnson and Johnston (1989), and increases are to be expected - particularly for a free boundary. We are currently attempting to check the span wise wall shear directly. A few of the last two near wall w´ component data points have been omitted until further checks can be performed. The u´v´ component is initially negative and then goes through 0 at about 60% of y_{max}. It then goes and remains positive as observed in other planar wall jets (Launder and Rodi,1981) investigations.

The integral turbulence scales on the wall jet centerline, for axial scales and for the lateral or vertical scales at y_{max} are shown in Figure 13. A boundary layer traverse of the axial scale is shown at x/h´ = 26.28 in Figure 14.
The scale is sensitive to the mean velocity and the facility

compressor operation which results in mean velocity fluctuations of 2%. Four to six scale measurements were made for each data point for both span and centerline profiles to assure reproducibility in the scale measurements.

Moffat and Maciejewski (1989) have observed a linear relationship of h, the heat transfer coefficient, with u'. These observations were also made in this investigation, with the addition that a family of these relationships, not just a single one were observed. This leads to the conclusion that other functional relationships are involved in the relationship for h. The ratio of turbulence scale to boundary layer thickness has been suggested by several investigators with a functional dependence proposed by Simonich and Bradshaw (1978), and this later modified by Blair (1981) for 2D flat plate boundary layers such that:

$$S_t - S_w / S_\infty = T_u * \alpha * \beta \qquad (2)$$

$$\alpha = (\Lambda/\delta + 2)$$

$$\beta = (3e^{-Re_\theta/400} + 1)$$

where S_t is the local x Stanton number and S_∞ is the fully turbulent local Stanton number from the Kays and Crawford relationship. The heat transfer at a 20% turbulence level is shown in Figure 15. The planar jet shows similar behavior to the axi-symmetric wall jet heat transfer, but is slightly higher at similar turbulence intensities. Figure 4 shows schematic wall jet heat transfer superimposed on engine data, indicating similar levels of heat transfer and dependence with Reynolds number.

The scale size ratio of y_{max} 3D / y_{max} planar is 2. Scales have also been measured for the axi-symmetric 3D jet, and this is considered a reasonable comparison of the two scales. The normalized turbulent kinetic energy of the 3D wall jet is .075, and for the planar wall jet (3 component LV measurements) is 053 at a x/D, x/h' of 8.63 and 7.8, respectively. The normalized heat transfer and scale dependence of equation 2 is shown in Figure 16. Here we see an increased heat transfer for the planar wall jet even though it has less turbulent kinetic energy at similar Reynolds numbers. The lack of collapse of the data would indicate that the functional dependence is not the appropriate relationship.

4. SUMMARY

There remains a very strong need to characterize the inlet flow to the turbine quantitatively in terms of three components of spatial and temporal velocities, the magnitudes of spatial and temporal temperature gradients, as well as the decay characteristics of these fluctuations. Typical gas turbine combustor flows are far from classical isotropic turbulence. The non conventional turbulence sources, as well as 3D Navier Stokes solvers are showing magnitudes of some effects such as T_u and scale but simulations and computations clearly require additional definition.

REFERENCES

1. Ames F. E., "Heat transfer with High Intensity, Large Scale Turbulence: The Flat Plate Turbulent Boundary Layer and the Cylindrical Stagnation Point," Ph.D. Dissertation, Department of Mechanical Engineering, Stanford University, Nov 1990.

2. Arts, T. and Lambert de Rouvroit, M., "Aero-Thermal Performance of a Two-Dimensional Highly Loaded Transonic Turbine Nozzle Guide Vane: A Test Case for Inviscid and Viscous Flow Computations," Journal of Turbomachinery, Vol. 114, pp. 147-154, January 1992.

3. Bayley, F.J. and Priddy, W.J., "Effects of Free-Stream Turbulence Intensity and Frequency on Heat Transfer to Turbine Blading," ASME Journal of Engineering for Power, Vol. 103, pp. 60-64, January 1981.

4. Binder, A., Forster, W., Kruse, H., and Rogge, H., "An Experimental Investigation Into the Effects of Wake on the Unsteady Turbine Rotor Flow," ASME Journal of Engineering for Gas Turbines and Power, Vol. 107, pp. 458-466, 1985.

5. Blair, M.F. and Werle, M.J., "Combined Influence of Free-Stream Turbulence and Favorable Pressure Gradients on Boundary Layer Transition and Heat Transfer," United Technologies Research Center, Report No. R81-914388-17, March 1981.

6. Consigny, H. and Richards, B.E., "Short Duration Measurements of Heat-Transfer Rate to a Gas Turbine Rotor Blade," ASME Journal of Engineering for Power, Vol. 104, pp. 542-551, July 1982.

7. Johnson P.L. and Johnston, J.P., "The Effects of Grid Generated Turbulence on Flat and Concave Turbulent Boundary Layers," Department of Mechanical Engineering, Stanford University, Report No. 14053, November 1989.

8. Kays, W.M. and Crawford, M.E., "Convective Heat and Mass Transfer", 2nd ed., McGraw-Hill, New York, p. 172, 1980.

9. Launder, B.E. and Rodi, W., "The Turbulent Wall Jet," Progress in Aerospace Science, Vol. 19, pp. 81-128, 1981.

10. Launder, B.E. and Rodi, W., "The Turbulent Wall Jet - Measurements and Modeling," Annual Review of Fluid Mechanics, pp. 429-458, 1983.

11. MacArthur, C.D., "Prediction of Free Stream Turbulence Effects on Boundary Layer Heat Transfer - An Evaluation of the Heat Transfer Code STAN5," Final Report on Contract F49620-82-0035, September 1983.

12. MacMullin, R., Elrod, W. and Rivir, R., "Free-Stream Turbulence From a Circular Wall Jet on a Flat Plate Heat Transfer and Boundary Layer Flow," ASME Journal of Turbomachinery, Vol 111, pp. 78-86, January 1989.

13. McCarthy, J.W., "The Effects of Free Stream Turbulence from a Slot Jet on Flat Plate Heat Transfer," Thesis Department of Mechanical Engineering, University of Dayton, July 1989.

14. Moffat, R. and Maciejewski, P.K., "Heat Transfer With Very High Free-Stream Turbulence," NASA Grant NAG3-522, Proceedings of the 1985 Turbine Engine Hot Section Technology Conference (NASA Conference Publication 2405), pp. 203-215.

15. Narayanan, M.A.B., Rivir, R. and MacArthur C.D., "Effect of High Turbulence on Wall Shear and Heat Transfer", Presented to Fifth Asian Congress of Fluid Mechanics, Asian Fluid Mechanics Committee, August 1992.

16. Rae, W.J., Taulbee, D.B., Civinskas, K.C., and Dunn, M.G., "Turbine-Stage Heat Transfer: Comparison of Short-Duration Measurements with State-of-the-Art Prediction," AIAA Paper 86-1465, AIAA/ASME/SAE/ASEE 22nd Joint Propulsion Conference, Huntsville, Alabama, June 1986.

17. Rivir, R.B., Roqumore, W.M. and McCarthy, J.W., "Visualization of Film Cooling Flows Using Laser Sheet Light," AIAA Paper 87-1914, AIAA/SAE/ASME/ASEE 23rd Joint Propulsion Conference, San Diego, CA, July 1987.

18. Sharma, O.P., Pickett, G.F. and Ni, R.H., "Assessment of Unsteady Flows in Turbines", Journal of Turbomachinery, Vol. 114, pp. 79-90, January 1992.

19. Simonich, J.C. and Bradshaw P., "Effect of Free-Stream Turbulence on Heat Transfer Through a Turbulent Boundary Layer," ASME Journal of Heat Transfer, Vol. 100, pp. 671-677.

20. Wittig, S., Schulz, A. Bauer, H.J. and Sill, K.H., "Effects of Wakes on the Heat Transfer in Gas Turbine Cascades," AGARD, CP-390, 1985.

21. Wygnanski, I., Katz, Y. and Horev, E., "On the Applicability of Various Scaling Laws to the Turbulent Wall Jet," Journal of Fluid Mechanics, Vol. 234, pp. 669-690, 1992.

22. Young, C.D., Han, J.C. Huang, Y., and Rivir, R. B., "Influence of Jet-Grid Turbulence on Flat Plate Turbulent Boundary Layer Flow and Heat Transfer," 3rd ASME-JSME Thermal Engineering Joint Conference, Reno, Nevada, March 1991.

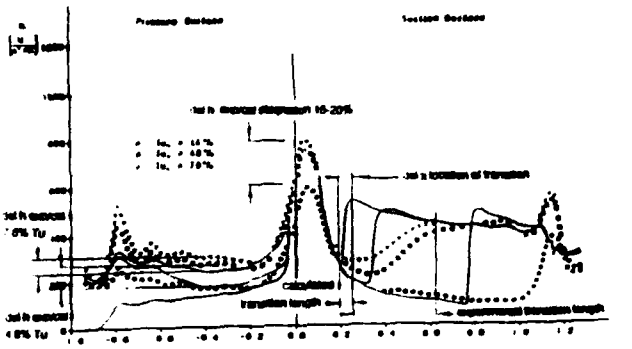

Figure 2. Linear cascade comparison of experimental calculations (Wittig, 1985)

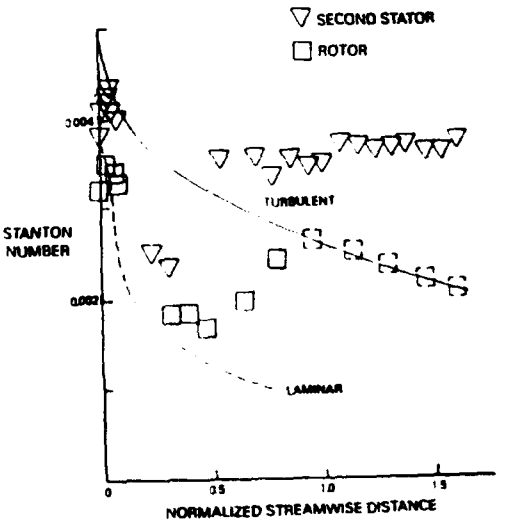

Figure 3. Large scale multi-stage rotating cascade comparison of experiment to fully turbulent flow (Sharma, et al., 1992)

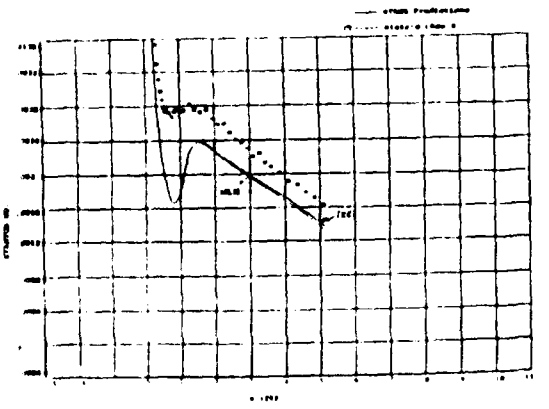

Figure 1. STAN5 calculation of flat plate Tu=4% a=7.5x10^5 (MacArthur, 1983)(Blair, 1981)

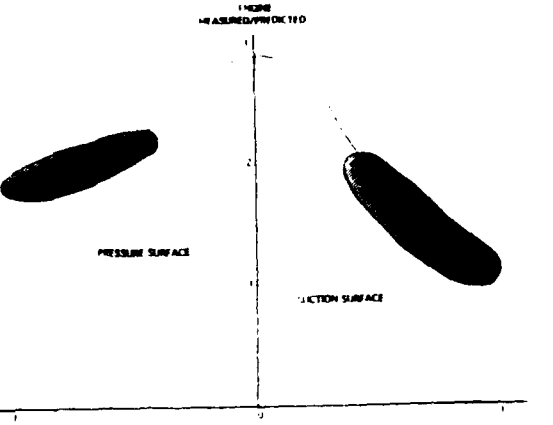

Figure 4. The measured/predicted heat transfer for turbine engine blades and vanes

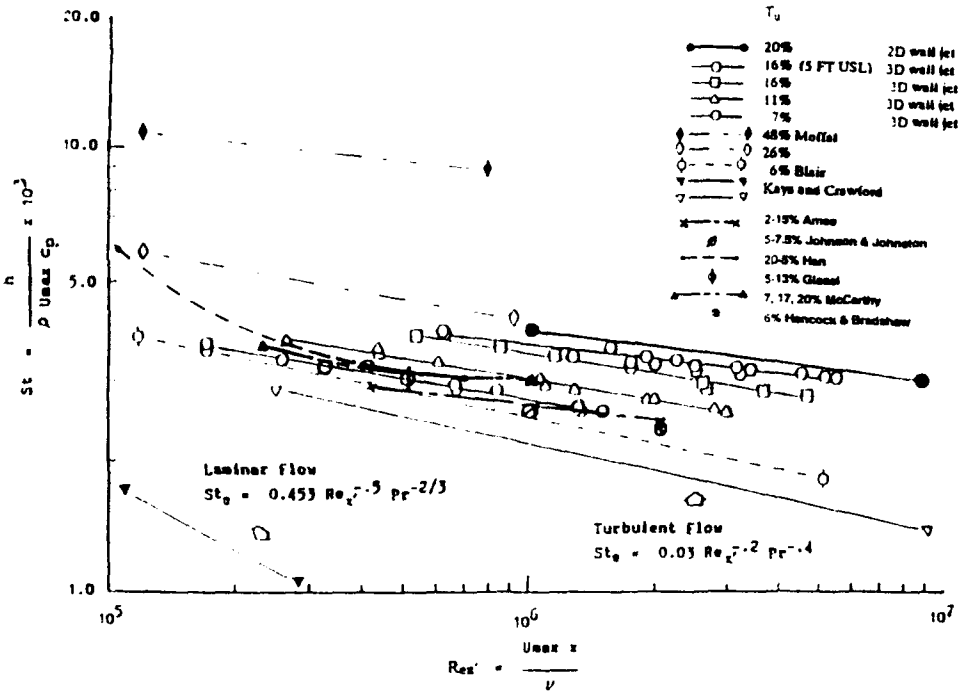

Figure 5. Heat transfer characteristics for non standard turbulence generators

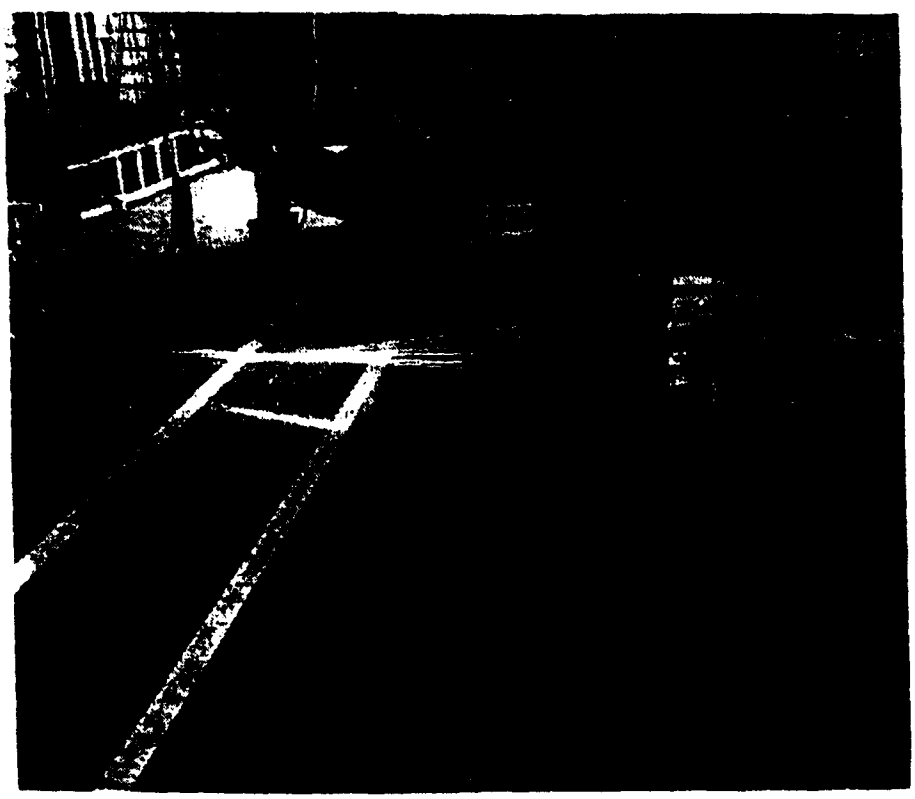

Figure 6. 2D wall jet

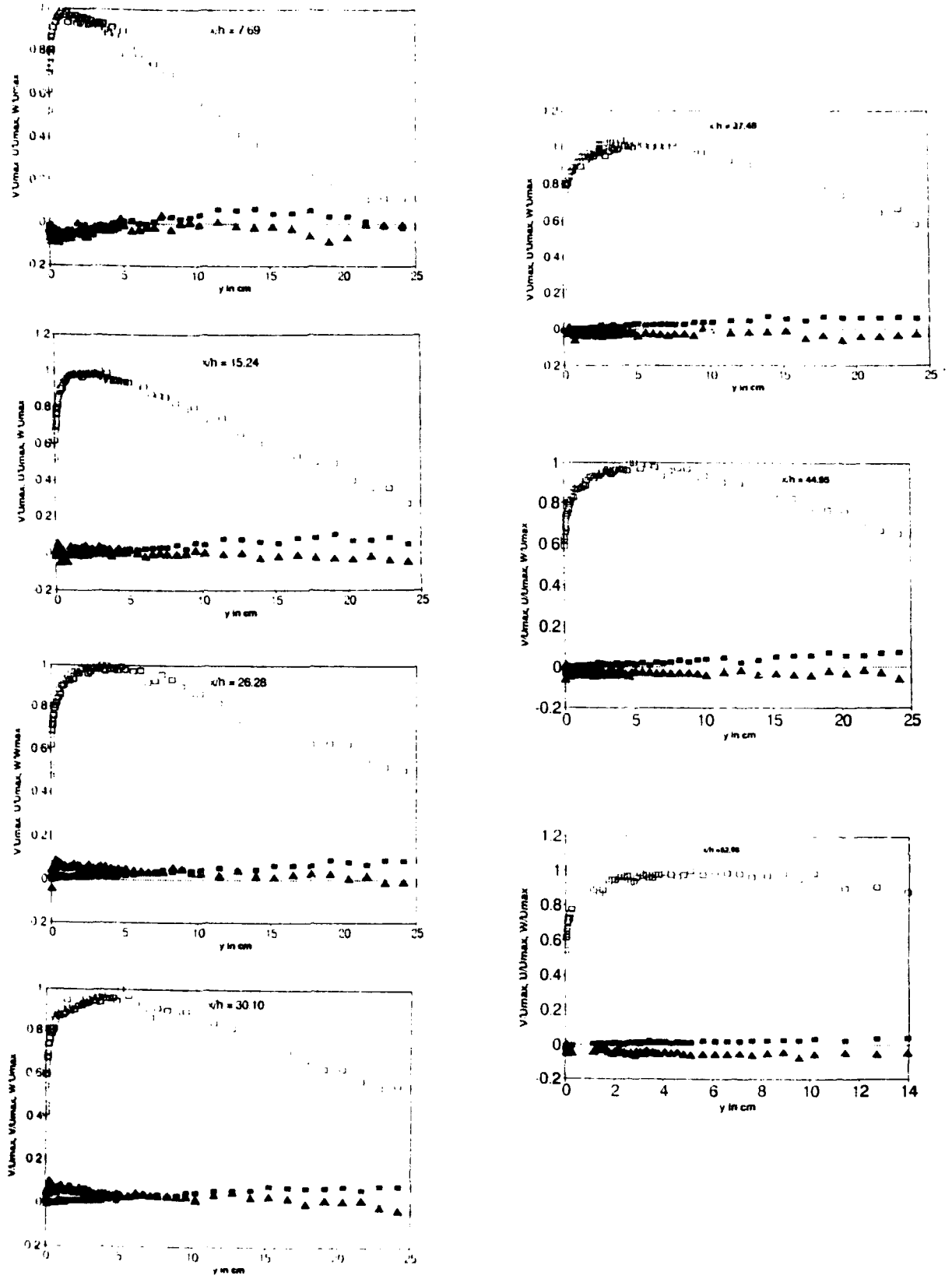

Figure 7. LV mean velocity profiles

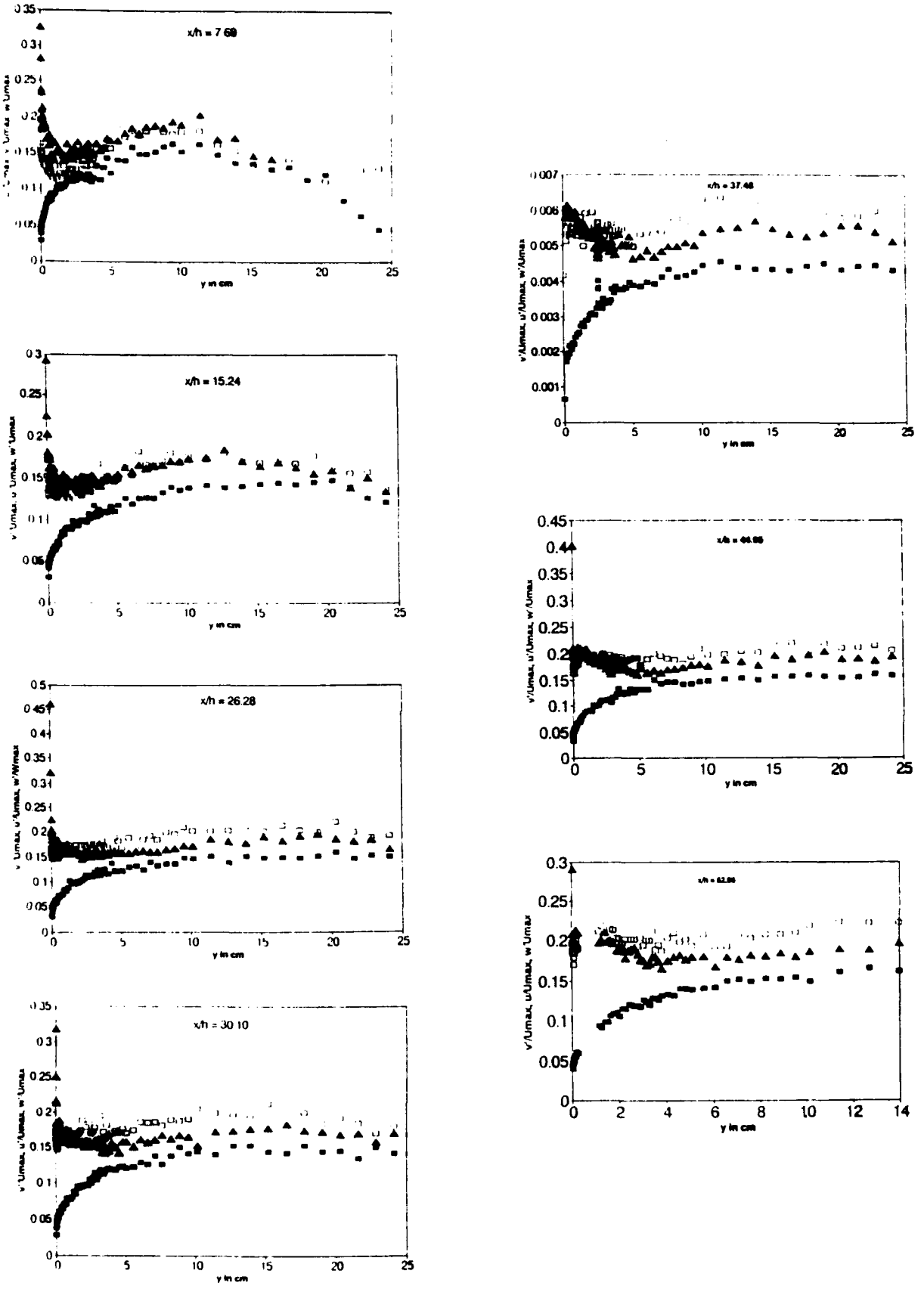

Figure 8. LV rms velocity profiles

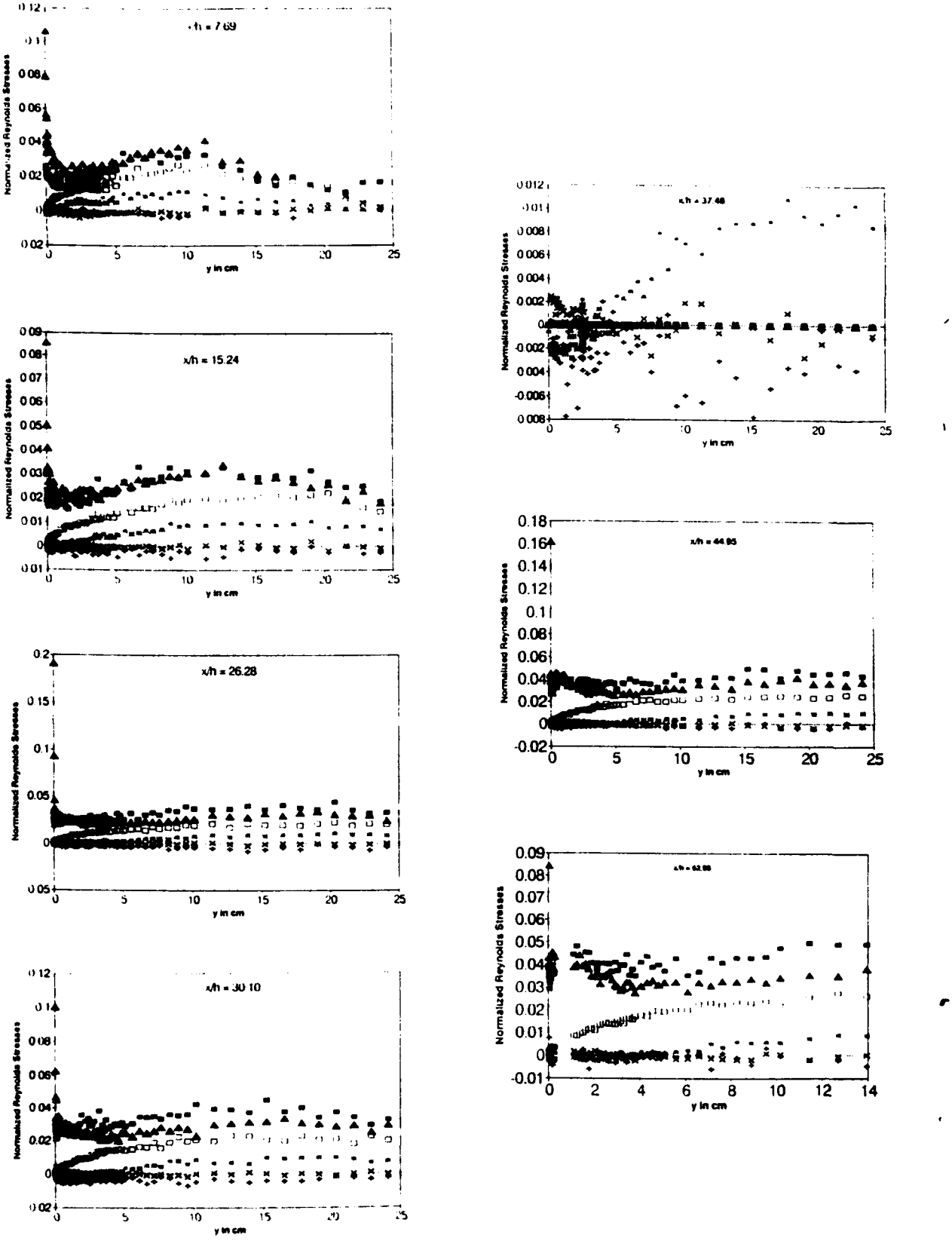

Figure 9. LV normalized Reynolds stress profiles

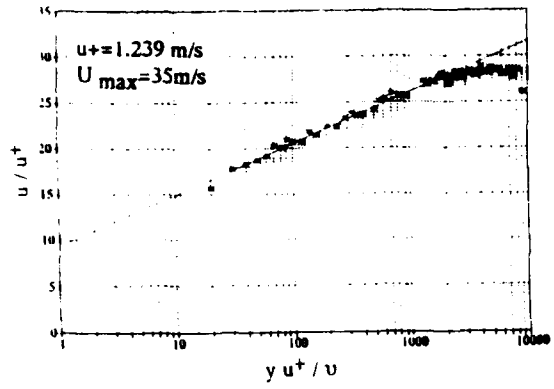

Figure 10. LV velocity protile at 353 cm, Tu -20%

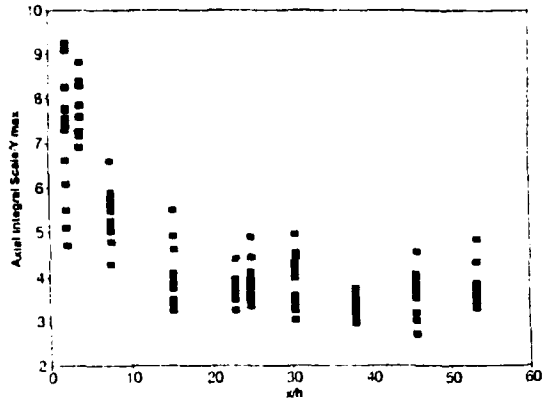

Figure 12. Axial integral scale

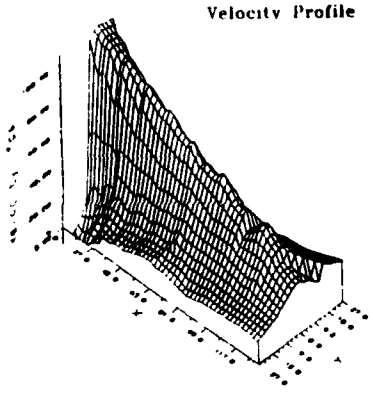

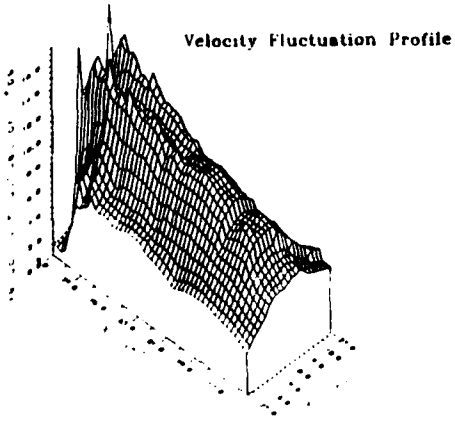

Figure 11. Span hot wire measurements of velocity and rms velocity

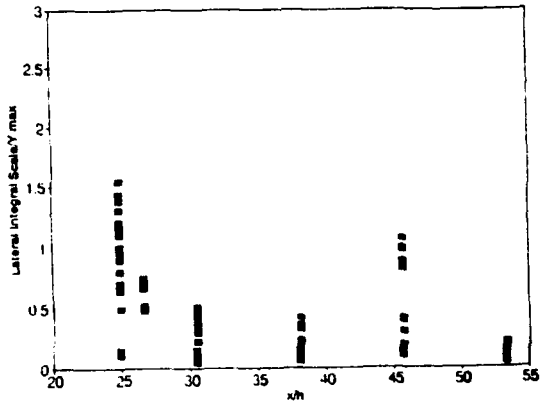

Figure 13. Lateral/vertical integral scale

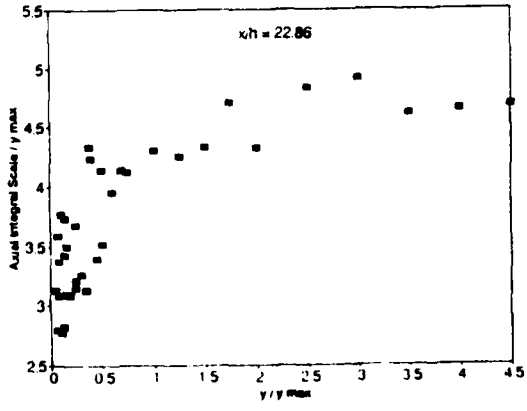

Figure 14. Axial scale distribution through the boundary layer

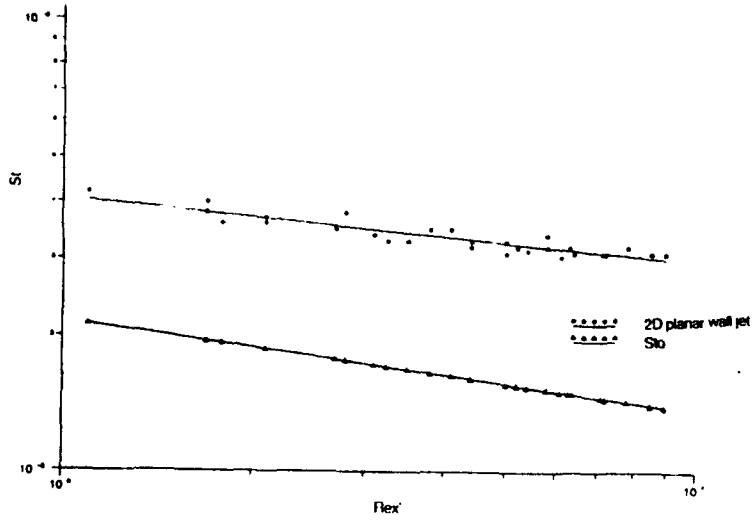

Figure 15. 2D wall jet heat transfer at Tu=20%

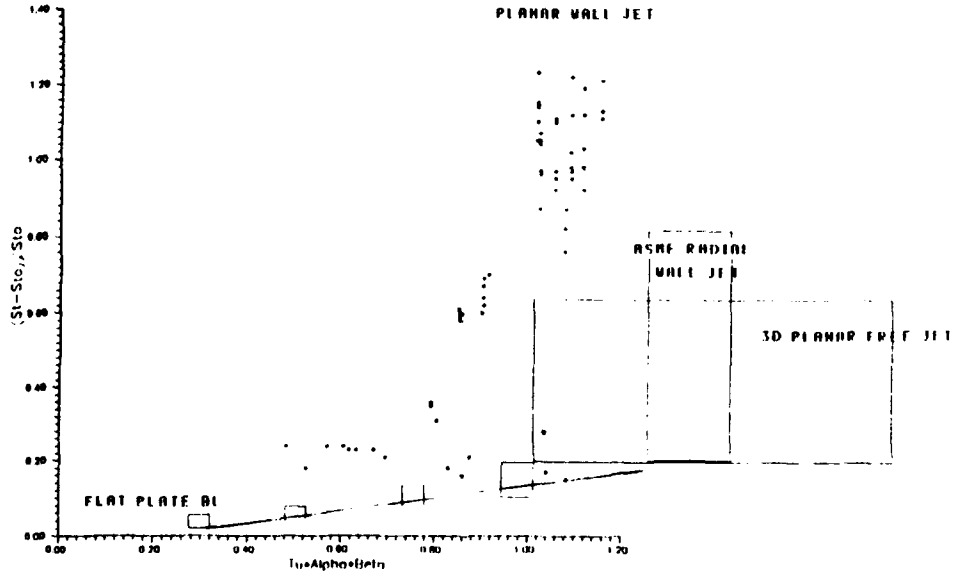

Figure 16. Comparison of 2D wall jet, 3D wall jet, and free jet

APPENDIX P

LIST OF PUBLICATIONS AND PRESENTATIONS

by

UNIVERSITY OF DAYTON RESEARCH INSTITUTE PERSONNEL

LIST OF PUBLICATIONS AND PRESENTATIONS

Journal Publications

[1] D. R. Ballal, "Joint Laser Raman Spectroscopy and Anemometry," **Combustion Measurements** (Edt. N. A. Chigier), Hemisphere Publishing Company, New York, 1991.

[2] D. R. Ballal, "Turbulence-Kinetics Interaction in Recirculatory Flows," **Major Research Topics in Combustion** (Edts. M. Y. Hussaini, A. Kumar, and R. A. Voigt), Springer Verlag Publishing Inc., New York, pp. 403-423, 1991.

[3] S. P. Heneghan and M. D. Vangsness, "Instrument Noise and Weighting Factors in Data Analysis," *Experiments in Fluids*, Vol. 9, pp. 290-294, 1990.

[4] F. Takahashi and W. J. Schmoll, "Lifting Criteria of Jet Diffusion Flames," *Twenty-Third Symposium (Int.) on Combustion*, The Combustion Institute, Pittsburgh, PA, pp. 677-683, 1991.

[5] G. J. Sturgess, D. G. Sloan, A. L. Lesmerises, D. R. Ballal, and S. P. Heneghan, "Design and Development of a Research Combustor for Lean Blow Out Studies," *ASME, Journal of Engineering for Gas Turbines and Power*, Vol. 114, pp. 13-20, 1992.

[6] J. C. Pan, W. J. Schmoll, and D. R. Ballal, "Turbulent Combustion Properties Behind a Conical Stabilizer," Paper No. 90-GT-51, *ASME, Journal of Engineering for Gas Turbines and Power*, 1991.

[7] S. P. Heneghan, M. D. Vangsness, and J. C. Pan, "Simple Determination of the Width of the Slit Function in Single-Shot CARS Thermometry," *Journal of Applied Physics*, Vol. 69, pp. 2692-2693, 1991.

[8] S. P. Heneghan and M. D. Vangsness, "Analysis of Slit Function Errors in Single-Shot Coherent Anti-Stokes Raman Spectroscopy (CARS)," *Reviews of Scientific Instruments*, Vol. 62, pp. 2093-2099, 1991.

[9] G. J. Sturgess, A. L. Lesmerises, S. P. Heneghan, M. D. Vangsness, and D. R. Ballal, "Isothermal Flowfields in a Research Combustor For Lean Blowout Studies," Paper No. 91-GT-37, *ASME, Journal of Engineering for Gas Turbines and Power*, 1991.

[10] G. J. Sturgess, A. L. Lesmerises, S. P. Heneghan, M. D. Vangsness, and D. R. Ballal, "Lean Blowout in a Research Combustor at Simulated Low Pressures, " Paper No. 91-GT-359, *ASME, Journal of Engineering for Gas Turbines and Power*, 1991.

[11] J. C. Pan, M. D. Vangsness, and D. R. Ballal, " Aerodynamics of Bluff-Body Stabilized Confined Turbulent Premixed Flames," Paper No. 91-GT-218, *ASME, Journal of Engineering for Gas Turbines and Power*, Vol. 114, pp. 783-789, 1992.

[12] J. C. Pan, M. D. Vangsness, S. P. Heneghan, and D. R. Ballal, "Scalar Measurements in Bluff-Body Stabilized Flames Using CARS Diagnostics," Paper No. 91-GT-302, *ASME, Journal of Engineering for Gas Turbines and Power*, 1991.

[13] S. P. Heneghan, M. D. Vangsness, D. R. Ballal, A. L. Lesmerises, and G. J. Sturgess, "Acoustic Characteristics of a Research Step Combustor," Paper No. AIAA 90-1851, *AIAA Journal of Propulsion*, 1991.

[14] G. J. Sturgess, A. L. Lesmerises, S. P. Heneghan, M. D. Vangsness, and D. R. Ballal, "Flame Stability and Lean Blowout in a Research Combustor," *Proceedings of the Tenth International Symposium on Air Breathing Engines*, Nottingham, U. K., pp. 372-384, September 1991.

[15] F. Takahashi, M. D. Vangsness, and W. J. Schmoll, "Near-Field Structure and The Local Extinction of Turbulent Jet Diffusion Flames of Methane in Air," *Proceedings of the 13th (Int.) Colloquium on the Dynamics of Explosions and Reactive Systems*, Nagoya, Japan, July 1991.

[16] S. P. Heneghan, C. R. Martel, T. F. Williams, and D. R. Ballal, "Studies of Jet Fuel Thermal Stability in Flowing Systems," *ASME, Journal of Engineering for Gas Turbines and Power, 1992.*

[17] J. C. Pan and D. R. Ballal, "Chemistry and Turbulence Effects in Bluff-Body Stabilized Flames," AIAA Paper No. 92-0771, Submitted to *AIAA Journal of Propulsion and Power.*

[18] S. P. Heneghan, R. J. Byrd, S. Locklear, S. Anderson, and W. D. Schultz, "Evaluation of Jet Fuel Additives in Static Systems," AIAA Paper No. 92-0686, Submitted to *AIAA Journal of Propulsion and Power.*

[19] G. J. Sturgess, S. P. Heneghan, M. D. Vangsness, D. L. Shouse, A. L. Lesmerises, and D. R. Ballal, "Effects of Back Pressure in a Lean-Blowout Research Combustor," Accepted for *ASME, Journal of Engineering for Gas Turbines and Power, 1992.*

[20] J. S. Chin, A. H. Lefebvre, and F. T. Sun, "Influence of Flow Conditions on Deposits from Heated Hydrocarbon Fuels," Accepted for *ASME, Journal of Engineering for Gas Turbines and Power, 1992.*

[21] F. Takahashi and L. P. Goss, "Near-Field Turbulent Structures and the Local Extinction of Jet Diffusion Flames," *Twenty-Fourth Symposium (Int.) on Combustion*, The Combustion Institute, Pittsburgh, PA, 1992.

[22] S. D. Anderson, J. T. Edwards, R. J. Byrd, T. B. Biddle, W. H. Edwards, S. P. Heneghan, C. R. Martel, T. F. Williams, J. A. Pearce, and W. E. Harrison, "Advanced Thermally Stable Jet Fuel Development," *Aviation Fuels: Thermal Stability Requirements*, ASTM STP 1138, P. W. Kirklin and P. David, Eds. ASTM Philadelphia, 1992.

Papers Under Review

[1] S. P. Heneghan and S. Zabarnick, "Oxidation of Jet Fuels and the Formation of Deposits," Submitted to Fuels, May 1992.

[2] S. P. Heneghan, C. R. Martel, T. F. Williams, and D. R. Ballal, "Effects of Oxygen and Additives on the Thermal Stability of jet Fuels," Submitted to 38th ASME (Int.) Gas Turbine and Aeroengine Conference, Cincinnati, OH, May, 1993.

Presentations

[1] S. P. Heneghan, W. J. Schmoll, and D. R. Ballal, "Studies of CARS-LDA Biasing in Reactive Flows," Fall Technical Meeting, Eastern States Section, The Combustion Institute, Clearwater Beach, FL, December, 1988

[2] S. P. Heneghan and M. D. Vangsness, "Mean Biasing in an LDA-CARS System," 15th AIAA Mini-Symposium, March, 1989, Dayton, Ohio

[3] F. Takahashi, W. J. Schmoll, and M. D. Vangsness, "Effects of Swirl on the Stability and Turbulent Structure of Jet Diffusion Flames," Paper No. AIAA 90-0036, 28th Aerospace Sciences Meeting, January, 1990, Reno, NV.

[4] S. P. Heneghan, "Determination of Bulk A-Factors From Surface Deposition Rates in Jet Fuel Thermal Stability Tests," AIAA, 16th Annual Mini-Symposium on Aerospace Science and Technology, March 29, 1990, Dayton, Ohio

[5] J. C. Pan, "Measurements of Turbulence Properties Behind a Confined Conical Stabilizer," 16th AIAA Mini-Symposium, March, 1990, Dayton, Ohio.

[6] D. R. Ballal, " Gas Turbine Combustion-Contribution of Academia to Research," Central States Section, The Combustion Institute, Cincinnati, OH, May, 1990.

[7] J. C. Pan, M. D. Vangsness, S. P. Heneghan, and D. R. Ballal, "Turbulent Scalar Properties Behind Conical Bluff Bodies Using Laser Diagnostics," Central States Section, The Combustion Institute, Cincinnati, Ohio, May, 1990.

[8] F. Takahashi and W. J. Schmoll, "Mean and Turbulent Velocity Characteristics of Swirling Jet Diffusion Flames," Central States Section, The Combustion Institute, Cincinnati, Ohio, May, 1990.

[9] M. D. Vangsness and S. P. Heneghan, "Probe Volume Effects on the Spatial Distribution of CARS Signal," Presented at Sixth Annual Interdisciplinary Laser Science Conference, Minneapolis, MN, September 16-19, 1990.

[10] S. P. Heneghan and M. D. Vangsness, "Analysis of Slit Function Errors in Single-Shot CARS," Presented at Sixth Annual Interdisciplinary Laser Science Conference, Minneapolis, MN, September 16-19, 1990.

[11] S. P. Heneghan, J. C. Pan, and M. D. Vangsness, "Analysis of The Instrument Slit Function in CARS Thermometry," Presented at The Spring Meeting, Central States Section, The Combustion Institute, Nashville, TN, April 21-24, 1991.

[12] J. C. Pan, M. D. Vangsness, S. P. Heneghan, and D. R. Ballal, "Laser Diagnostic Studies of Bluff-Body Stabilized Confined Turbulent Premixed Flames," Presented at The Spring Meeting, Central States Section, The Combustion Institute, Nashville, TN, April 21-24, 1991.

[13] F. Takahashi, M. D. Vangsness, W. J. Schmoll, and V. M. Belovich, "Turbulent Flow Characteristics of Swirling Jets and Jet Diffusion Flames," Presented at The Spring Meeting, Central States Section, The Combustion Institute, Nashville, TN, April 21-24, 1991.

[14] M. D. Vangsness and F. Takahashi, "LDA/CARS Studies on a Confined Diffusion Flame," 17th AIAA Mini-Symposium, Dayton, OH, March (1991)

[15] F. Takahashi, M. D. Vangsness, and V. M. Belovich, "Conditional LDV Measurements in Swirling and Non-Swirling Coaxial Turbulent Air Jets for Model Validation," Paper No. AIAA-92-0580, AIAA 30th Aerospace Sciences Meeting, Reno, Nevada, Jan. 6-9, 1992.

[16] F. Takahashi, "Intermittency and Conditional Statistics in Reacting and Non-Reacting Turbulent Jets," 18th AIAA Mini-Symposium, Dayton, OH, March 1992.

[17] S. P. Heneghan and W. E. Harrison III, "Anti-Oxidants in Jet Fuels: A New Look," Symposium on Structures of Jet Fuels, American Chemical Society, San Francisco, CA, April 5-10, 1992.

[18] M. D. Vangsness and S. P. Heneghan, "Coherent Anti-Stokes Raman Spectroscopy: System Characterization and Reproducibility," Presented at The Spring Meeting, Central States Section, The Combustion Institute, Columbus, OH, April 26-28, 1992.

[19] F. Takahashi, M. D. Vangsness, and L. P. Goss, "Dynamic Vortex-Flame Interactions in Turbulent Jet Diffusion Flames Near Local Extinction," Presented at The Spring Meeting, Central States Section, The Combustion Institute, Columbus, OH, April 26-28, 1992.

[20] S. P. Heneghan, "Chemistry of Antioxidants and Their Role in the Formation of Solids in Jet Fuels," Coordinating Research Council Meeting, Washington D.C., April 1992.

[21] S. P. Heneghan, D. L. Gieger, and E. Stewart, "Quantitative determination of Sulfur Content in Jet Fuels using Atomic Emission Detection and Gas Chromatography, " Ohio Valley Chromatographic Symposium, June, 1992.

[22] F. Takahashi and M. D. Vangsness, "Structure Measurements in Swirling and Non-Swirling Turbulent Jets and Jet Diffusion Flames," Twenty-Fourth Symposium (Int.) on Combustion, Sydney, Australia, July, 1992.

UDRI Reports

[1] J. C. Pan, "Laser Diagnostic Studies of Confined Turbulent Premixed Flames Stabilized by Conical Bluff Bodies: Vol. I: Theory and Experiments," UDR-TR-91-101, Ph. D. Dissertation, University of Dayton, Dayton, OH, July 1991.

[2] J. C. Pan, M. D. Vangsness, S. P. Heneghan, W. J. Schmoll, and D. R. Ballal, "Laser Diagnostic Studies of Confined Turbulent Premixed Flames Stabilized by Conical Bluff Bodies: Vol. II: Data Set," UDR-TR-91-102, University of Dayton, Dayton, OH, July 1991.

[3] F. Takahashi and M. D. Vangsness, "LDV Measurements in Swirling and Non-Swirling Coaxial Turbulent Air Jets: Report 1: No Swirl, 100 m/s," UDR-TR-91-160, University of Dayton, Dayton, OH, April 1991.

[4] F. Takahashi and M. D. Vangsness, "LDV Measurements in Swirling and Non-Swirling Coaxial Turbulent Air Jets: Report 2: No Swirl, 25 m/s," UDR-TR-91-161, University of Dayton, Dayton, OH, May 1991.

[5] F. Takahashi, M. D. Vangsness, and V. M. Belovich, "LDV Measurements in Swirling and Non-Swirling Coaxial Turbulent Air Jets: Report 3: 30-degree Swirl, 100 m/s," UDR-TR-91-162, University of Dayton, Dayton, OH, July 1991.

[6] F. Takahashi, M. D. Vangsness, and V. M. Belovich, "LDV Measurements in Swirling and Non-Swirling Coaxial Turbulent Air Jets: Report 4: 30-degree Swirl, 100 m/s," UDR-TR-91-163, 30-degree Swirl, 25 m/s," University of Dayton, Dayton, OH, August 1991.

[7] W. D. Schulz, "A Chemical Investigation of the Nature of Jet Fuel Oxidation Deposits and the Effects of additives on Deposits," Subcontractor Final Report, April 1992.

[8] C. R. Martel, T. F. Williams, and H. L. Imwalle, "Studies of Jet Fuel Thermal Stability in a Flowing System-Report I: Analyses," Report No. UDR-TR-92-98, University of Dayton, Dayton, OH, July 1992.

[9] C. R. Martel, T. F. Williams, and H. L. Imwalle, "Studies of Jet Fuel Thermal Stability in a Flowing System-Report II: Data Set," Report No. UDR-TR-92-99, University of Dayton, Dayton, OH, August 1992.